Elucidating the Origin of Expiratory Abdominal Activity During Sleep and Analysis of its Manifestation in Conditions of an Impaired Inspiratory Drive

by

Annette Pisanski

A thesis submitted in partial fulfillment of the requirements for the degree of

Doctor of Philosophy

Department of Physiology

University of Alberta

Abstract

This dissertation explored respiratory control mechanisms during sleep, with a specific focus on the contribution of the lateral parafacial area (pFL) to the generation of abdominal recruitment. Existing theories posit the preBötzinger complex (preBötC) as the inspiratory oscillator and identify the pFL as the driver of active expiration through abdominal muscle (ABD) recruitment. Despite induced muscle paralysis during REM sleep, ABD recruitment persists, exhibiting correlations with heightened tidal volume and the regularization of respiratory periods. Utilizing chemogenetic modulation of the pFL activity, this study revealed a state-dependent impact: inhibiting the pFL reduced REM events expressing ABD recruitment, while activation increased both the frequency and intensity of such events. Intriguingly, ABD recruitment during NREM sleep and wakefulness remained unaffected. Additionally, this thesis investigated the rostrocaudal localization of the pFL core, addressing the variability in prior studies regarding the pFL response coordinates. Through the measurement of the impact of GABAergic disinhibition on respiration at distinct rostro-caudal sites, this study identified that more rostral pFL locations are pivotal for substantial and enduring changes in ABD recruitment and respiratory responses. Moreover, this dissertation explored the occurrence of ABD recruitment in sleep-disordered breathing (SDB), a health concern with cardio-metabolic implications. By leveraging the Kappa-opioid-receptor-DREADD (KORD) system to depress preBötzinger complex activity in rats, this study observed heightened respiratory disturbances and ABD recruitment during REM sleep following KORD receptor ligand administration. These findings offer valuable insights into the role of the pFL in sleep-related respiratory control, elucidating state-dependent mechanisms and identifying potential therapeutic targets for sleep-related breathing disorders.

Preface

Section 1.2 of Chapter 1 in this thesis is an updated version of a literature review published as A. Pisanski and S. Pagliardini "The parafacial respiratory group and the control of active expiration", *Respiratory Physiology & Neurobiology,* vol. 265, 153-160 with permission from the publisher. I was responsible for the literature review and manuscript composition. S. Pagliardini was the senior author and was involved in manuscript composition.

Chapter 2 of this thesis has been published as A. Pisanski, X. Ding, N. Koch and S. Pagliardini "Chemogenetic modulation of the parafacial respiratory group influences the recruitment of abdominal activity during REM sleep", *Sleep*, vol. 43, issue 5 and is included in this thesis with permission from the publisher. I was responsible for the experimental design, data collection and analysis as well as the manuscript composition. X. Ding was responsible for the instrumentation of experimental animals and immunohistochemistry. N. Koch assisted with data collection and contributed to manuscript edits. S. Pagliardini was the senior author and was involved with concept formation, experimental design and manuscript composition.

Chapter 3 of this thesis has been submitted for publication to *eLife* and is currently under review and available on BioRxiv as A. Pisanski, M. Prostebby, C.T. Dickson and S. Pagliardini "Mapping responses to focal injections of bicuculline in the lateral parafacial region identifies core regions for maximal generation of active expiration". I contributed with the concept formation and experimental design, and was responsible for the data collection and analysis, as well as the manuscript composition. M. Prostebby assisted with data analysis, particularly the multivariate analysis of respiratory measures and contributed to manuscript composition. C. T. Dickson contributed to manuscript edits. S. Pagliardini was the senior author and was involved with concept formation, experimental design and manuscript composition.

Chapter 4 of this thesis is a collaborative work that will be submitted for publication as A. Pisanski, N. Koch, X. Ding and S. Pagliardini "Characterization of respiratory disturbances and abdominal recruitment during sleep in conditions of impaired inspiratory drive". I was responsible for the experimental design, data collection and analysis, as well as the manuscript composition. X. Ding was responsible for the instrumentation of experimental animals and immunohistochemistry. N. Koch assisted with data collection. S. Pagliardini was the senior author and was involved with concept formation, experimental design and manuscript composition.

A loyal companion and a true friend, in loving memory of Pirri

"The world would be a better place if everyone
had the ability to love as unconditionally as a dog"
-M.K. Clinton

"Dogs come into our lives to teach us about love,
they depart to teach us about loss.
A new dog never replaces an old dog;
it merely expands the heart"
-Erica Jong

Acknowledgements

I extend my profound gratitude to those whose invaluable contributions were instrumental in the completion of this doctoral thesis. My academic journey has been enriched by the unwavering support and guidance I received.

Table of Content

x

List of Tables

List of Figures

Chapter 1.   Introduction

The generation of rhythmic respiratory behaviors has long been a subject of scientific inquiry, with a prevailing hypothesis positing the existence of distinct yet interconnected oscillators within the medulla. These oscillators, each with specific roles in the respiratory cycle, are currently understood as follows: the preBötzinger Complex (preBötC), responsible for instigating the inspiratory rhythm (Gray te al., 2001; Smith et al., 1991; Tan et al., 2008), the lateral parafacial area (pFL), driving active expiration through the recruitment of expiratory abdominal (ABD) muscles (Huckstepp et al., 2015; Janczewski & Feldman, 2006; Janczewski et al., 2002; Pagliardini et al., 2011), as well as the post-inspiratory Complex (PiCo), proposed to generate the post-inspiratory phase characterized by diaphragmatic eccentric contraction and airway muscle adduction to slow expiration (Anderson et al., 2016) and whose existence is still debated (Ashhad et al., 2022)..

In resting conditions, the preBötC plays an essential role in maintaining ventilation, with subpopulations within it contributing to specialized orofacial behaviors associated with breathing (Gray et al., 2001; Deschênes & Ulanovsky, 2016; Li et al., 2016; Tan et al., 2008; Yackle et al., 2017). Conversely, the pFL remains silent during rest and becomes active only in response to heightened respiratory demands, such as exercise, hypercapnia, or hypoxia (de Britto & Moraes, 2017; Huckstepp et al., 2015; Pagliardini et al., 2011). Investigations into the interplay between the expiratory and inspiratory oscillators in adult rodents have demonstrated the pFL's inability to sustain activity when the inspiratory oscillator is compromised (Huckstepp et al., 2016). However, these experiments were conducted in anesthetized preparations, where autoresuscitation processes are impaired (Krause et al., 2016). Therefore, the evaluation of active expiration's contributions to breathing under conditions of preBötC inhibition in unanesthetized freely behaving animals remains an intriguing avenue of research.

The anatomical origin, mechanism of generation, and modulation of inspiratory rhythm have been subjects of intensive investigation (Del Negro et al., 2018; Kam et al., 2013). Recently, interest has expanded to examine the role of active expiration, particularly the involvement of the pFL, in ventilation across various physiological and vigilance states (de Britto & Moraes, 2017; Huckstepp

et al., 2015; Pagliardini et al., 2011). While active expiration has been observed during sleep (Andrews & Pagliardini, 2015; Saini et al., 2022; Saini & Pagliardini, 2017), the precise engagement of the pFL in this phenomenon remains incompletely understood. To address this, it becomes imperative to inhibit and activate the pFL during sleep and assess the resultant changes in ABD recruitment.

Moreover, the precise anatomical location of the pFL remains a matter of debate. Previous investigations have employed pharmacological methods (Boutin et al., 2017; de Britto et al., 2020; de Britto & Moraes, 2017; Huckstepp et al., 2018; Magalhães et al., 2021; Pagliardini et al., 2011; Zoccal et al., 2018) and chemogenetic/optogenetic techniques (Huckstepp et al., 2015; Pagliardini et al., 2011; Pisanski et al., 2019) to probe the function of the pFL. The observed core location of the pFL varies, with some studies placing it proximate to the caudal tip of the facial nucleus (VIIc) (-0.2 to +0.5 mm from VIIc) (Boutin et al., 2017; de Britto et al., 2020; de Britto & Moraes, 2017; Huckstepp et al., 2018; Magalhães et al., 2021; Pagliardini et al., 2011), while others suggest a more rostral position (+0.3 to +1.0 mm from VIIc) (Silva et al., 2019). Notably, chemogenetic inhibition at various coordinates did not completely suppress the ABD recruitment observed during sleep or in response to Bicuculline injection, underscoring the incomplete understanding of the pFL's anatomical and functional boundaries (Huckstepp et al., 2015; Pisanski et al., 2019).

Therefore, in this thesis, I seek to address the following aims:

   I.   Understand the role of the pFL in the generation of active expiration during sleep.
  II.   Identify the rostro-caudal distribution of the pFL along the ventral medulla.
 III.   Determine the contribution of active expiration during sleep in conditions of an impaired inspiratory drive.

In Chapter 1 of this thesis, we will delve into the historical and contemporary research literature concerning the generation and modulation of inspiratory rhythm and active expiration in rodent models. We will also explore the emergence of expiratory ABD activity during sleep and its contributions to ventilation across different physiological and developmental states. This review aims to elucidate existing gaps in the literature and provide a foundation for this thesis's research objectives, which will be discussed in detail.

1.1 The Inspiratory Oscillator: preBötzinger Complex

After the discovery of the preBötzinger Complex (preBötC) by Smith et al. in 1991, the molecular markers associated with this inspiratory rhythmic oscillator remained unidentified for almost a decade. A pivotal study conducted by Gray et al. in 1999 successfully delineated the boundaries of this brain region by identifying a cell population expressing neurokinin 1 (NK1R) and μ-opioid receptors (μOR) (Gray et al., 1999). This study marked the first to report that preBötC NK1R and μ-opioid receptor-expressing cells are excitatory and involved in frequency modulation. Based on the response of individual cells to peptidergic modulation, they proposed that pre-inspiratory rhythmogenic neurons in the preBötC are sensitive to both substance P (NK1R ligand) and DAMGO (μ-opioid receptor agonist), whereas inspiratory pattern-generating neurons are only sensitive to substance P (Gray et al., 1999; Kam et al., 2013). Subsequent research revealed that the NK1R+ cell population consists of various cell types differing in size and anatomical projections, located throughout the ventral respiratory group (VRG) area, including the preBötC (Guyenet et al., 2002; Stornetta et al., 2003). Although somatostatin (SST) cells constitute only a subpopulation of the preBötC, it is being used as a marker for identifying the anatomical boundaries of the preBötC in both adult and perinatal rats (Pagliardini et al., 2003; Stornetta et al., 2003). Interestingly, the excitatory respiratory neurons expressing the aforementioned markers originate from the ventral domain of Developing brain homeobox 1 (Dbx1) progenitors (Bouvier et al., 2010; Gray et al., 2010) which has also been shown to be essential for coordination of locomotion (Lanuza et al., 2004). Furthermore, although the generation of rhythmic activity in the preBötC relays on excitatory Dbx1-glutamatergic neurons (Del Negro et al., 2018), inhibitory neurons which make up a substantial fraction of the preBötC cell population, modulate inspiratory pattern generation (Sherman et al., 2015)

The discovery of the embryonic origin and cellular markers for respiratory preBötC neurons has opened the door to cell-specific targeted studies and molecular manipulations. However, the contribution of these anatomically identified cell populations to rhythm and pattern generation remains uncertain and is a central focus of current respiratory research. Recent studies have challenged the conventional view of preBötC as a nucleus exclusively dedicated to the generation of respiratory rhythm. These studies propose that different subpopulations of cells within the preBötC may play essential roles in generating cardiorespiratory oscillations and orofacial

behaviors such as sighs, gasps, and vocal communication (Li et al., 2016; Lieske et al., 2000; Menuet et al., 2020; Tupal et al., 2014; Yackle et al., 2017).

1.1.1 Functional Characterization of Dbx1-Derived Neurons

Drawing parallels between the spinal cord, where Dbx1-derived cells are vital for bilateral synchronization, and hindbrain progenitors, led to the hypothesis that Dbx1 neurons in the preBötC may also play a pivotal role in respiration (Bouvier et al., 2010; Gray et al., 2010). Transgenic mice with a loss of Dbx1 gene function exhibit viable cardiovascular and locomotor systems, yet they do not initiate inspiratory efforts, becoming cyanotic and succumbing shortly after birth (Bouvier et al., 2010; Gray et al., 2010). Network activity recordings in medullary slice preparations from the preBötC region of the embryos lacking Dbx1 gene function, confirm the absence of inspiratory rhythm (Figure 1.1) (Bouvier et al., 2010; Gray et al., 2010). Interestingly, the absence of the Dbx1 genetic product does not impact the survival and migration of the progeny cell line. Instead, it eliminates the expression of SST, NK1R, and VGlut2 in Dbx1-derived preBötC cell subpopulations that would otherwise express these markers (Bouvier et al., 2010). The inability of these mice to produce rhythmic inspiratory movements is most likely attributable to the absence of glutamatergic transmission in preBötC Dbx1-derived cells, which are a core element of rhythmogenic inspiratory activity. The necessity of these cell populations for respiratory rhythm is confirmed by laser ablation of Dbx1-derived cells in the preBötC, leading to a gradual decline in frequency and motor output, ultimately causing respiratory rhythm cessation after ablating approximately 15% of the Dbx1 population in the preBötC (Wang et al., 2014).

Overall, data from anatomical and targeted ablation studies provide insights into the function and types of Dbx1-derived preBötC cells. These findings suggest that the ventral domain of Dbx1 progenitors primarily gives rise to glutamatergic preBötC neurons, which are essential for both the generation of respiratory rhythm and the shaping of motor output. While it is known that a subpopulation of preBötC Dbx1-derived cells also expresses NK1R and SST, the degree of overlap among these three populations remains unclear.

1.1.2 Functional Characterization of NK1R+ preBötC Neurons

Modulating respiratory frequency through the bath application of substance P, the NK1R ligand, in medullary slice preparations (Gray et al., 1999; Pagliardini et al., 2003; Stornetta et al., 2003) suggests that the NK1R+ preBötC subpopulation may play a direct role in either respiratory rhythm generation or non-respiratory modulation of the rhythmogenic kernel (Gray et al., 1999). Further evidence, stemming from slow (over the course of days) targeted ablation of preBötC NK1R+ neurons (Gray et al., 2001), suggests that these cells are essential for the generation of normal breathing. The chronic elimination of NK1R+ cells in the preBötC through local injections of the toxin saporin conjugated to substance P (SP-SAP) results in patterns of ataxic breathing sufficient to sustain life in conscious rats (Gray et al., 2001). A similar study, involving the monitoring of sleep over post-lesion days, reveals an increasing number of respiratory disturbances during sleep (Figure 1.2 A), such as apneas and hypopneas, and an ataxic breathing pattern during wakefulness (Figure 1.2 B) (McKay et al., 2005). However, the incomplete silencing of the inspiratory rhythm in these conditions may be the result of neural plasticity occurring over the course of days or the limited number of cells affected by the ablation.

1.1.3 Functional Analysis of SST+ Neurons in the PreBötzinger Complex

A study in which viral vectors were employed to selectively express the allatostatin receptor (AlstR) in SST+ preBötC neurons, demonstrated that rapid and temporary silencing of the SST+ subpopulation resulted in prolonged apneas, necessitating mechanical ventilation to prevent asphyxiation in both anesthetized and conscious animals (Figure 1.3 A-C) (Tan et al., 2008). These findings supported the notion that perturbation of SST+ neurons significantly disrupts normal rhythmogenesis. However, experiments in which VGlut2 expression was selectively eliminated from the SST+ subpopulation indicated that excitatory synaptic transmission from SST+ preBötC neurons was not a prerequisite for the generation and stability of the respiratory rhythm (Tupal et al., 2014). Similarly, other studies have raised doubts regarding the role of SST+ neurons in respiration (Le et al., 2016; Stornetta et al., 2003; Tupal et al., 2014). The challenges associated with identifying and recording from SST+ neurons exhibiting a respiratory discharge pattern (Stornetta et al., 2003), coupled with evidence indicating that the SST+ preBötC subpopulation is

not evolutionarily conserved across mammalian species (Tupal et al., 2014), casted uncertainty on the relevance of SST+ neurons in respiratory function.

Interestingly, Koizumi et al. (2016) not only demonstrated that SST+ neurons in the preBötC are indeed respiratory neurons, characterized by a phasic discharge pattern synchronized with hypoglossal inspiratory bursts, but also revealed that SST+, glutamatergic, and Dbx1-derived cell populations may exhibit functional overlap. Following laser stimulation of cells expressing archaerhodopsin (Arch2) in SST, Dbx1, or VGlut2-transgenic mice, all three neuronal subpopulations were equally capable of modulating the respiratory rhythm through the same voltage-dependent mechanism (Koizumi et al., 2016). Additionally, other studies have suggested that a subset of SST+ neurons within the preBötC may have an inhibitory role that potentially modulates the respiratory rhythm, while a different subset of excitatory SST+ neurons contribute to the generation of motor output patterns (Cui et al., 2016; de Sousa Abreu et al., 2022).

1.1.4 PreBötzinger Complex Ontogeny, Transcription Factors, and Rhythmogenesis

Studies in which the loss of Dbx1 gene function leads to the inability to produce respiratory rhythmic bursts strongly suggest that Dbx1-derived cells are vital for generating inspiratory efforts (Bouvier et al., 2010; Gray et al., 2010). PreBötC NK1R+ and SST+ cell populations, which are required for the generation of normal respiratory rhythm and pattern (Cui et al., 2016; Gray et al., 2001; Tan et al., 2008), are primarily glutamatergic and arise from the ventral domain of Dbx1 progenitors (Bouvier et al., 2010; Gray et al., 2010). Furthermore, Dbx1-derived cells in the preBötC expressing the roundabout homolog 3 (Robo3) gene, have commissural properties and are essential for the synchrony of the preBötC (Bouvier et al., 2010). Both the high-frequency inspiratory discharges in the preBötC and bilateral synchrony of the respiratory rhythm emerge simultaneously during embryonic development, coinciding with the presence of overlapping populations of NK1R+ and SST+ cells within the preBötC (E15) (Bouvier et al., 2010; Pagliardini et al., 2003; Stornetta et al., 2003; Thoby-Brisson et al., 2005).

The mechanism underlying rhythmic inspiratory activity undergoes developmental changes: initially relying more on endogenous pacemaker activity, potentially driven by calcium activated non-specific conductance (ICAN) and persistent sodium currents (INaP), during earlier stages of embryonic development and shifting toward greater dependence on network electrical and

glutamatergic connectivity closer to birth (Chevalier et al., 2016; Thoby-Brisson et al., 2005). Specifically, recent theories postulate that rhythmicity of the inspiratory oscillator is based on the summation and synchronization of subthreshold recurrent excitatory post-synaptic potentials (EPSPs) from a small fraction of Dbx1+ preBötzinger Complex neurons to generate a burst that is transmitted to pattern generating SST+ neurons and motor output (Burstlet Theory) (Ashhad et al., 2022; Del Negro et al., 2018; Feldman & Kam, 2015; Kam et al., 2013; Phillips & Rubin, 2022; Prajkta et al., 2020).

1.1.5 Functional role of inhibitory neurons in the preBötzinger Complex

While inhibition is not essential for respiratory rhythmogenesis (Funk et al. 1993, Wallén-Mackenzie et al. 2006, Janczewski et al. 2013), it has been shown that plays a crucial role in modulating breathing patterns, as evidenced by its profound effects on burst amplitude and frequency (Cui et al. 2016, Cregg et al. 2017, Baertsch et al. 2018, Yang & Feldman 2018). Approximately half of preBötC neurons exhibit inhibitory characteristics, representing a combination of glycinergic and GABAergic neurons (Kuwana et al. 2006, Winter et al. 2009). Furthermore, optogenetic activation of preBötC glycinergic neurons in vivo results in delayed inspiration and the occurrence of apneas. Conversely, photoinhibition of these neurons increases tidal volume and shortens expiratory duration (Sherman et al. 2015). This evidence suggests that overall, inhibitory neurons in the preBötC modulate breathing frequency by controlling the refractory properties of the excitatory neurons and can also modulate the generation of the inspiratory pattern (Cui et al. 2016; Sherman et al. 2015; Baertsch et al. 2018).

1.1.6 Connectivity of the PreBötzinger Complex

Within the brainstem, numerous clusters of neurons, including those from the contralateral preBötC, Bötzinger Complex, nucleus of the solitary tract (NTS), parafacial region (pFL/pFV), and parabrachial nuclei (PB), establish direct connections with both excitatory and inhibitory neurons in the preBötC (Yang et al., 2020). Moreover, suprapontine inputs to these excitatory and inhibitory preBötC neurons encompass regions like the superior colliculus, red nucleus, amygdala, hypothalamus, periaqueductal gray (PAG) and cortex (Trevizan-Baú et al., 2021; Yang et al., 2020). Notably, cholinergic neurotransmission exerts an influence on both respiratory rhythm-generating neurons and inhibitory glycinergic neurons within the preBötC (Shao & Feldman, 2009;

Zheng et al., 2020). In a recent investigation, the source of these cholinergic projections to the preBötC was identified as the intermediate reticular formation, the lateral paragigantocellularis, and the nucleus of the solitary tract (Biancardi et al., 2023). Surprisingly, recent evidence contradicts earlier hypotheses that the laterodorsal and pedunculopontine tegmental nuclei (LDT/PPT) were the primary sources of cholinergic activation for the preBötC (Muere et al., 2012, 2015; Shao & Feldman, 2005; Shao & Feldman, 2009), demonstrating instead that these nuclei predominantly dispatch glutamatergic and GABAergic/glycinergic projections to the preBötC, rather than cholinergic ones (Biancardi et al., 2023).

On the other hand, an exploration of the excitatory efferent projections originating from the preBötC has revealed labeling in various regions, including the contralateral preBötC, Bötzinger Complex (BötC), ventral respiratory group, nucleus of the solitary tract, parahypoglossal nucleus, parafacial region (pFL/pFV), parabrachial and Kölliker-Füse nuclei (Yang & Feldman, 2018). Furthermore, significant projections extend into the midbrain periaqueductal gray. Interestingly, in terms of forebrain efferent projections, these are notably sparse and primarily restricted to specific nuclei within the thalamus and hypothalamus, with minimal presence in areas like the cortex, basal ganglia, or other limbic regions, such as the amygdala or hippocampus (Yang & Feldman, 2018). While the connectivity of the preBötC with other respiratory nuclei in the ventral medulla and suprapontine nuclei emphasizes its role as a conductor of the respiratory rhythm and its' involvement in other orofacial behaviors, for this study, it is of particular interest the afferent and efferent connections between the preBötC and the pFL.

1.2 Expiratory Oscillator: Lateral parafacial area (pFL)

The discovery of pre-inspiratory/late-expiratory rhythmogenic neurons within the parafacial region (Onimaru & Homma, 2003) and their subsequent association with active expiration (de Britto & Moraes, 2017; Magalhães et al., 2021; Pagliardini et al., 2011) has sparked an enduring debate surrounding the characterization and functional disparities between chemosensitive neurons residing in the retrotrapezoid nucleus (RTN) and late expiratory neurons situated in the lateral parafacial area (pFL). Accumulated evidence suggests that phox2b-negative late-expiratory neurons observed in the pFL are distinguishable from phox2b-positive, chemosensitive RTN neurons found in the adult rat. Notably, these pFL neurons remain quiescent during rest but exhibit

rhythmic activity in response to heightened respiratory demands, driving active expiration by recruiting oblique abdominal (ABD) muscles (de Britto & Moraes, 2017; Huckstepp et al., 2015; Magalhães et al., 2021; Pagliardini et al., 2011).

Moreover, active expiration has been demonstrated to be inducible through various pharmacological manipulations, including the release from glycinergic and GABAergic inhibition, as well as via glutamatergic and cholinergic excitation (Boutin et al., 2017; Huckstepp et al., 2018; Pagliardini et al., 2011). Intriguingly, while it has been established that active expiration manifests during sleep in both adult and neonates (Andrews & Pagliardini, 2015; Saini et al., 2022; Saini & Pagliardini, 2017), the direct involvement of the pFL in this phenomenon has only recently begun to receive in-depth exploration (Pisanski et al., 2019). This newfound understanding emerged as a result of chemogenetic manipulations within the pFL during sleep, demonstrating its role in the generation of ABD recruitment during sleep, a topic that will be comprehensively discussed in Chapter 2.

1.2.1 Ventral and Lateral Parafacial Areas: two independent nuclei?

Since the discovery of the rhythmogenic properties in the region surrounding the facial nucleus, there has been an ongoing debate on whether the chemosensitive neurons in the retrotrapezoid nucleus (RTN) and the late expiratory neurons in the pFL are the same neuronal population of identical genetic origin, or partially overlapping distinct neuronal populations. Embryonic studies in mice identified the precursor of pFL neurons (embryonic parafacial, epF) as a unique population derived from the early growth response protein 2 transcription factor (Egr2) progenitors and expressing the transcription factor Phox2b and the neurokinin1 receptor (Thoby-Brisson et al., 2009). Rhythmogenic activity of these neurons, which were initially described as the parafacial respiratory group (pFRG), is present in late stages of embryonic development (Onimaru & Homma, 2003; Thoby-Brisson et al., 2009), progressively declines in the postnatal period (Oku et al., 2007) and disappears in adulthood, making the identification and characterization of these adult neurons at rest challenging (de Britto & Moraes, 2017; Pagliardini et al., 2011). Recently it has been more widely accepted to subdivide the RTN and pFRG areas into ventral and lateral parafacial areas respectively (pFV and pFL) (Huckstepp et al., 2015).

Late expiratory/pre-Inspiratory pFL neurons are sensitive to pH in P0-P2 in vitro preparations (Kawai et al., 2006; Onimaru et al., 2008). However, the pH responses were heterogeneous and allowed for the identification of distinct subpopulation of parafacial neurons: Phox2b$^+$ CO2 sensitive pre-Inspiratory neurons, Phox2b$^-$ CO2 insensitive pre-Inspiratory neurons intermingled with tonically active Phox2b$^+$ CO2 sensitive RTN neurons (Kawai et al., 2006; Onimaru et al., 2008).

In juvenile and adult rats, chemosensitive cells of the pFV have been characterized in detail: these cells are tonically activated by low pH, they express the transcription factor Phox2b in addition to glutamatergic markers (vesicular glutamate transporter 2), neuromedin B (Shi et al., 2021) and NK1R (Abbott et al., 2009; Mulkey et al., 2004; Stornetta et al., 2006). Functional and anatomical studies have localized these cells mostly around the ventral and medial edges of the facial nucleus (Huckstepp et al., 2015). In both juvenile and adult rats pFV neurons fire tonically in resting conditions, increase their firing rate with lowered blood pH (Mulkey et al., 2004; Stornetta et al., 2009) and acute inactivation of Phox2b expressing neurons in pFV silences chemosensitive cells, blunts responses to low pH and reduces both CO2-driven inspiratory and expiratory output (Abbott et al., 2011; Abbott et al., 2009; Huckstepp et al., 2015; Marina et al., 2010). On the contrary, phox2b negative late expiratory neurons of the pFL have been identified on the ventral and lateral edge of the facial nucleus of juvenile and adult rats: these neurons are silent in resting conditions and when activated by hypercapnia or chemical disinhibition, they become rhythmically active during late expiration, in phase with abdominal muscle activity (Abdala et al., 2009; de Britto & Moraes, 2017; Huckstepp et al., 2015; Huckstepp et al., 2016; Pagliardini et al., 2011). In adult rats, late expiratory neurons do not express the transcription factor Phox2b, the pH sensor TASK2 and GPR, but display NK1R immunoreactivity and are glutamatergic (de Britto & Moraes, 2017; Huckstepp et al., 2015; Pagliardini et al., 2011).

A clear genetic and physiological distinction between late expiratory pFL neurons and the ventral chemosensitive pFV neurons regions remains to be established, but additional evidence supporting distinct functionalities between these two regions include: 1) selective hyperpolarization of either pFV or pFL induces distinct effects on various respiratory variables in normoxia, and under hypoxic and hypercapnic challenges while producing a similar attenuation of the ABD recruitment elicited by hypercapnia and hypoxia (Huckstepp et al., 2015). 2) Injection of cholinomimetics in

the pFL induces a stronger ABD recruitment of expiratory activity and a stronger reduction in respiratory frequency compared to similar injections in the pFV (Boutin et al., 2017). 3) Although tested in slightly different experimental conditions, optostimulation of Phox2b cells in pFV (Abbott et al., 2011) or neurons located in the pFL (Pagliardini et al., 2011) induced distinct respiratory responses when tested in the inspiratory phase. When Phox2b pFV cells were stimulated, there were few effects on either respiratory rhythm, tidal volume, or phrenic nerve activity. In contrast, when pFL neurons were stimulated, there was complete inhibition of inspiratory effort and immediate recruitment of ABD activity followed by an inspiratory event. Differences in the respiratory responses and reset plots can be directly observed in Figures 6E and 7A in Abbott et al. 2011 and compared to Figures 7A and S1 in Pagliardini et al. 2011); 4) While pFL neurons in adult rats appear to be silent at rest and active during late expiration upon CO2 stimulation or disinhibition, activity of Phox2b-positive pFV chemosensitive neurons has consistently been reported to be tonic through the respiratory phase and not late expiratory modulated (Abdala et al., 2009; de Britto & Moraes, 2017; Marina et al., 2010; Pagliardini et al., 2011).

Based on this evidence, it is conceivable to propose that two distinct populations, located in close proximity to the facial nucleus have two important roles in respiratory control. In adult rodents, Phox2b positive, CO2 sensitive RTN neurons in pFV control respiratory responses to changes in blood pH and affect both inspiratory and expiratory activity, while pFRG neurons in the pFL act as a conditional oscillator activated directly or indirectly by chemosensitive areas during hypercapnia and are critical for the generation of active expiration. While epF and pFRG neurons in the pFL region express Phox2b in the embryonic and early postnatal period, current evidence suggest that Phox2b expression may be downregulated in adulthood, similar to other cell populations in the sympathetic system (Kang et al., 2007), and therefore they may have a similar genetic origin to RTN neurons in the pFV but differentiate into a unique neuronal population responsible for generation of active expiration in presence of high metabolic demands.

1.2.2 Relationship between inspiratory and expiratory oscillators across development

The relationship between inspiratory and expiratory oscillators has been studied across different developmental stages in rodents (for a concise summary, see Figure 9 in Huckstepp et al. 2016).

In the early stages of fetal development, rhythmic activity of the embryonic pFL (Thoby-Brisson et al. 2009) commences in mice just before the inception of preBötC activity (embryonic day E14) and later on it couples with and entrains the activity of the independently formed preBötC (Thoby-Brisson et al., 2009). With progression of fetal rodent development and within the first post-natal week, the preBötC assumes the primary role in driving rhythmic respiratory activity but remains functionally coupled with the pFL (Mellen et al., 2003; Oku et al., 2007; Pagliardini et al., 2003; Smith et al., 1991; Thoby-Brisson et al., 2005).

The two oscillators are differentially affected by opioids: while activity of preBötC neurons and its inspiratory output are depressed, the activity in the late expiratory/pre-inspiratory neurons of the pFL persists in the first postnatal week, pacing inspiratory rhythm and providing an essential input to drive expiratory motor output and respiration (Janczewski & Feldman, 2006; Janczewski et al., 2002; Mellen et al., 2003).

In juvenile and adult rats, the pFL is silent in resting conditions and acts as a conditional oscillator, recruited during periods of increased respiratory drive to increase tidal volume and ventilation (de Britto & Moraes, 2017; Huckstepp et al., 2015; Pagliardini et al., 2011). Interestingly, selective inhibition and stimulation of the preBötC and/or the pFL in adult rats, demonstrate that activation of the pFL induces expiratory motor output, but the pFL is unable to sustain its activity when the preBötC rhythmicity is persistently silenced (Huckstepp et al., 2016). These results suggest that in adult rats the pFL is unable to drive expiratory activity or a breathing rhythm in absence of input from the preBötC. However, since those experiments were performed under urethane anesthesia, it will be interesting to test the ability of the pFL to support ventilation in physiological and pathological conditions where simultaneous recordings of pFL and preBötC neuronal activity, inspiratory and expiratory motoneuron activity, and expiratory motor output can be performed without the confounding effects of anesthesia.

1.2.3 Active expiration and sleep in vivo

Studies investigating the interactions between respiratory oscillators and their corresponding motor outputs have been performed mostly in *in vitro* and *in situ* reduced preparations or in *in vivo* anesthetized rodents (Abdala et al., 2009; Iizuka, 2001, 2003; Janczewski & Feldman, 2006; Janczewski et al., 2002). Recent observations in unanesthetized conditions are beginning to

provide insight into the contribution of active expiration to ventilation across different species, developmental stages and behavioural states (Andrews & Pagliardini, 2015; Leirao et al., 2017; Saini & Pagliardini, 2017). The pattern of expiratory ABD activity across sleep/wake cycles in normocapnic conditions was initially described by Sherrey et al. in 1988 and further investigated in detail by our group (Andrews & Pagliardini, 2015). Expiratory activity occurs during both NREM and REM sleep (Andrews & Pagliardini, 2015; Sherrey et al., 1988), but it is more likely to occur after the irregular breathing (i.e. apneas and high respiratory variability) observed during REM sleep (Andrews & Pagliardini, 2015). Moreover, frequent expiratory ABD recruitment in REM sleep is associated with increased respiratory stability and improved ventilation (Figure 1.5; Andrews and Pagliardini 2015). Abdominal recruitment events during NREM sleep are less frequent than in REM sleep (21.4% in NREM as compared to 49% in REM epochs) and not associated with a significant change in respiratory frequency or respiratory variability (Andrews & Pagliardini, 2015). On the contrary, other studies have reported the absence of expiratory ADB recruitment during NREM sleep in normocapnia (Leirao et al., 2017). While factors like animal posture during sleep could differentially influence the strength of the signal recorded from oblique ABD muscles (Sherrey et al., 1988), differences in the reported occurrence of expiratory ABD activity during NREM sleep (Andrews & Pagliardini, 2015; Sherrey et al., 1988) vs (Leirao et al., 2017) could also be due to differences in the experimental procedures, such as the placement of EMG electrodes, the duration of the habituation period and recording sessions, or to differences with respect to analyses and identification of active expiration. While the precise involvement of the parafacial region (pFL) in the induction of abdominal (ABD) muscle activity during sleep under normocapnic conditions remains to be elucidated, recent findings, to be elaborated on in Chapter 2, propose a potential role for the pFL in the recruitment of active expiration during sleep (Pisanski et al., 2019). To gain deeper insights into the state-dependent activity of pFL neurons in adult rats, concurrent recording of unit activity from pFL neurons, ABD motoneurons, and respiratory motor output during natural sleep are required.

1.2.4 Active expiration throughout development

Because the functional relationship between inspiratory and expiratory oscillators changes so much during development, a natural question is whether the ABD activity observed in adult rats during sleep is also present during postnatal development. A recent study in behaving neonate and

juvenile rats under normocapnic conditions (from post-natal days 0 to 15: P0 to P15) indicates that expiratory ABD activity is recruited during both NREM and REM sleep throughout development (Saini & Pagliardini, 2017a). Similar to adult rats, ABD recruitment during REM sleep in post-natal rats was associated with an increase in tidal volume and minute ventilation, as well as a reduction in respiratory variability (Figure 1.6; Saini and Pagliardini, 2017). Moreover, while the rate of ABD recruitment during REM sleep remains stable across postnatal development and adulthood (Andrews & Pagliardini, 2015; Saini & Pagliardini, 2017a), ABD recruitment during NREM sleep varies during postnatal development: it is highest in neonates and gradually decreases to adult levels by P15 (Andrews & Pagliardini, 2015; Saini & Pagliardini, 2017). Whether these differences reflect developmental changes in networks controlling breathing, sleep or their interactions remains to be investigated. Furthermore, recent evidence suggests that ABD recruitment is not exclusive to rodent neonates but is also present during the postnatal period in humans (Saini et al., 2022). This marks the first study to report the occurrence of active expiration in human children. Analogous to observations in rodents, ABD recruitment in human neonates occurs during both NREM and REM sleep and is associated with regular breathing as well as respiratory irregularities (Saini et al., 2022).

Experiments in medullary slices and in *en bloc* preparations of neonatal rodents indicate that both the preBötC and pFL oscillators are active and coupled during the first days after birth (Mellen et al., 2003; Oku et al., 2007; Pagliardini et al., 2003; Smith et al., 1991; Thoby-Brisson et al., 2005). This suggests that the motor output during inspiration and expiration would have an expected coupling ratio of one-to-one (inspiration always followed by expiration) during the first hours and days after birth (P0-P1). Interestingly, expiratory ABD activity during sleep in behaving neonates is not constantly present and coupled with the inspiratory intercostal (INT) muscle activity (Saini & Pagliardini, 2017a) as would be expected if pFRG was continuously active and driving expiratory ABD activity. Possible explanations for this intriguing results, are: i) key modulatory networks are absent in the *in vitro* preparation compared to the behaving animals; this would suggest that although the pFL is rhythmic in slice and *en bloc* preparations of neonates, it may be silent in the behaving animals, becoming sporadically active during sleep; ii) the pFL rhythmic activity observed in *in vitro* preparations of neonates is maintained in behaving animals, but its drive remains subthreshold and does not generate an expiratory motor output by itself. This would mean that either the pFL itself, or the expiratory premotor and motor neurons would require some

type of additional excitatory drive to generate expiratory muscle activity (Huckstepp et al,. 2016). The simultaneous measurement of pFL unit activity and motor output in behaving neonates, although challenging, would be enlightening to better understand the coupling of the preBötC and pFL in vivo in perinatal rodents, and the contribution of the pFL activity to ventilation in different arousal and sleep states throughout development.

1.2.5 Increased respiratory drive

Hypercapnia potentiates active expiration in every state of arousal and sleep in adult rats; however, it is not continuously recruited throughout the entire CO_2 exposure period (Leirao et al., 2017; Sherrey et al., 1988). Moreover, during hypercapnia ABD recruitment is more frequent during NREM sleep than during quiet wakefulness (REM stage was not analyzed), and it was associated with enhanced ventilation (Leirao et al., 2017). All together, these results suggest that recruitment of ABD muscles by chemosensory or vigilance drives could be mediated through different neuromodulatory systems (Leirao et al., 2017; O'Halloran, 2017).

Active expiration can also be initiated under hypoxic conditions (Mendoca-Juniro et al., 2021; Zoccal & Machado, 2010). Malheiros-Lima and colleagues (2017) propose the involvement of a catecholaminergic mechanism in generating active expiration during hypoxia. Their research shows that selective ablation of catecholaminergic C1 neurons in the rostral ventrolateral medulla (RVLM) reduces the late-expiratory flow observed during hypoxia in non-anesthetized rats (Malheiros-Lima et al., 2017) and entirely eliminates late-E ABD activation associated with peripheral chemoreceptor stimulation, in anesthetized rats (Malheiros-Lima et al., 2020). Furthermore, additional evidence suggests the presence of direct catecholaminergic and glutamatergic projections from C1 neurons to the lateral parafacial region (pFL), hinting at a potential glutamatergic pathway from C1 neurons to the pFL, which may contribute to the recruitment of active expiration during hypoxia (Malheiros-Lima et al., 2020).

1.2.6 Induction of Active Expiration through pharmacology

In adult anesthetized rats, active expiration is tonically supressed via active synaptic inhibition (Pagliardini et al., 2011). Pharmacological disinhibition of the pFL allows silent pFL neurons to become rhythmically active during late expiration, driving the recruitment of expiratory ABD

activity (Figure 1.7; Pagliardini et al. 2011). A similar mechanism may be responsible for the activation of non-chemosensitive late expiratory pFL neurons in hypercapnia-evoked active expiration (de Britto & Moraes, 2017). While blocking glutamatergic excitation has no effect on hypercapnia-induced active expiration, activation of GABAergic and glycinergic receptors in the pFL eliminates hypercapnia-induced active expiration and silences non-chemosensitive late-expiratory neurons in this area (de Britto & Moraes, 2017). Furthermore, recent studies on inhibitory post-synaptic potentials of late-E pFL neurons (Magalhães et al., 2021) indicates that GABAergic inhibition occurs during the inspiratory phase and glycinergic inhibition occurs throughout the entire respiratory cycle in baseline conditions, whereas hypercapnia increases GABAergic phasic inhibition but reduces glycinergic inhibition in the late-E phase of the respiratory cycle. Altogether, these data suggest that disinhibition of the pFL, may be important in the initiation of hypercapnia-induced active expiration (de Britto & Moraes, 2017). The source of the inhibition to pFL neurons under resting conditions is currently unknown. It could come directly or indirectly from chemosensitive areas of the brain like the retrotrapezoid nucleus (also referred to as pFV), the nucleus of the solitary tract, the locus coeruleus or the medullary raphe (de Britto & Moraes, 2017; Nattie & Li, 2012; Pagliardini et al., 2011). The Kölliker-Fuse is strongly implicated in the generation of hypercapnia-elicited active expiration through disinhibition of the pFL (Barnett et al., 2018; Jenkin et al., 2017). However, it is possible that the modulatory effects of Kölliker-Fuse on the pFL are mediated through inhibitory cells located in the Bötzinger or preBötzinger areas (Barnett et al., 2018). More studies on the connectivity between the pFL and the rest of the respiratory network, and the phenotype of pFL neurons are necessary to elucidate these mechanisms.

It was also recently demonstrated that local inhibition of acetylcholinesterases or the application of the cholinomimetic carbachol in the pFL induces active expiration (Figure 1.8) (Boutin et al., 2017) suggesting that the pFL is also under cholinergic modulation. The source of cholinergic input to the pFL and its contribution to the recruitment of active expiration in different physiological scenarios is still unknown. Cholinergic mechanisms could play an important role for the generation of active expiration during sleep (Andrews & Pagliardini, 2015; Saini & Pagliardini, 2017; Sherrey et al., 1988). If so, the pedunculopontine tegmental (PPT) and the laterodorsal tegmental (LDT) nuclei would be likely candidates since they send cholinergic projections to the reticular formation and are important for the generation and maintenance of REM sleep (Jones,

1990; Van Dort et al., 2015; Woolf & Butcher, 1989). However, a recent study mapping afferent projections to the pFL found no cholinergic projections from these areas (Biancardi et al., 2020). This recent evidence has raised questions about the role of cholinergic modulation in the ABD activity observed during sleep, casting uncertainty on its involvement in controlling active expiration during sleep and paving the way for further investigation into the potential impact of cholinergic activation on the recruitment of ABD activity in different physiological contexts.

Recent research has accumulated a growing body of evidence regarding the role of glutamate in inducing active expiration (Korsak et al., 2018; Malheiros-Lima et al., 2020; Zoccal et al., 2018). Studies have shown that bilateral injections of glutamate or the glutamatergic agonist AMPA into the parafacial region (pFL) of anesthetized rats and in situ preparations, induce active expiration (Huckstepp et al., 2018; Malheiros-Lima et al., 2020). This effect is characterized by an increase in late-E abdominal (ABD) muscle activity, enhanced diaphragmatic (DIA) amplitude, and a simultaneous reduction in respiratory frequency (Huckstepp et al., 2018; Malheiros-Lima et al., 2020). Interestingly, while glutamate injections appear to engage ABD muscles, blocking glutamatergic transmission in the lateral parafacial region of *in situ* preparations while diminishing the intensity of ABD activity does not entirely suppress active expiration triggered by hypercapnia (Britto & Moraes, 2017; Zoccal et al., 2018). However, contrasting findings exist, demonstrating that the injection of kynurenic acid, a glutamate receptor antagonist, into the pFL of anesthetized, vagotomized, and artificially ventilated rats, entirely abolishes active expiration during hypercapnia (Malheiros-Lima et al., 2020). These discrepancies may stem from the different preparations employed (*in situ* vs. *in vivo*) or the age of the animals used (juveniles for in situ experiments vs. adults for anesthetized in vivo preparations). Moreover, blocking of glutamatergic transmission in the pFL of anesthetized rats, eliminated active expiration elicited by hypoxia (Malheiros-Lima et al., 2020). This evidence, coupled with the observation that the removal of C1 neurons projecting to the pFL abolishes the ABD recruitment typically seen during peripheral chemoreceptor activation (Malheiros-Lima et al., 2020; Malheiros-Lima et al., 2017), implies the existence of a potential mechanism for pFL activation during hypoxia, likely involving glutamatergic C1 neurons.

1.3 Sleep

Sleep, a fundamental physiological phenomenon observed in both humans and rodents, manifests as a reversible state of unconsciousness, associated with species-specific behavioral characteristics (Carskadon & Dement, 2005; Chokroverty, 2010). Sleep is divided into two distinct phases: non-rapid eye movement (NREM) and rapid eye movement (REM), each delineated by unique electroencephalographic patterns and associated muscle dynamics. During NREM sleep, skeletal muscle tone is sustained, in contrast to REM sleep, wherein a comprehensive atonia of skeletal musculature prevails, except for ocular muscles responsible for rapid eye movements (Benington & Heller, 1994; Benington et al., 1994; Carskadon & Dement, 2005; Chokroverty, 2010). The vulnerability of the respiratory system is most pronounced during sleep, when the tonic excitation within the ventral medulla, normally observed during wakefulness, decreases (Orem et al., 2000). The source of this tonic excitation has engendered debate, attributing it to either the reticular activating system or serotoninergic Dorsal Raphe neurons (Al-Zubaidy et al., 1996; Arita & Ochiishi, 1991; Kubin et al., 1992; Lindsay & Feldman, 1993; McGinty et al., 1977; Orem, 1980; Orem & Lydic, 1978; Orem et al., 1985; Sakai & Crochet, 2001). Upper airway musculature also experiences a reduction in tone during both NREM and REM sleep, which results in heightened airway resistance (Orem & Lydic, 1978). Additionally, ventilatory responses to alterations in carbon dioxide and oxygen levels are attenuated during sleep (Burke et al., 2015; Douglas et al., 1982; Phillipson et al., 1976). Recently, attention has been directed toward the phenomenon of active expiration during sleep in both rodents and humans, as an interesting research avenue with potential for clinical applications (Andrews & Pagliardini, 2015; Saini et al., 2022; Saini & Pagliardini, 2017).

1.3.1 Stages of sleep in humans and rodents

In both humans and rodents, sleep is characterized behaviorally as a reversible state of unconsciousness marked by immobility in a species-specific sleeping posture and an unresponsiveness to external stimuli (Carskadon & Dement, 2005; Chokroverty, 2010). From a physiological perspective, sleep is defined by the analysis of readings obtained through electroencephalography (EEG), electrooculography (EOG), and electromyography (EMG) in the case of humans (Carskadon & Dement, 2005; Chokroverty, 2010). In contrast, for rodents, sleep

is primarily defined based on EEG and EMG recordings (Mandile et al., 1996; Mendelson & Bergmann, 1999). Utilizing physiological measurements in adult humans and rodents, sleep can be categorized into two distinct phases: non-rapid eye movement (NREM) and rapid eye movement (REM) (Carskadon & Dement, 2005; Chokroverty, 2010; Mendelson & Bergmann, 1999). NREM sleep is commonly described by its synchronous EEG pattern, featuring characteristic waveforms such as sleep spindles, K-complexes, and high voltage slow delta waves (2-4 Hz) (Carskadon & Dement, 2005; Mendelson & Bergmann, 1999). However, it's essential to note that while NREM sleep can be further subdivided into four stages in humans, it is conventionally considered a single stage for rodents, as pertains to this research (Benington et al., 1994; Mendelson & Bergmann, 1999). During NREM sleep, skeletal muscle tone is retained (Benington et al., 1994; Carskadon & Dement, 2005; Chokroverty, 2010; Mendelson & Bergmann, 1999). Conversely, REM sleep is characterized by a complete atonia of skeletal muscles, with the exception of the ocular muscles responsible for generating the rapid eye movements characteristic of this stage (Benington et al., 1994; Carskadon & Dement, 2005; Chokroverty, 2010; Mendelson & Bergmann, 1999). Moreover, EEG activity during REM sleep is marked by fast theta waves (6-7 Hz) and can be subdivided into phasic and tonic stages (Benington et al., 1994; Carskadon & Dement, 2005; Chokroverty, 2010; Mendelson & Bergmann, 1999; Simor et al., 2020). Sleep cycles cyclically shift between NREM, REM, and wakefulness throughout the sleep period, and the duration of these cycles can vary between species (e.g., 90-110 minutes in adult humans versus 5-10 minutes in adult rodents), resulting in differences in the fragmentation of sleep (Benington et al., 1994; Chokroverty, 2010).

1.3.2 Breathing changes during sleep

The vulnerability of the respiratory system is most pronounced during normal sleep. When an individual is awake, the ventral medulla's respiratory system receives a continuous excitation, referred to as tonic excitation, which subsides when the person enters a state of sleep (Orem & Lydic, 1978). The source of this tonic excitation during wakefulness has been a subject of debate. Some researchers have suggested that it may be linked to the reticular activating system (Orem & Lydic, 1978; Orem et al., 2005), while others propose that serotoninergic Dorsal Raphe neurons play a role (Arita & Ochiishi, 1991; McGinty et al., 1977; Schmidt-Nowara et al., 1990). These neurons stimulate the respiratory nuclei and are most active during wakefulness, with their activity

diminishing during non-rapid eye movement (NREM) sleep and virtually ceasing during rapid eye movement (REM) sleep (Al-Zubaidy et al., 1996; Arita & Ochiishi, 1991; Kubin et al., 1992; Lindsay & Feldman, 1993; McGinty et al., 1977; Sakai & Crochet, 2001; Schmidt-Nowara et al., 1990). Muscle tone in the upper airway experiences a slight decrease during NREM sleep and a more substantial reduction, eventually disappearing, in REM sleep. This decrease in muscle tone results in an increased upper airway resistance (Orem & Lydic, 1978) and development of obstructive sleep apnea (OSA). Obstructive sleep apnea is one of several conditions that collectively make up the category of sleep-disordered breathing. Sleep-disordered breathing is characterized by interruptions in breathing or a decrease in breath volume, known as apneas and hypopneas, respectively, occurring five or more times per hour during sleep (Davis & O'Donnell, 2013). These disruptions in breathing can be attributed to the narrowing or collapse of the upper airway (referred to as an obstructive event), a decrease or cessation of respiratory motor activity (central), or a combination of both factors (Dempsey et al., 2010).

Furthermore, during NREM sleep, both hypercapnic and hypoxic ventilatory responses are moderately reduced, indicating that the body's ability to respond to elevated levels of carbon dioxide and reduced oxygen in the blood is dampened. This reduction is even more pronounced during REM sleep (Burke et al., 2015; Douglas et al., 1982; Phillipson et al., 1976). It has also been reported that several pathological conditions can lead to sleep-related hypoventilation, which is more severe during NREM sleep (Böing & Randerath, 2015). Abdominal activity reminiscent of active expiration has been observed during sleep and associated with stabilization of breathing following respiratory disturbances in naturally sleeping healthy rodents and in anesthetized models of sleep (Andrews & Pagliardini, 2015; Pagliardini et al., 2013; Pagliardini et al., 2012). Interestingly, the role of active expiration during sleep has only started to receive some attention, with recent descriptive experiments being done in sleeping neonate rodents and humans (Saini et al., 2022; Saini & Pagliardini, 2017). These studies pave the way for exploring the potential therapeutic application of active expiration to stabilize breathing in cases of pathological conditions.

1.4 Research Aims and Objectives

This research aims to fill the gaps in existing literature concerning the role of active expiration in conditions of an impaired inspiratory drive in naturally behaving animals, the contribution of the lateral parafacial area (pFL) in generating active expiration during sleep, as well as to pinpoint the specific pFL area with the most pronounced respiratory effects. The following objectives and goals have been delineated to direct this research:

I.   Understand the role of the pFL in the generation of active expiration during sleep.

To achieve this aim, our objectives are to:

   i.   Transfect pFL cells with a pan-neuronal vector carrying either DREADD-Gi or DREADD-Gq, allowing us to respectively hyperpolarize or depolarize the transfected cells through the injection of the designer ligand CNO.
   ii.   Quantify the occurrences of ABD recruitment events during sleep in freely behaving unanesthetized rats, both before and after chemogenetic modulation of the pFL.
   iii.   Characterize respiratory measures preceding chemogenetic modulation and following inhibition and excitation of the pFL during sleep.

II.   Identify the rostro-caudal distribution of the pFL along the ventral medulla.

To achieve this, our objectives are to:

   i.   Inject bicuculline at various coordinates along the rostro-caudal portion of the ventral medulla to disinhibit the pFL.

   ii.   Identify injection sites and categorize experimental animals based on the proximity of the injections.

   ii.   Evaluate the intensity of ABD response elicited, alongside other respiratory measures, to pinpoint the injection site most effective in generating active expiration.

III.   Determine the contribution of active expiration during sleep in conditions of an impaired inspiratory drive.

For this purpose, our objectives are to:

i.   Transfect preBötC cells with a pan-neuronal viral vector carrying Kappa-Opioid-Receptor-DREADD (KORD) to hyperpolarize transfected cells using Salvinorin B (SalB), thereby inducing impaired inspiratory drive.

ii.   Assess the occurrence of respiratory disturbances following KORD ligand injection in freely behaving unanesthetized rats during their sleep period.

iii.   Characterize ABD recruitment occurrence in both healthy (DMSO) and impaired inspiratory drive (SalB) conditions in unanesthetized freely behaving rats during their sleep.

1.5 Figures and Figure Captions
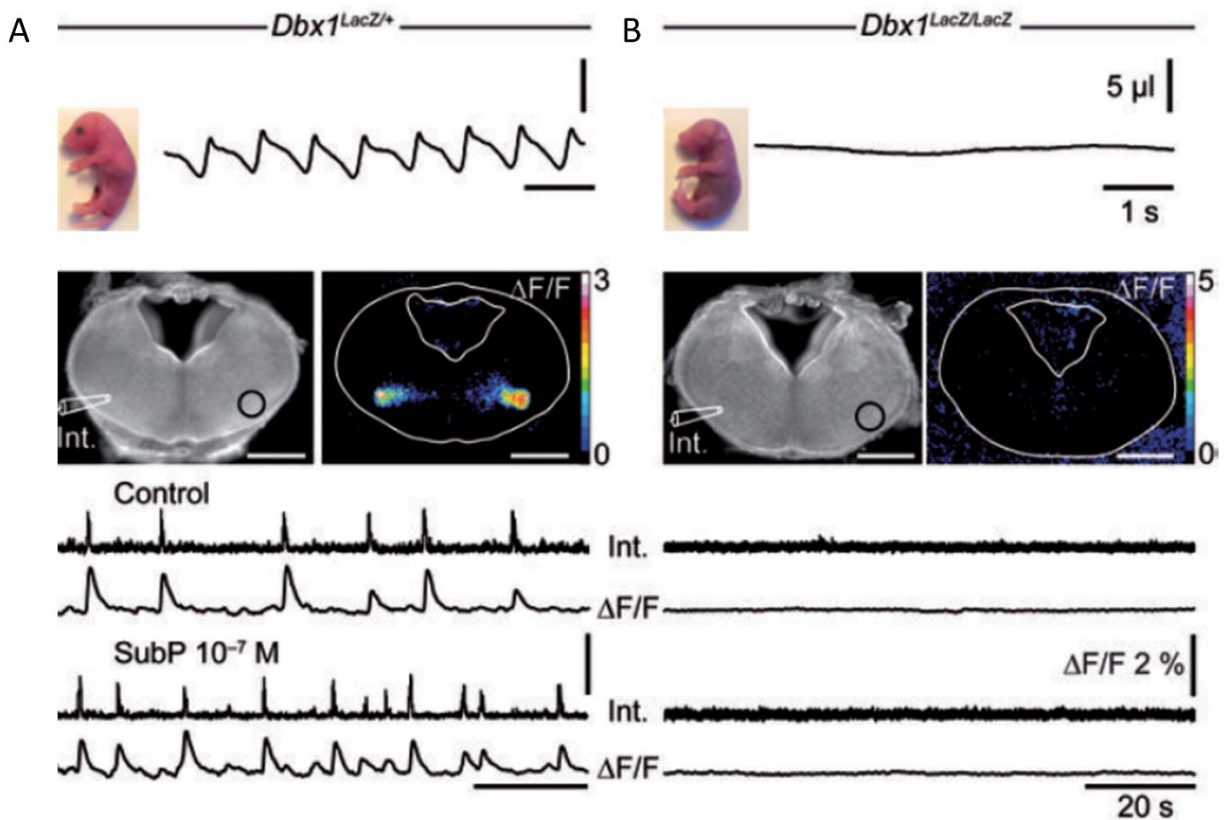
Figure 1.1 Disrupted breathing and rhythm generation in the preBötC of Dbx1 null mice

Plethysmographic recordings of E 18.5 embryos and calcium imaging fluorescence ($\Delta F/F$) in slice preparations of CTRL (Dbx1LacZ/$^+$) (**A**) and Dbx1 null (Dbx1LacZ/LacZ) mice (**B**) reveal the absence of respiratory rhythm generation in the Dbx1 LacZ/LacZ mice (**B**) which did not show any sign of ventilation an eventually died cyanotic. Modified from Bouvier, J., Thoby-Brisson, M., Renier, N. et al. Hindbrain interneurons and axon guidance signaling critical for breathing. *Nat Neurosci* 13, 1066–1074 (2010). https://doi.org/10.1038/nn.2622 with permission from *Nature Neuroscience.*
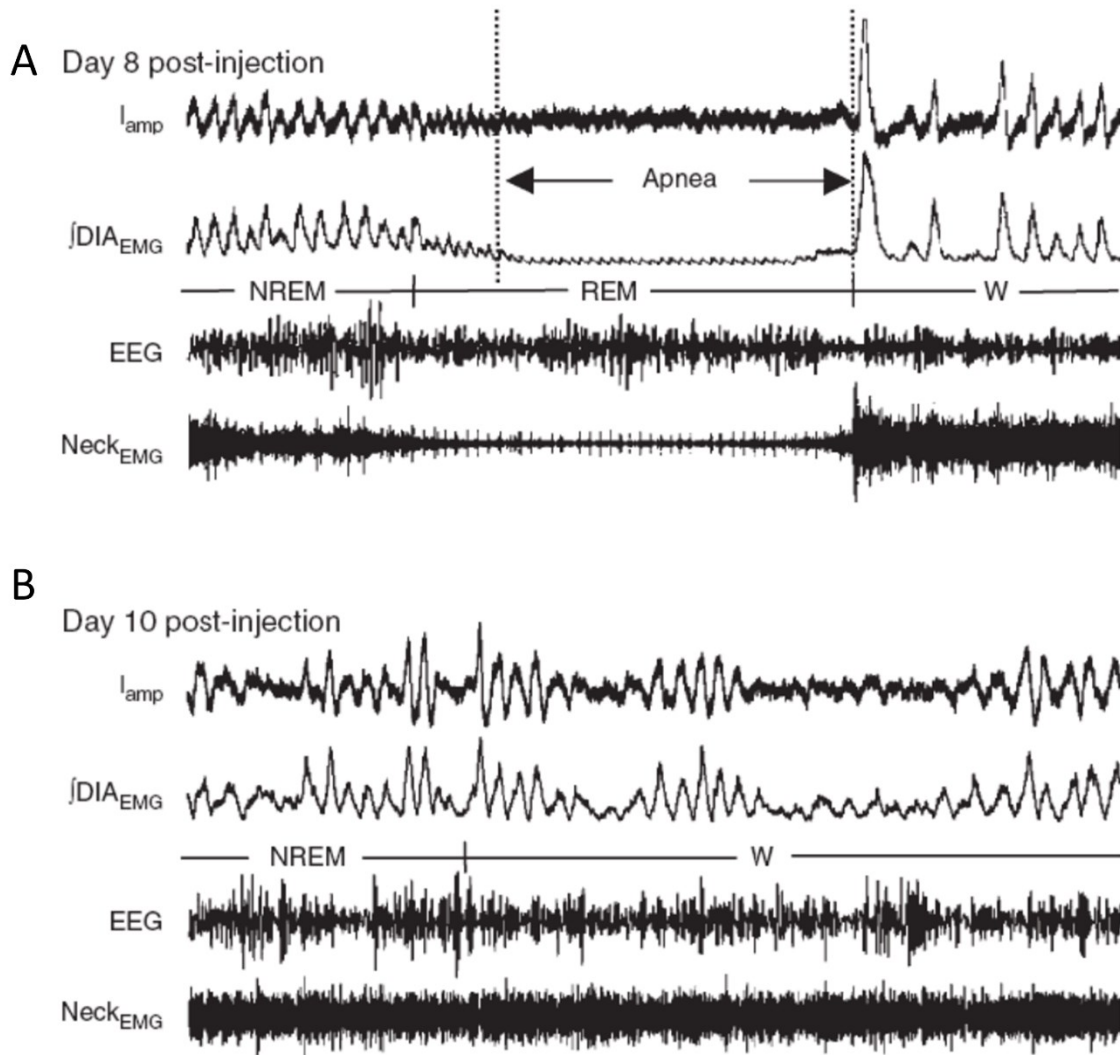
Figure 1.2 Slow ablation of preBötC NK1R+ neurons disrupts breathing during sleep and induces ataxic breathing in awake rats

A: Respiratory disruptions (i.e. apneas and hypopneas) during sleep increase in number and duration after bilateral injections of substance P conjugated to saporin in the preBötC. Eventually, injected rats develop ataxic breathing during wakefulness (**B**). ∫DIAEMG: integrated diaphragm EMG. Neck$_{EMG}$: dorsal neck EMG. EEG: electroencephalogram. Modified from McKay, L., Janczewski, W. & Feldman, J. Sleep-disordered breathing after targeted ablation of preBötzinger complex neurons. *Nat Neurosci* 8, 1142–1144 (2005). https://doi.org/10.1038/nn1517 with permission from *Nature Neuroscience.*
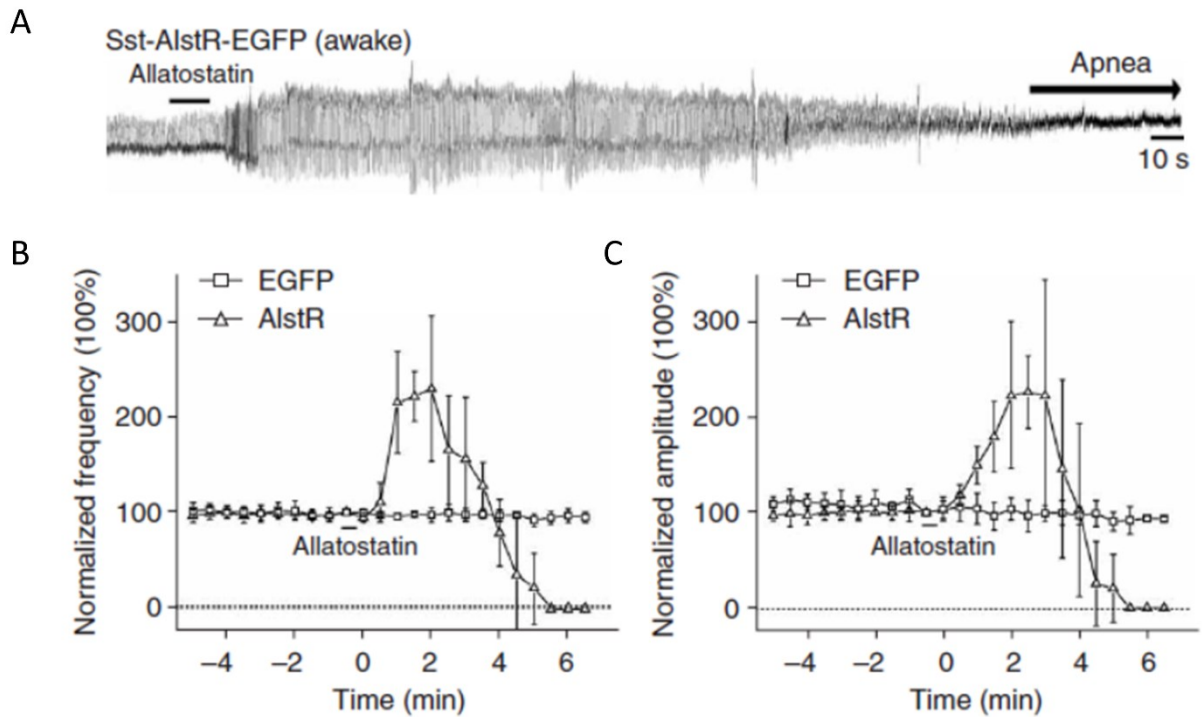
Figure 1.3 Role of SST+ neurons in the respiratory rhythmogenesis and pattern generation

A: Hyperpolarization of AlstR-expressing preBötC SST-neurons produces long lasting apneas. Silencing of SST+ cells affects both, rhythmogenesis and pattern generation (**B-C**) compared to the control (EGFP). Modified from Tan, W., Janczewski, W., Yang, P. et al. Silencing preBötzinger Complex somatostatin-expressing neurons induces persistent apnea in awake rat. *Nat Neurosci* 11, 538–540 (2008). https://doi.org/10.1038/nn.2104 with permission from *Nature Neurosciences*
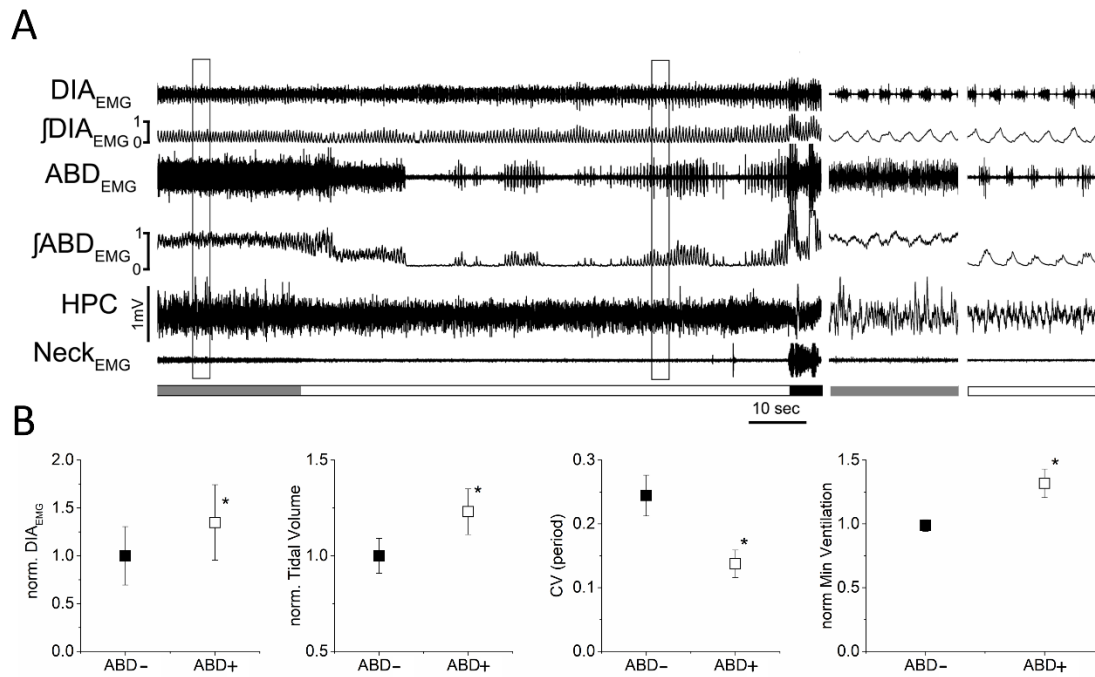
Figure 1.4 Abdominal recruitment observed during REM sleep in adult normocapnic rats is associated with stabilization of breathing

A: Abdominal muscle recruitment during transition from NREM to REM sleep. Long traces recording of diaphragm (DIA_{EMG}) and abdominal (ABD_{EMG}) muscles, their integrated EMG activity, hippocampal activity (HPC), and neck EMG activity in NREM (gray bar) and REM (white bar) epochs in which ABD muscle activity is recruited. Details of EMG and EEG traces during NREM and REM epochs are displayed in panels on the right. Schematic blocks at the bottom of the traces indicate time spent in NREM (grey), REM (white), and wakefulness (black). **B**: ABD recruitment within REM epochs significantly improves breathing. Plots display a comparison of the peak DIA_{EMG}, tidal volume, coefficient of variation of the respiratory period (CV) and minute ventilation before (ABD-) and during (ABD+) the occurrence of ABD recruitment within REM epochs. Figure modified from Andrews, C. G., and S. Pagliardini. 2015. 'Expiratory activation of abdominal muscle is associated with improved respiratory stability and an increase in minute ventilation in REM epochs of adult rats', *J Appl Physiol* (1985), 119: 968-74 with permission from *Journal of Applied Physiology*.
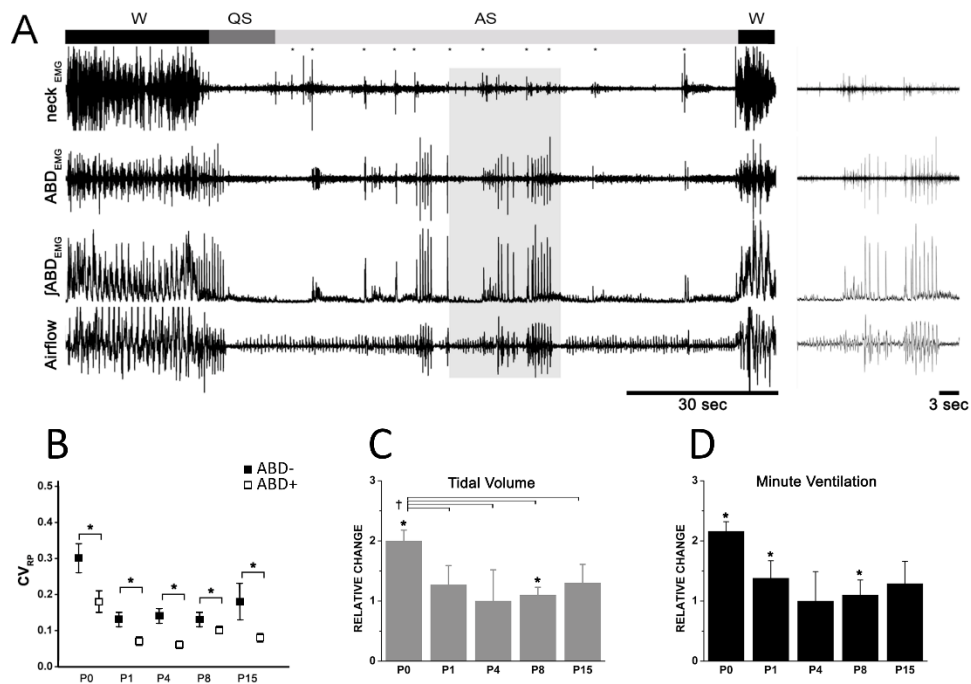
Figure 1.5 The effects of abdominal recruitment during REM or active sleep (AS) in normocapnic neonatal rats varies throughout development

(A) Abdominal muscle recruitment during transition from wakefulness (W) to quiet sleep (QS, the precursor of NREM sleep in infants) to active sleep (AS, the precursor of REM sleep in infants) in a P0 rat. Long traces recording of abdominal (ABD_{EMG}) muscles, its integrated EMG activity, neck EMG activity and whole-body plethysmograph traces during a AS (light gray bar) epoch in which ABD muscle activity is recruited. Abdominal activity is recruited during AS, most frequently following a twitch event (indicated by *). Details of traces during AS in the grey box are displayed in the right panel. Schematic blocks at the top of the traces indicate time spent in wakefulness (W, black), QS (dark grey) and AS (light gray). (B-D) ABD recruitment within AS epochs significantly improves breathing across different age groups. (B) Comparison of the coefficient of variation (CV) of the respiratory period before (ABD-) and during (ABD+) ABD recruitment within AS sleep epochs across different ages (P0-P15) shows a significant decrease for all age groups. Relative measurements of tidal volume (C) and minute ventilation (D) indicate that there is an overall trend for tidal volume to increase with the onset of recruitment (ABD+) but

this change is significant only in P0 and P8 rats, whereas minute ventilation increased with ABD recruitment at all age groups except in P4 and P15 rats. Figure modified from Saini, J. K., and S. Pagliardini. 2017. 'Breathing During Sleep in the Postnatal Period of Rats: The Contribution of Active Expiration', *Sleep*, 40 with permission from *Sleep*.
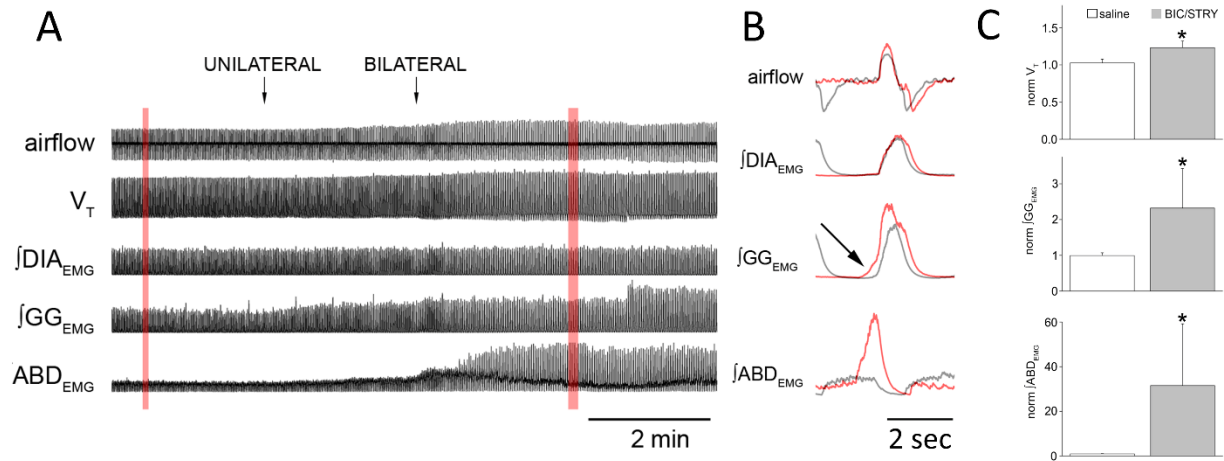
Figure 1.6 Disinhibition of pFRG induces active expiration with the recruitment of ABD muscles

A: Response to unilateral and bilateral application of (bicuculine and strychnine) BIC/STRY (50μM; 200 nl) in pFRG. The airflow, integral of abdominal (ABD_{EMG}), diaphragm (DIA_{EMG}) and genioglossus (GG_{EMG}) traces in red boxes are expanded and superimposed in (**B**) before (black) and after (red) BIC/STRY application. The arrow in B indicates effect of BIC/STRY on GG_{EMG} onset. **C**: Plots display comparisons of the tidal volume (VT), peak GG_{EMG}, and DIA_{EMG} amplitude in control (white bars) and after the injection of BIC/STRY (gray bars). Figure modified from Pagliardini, S., W. A. Janczewski, W. Tan, C. T. Dickson, K. Deisseroth, and J. L. Feldman. 2011. 'Active expiration induced by excitation of ventral medulla in adult anesthetized rats', *J Neurosci*, 31: 2895-905 with permission from *Journal of Neurosciences*.
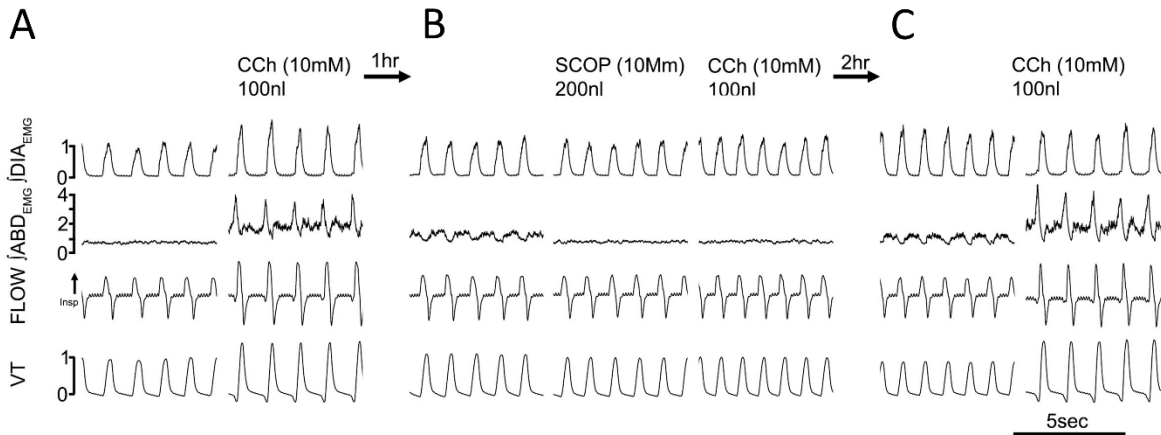
Figure 1.7 Active expiration is induced by cholinergic modulation of pFRG

Traces show details of the airflow, tidal volume (VT), and the integrals of diaphragm (DIA_{EMG}) and abdominal (ABD_{EMG}) muscle activity. **A**: Injection of the cholinomimetic carbachol (CCh) in pFRG induces active expiration and increases peak DIAEMG amplitude and VT. **B**: The injection of the muscarinic antagonist scopolamine (SCOP) in pFRG blocks the effects of CCh injection in pFRG. **C**: After washout from SCOP application, the effects of CCh injection in pFRG are recovered. Figure modified from Boutin, R. C., Z. Alsahafi, and S. Pagliardini. 2017. 'Cholinergic modulation of the parafacial respiratory group', *J Physiol,* 595: 1377-92 with permission from *Journal of Physiology*.

Chapter 2.   Chemogenetic modulation of the parafacial respiratory group influences the recruitment of abdominal activity during REM sleep

2.1 Introduction

Breathing requires the synchronization of a complex motor program to control gas exchange and adequately respond to various physiological and environmental conditions. The central pattern generator that orchestrates the respiratory rhythm lies in the medulla and is hypothesized to be composed by at least two coupled oscillators (Del Negro et al., 2018; Pisanski & Pagliardini, 2018). The preBötzinger complex (preBötC) is essential for respiratory rhythmogenesis through contraction of inspiratory muscles (Gray et al., 2001; Smith et al., 1991; Tan et al., 2008; Wang et al., 2014). The parafacial respiratory group (pFRG), silent in resting conditions, is recruited during periods of increased respiratory demand and generates active expiration through contraction of abdominal (ABD) muscles (de Britto & Moraes, 2017; Huckstepp et al., 2015; Pagliardini et al., 2011; Pisanski & Pagliardini, 2018). Recently, the existence of a third generator, the post-inspiratory complex (PiCo), has been proposed to regulate respiratory braking during post-inspiration (Anderson et al., 2016; Del Negro et al., 2018).

Rhythmic activity of neurons in the parafacial area was initially described in brainstem-spinal cord preparations of newborn rats (Arata et al., 1990; Onimaru et al., 1987; Onimaru & Homma, 1992). Parafacial neuronal oscillations commence during embryonic development before preBötC activity inception (Thoby-Brisson et al., 2009) and eventually become silent by adulthood (de Britto & Moraes, 2017; Pagliardini et al., 2011). Mounting evidence obtained in anesthetized adult and juvenile rats highlights the dependence on pFRG late-expiratory activity for the recruitment of ABD muscles during active expiration (Boutin et al., 2017; de Britto & Moraes, 2017; Huckstepp et al., 2015; Huckstepp et al., 2016; Pagliardini et al., 2011). The convergence of several modulatory mechanisms into the parafacial area (e.g. GABAergic, Glycinergic, Cholinergic and Glutamatergic inputs) suggests that pFRG activation and the generation of active expiration throughout different physiological conditions may be more complex than previously thought, depending not only on central and peripheral chemosensitive inputs but also on developmental stage and vigilance state (Andrews & Pagliardini, 2015; de Britto & Moraes, 2017; Huckstepp et al., 2018; Leirao et al., 2017; Pagliardini et al., 2011; Saini & Pagliardini, 2017).

In recent years, attention has been drawn to the functional implications of expiratory activity observed in sleeping healthy rodents. While the occurrence of ABD recruitment during REM sleep seems to be consistent, occurring throughout postnatal development and into adulthood, the ABD recruitment during NREM is present at a higher rate during the first days of postnatal development and gradually decreases until it becomes almost non-existent by adulthood (Andrews & Pagliardini, 2015; Leirao et al., 2017; Saini & Pagliardini, 2017; Sherrey et al., 1988). Interestingly, the occurrence of ABD muscle recruitment during both REM and NREM sleep across development, was preceded by periods displaying higher respiratory disturbances (i.e. apneas and hypopneas) and breathing variability (Andrews & Pagliardini, 2015; Saini & Pagliardini, 2017). Moreover, the recruitment of ABD muscles during REM sleep was associated with increased tidal volume and reduced breathing variability, whereas ventilation was not affected during NREM sleep (Andrews & Pagliardini, 2015; Saini & Pagliardini, 2017). The urethane-anesthetized preparation has been proposed as a model of natural sleep (Clement et al., 2008; Pagliardini et al., 2013; Pagliardini et al., 2013b; Pagliardini et al., 2012). In this model, despite absence of respiratory disturbances, ABD recruitment can be occasionally observed during activated (REM-like) epochs, but not during inactivated (NREM-like) states (Pagliardini et al., 2012). This evidence suggests that factors like respiratory variability and brain states may affect the occurrence of ABD recruitment during both natural sleep and urethane anesthesia. However, the role played by the pFRG in the generation of these events is still to be determined. To investigate the role of pFRG in the generation of ABD recruitment across sleep states we used a chemogenetic approach to manipulate pFRG activity and evaluated ABD occurrence during sleep. Our results suggest that pFRG modulates the occurrence, strength and prevalence of expiratory ABD activity, specifically during REM sleep.

2.2 Methods

2.2.1 Ethical Approval

Experimental procedures were approved by the Animal Care and Use Committee (ACUC) of the University of Alberta (AUP#461) according to the guidelines defined by the Canadian Council of Animal Care.

2.2.2 Viral Injections into the pFRG

To test the hypothesis that pFRG activation underlies the occurrence of ABD recruitment during sleep, we transfected pFRG neurons with a DREADD (i.e. Designer Receptors Exclusively Activated by Designer Drugs) adeno-associated virus expressing either an inactivating G_i protein-coupled receptor driven by the synapsin promoter (AAV2/2, hSyn-HA-hM4D(G_i)-IRES-mCitrine; n=7; UNC Vector Core, NC, USA) or a stimulatory G_q protein-coupled receptor (AAV2/2, hSyn-HA-hM3D(G_q)-IRES-mCitrine; n=8; UNC Vector Core, NC, USA) (Rogan & Roth, 2011). An additional cohort of rats (n=6) was transfected with viruses expressing Cre-eYFP only (AAV2/2-hSyn-IRES-Cre-eYFP; UNC Vector Core, NC, USA) to assess the possibility of non-specific effects associated with viral expression, and the use of the DREADD receptors ligand clozapine-N-oxide, (CNO) or its metabolite clozapine (Gomez et al., 2017; Mahler & Aston-Jones, 2018; D. F. Manvich et al., 2018).

Sprague Dawley adult male rats (250-300 g) were anesthetized via intraperitoneal injection of ketamine (90 mg/kg) and xylazine (10 mg/kg) and positioned prone on a stereotaxic frame. The incision area was trimmed, aseptically cleaned, and local anesthetic was applied (Bupivacaine 0.25% solution). Access to the medullary region was obtained through the partial removal of the occipital bone. Bregma was positioned 5 mm below lambda and viruses were pressure injected bilaterally into the pFRG (1.8 mm rostral, 2.5 mm lateral and 3.4 mm ventral to the obex) through a sharp glass micropipette (30 µm tip diameter) at a rate of 100 nL/min (volume injected was 200-300 nL per side). Following injections, the micropipette was left in place for 5 min to avoid backflow of the virus along the track. Incisions were sutured closed, rats were provided with oral analgesics (Metacam, 2 mg/kg) and monitored for recovery during 5 days with food and water *ad libitum*.

2.2.3 Chronic instrumentation

Three weeks after viral injections rats were instrumented with EEG and EMG electrodes according to previously published protocols (Andrews & Pagliardini, 2015; Pagliardini et al., 2012). Rats were anesthetized with ketamine/xylazine and bipolar multistranded PFA-insulated stainless-steel EMG electrodes (Cooner wire, CA, USA) were inserted into the oblique abdominal (ABD), diaphragm (DIA) and neck muscles. The wires were then tunneled under the skin and attached to

an electrical socket (Ginder scientific, ON, Canada) placed between the shoulder blades. Subsequently, rats were positioned prone on a stereotaxic frame with bregma and lambda at the same level. Bipolar, multistranded PFA-insulated stainless-steel EEG wires (AM-System, WA, USA) were implanted in the neocortex (nCTX) and hippocampus (HPC) according to the following coordinates (in mm) relative to bregma: for nCTX: rostro-caudal (RC), +2.5; mediolateral (ML), +1.2; dorsoventral (DV), -1.5 to -2.0; for HPC: RC, -3.3; ML, -2.4; DV, -2.5 to -3.0 mm. The distance between the two ends of the wires was kept at ~1 mm for optimal recordings. Additional wires to be used as surface EEG and ground were soldered to jeweler's screws and positioned in the parietal/frontal bones and occipital bone, respectively. All electrodes were fixed to the skull with dental acrylic and wires were then tunneled under the skin and attached to a second electrical socket positioned on the neck. Rats were monitored postoperatively and provided with oral analgesics (Meloxicam, 2 mg/kg) for 5 days thereafter.

2.2.4 Recording procedures

One week after implantation rats were accommodated to a whole-body plethysmograph (Buxco Respiratory Products, DSI, USA) for 5hrs on three consecutive days with constant airflow delivered (1.5 litres/min). On days four and five, signals of implanted EEG and EMG were recorded during the rats' natural sleep period from 12 to 5 PM after systemic (IP) injection of either vehicle (CTRL, 0.9% sterile saline + 0.02% D-methyl sulfate on day 4) or clozapine-N-Oxide (CNO dosage of 3 mg/kg of a 0.3 mg/ml solution, day 5). Data from EEG and EMG activity was sampled at 1 kHz and acquired using PowerLab (AD Instruments, CO, USA). HPC and nCTX signals were amplified at x1000 gain and filtered between 0.1 and 500 Hz (model P511, Grass Technologies, USA), whereas EMG activity was amplified at x10000 and filtered between 100 and 500 Hz (model 1700 A-M Systems, USA).

2.2.5 Histology

At the end of the *in vivo* recordings, rats were anesthetized with an IP injection of urethane (1.7 mg/kg) and transcardially perfused with saline 0.9 % followed by 4% paraformaldehyde (PFA) in phosphate buffer (PB). Brains were collected, post-fixed in 4% PFA overnight and sectioned (50 µm) in a vibratome (model VT1000S, Leica Mycrosystems, USA) for immunodetection of the viral reporter proteins and specific neuronal markers. All immunostaining procedures were

performed at room temperature. Free floating sections were incubated for 1hr with 0.3% Triton X-100 and 10% normal donkey serum (NDS) in saline PB (PBS) to increase membrane permeability to antibodies and reduce non-specific binding. Following blocking, sections were incubated overnight with primary antibodies diluted in a solution containing PBS, 1% NDS and 0.3% Triton X-100. Primary antibodies used were as follows: anti-hemagglutinin (HA; rabbit; 1:800; Cell Signaling Technologies, USA), anti-green fluorescent protein (GFP; chicken; 1:800; Aves Labs Inc., USA), anti-choline acetyl transferase (ChAT; goat; 1:800; EMD Millipore, ON, Canada) anti-neuronal nuclei (NeuN ;mouse; 1:500; EMD Millipore). The following day, sections were washed three times in PBS and incubated with specific secondary antibodies (1:200; Cy2-donkey anti-rabbit; Cy3-donkey anti-goat; Cy5-donkey anti mouse; Cy2-donkey anti-chicken; Jackson Immuno Research, USA) diluted in PBS and 1% NDS for 2 hours. Subsequently, sections were washed with PBS three times, mounted and coverslipped with Fluorsave mounting medium (EMD Millipore). Slides were observed under an AxioCam2 Zeiss fluorescent microscope connected with Metamorph acquisition software or Evos FL fluorescent microscope (Thermofisher, USA). Images were acquired as TIFF files and used for cell counting and analysis of injection sites using ImageJ. Expression of the virus was investigated in the parafacial area. Serial sections (150 µm interval) spanning the caudal end of the facial nucleus (VII) (from 650 µm caudal to 850 µm rostral to the caudal tip of VII) were investigated. The core of pFRG was identified as the non-cholinergic cells in a square area (Figure 2.1 A; 2.5-3.2 mm ML and 9.8-10.6 mm DV relative to bregma (Paxinos & Watson, 2005)) ventrolateral to the caudal tip of VII (VIIc) and extending for 600 µm rostro-caudally (from -0.35 mm to +0.25 mm from VIIc). Expression of neurons in the pFRG (pF_L) was also assessed in relation to the more medial parafacial area (pF_M) where chemosensitive neurons of the retrotrapezoid nucleus (RTN) are localized (Stornetta et al 2006).

2.2.6 Data analysis and statistics

Sleep scoring was assessed manually using traces from HPC, nCTX and neck EMG according to previously established sleep scoring criteria (Andrews & Pagliardini, 2015; Pagliardini et al., 2012). EEG traces were bandpass filtered between 0.2 and 50 Hz to reduce noise associated to movement of the tethered cables or electrical current. Wakefulness was identified by the presence of strong neck EMG activity associated with activated EEG in the nCTX (low amplitude fast signal) and HPC (theta frequency; 4-10 Hz). Muscle tone during sleep was generally low, reaching

even lower levels during REM stage. Distinction between NREM and REM sleep was performed by analyzing the EEG and neck EMG signals. NREM stage was identified due to the presence of low frequency (delta waves: 2-4 Hz) and high amplitude signals in nCTX, whereas REM sleep was identified due to the presence of theta activity in the HPC (lasting 10 seconds or longer) and minimal neck$_{EMG}$ activity. Possible effects of CNO, its metabolite clozapine, or modulation of pFRG on sleep architecture (Gomez et al., 2017; Mahler & Aston-Jones, 2018; D. F. Manvich et al., 2018) were evaluated through the analysis of the number and duration of REM and NREM epochs per hour of recording, as well as the percentage of time spent in each sleep stage. Additionally, sleep fragmentation was further analyzed through the calculation of the number of transitions between sleep stages throughout the recording sessions. Sleep characteristics were analyzed using Labchart 8-Pro (AD-Instruments, Sydney, AU), SleepSign (Kissei Comtec, Japan), Excel and Origin 8 software.

Respiratory variables were analyzed using signals recorded from the DIA and ABD EMG. The absolute value of EMG traces was integrated with a time constant decay of 0.08 s to perform peak analysis. Integrated DIA traces were used to calculate respiratory rate (RR) and period. DIA$_{EMG}$ peak amplitude values during ABD recruitment and in baseline conditions were used to estimate relative changes in DIA amplitude (DIA$_{amp}$) and minute respiration (i.e. the product of RR and DIA$_{amp;}$ MR) and used as proxy for rats' minute ventilation similar to previous studies (Dumont et al.,2011). Respiratory variability was calculated and is reported as percentage of coefficient of variation (CV) of the respiratory period. Central and post-sigh apneas were identified as pauses of 2 seconds or longer in the DIA$_{EMG}$ signals. Additionally, sigh rate and the ratio of sighs in which post-sigh apneas (PSA) were observed was also calculated.

REM, NREM and quiet wakefulness events were classified as ABD$^+$ or ABD$^-$ based on the presence or absence of ABD recruitment during each epoch. ABD recruitment was determined as three or more consecutive ABD bursts occurring during the later half of inspiratory inter-burst intervals with an amplitude 50% larger than baseline non-respiratory related tonic ABD muscle activity (as illustrated in Figure 2.3 Ai-Aii). The incidence of ABD recruitment was evaluated by calculating the ratio of epochs in which ABD recruitment was observed (e.g. ABD$^+$/REM$_{Tot}$ or ABD$^+$/NREM$_{Tot}$). The effect of CNO on the occurrence of ABD recruitment was further tested by assessing the prevalence and strength of these events in CTRL and CNO conditions. Prevalence

of ABD recruitment was evaluated through the ratio of ABD to DIA burst frequency (as illustrated in Figure 2.4 Bi-Bii), whereas strength was assessed through the average ABD_{EMG} amplitude relative to baseline non-respiratory tonic ABD activity in CTRL and CNO conditions within each sleep epoch. Respiratory parameters (i.e. respiratory rate, respiratory variability, relative DIA_{amp}, and relative MR) were further compared within sleep epochs: respiratory parameters were analyzed throughout the duration of ABD recruitment events and compared to a similar number of breaths before the onset of ABD recruitment. Traces were analyzed using Labchart 8 Pro (AD-Instruments; Sydney, AU), Excel and Origin 8 (OriginLab Corp.; USA) software, and images of recorded traces were prepared with IgorPro (Wavemetrics; USA).

Respiratory parameters and ratios are reported as mean ± SEM. Assumptions of homogeneity of variance and normal distribution were tested through Brown-Forsythe ($\alpha = 0.05$) and Shapiro-Wilk ($\alpha = 0.05$) tests respectively. All within individual (CTRL vs CNO) and in-between groups (EYFP vs DREADD-G_i vs DREADD-G_q) comparisons were performed with a two-factor repeated-measures analysis of variance (Two-Way RM ANOVA; one repeated factor; $\alpha = 0.05$). Repeated measures in the Two-Way RM ANOVA were composed of only two levels (CTRL and CNO), therefore the sphericity assumption was always met. If significant main effects were found, Two-Way RM ANOVAs were followed by all pairwise multiple comparison post-hoc procedures (Holm-Sidak method; $\alpha = 0.05$). When applicable, comparisons of CNO/CTRL ratios across different groups (EYFP vs DREADD-G_i vs DREADD-G_q) were performed using a one-factor analysis of variance (One-Way ANOVA; $\alpha = 0.05$). When significant main effects were resolved, One-Way ANOVAs were followed by Tukey's honestly significant difference (HSD) post hoc test ($\alpha = 0.05$). If normality test failed ($p < 0.05$), we performed a Kruskal-Wallis One Way analysis of variance on ranks ($\alpha = 0.05$) as a non-parametric equivalent of One-Way ANOVA. If main effects were found, Kruskal Wallis test was followed by all pairwise multiple comparison post-hoc procedures (Dunn's Method; $\alpha = 0.05$). All statistical analyses were performed in SigmaPlot 14.0 (Systat Software Inc.; USA).

2.3 Results

A total of 21 rats underwent successful pFRG viral injections and electrode instrumentation for the analysis of respiratory variables during natural sleep in healthy conditions: 6 for control

experiments with Cre-eYFP viruses, 7 for the inhibitory experiments with DREADD-G_i and 8 for the excitatory experiments with DREADD-G_q.

2.3.1 Histological Analysis

To verify that viral injections were effectively located in the area that was previously identified as pFRG (Del Negro et al., 2018; Li et al., 2016; Huckstepp et al., 2015; Li et al., 2016; Pagliardini et al., 2011), we inspected an area comprising 1500 µm rostro-caudally, from -0.6 mm caudal to +0.6 mm rostral to the tip of the facial nucleus (VIIc). We analyzed a rectangular area in the perifacial region, which included both chemosensitive RTN neurons in the region ventromedial to the facial nucleus (pF_M) and late expiratory pFRG neurons in the region ventrolateral to the facial nucleus (pF_L) (Figure 2.1 A). The analyzed area extended from the lateral border of the pyramidal tract to the medial edge of the spinal trigeminal tract, mediolaterally, and from the ventral surface of the medulla to the dorsal edge of the facial nucleus, dorso-ventrally. The average number of cells expressing the reporter protein was 152 ± 5.3 per animal (n=14; 1 section every 150 µm) in an area that extended 600 µm caudal and rostral to the caudal tip of VII. On average, the majority of the transfected cells (approximately 129 ± 6.8 per animal or 88.7 ± 4.2% of the total number of transfected cells counted per animal) were located in the perifacial area that includes the RTN/pFRG region from -0.35 mm to +0.25 mm from VIIc (Figure 2.1 Bi-Ci) according to the current literature (Huckstepp et al., 2015; Pagliardini et al., 2011; Del Negro et al., 2018). Only a few of those cells (36.9 ± 3.4 per animal; Figure 2.1 Cii) were located more medially, in the ventral parafacial area (i.e., pF_M, RTN; 1.0-2.4 mm lateral to the midline Huckstepp et al., 2015; Paxinos & Watson, 2005) whereas the majority of transfected neurons were located in the lateral parafacial area (i.e. pF_L or pFRG ; >2.4 mm lateral to the midline; Figure 2.1 Ciii). We also evaluated the spread of the virus to cholinergic motoneurons in VII. On average, 34 ± 4.7 ChAT positive motoneurons per animal also expressed viral vectors along the rostro-caudal area analyzed (10.1 ± 1.4% of motoneurons in that area). No cell bodies expressing viral reporter proteins were observed in adjacent areas of the medulla (i.e. spinal trigeminal tract, Bötzinger Complex, preBötzinger Complex).

2.3.2 Sleep architecture and general respiratory characteristics

It has been recently demonstrated that CNO can be reversibly metabolized to clozapine and therefore induce clozapine-mediated effects (Manvich et al., 2018). Furthermore, clozapine has sedative properties and may influence sleep architecture (Hinze-Selch et al., 1997; Touyz et al., 1977; Touyz et al., 1978). In our study, the frequency, average duration, and percentage of time spent in each sleep phase (i.e. REM and NREM sleep) remained unaffected after systemic injection of CNO in rats transfected with either Cre-eYFP, DREADD-G_i or DREADD-G_q (p>0.05; Table 1), suggesting that, even though CNO is metabolized to clozapine, the amount of circulating clozapine was not sufficient to induce alterations in the sleep architecture. Representative examples of hypnograms in each condition are presented in Figure 2.2 Ai-Aiii. A chronological analysis of the time spent in each sleep stage throughout the recordings (Figure 2.2 Bi-Biii) indicates that rats spent 39-48% of the recording time awake, whereas 49-56% and 3-5% of the recording time was spent in NREM and REM sleep respectively. No difference was observed between CTRL and CNO and between groups for the percentage of time spent in REM and NREM sleep (Two-Way RM ANOVA, p > 0.05, Table 1). In addition, the frequency of transitions between sleep stages was not significantly different after CNO administration across groups (Two-Way RM ANOVA, p>0.05; Figure 2.2 Ci-Ciii). Most of the NREM epochs ended in wakefulness events (NRW/hr = 6.14 ± 0.78 vs NRR/hr = 3.19 ± 0.31, two tail unpaired Student t-test, p = 0.01) whereas REM epochs indistinctively finalized in either wakefulness or transitions to NREM sleep (RW/hr = 1.69 ± 0.27 vs RR/hr = 1.50 ± 0.10, two tail unpaired Student t-test, p = 0.519; Figure 2.2 Ci-Ciii).

Group analysis of the respiratory rate (RR) in CTRL conditions vs CNO and in between groups suggests that RR was not affected by modulation of pFRG during either NREM sleep or REM sleep (p > 0.05; Two-Way RM ANOVA for NREM and for REM). On average, pooled data of RR during REM sleep was not different from NREM sleep (89.4 ± 1.3 bpm in REM vs 90.1 ± 1.7 bpm in NREM, unpaired Student t-test, p = 0.52). Similarly, respiratory variability (measured by the CV of the period) was not different between CTRL and CNO conditions and across groups in either REM or NREM sleep (p > 0.05; Two-Way RM ANOVA for REM and NREM). Overall, analysis of the pooled data suggests that breathing during REM epochs was more variable than during NREM sleep (24.9 ± 1.5% in REM vs 17.8 ± 1.4% in NREM, two tail unpaired Student t-

test, p = 0.006). We conclude that the commonly used dose of CNO applied in this study (3mg/kg) did not mediate non-specific effects in the sleep architecture or respiratory characteristics of adult male Sprague Dawley rats. Additionally, targeted inhibition and/or excitation of the pFRG area did not affect the generation of the respiratory rhythm across sleep states.

2.3.3 Effect of pFRG modulation on the recruitment of ABD muscles across vigilance states

To understand the effects of pFRG modulation in the generation of ABD recruitment across sleep states, we analyzed the percentage of Wake, NREM and REM sleep epochs in which ABD recruitment was observed, as well as the ABD/DIA ratios and the amplitude of ABD_{EMG} signals during the different sleep stages. Vigilance states were considered ABD+ when three or more consecutive late expiratory ABD bursts surpassed the threshold of 50% of baseline activity (Figure 2.3 Ai-Aii) during the duration of the epoch. All respiratory parameters analyzed, were not significantly different across groups in CTRL (vehicle) conditions ($p > 0.05$; Two-Way RM ANOVA). Therefore, all CTRL data was pooled for subsequent interpretation of the results. During quiet wakefulness and NREM sleep, ABD recruitment was sparsely observed (Figure 2.3 Bi-Ciii). Specifically, only $0.5 \pm 1.3\%$ of the wake events displayed ABD recruitment in CTRL and this value did not change after administration of CNO across groups ($p > 0.05$; Two-Way RM ANOVA; Figure 2.3 Bi-Biii). Similarly, ABD recruitment was present in only $3.0 \pm 0.58\%$ of NREM epochs in CTRL conditions and this value did not change after CNO administration across groups ($p > 0.05$; Two-Way RM ANOVA; Figure 2.3 Ci-Ciii). Interestingly, ABD recruitment events occurred in ~$27.1 \pm 3.3\%$ of REM sleep epochs in CTRL conditions and this value was affected by modulation of pFRG ($p < 0.05$, Two-Way RM ANOVA; Figure 2.3 Di-Diii). Inhibition of pFRG resulted in a decrease of the percentage of REM sleep epochs in which ABD recruitment was observed ($9.4 \pm 5.4\%$ in CNO, $p = 0.04$; Holm-Sidak post-hoc test; Figure 2.3 Dii), whereas excitation increased them ($50.4 \pm 8.2\%$ in CNO, $p = 0.001$; Holm-Sidak post-hoc test; Figure 2.3 Diii).

An in-depth analysis of the inspiratory and expiratory outputs during REM sleep suggests that both the prevalence and amplitude of ABD recruitment is affected by modulation of pFRG (Figure 4A). The prevalence of ABD bursts within each REM epoch was analyzed through the ratio of ABD/DIA bursts (a value closer to 1 indicates stronger prevalence of ABD burst, whereas a value

closer to 0 indicates lower prevalence of ABD bursts within the sleep epoch analyzed; Figure 4Bi-Bii).

The prevalence of ABD bursts within REM events was ~0.30 ± 0.04 in CTRL conditions and inhibition of pFRG reduced this value to 0.11 ± 0.04 (Holm-Sidak post-hoc test, p = 0.03; Figure 2.4 Cii), whereas excitation increased it to 0.49 ± 0.08 (Holm-Sidak post-hoc test, p = 0.015; Figure 2.4 Ciii).

Next, we evaluated the strength of the ABD_{EMG} signals in response to modulation of pFRG, specifically during REM epochs, by analyzing the ratio of the ABD_{EMG} amplitude and ABD_{EMG} frequency in CNO and CTRL conditions across groups. The amplitude of ABD_{EMG} signals after inhibition of pFRG in DREADD-G_i rats was ~27% of that observed in baseline (ABD_{amp} CNO/baseline = 0.27 ± 0.17; Figure 2.4 Di), whereas excitation in DREADD-G_q rats induced an increase of ~82% on the ABD_{EMG} signal amplitude compared to baseline values (ABD_{amp} CNO/baseline = 1.82 ± 0.68; Figure 2.4 Di). Similarly, excitation of pFRG after CNO administration in DREADD-G_q rats, increased the frequency of ABD bursts within REM events compared to baseline conditions (ABD_{freq} CNO/baseline = 3.11 ± 1.18; Figure 2.4 Dii), whereas pFRG inhibition reduced the ABD bursting rate to ~45% of the baseline values (ABD_{freq} CNO/baseline = 0.45 ± 0.20; Figure 2.4 Dii). Overall these results suggest that chemogenetic modulation of pFRG affects the occurrence of ABD recruitment, as well as the ABD burst prevalence and ABD_{EMG} signal amplitude during REM sleep, but it has no apparent influence on the recruitment of ABD muscles or the strength of ABD_{EMG} recruitment during quiet wakefulness and NREM sleep in adult male Sprague Dawley rats.

2.3.4 Effect of ABD recruitment and pFRG modulation on respiratory variables

To evaluate the effects of pFRG modulation during REM sleep, we proceeded to analyze various respiratory parameters (i.e. respiratory rate, coefficient of variation of the respiratory period, diaphragm amplitude and minute respiration). More specifically, we evaluated the changes in these parameters associated with the recruitment of ABD muscles by normalizing these values to their baseline immediately before ABD recruitment occurrence (a value higher than 1 indicates that ABD recruitment was associated with a value increase, whereas a value lower than 1 indicates that ABD recruitment was associated with a decrease in those values; Figure 2.5 A). Normalized values

of RR, CV, DIA$_{amp}$ and MR were not different between CTRL and CNO conditions across experimental groups (p > 0.05; Two-Way RM ANOVA). The respiratory rate during ABD recruitment was no different from the baseline values in either CTRL conditions (1.05 ± 0.06, paired Student t-test, p = 0.575; Figure 2.5 Bi) or after modulation of pFRG through the administration of CNO in DREADD-G$_i$ (0.98 ± 0.06, paired Student t-test, p = 0.297; Figure 2.5 Bi) and DREADD-G$_q$ rats (1.08 ± 0.03, paired Student t-test, p = 0.451; Figure 2.5 Bi). Interestingly, the occurrence of ABD recruitment was associated with a decrease in respiratory variability in CTRL conditions (normCV = 0.67 ± 0.08, paired Student t-test, p = 0.007; Figure 2.5 Bii) and after excitation of pFRG (normCV = 0.61 ± 0.20, paired Student t-test, p = 0.029; Figure 5Bii), but had no significant effect after inhibition of pFRG (normCV = 1.16 ± 0.48, Student t-test, p = 0.297; Figure 2.5 Bii). Similarly, ABD recruitment was associated with an increase in diaphragm amplitude (DIA$_{amp}$) and minute respiration (MR) in CTRL (paired Student t-tests, normDIA$_{amp}$ = 1.10 ± 0.03, p = 0.033; normMR = 1.16 ± 0.07, p = 0.035; Figure 2.5 Biii-Biv) and excitatory conditions (paired Student t-tests, normDIA$_{amp}$ = 1.12 ± 0.03, p = 0.029; normMR = 1.15 ± 0.05, p = 0.043; Figure 2.5 Biii-Biv), but these enhancements in breathing were no longer observed after inhibition of pFRG (paired Student t-test, normDIA$_{amp}$ = 0.95 ± 0.08, p = 0.484; normMR = 0.91 ± 0.05, p = 0.186; Figure 2.5 Biii-Biv).

We previously observed that the occurrence of ABD recruitment during sleep was usually associated with REM epochs in which respiratory disturbances were more predominant (C. G. Andrews & S. Pagliardini, 2015). Therefore, we further examined the effects of pFRG modulation on the frequency and duration of apneas in rats transfected with Cre-EYFP, DREADD-G$_i$ and DREADD-G$_q$ viruses. Chemogenetic modulation of pFRG had no influence in the number or the duration of apneas and post-sigh apneas (PSA) observed in both DREADD-G$_i$ and DREADD-G$_q$ treated rats (p > 0.05, Two-Way RM ANOVA; Table 2). On average, respiratory disturbances oscillated around 2.23 ± 0.6 apneas/hr, whereas PSA were present at a rate of 8.33 ± 1.9 events/hr. The durations of both apneas and PSA were similar and oscillated around 3.41 ± 0.21 seconds.

We conclude that pFRG activity, in addition to being responsible for the occurrence of ABD recruitment within REM epochs, is also responsible for the regularization of breathing and enhancement in diaphragm amplitude and minute respiration associated with ABD activity. Because inhibition of pFRG eliminated the expected enhancement in breathing otherwise caused

by the recruitment of ABD muscles, it is possible that those effects could be mediated through central modulation (Pisanski and Pagliardini, 2018). However, the improvement in breathing observed in CTRL and excitatory conditions was not due to a reduction on the number of respiratory disturbances, but to a stabilization of breathing on a burst to burst basis instead.

2.4 Discussion

We used a chemogenetic approach to investigate whether pFRG could be responsible for the ABD recruitment previously observed during sleep (Andrews & Pagliardini, 2015; Leirao et al., 2017; Saini & Pagliardini, 2017; Sherrey et al., 1988). Our results suggest that pFRG modulation impacts the frequency, prevalence and amplitude of ABD recruitment during REM sleep but does not seem to influence ABD activity during quiet wakefulness and NREM sleep. This evidence suggests that the mechanism underlying the generation of ABD recruitment during sleep may depend on the vigilance state. Furthermore, our study also found that the effects of potentiation of ventilation observed at the onset of ABD recruitment in CTRL and excitatory conditions was blunted in inhibitory conditions. Finally, we found that the modulation of pFRG and the occurrence of ABD recruitment did not stabilize breathing by reducing the number of respiratory disturbances but had an effect on a breath to breath basis.

2.4.1 Technical considerations

In this study, we used a chemogenetic approach to specifically manipulate the activity of the pFRG brain region. Although the DREADD technology is being portrayed as a powerful tool to remotely manipulate cell activity (Armbruster et al., 2007; Zhu & Roth, 2014), a few reports have highlighted some limitations that could compromise the interpretation of findings unless rigorous control experiments are performed (Gomez et al., 2017; MacLaren et al., 2016; Mahler & Aston-Jones, 2018; Manvich et al., 2018; Raper et al., 2017). For example, systemic administration of the "inert" ligand CNO may produce locomotion-related and behavioural effects that are possibly associated with CNO's reverse metabolism into clozapine and N-desmethylclozapine (MacLaren et al., 2016; Manvich et al., 2018; Raper et al., 2017). Additionally, it was recently proposed that DREADD-specific effects may be mediated by clozapine rather than CNO, since CNO sparingly crosses the blood brain barrier and DREADD receptors display a higher affinity for clozapine (Gomez et al., 2017; Raper et al., 2017). Additionally, due to the slow conversion of CNO into

clozapine, systemic injection of CNO may delay and extend the duration of DREADD-mediated effects, which could be advantageous for extended experiments (> 2-hour duration), as in our current study (Mahler & Aston-Jones, 2018). Despite its limitations, the DREADD technology remains a powerful tool for the specific manipulation of brain activity (Mahler & Aston-Jones, 2018; Roth, 2016). In this study we controlled for potential off-target effects of the CNO metabolic by-products by administering identical commonly used doses of CNO to rats transfected with both DREADD and non-DREADD viruses (i.e., the Cre-eYFP experimental group). Our results suggest that CNO did not produce non-DREADD mediated effects in the sleep architecture, respiratory variables or the recruitment of ABD muscles during sleep, suggesting that the observed results are not associated with off target effects caused by CNO and its metabolites.

2.4.2 Histological analysis and extent of pFRG chemogenetic modulation

Since specific anatomical or genetic markers for the identification of pFRG cells remain to be determined, we based our injection on stereotaxic coordinates that target pFRG according to previous work that assessed recruitment of active expiration and late expiratory neurons by pharmacological, chemogenetic and optogenetic manipulations of the area ventrolateral to VII (Boutin et al., 2017; de Britto & Moraes, 2017; Huckstepp et al., 2015; Huckstepp et al., 2016; Pagliardini et al., 2011).

In our study, viral expression extended 1200 μm rostro-caudally around the caudal tip of the facial nucleus, with most transfected cells being circumscribed to a smaller area of 600 μm lateral to the facial nucleus. Although the expression of DREADD receptors was not dependent on a specific marker and therefore may affect other respiratory and non-respiratory structures in the surrounding area, the majority of the cells were located ventrolateral to the facial nucleus. A fraction of transfected cells was also present in the more medial, chemosensitive area of the RTN. This area has an important role in driving both inspiratory and expiratory activities (Abbott et al., 2011) and it displays an exquisite state-dependent activity (Burke et al., 2015; Curran et al., 2001; Kuwaki et al., 2010; Li & Nattie, 1997; Nattie et al., 2001; Souza et al., 2019). Our results suggest that RTN function may have minimally, if at all, affected our results, given that: i) DREADD-Gi activation did not change inspiratory activity at any given vigilance state; ii) DREADD-Gq and DREADD Gi activation had no effect on either inspiratory or expiratory activity when RTN neurons are more

excitable, i.e., during wakefulness and NREM sleep; iii) DREADD-Gq activation increased EMG amplitude and expiratory activity in REM sleep, when expiratory activity has been previously observed (Andrews & Pagliardini, 2015) and when RTN neurons are in their least excitable state (Burke et al., 2015). We therefore conclude that DREADD modulation of neuronal activity most likely affected the more ventrolateral region of the parafacial area corresponding to the putative region of the pFRG.

The non-specific transfection of cells in the parafacial area, combined with the localized viral injections may also be responsible for the incomplete silencing or activation of ABD recruitment during sleep in our study. Alternatively, the influence of competing inhibitory and excitatory state-dependent modulatory mechanisms on pFRG neurons or on premotor and motor neurons could also explain the incomplete effects on the recruitment of ABD muscles in DREADD-G_i and DREADD-G_q rats in comparison to previous work where pFRG activity was pharmacologically modulated under anesthesia (Boutin et al., 2017; Huckstepp et al., 2015; Huckstepp et al., 2016; Huckstepp et al., 2018; Pagliardini et al., 2011).

2.4.3 The mechanism for ABD recruitment during sleep may depend on vigilance state

Previous research has demonstrated the occurrence of expiratory ABD recruitment during REM sleep and to a lesser extent during NREM sleep (Andrews & Pagliardini, 2015; Leirao et al., 2017; Saini & Pagliardini, 2017; Sherrey et al., 1988). Our results show that chemogenetic modulation of the expiratory oscillator specifically influences the frequency of occurrence and strength of ABD$_{EMG}$ activity during REM sleep and not during NREM sleep. This is in clear contrast to what has been observed with RTN manipulations (Burke et al., 2015). Vigilance state-dependent changes in respiratory frequency, minute ventilation, breathing regularity, and/or diaphragm amplitude have previously been described in dogs, cats, and rats (Lydic et al., 1991; Megirian et al., 1980; Phillipson et al, 1976; Sherrey et al., 1988; Smith et al., 1997; Souza et al., 2018). Furthermore, important regulatory mechanisms such as chemosensation have been found to be reduced during REM sleep in comparison to wakefulness and NREM sleep (Burke et al., 2015; Lydic et al., 1991; Smith et al., 1997). The mechanisms underlying such state-dependent variations remain to be fully investigated and may account for the distinct effects of our chemogenetic manipulations across vigilance states.

The activity of pFRG is influenced by a combination of inhibitory and excitatory mechanisms that are still poorly understood (Boutin et al., 2017; Huckstepp et al., 2018; Pagliardini et al., 2011; Pisanski & Pagliardini, 2018) and seem to be dependent on vigilance state and physiological conditions (Andrews & S. Pagliardini, 2015; Saini & Pagliardini, 2017). Specifically, the cholinergic modulation of pFRG may be of particular interest to better understand state dependent expiratory ABD activity (Boutin et al., 2017). Cholinergic neurons of the latero-dorsal and pedunculopontine tegmental nucleus (LDT/PPT) seem to be involved in the initiation of REM sleep, whereas cholinergic cells in the basal forebrain have been demonstrated to influence the duration of REM epochs and the homeostatic sleep response in sleep deprived animals (Han et al., 2014; Kalinchuk et al., 2015; Van Dort et al., 2015). It is possible that the state-dependent activity of cholinergic neurons in the LDT/PPT and basal forebrain regions could modulate the recruitment of ABD muscles either through direct or indirect stimulation of pFRG rhythmicity or through modulation of ABD motor neurons specifically during REM sleep. This could explain the observation of strongest effects of pFRG modulation during REM sleep in the current study. Other potential explanations for the observation of ABD recruitment specifically during REM sleep could be the withdrawal of inhibitory inputs or the activation of glutamatergic pathways impingent on the pFRG (Huckstepp et al., 2018; Pagliardini et al., 2011). Previous studies have demonstrated fluctuations in the neurotransmitters release across sleep-wake cycles in various brain regions (Lena et al., 2005; Lopez-Rodriguez et al., 2007; Vanini et al., 2011). Therefore, it is possible that these vigilance state-dependent fluctuations in neurotransmitters release could also influence pFRG activity. Further studies will be required to confirm phenotype-specific anatomical connections to neurons in the pFRG and their possible implication in the modulation of ABD recruitment during sleep.

2.4.4 Breathing enhancement following the recruitment of ABD muscles

Our results show that increased excitability of pFRG through chemogenetic modulation produces an augmented occurrence of REM events displaying ABD recruitment, whereas its inhibition reduces the number of these events. Furthermore, in CTRL and excitatory conditions ABD recruitment events are associated with a reduction in respiratory variability, as well as an increase in ventilation, similar to previous reports (Andrews & Pagliardini, 2015; Saini & Pagliardini, 2017). However, following chemogenetic inhibition of pFRG, ABD recruitment did not elicit

reductions in respiratory variability or increased ventilation. It was previously proposed that activation of pFRG may stabilize breathing through either mechanical facilitation of air outflow with ABD muscle recruitment, or through direct and indirect excitation of the preBötC (Pisanski & Pagliardini, 2018). As the facilitatory component of air outflow produced by ABD muscle recruitment is still present in the inhibitory conditions of our study, we hypothesize that the enhancements in breathing occurring with ABD activity could be due to central mechanisms associated with pFRG activation. Although anatomical evidence to support the idea of a direct or indirect excitatory connectivity from pFRG to preBötC is non-existent to our knowledge, it has previously been proposed in embryonic and neonatal stages (see Figure 9 in Huckstepp et al. 2016; Thoby-Brisson et al., 2009) and has been inferred from physiological evidence in adult rats (Pagliardini et al., 2011).

Abdominal muscle recruitment in REM sleep is associated with reduced respiratory variability during its transient occurrence (Andrews & Pagliardini, 2015; Saini & Pagliardini, 2017). Therefore, we hypothesized that impairment of ABD recruitment would increase the number of respiratory disturbances observed in healthy animals, whereas potentiation of these events could reduce the respiratory disturbances naturally occurring in healthy rats. However, the analysis of respiratory disturbance frequency revealed that chemogenetic modulation of the expiratory oscillator had no influence on apnea occurrence.

Breathing is a robust process of vital importance for survival (Del Negro et al., 2018). Previous studies have demonstrated that ablation and/or inhibition of specific cell populations at the level of the inspiratory oscillator can compromise the integrity of breathing (Gray et al., 2001; Huckstepp et al., 2016; Li et al., 2016; McKay & Feldman, 2008; McKay et al., 2005; Vann et al., 2016; Wang et al., 2014). However, pFRG is silent during restful breathing (Huckstepp et al., 2015; Pagliardini et al., 2011) and further hyperpolarization of pFRG neurons (current study) decreases the occurrence of ABD recruitment and the enhancement of breathing associated with ABD activity but does not induce further disruptions of breathing (i.e. apneas). Similarly, potentiation of pFRG increases occurrence of ABD recruitment during sleep but does not affect naturally occurring apneas. Respiratory disturbances in healthy rats are minimal and occur at an average rate of 2 apneas per hour (Carley et al, 1996). Potentiation of pFRG activity in conditions in which apneas are nearly non-existent, as in the current study, may not allow for an accurate

evaluation of the benefits associated with an enhancement of ABD recruitment during sleep, although effects may be beneficial in pathological conditions such as sleep disordered breathing.

2.5 Figures and Figure captions
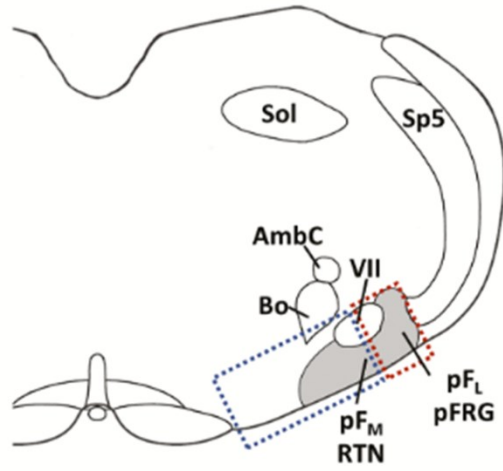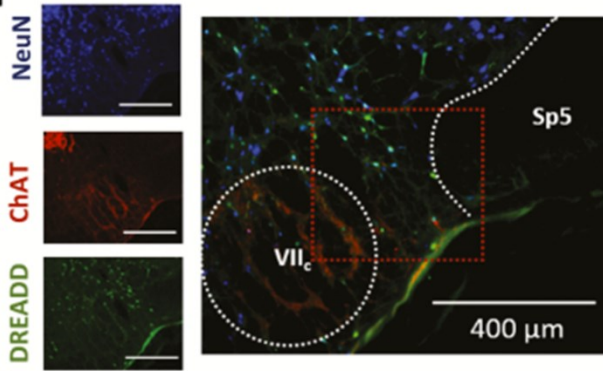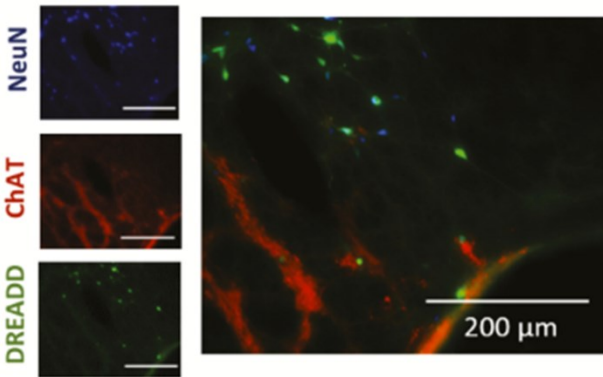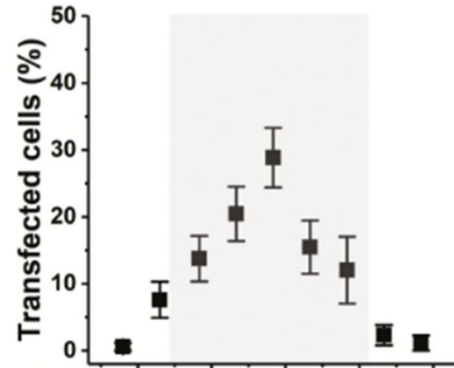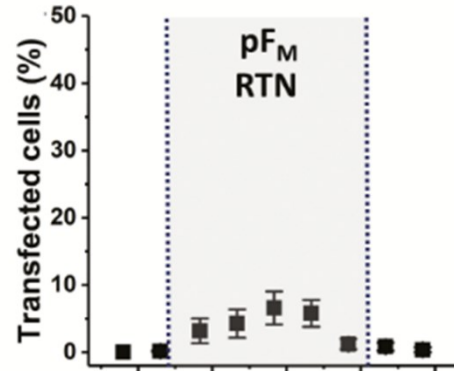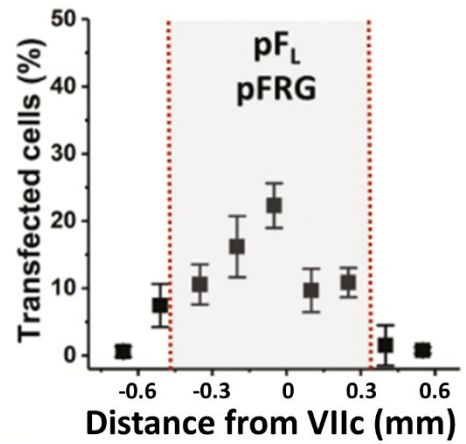
Figure 2.1 Expression of viral reporter proteins in the parafacial area

A: Schematic representation of the area analyzed at the caudal tip of the facial nucleus (VIIc). Neurons within the gray area were considered to be located in the medial parafacial area pF_M/RTN (blue square) and lateral parafacial area $pF_L/pFRG$ (red square). This logic was applied to every slice analyzed from –0.6 mm to +0.6 mm from VIIc. **Bi-Bii**: Immunofluorescent images taken just caudal to the facial nucleus (VIIc, -0.15 mm). Red square in Bi is represented in Bii. Immunostaining for cholinergic markers (red) revealed immunopositive processes caudal to the tip of the VII (circled area in Bi). Immunostaining for viral reporter proteins expressed by DREADD (green) revealed transfection of cells located lateral to the caudal tip of VII and adjacent to the spinal trigeminal tract (Sp5). ChAT: Choline Acetyl Transferase; NeuN: Neuronal nuclei marker; DREADD: Designer receptor exclusively activated by designer drug. **Ci-Ciii**: Rostro-caudal distribution of total transfected cells (**Ci**), as well as cells transfected within pFM/RTN (**Cii**) and pFL/pFRG areas (**Ciii**). Values are percentages of total cells transfected in a rostro-caudal span of 1200 µm (analysis of 1 transverse section every 150 µm). Shaded region on graphs indicates the area corresponding to the core of pF_M/RTN and $pF_L/pFRG$ respectively (from -0.35 mm to +0.25 mm from the tip of VIIc).
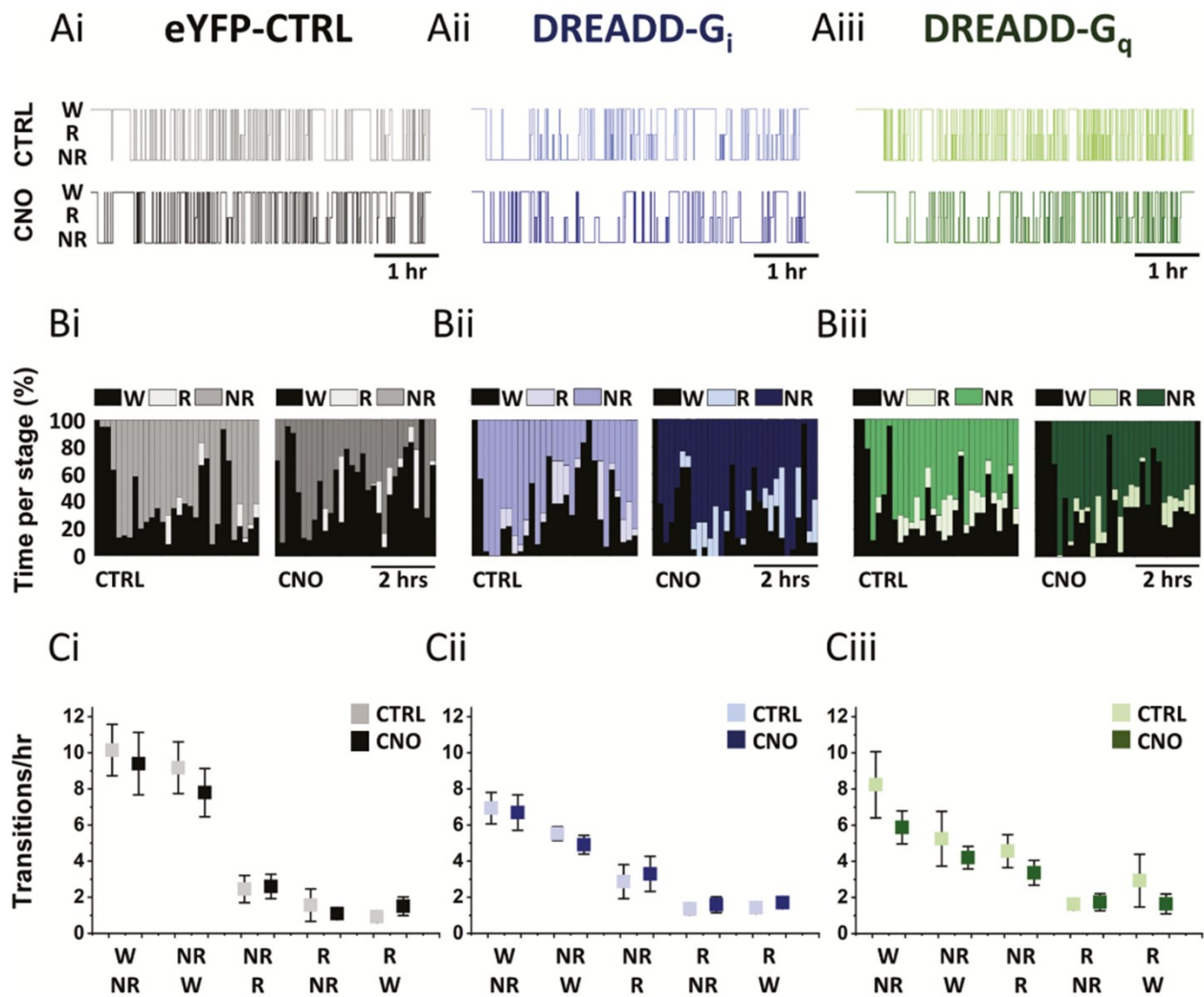
Figure 2.2 Sleep architecture is not affected by chemogenetic modulation of pFRG

Ai-Aiii: Hypnograms from 3 rats transfected with CTRL-eYFP (gray scale), DREADD-G_i (blue scale) or DREADD-G_q (green scale) viruses. Hypnograms show the transitions between wakefulness (W), non-rapid-eye-movement (NREM) and rapid-eye-movement (REM) sleep throughout 5 hours of continuous recordings. The percentage of time spent in each sleep stage (**Bi-Biii**) and the rate of transition between sleep stages (i.e. sleep fragmentation; **Ci-Ciii**) were not affected by the systemic administration of CNO (darker tone in each colour scale) in either CTRL-eYFP, DREADD-G_i, or DREADD-G_q rats.
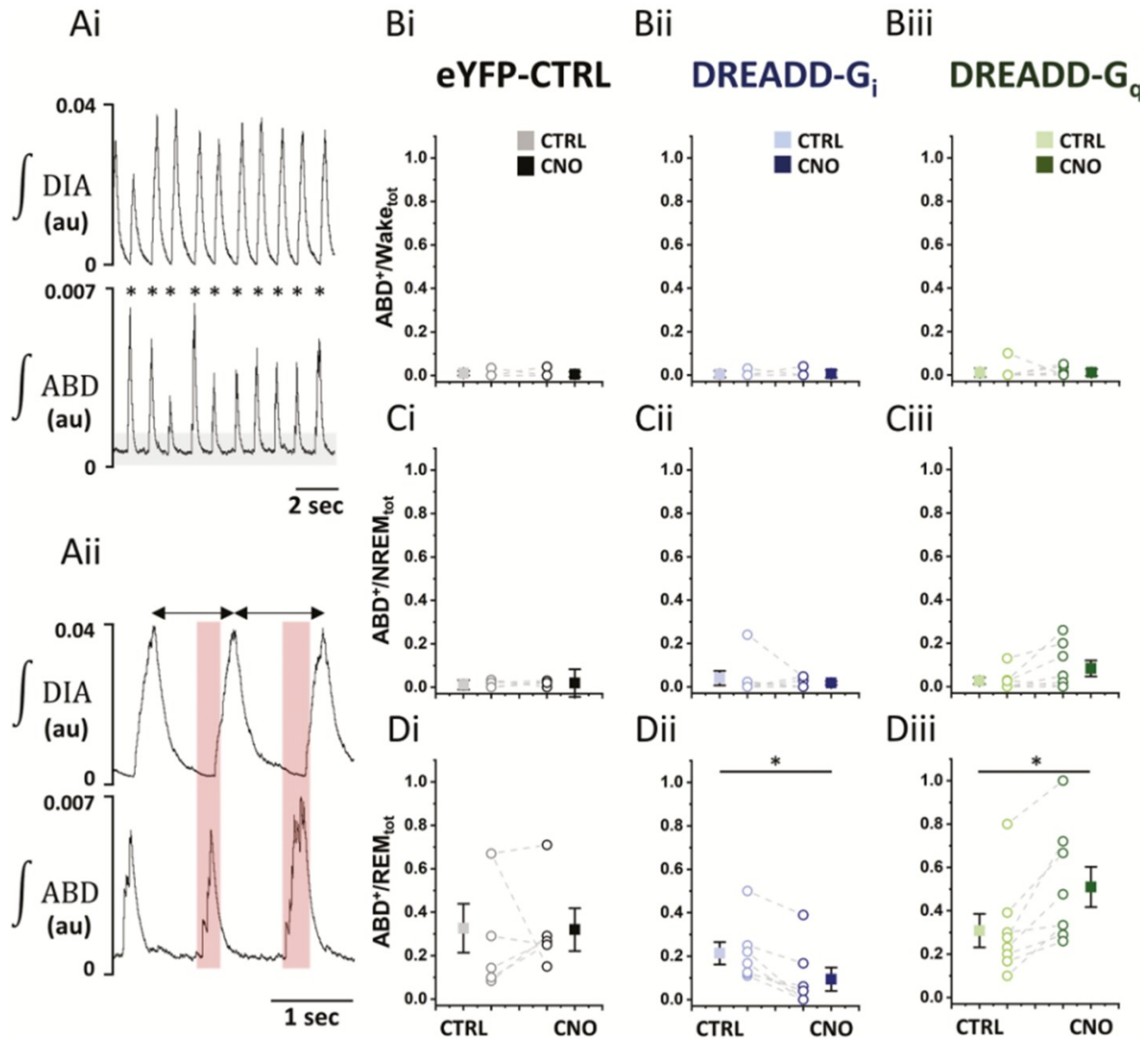
Figure 2.3 Modulation of pFRG influences the occurrence of ABD recruitment during REM sleep

Ai-Aii: Identification of occurrence of ABD recruitment across vigilance states in representative integrated traces of diaphragm (DIA) and abdominal (ABD) activity. Vigilance states were considered to be ABD^+ when three or more consecutive ABD bursts exceeded a threshold of 50% of baseline ABD activity (gray shaded area **Ai**) and occurred during the later half of the inter-inspiratory period (red shaded area **Aii**). **Bi-Diii**: Changes in the ratio of vigilance state epochs in which ABD recruitment was observed in CTRL-eYFP (gray scale), DREADD-G_i (blue scale) and DREADD-G_q (green scale) rats following systemic administration of vehicle (CTRL; lighter tone in each colour scale) or CNO (darker tone). Modulation of pFRG had no effect on the number of

sparse ABD recruitment events during quiet wakefulness (**Bi-Biii**) or NREM sleep (**Ci-Ciii**), but it affected the occurrence of ABD recruitment during REM sleep (**Di-Diii**). Graphs include mean values and SEM (square), as well as individual paired data (circles) for each group.

A

eYFP-CTRL   DREADD-G$_i$ DREADD-G$_q$

$\int$ DIA (au)

$\int$ ABD (au)

Neck$_{EMG}$

HPC (V)

Flow
Inspiration ↑

100 mV

2 sec

Bi $\boxed{\frac{\text{ABD}}{\text{DIA}} = 1}$

$\int$ DIA

$\int$ ABD

Bii $\boxed{\frac{\text{ABD}}{\text{DIA}} = 1/3}$

$\int$ DIA

$\int$ ABD

Di

ABD$_{amp}$(CNO/CTRL)

Ci

ABD/DIA

CTRL   CNO

Cii

CTRL   CNO

*

Ciii

CTRL   CNO

*

Dii

ABD$_{freq}$(CNO/CTRL)

eYFP   G$_i$ G$_q$

54
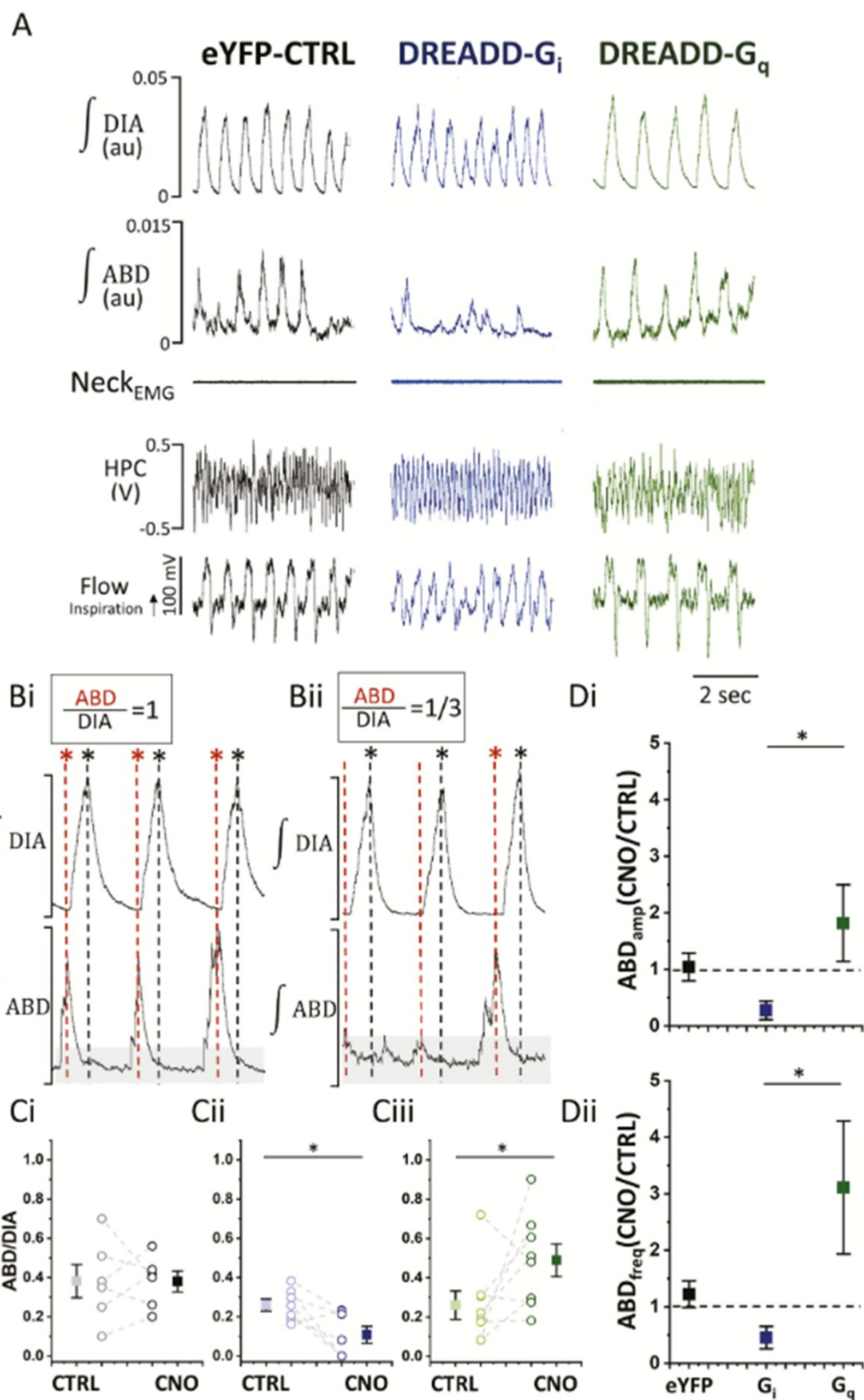
Figure 2.4 Modulation of pFRG influences the prevalence and strength of abdominal recruitment during REM sleep

A: Integrated traces of diaphragm (DIA), abdominal (ABD) and neck electromyogram, as well as hippocampus (HPC) and airflow recordings during a REM epoch after systemic administration of CNO in CTRL-EYFP (black), DREADD-G_i (blue) and DREADD-G_q (green) rats. **Bi-Bii**: Procedure for the calculation of ABD to DIA ratios in representative traces. Black dashed lines and asterisks indicate inspiratory peaks, whereas red dashed lines and asterisks indicate late expiratory ABD bursts that surpassed the threshold (gray shaded area). Red dashed lines without asterisks indicate respiratory event in which ABD bursts did not cross the threshold. **Ci-Ciii**: Changes in the ratio of ABD to DIA bursts in CTRL-eYFP (gray scale), DREADD-G_i (blue scale) and DREADD-G_q (green scale) rats following systemic administration of vehicle (CTRL; lighter tone in each colour scale) or CNO (darker tone). Graphs include mean values and SEM (square), as well as individual data (circles) for each treatment. **Di-Dii**: Relative change in the amplitude (ABD_{amp} CNO/CTRL; E) and frequency of ABD bursts (ABD_{freq} CNO/CTRL; F) after chemogenetic modulation of pFRG in rats transfected with CTRL-eYFP (gray) DREADD-G_i (blue) and DREADD-G_q (green) viruses.
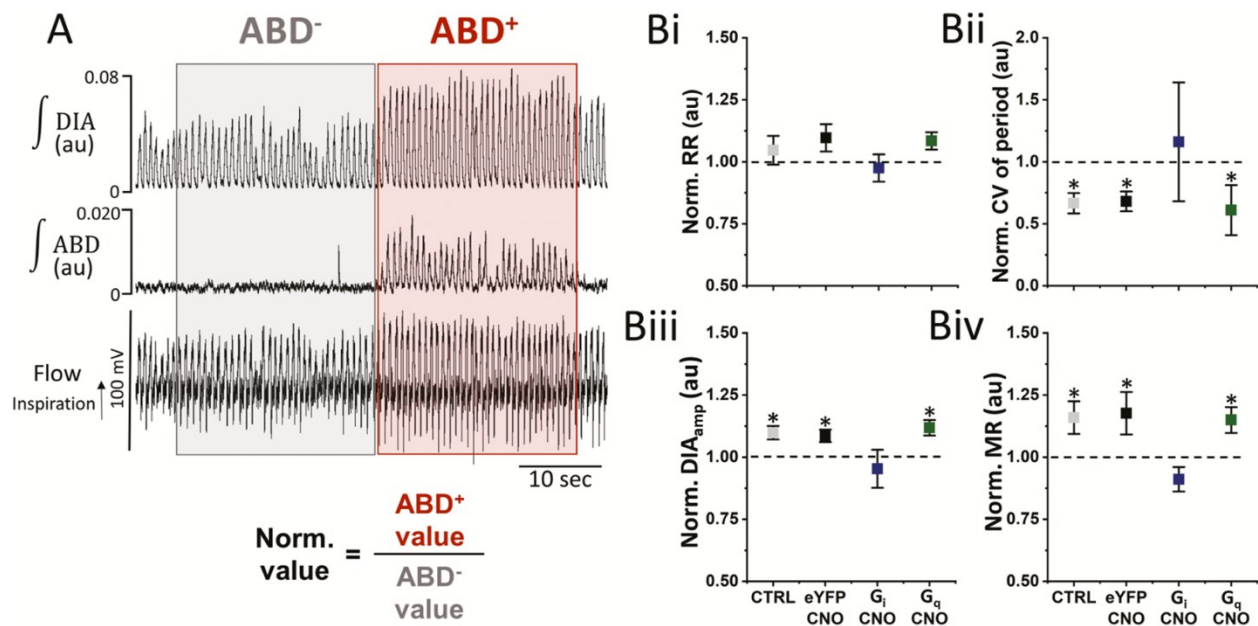
Figure 2.5 Effects of ABD recruitment and pFRG modulation on respiratory parameters

A: Process of normalization for each of the respiratory parameters analyzed on representative electrophysiological traces. Respiratory parameters during the occurrence of ABD activity (ABD$^+$; red shading) were normalized to baseline values (i.e. before the occurrence of ABD recruitment; ABD$^-$; gray shading). **Bi-Biv**: Comparison of respiratory parameters after vehicle (CTRL) and CNO administration across experimental groups (Gray scale: CTRL-eYFP; blue: DREADD-G$_i$; green: DREADD-G$_q$. RR: respiratory rate; CV: coefficient of variation; DIA$_{amp}$: diaphragm amplitude; MR: minute respiration. Values above or below dotted lines imply that ABD recruitment was associated with respective increases or decreases in the corresponding respiratory parameters.

2.6 Tables

Table 2.1 *Effects of chemogenetic modulation of pFRG on sleep architecture.*

Systemic administration of the DREADD ligand clozapine-N-oxide (CNO) had no effect in the sleep architecture of rats across experimental groups. Sleep was monitored throughout 5 hours during the natural sleep period of the rats after either vehicle (CTRL) or CNO administrations. Two-Way repeated measures ANOVA within individual factors (CTRL and CNO); in-between group factors (CTRL-eYFP, DREADD-Gi, DREADD-Gq). No significant main effects were resolved for in-between group comparisons (¤), within individual comparisons (¥) and interaction between within and in-between factors (§).

		Average epoch duration (min) (mean ± SEM)			Epochs/hr (mean ± SEM)			Percentage of time spent in sleep stage (mean ± SEM)		
		CTRL	CNO	p value	CTRL	CNO	p value	CTRL	CNO	p value
NREM	**eYFP-CTRL**	3.14 ± 0.61	3.73 ± 0.74	0.47¤	11.81 ± 1.60	10.54 ± 1.76	0.25¤	48.76 ± 9.80	56.46 ± 4.86	0.88¤
	DREADD-G$_i$	3.53 ± 0.44	4.76 ± 0.74	0.08¥	7.36 ± 0.92	8.28 ± 1.16	0.18¥	47.56 ± 3.55	56.29 ± 4.85	0.10¥
	DREADD-G$_q$	3.78 ± 0.50	5.03 ± 0.69	0.74§	16.57 ± 4.87	8.03 ± 1.17	0.18§	52.45 ± 1.91	56.36 ± 4.21	0.86§
REM	**eYFP-CTRL**	0.78 ± 0.11	1.05 ± 0.24	0.69¤	2.49 ± 0.77	2.60 ± 0.68	0.36¤	3.00 ± 1.31	4.55 ± 1.34	0.40¤
	DREADD-G$_i$	1.10 ± 0.10	1.05 ± 0.21	0.12¥	2.92 ± 0.37	3.29 ± 0.52	0.70¥	5.43 ± 0.97	5.74 ± 1.50	0.36¥
	DREADD-G$_q$	0.92 ± 0.12	1.14 ± 0.09	0.32§	4.31 ± 1.13	3.15 ± 0.49	0.49§	5.43 ± 0.71	5.44 ± 0.92	0.63§

Table 2.2 *Effects of chemogenetic modulation of pFRG on respiratory disturbances.*

Chemogenetic modulation of pFRG following the systemic administration of CNO in transfected rats had no effect in the occurrence of respiratory disturbances. The rate of apneas and post-sigh (PS) apneas, as well as their duration was not affected by modulation of pFRG. All values are mean and standard error of the mean (SEM). Two-Way repeated measures ANOVA within individual factors (CTRL and CNO); in-between group factors (CTRL-eYFP, DREADD-Gi, DREADD-Gq). No significant main effects were resolved for in-between group comparisons (¤), within individual comparisons (¥) and interaction between within and in-between factors (§).

	Apneas/hr (mean ± SEM)			Avg. apnea duration (sec) (mean ± SEM)			Sighs/hr (mean ± SEM)		
	CTRL	CNO	p value	CTRL	CNO	p value	CTRL	CNO	p value
eYFP-CTRL	2.17 ± 0.64	2.45 ± 0.62	0.46¤	3.48 ± 0.27	3.26 ± 0.22	0.18¤	20.58 ± 2.06	17.83 ± 1.96	0.33¤
DREADD-G$_i$	3.29 ± 0.97	1.93 ± 0.32	0.36¥	3.37 ± 0.19	3.38 ± 0.26	0.52¥	22.49 ± 2.62	23.00 ± 1.76	0.84¥
DREADD-G$_q$	1.87 ± 0.32	1.66 ± 0.58	0.34§	3.00 ± 0.19	2.88 ± 0.20	0.86§	21.91 ± 1.17	23.29 ± 2.42	0.46§

	PS apneas/hr (mean ± SEM)			Avg. PS apnea duration (sec) (mean ± SEM)			PS apneas/Sighs (mean ± SEM)		
	CTRL	CNO	p value	CTRL	CNO	p value	CTRL	CNO	p value
eYFP-CTRL	9.45 ± 1.34	7.69 ± 1.72	0.25¤	3.84 ± 0.11	3.54 ± 0.18	0.44¤	0.47 ± 0.06	0.44 ± 0.08	0.30¤
DREADD-G$_i$	9.73 ± 1.75	10.37 ± 2.06	0.18¥	3.64 ± 0.22	3.75 ± 0.23	0.41¥	0.43 ± 0.08	0.48 ± 0.10	0.19¥
DREADD-G$_q$	7.32 ± 2.94	5.43 ± 1.56	0.19§	3.43 ± 0.12	3.35 ± 0.29	0.33§	0.26 ± 0.07	0.35 ± 0.06	0.19§

Chapter 3.   Mapping responses to focal injections of bicuculline in the lateral parafacial region identifies core regions for maximal generation of active expiration

3.1 Introduction

The neural control of respiration is a complex physiological process that requires precise coordination among multiple brainstem nuclei. One such nucleus, the preBötzinger Complex (preBötC), plays a crucial role in generating the inspiratory rhythm and pattern (Gray et al., 2001; Smith et al., 1991; Tan et al., 2008; Wang et al., 2014). In contrast, the lateral parafacial region (pFL), also referred to as pFRG in the initial studies, has emerged as an important neuronal structure containing neurons that are responsible for the generation of active expiration via the recruitment of expiratory musculature, such as the ABD muscles (de Britto & Moraes, 2017; Huckstepp et al., 2015; Pagliardini et al., 2011; Pisanski & Pagliardini, 2019). Although the involvement of the preBötC in respiration, as well as its origin, anatomical markers, and anatomical location has been extensively studied (Biancardi et al., 2023; Del Negro et al., 2018; Gray et al., 2001; Hayes et al., 2017; Tan et al., 2008; Wang et al., 2014; Yackle et al., 2017; Yang & Feldman, 2018; Yang et al., 2020), the expiratory oscillator remains a challenging structure to locate accurately due to the absence of a definite anatomical marker and the lack of its activation during experimental resting conditions (de Britto & Moraes, 2017; Magalhães et al., 2021; Pagliardini et al., 2011). Understanding the precise location and functional properties of the expiratory oscillator is crucial for unraveling the complete neural circuitry underlying respiratory control.

Previous research has employed a variety of techniques to study and elucidate this expiratory oscillator that include pharmacological disinhibition and excitation (Boutin et al., 2017; de Britto et al., 2020; de Britto & Moraes, 2017; Korsak et al., 2018; Magalhães et al., 2021; Pagliardini et al., 2011; Zoccal et al., 2018), as well as chemogenetic and optogenetic approaches (Huckstepp et al., 2015; Pagliardini et al., 2011; Pisanski et al., 2019). The coordinates used for the latter studies considered the core of the expiratory oscillator proximal to the caudal tip of the facial nucleus (VIIc) (-0.2 to +0.5 mm from VIIc). Interestingly, the use of chemogenetics to inhibit pFL at the level of the caudal tip of the facial nucleus (-0.3 to +0.3 mm from VIIc) was unable to achieve complete inhibition of the putative expiratory muscle output, with ABD recruitment still occurring

naturally during sleep, albeit at a diminished rate (Pisanski et al., 2019). Similarly, chemogenetic inhibition of pFL at +0.5 mm from VIIc decreased the intensity of the ABD signals obtained in response to bicuculline/strychnine injections, but did not silence it entirely (Huckstepp et al., 2015). This evidence could suggest that the expiratory oscillator extends beyond the limits of the viral expression achieved in said studies as proposed by Huckstepp et al., (2015). Intriguingly, other studies (Silva et al., 2019) located its core at more rostral coordinates (+0.3 to +1.0 mm from VIIc). This dichotomy in the coordinates used to study the functional properties of the expiratory oscillator demonstrates that the characterization of the anatomical and functional boundaries of pFL is incomplete.

To address this gap, we used focal injections along different rostrocaudal locations of the brainstem to create a functional map of the pFL. Bicuculline, a competitive antagonist of γ-aminobutyric acid type A (GABA-A) receptors, has been widely employed to study neuronal excitability and functional circuitry in various brain regions, including the pFL (Pagliardini et al., 2011). By strategically administering localized volumes of bicuculline at multiple rostrocaudal levels of the ventral brainstem, we aimed to selectively enhance the excitability of neurons driving active expiration, thereby revealing the precise location and functional boundaries of the expiratory oscillation within the pFL. Using a novel multidimensional cycle-by-cycle analysis specifically developed for this study, we characterized the effect that bicuculline elicited on the different phases of the respiratory cycle at each injection site, as the differences in area under the curve of the airflow, ∫DIA EMG and ∫ABD EMG, as well as the combined differences of these three respiratory signals using a novel phase-plane analysis. This approach enabled us to construct a comprehensive functional map of the pFL in conjunction with anatomical immunostaining techniques.

Our results indicate that the injection of bicuculline produced active expiration at all locations studied (-0.2 mm to +0.8 mm from VIIc). However, the strongest effects in terms of changes in tidal volume (V_T), minute ventilation (V_E) and differences in combined respiratory signals were observed at the two most rostral locations (+0.6 mm and +0.8 mm). Similarly, ABD activation lasted longer at these sites and the swiftest onset of the ABD response was observed at the +0.6 mm location. Interestingly, our multivariate analysis of the respiratory cycle permitted further differentiation of the response elicited in the two rostral locations, with the strongest deformations of the respiratory loop during late-Expiration (late-E) and post-Inspiration (post-I) with injections

at the +0.8 mm locations, whereas injections at the level of +0.6 mm producing more pronounced deformations of the respiratory cycle during the inspiratory phase. The use of the multi dimensional trajectory map will certainly enhance our understanding of the role that the expiratory oscillator plays in respiratory control. Additionally, it will provide a crucial foundation for future investigations into its modulation, plasticity, and potential therapeutic targets for respiratory disorders.

3.2 Methods

3.2.1 Experimental Subjects

Thirty-five adult male Sprague Dawley rats weighing 340.4 g ± 13.2 were used for the study. The rats were housed in a controlled environment with a 12-hour light-dark cycle and were allowed unrestricted access to food and water. All experimental procedures followed the guidelines set by the Canadian Council of Animal Care and received approval from the Animal Care and Use Committee (ACUC) of the University of Alberta (AUP#461).

3.2.2 Surgical Preparation

Prior to the experiment, the rats were initially anesthetized using 5% isoflurane in air for induction, followed by 1-3% isoflurane for maintaining a surgical plane of anesthesia. During this time, we cannulated the femoral vein to facilitate the gradual administration of urethane (1.5-1.7 g/kg body weight) for inducing permanent and irreversible anesthesia. We assessed the depth of anesthesia by monitoring the absence of the withdrawal reflex. We cannulated the trachea and used a flow head connected to a transducer (GM Instruments, UK) to detect respiratory flow. We provided supplemental oxygen (30%) throughout the experiment and connected a gas analyzer to the tracheal tube. The gas analyzer measured fractional concentration of O_2 and CO_2. Based on this and flow rate we calculated O_2 consumption. Paired electromyogram (EMG) wire electrodes (Cooner Wire, CA, USA) were inserted into the oblique ABD and diaphragm (DIA) muscles. The wires were connected to differential amplifiers (AM Systems, WA, USA), and we sampled the activity at a rate of 1kHz using the Powerlab 16/30 system (AD Instruments, CO, USA). We performed vagotomy by resecting a 2 mm portion of the vagus nerve at the mid-cervical level, and

the rats' body temperature was maintained at a constant level of 37±1°C using a servo-controlled heating pad (Harvard Apparatus, MA, USA).

3.2.3 Bicuculline Injections

Following the surgical preparation, we placed the instrumented rats in a prone position on a Kopf stereotaxic frame. We trimmed and aseptically cleaned the incision area and achieved access to the brainstem by partially removing the occipital bone. We determined the coordinates for injection into the ventral medulla with Bregma positioned 5 mm below lambda. The bicuculline/fluorobeads solution (n=28, Bicuculline: 200 µM in HEPES, Sigma-Aldrich) or saline/fluorobead (CTRL, n=7) was bilaterally pressure-injected into specific coordinates using a sharp glass micropipette (30 µm tip diameter) at a rate of 100 nL/min (total volume injected was 200 nL per side). Each rat was injected at a specific coordinate based on the following groups: -0.2 mm from the caudal tip of the facial nucleus (VIIc) (n=5), +0.1 mm from VIIc (n=7), +0.4 mm from VIIc (n=5), +0.6 mm from VIIc (n=6), +0.8 mm from VIIc (n=5), and CTRL (n=7). Prior to injections we recorded baseline activity for a period of 15 min following surgical procedures. During the injections, we took measures to ensure that the timing between the first and the second injection did not exceed 5 minutes and recorded the physiological responses induced by bicuculline for 20-25 min post second injection.

3.2.4 Histology Procedures

Upon completion of the experiments, we transcardially perfused the rats with saline (0.9% NaCl), followed by 4% paraformaldehyde in phosphate buffer. We then collected, postfixed, cryoprotected, and sectioned the brains in a cryostat (Leica, CM1950) to obtain 30 µm thick transverse slices. To prepare the brain tissue for immunohistochemistry, we washed the brain sections multiple times with phosphate-buffered saline (PBS) to remove the cryoprotectant solution. All immunostaining procedures were conducted at room temperature. We incubated the sections in a blocking solution (0.3% Triton X-100 and 10% normal donkey serum (NDS) in PBS) for 1 hour to enhance membrane permeability to antibodies and minimize nonspecific binding. After blocking, we incubated the tissue overnight with the primary antibody solution, which consisted of PBS, 1% NDS, and 0.3% Triton X-100. In order to identify specific brain structures relevant to this study, we used the following primary antibodies: anti-choline acetyltransferase

(ChAT; goat; 1:800; EMD Millipore, ON, Canada), anti-phox2b (phox2b; mouse; 1:100; Santa Cruz Biotechnology, TX, US), anti-cFos (cFos, rabbit, Cell Signaling Technology, MA, US), and anti-tyrosine hydroxylase (TH, chicken, EMD Millipore, ON, Canada). The next day, we washed the tissue three times in PBS and incubated it for 2 hours in a secondary antibody solution containing PBS, 1% NDS, and specific secondary antibodies (1:200; Cy3-donkey anti-goat; Cy5-donkey anti-mouse; Cy2-donkey anti-rabbit; rhodamine-red-donkey anti-chicken; Jackson ImmunoResearch Laboratories, PA, US). Following the incubation with the secondary antibodies, we washed the sections three times and mounted them with Fluorsave mounting medium (EMD Millipore, ON, Canada). We observed the slides under an Evos FL fluorescent microscope (Thermofisher Scientific, MA, US) and acquired TIFF files for cFos+ cell counting and analysis of the rostrocaudal, mediolateral, and dorsoventral coordinates of the injection sites using ImageJ. We examined serial sections with a 120 μm interval, spanning from 400 μm caudal to 1000 μm rostral to the caudal tip of the facial nucleus (VIIc). To group the animals according to the location of the injections, we calculated a 3D distance from the VIIc using the rostrocaudal, mediolateral, and dorsoventral coordinates of each injection site.

3.2.5 Data Acquisition and Analysis

EMG activity was amplified at x10 000 and filtered between 100 and 500 Hz (model 1700 A-M Systems, USA). The data was sampled at a rate of 1 kHz using the PowerLab 16/35 acquisition system and analyzed using LabChart7 Pro (ADInstruments), Excel 2013, Origin 9 (OriginLab Corp., Northampton, MA, USA), as well as custom scripts written in MATLAB (The Mathworks Inc.). All raw EMG data were digitally rectified and integrated using a time-constant decay of 0.08s. Respiratory airflow was further used to determine respiratory rate, V_T, and Ve. The tidal volume was obtained by integrating the airflow amplitude and converting it to milliliters using a five-point calibration curve (0.5–5 ml range).

Airflow and integrated EMG signals were standardized across rats by first zeroing signals in the rest period phases between breaths as recorded during baseline conditions and then converting the remaining amplitude values into standard deviation units (SD) based on a time-collapsed amplitude distribution. Data were tracked in time bins of 2-minute duration from the baseline period prior to injections and spanned 20 min of recording post-injection. Mean-cycle

measurements for each signal were computed by averaging across all cycles within a given time bin. To assess the changes within each of the phases of the breathing cycle, each mean-cycle was subdivided into the Late-E, inspiratory, Post-I, and resting phases using the zero-crossings of the mean airflow signal (Green lines, Figure 3.1 B). The inspiratory phase begins with an inward (positive going) intake of air as airflow increases above zero and ends when airflow crosses zero towards the negative direction. This negative going deflection begins the Post-I phase, which lasts until airflow returns to zero during the rest period. The Late-E phase is defined in two ways. In cases where a significant negative deflection in airflow was observed prior to inspiration, the late-E phase was determined to have begun when airflow decreased below zero and ended when airflow crossed back above zero to begin the subsequent inspiratory phase. When airflow did not decrease below zero prior to inspiration, as was often the case during baseline conditions, the late-E phase was determined as the last quarter of the expiratory period (Figure 3.1 B). The Area under the curve (AUC) was measured during baseline and was subtracted from the corresponding AUC of the response for each time bin (Figure 3.1 C). Note that areas calculated below the zero- (0) line, as would be expected from a negative airflow during expiration, yields negative AUC values. Any changes to the duration of the three respiratory phases, as well as changes to the entire respiratory period were independently assessed using the triggers described above.

We further contrasted the overall changes to the three respiratory signals elicited across injection locations by combining them into a multi-dimensional (3D) space (Figure 3.1 D). In a manner similar to respiratory pressure-volume loops, each point in time is defined as a dot in this 3D space based on the 3 simultaneous physiological measurements of respiration we recorded (airflow, together with the $\int DIA_{EMG}$, and $\int ABD_{EMG}$). Each respiratory cycle could then be plotted as a trajectory of points in this space, represented as a loop. Example loops for the baseline and the first 2-minute time bin of the elicited response are shown in Figure 3.1 D and are also projected onto separate 2D planes in Figure 3.1 E. Our approach was to measure how the trajectories of response loops changed relative to the baseline loop during each phase of the respiratory cycle, as per the color scheme (same as in Figure 3.1 B). Given these loops may be deformed as a result of changes to any one of the three signals which form the basis of this 3D space, this method determines the *total* extent to which breathing is altered in response to stimulation. We quantified changes to respiratory trajectories elicited by bicuculline injection using the sum of the "straight-line" or "Euclidean" distances between points on the response and baseline loops in each respiratory phase.

An example of the Euclidean distance between the peak of inspiration in baseline and response loops is shown in Figure 3.1 F (pink line). To compute this distance for all time points, we resampled the response to ensure that that baseline and response mean-cycles had the same number of comparison phase points in a given respiratory phase. Distances were then calculated between these baseline and response loops at each timepoint t using the Euclidean distance formula:

$$Euclidean\ Distance_t = \sqrt{AirDiff_t^2 + DiaDiff_t^2 + AbdDiff_t^2}$$

where AirDiff$_t$, DiaDiff$_t$ and AbdDiff$_t$ are the differences between the response and baseline mean-cycles at timepoint t. Averaging the distances measured at every timepoint in a given respiratory phase yields the mean Euclidean distance measure used in the analyses displayed in Figure 3.6 G.

We extended our multivariate analysis of respiration to account for the cycle-by-cycle variability in the recorded signals. At each timepoint, we compared how far away the response mean-cycle is from the baseline mean-cycle relative to the covariance across all baseline cycles. Thus, this measure can be interpreted as having units of standard deviation, as it describes how likely it is to observe the response given the distribution of baseline measurements gathered across many respiratory cycles. This measure is known as the Mahalanobis distance and is exemplified as the pink distance relative to the black cloud of points in the baseline mean-cycle of Figure 3.1 F. Similarly to above, this distance is computed for each timepoint t:

$$Mahalanobis\ Distance_t = \sqrt{(R_t - \mu_t)\Sigma_t^{-1}(R_t - \mu)'}$$

where R_t is the response mean-cycle at timepoint t, μ_t is the baseline mean-cycle at timepoint t, and Σ_t is the covariance of all baseline cycles at timepoint t. Similar to the Euclidean distance above, we the calculated Mahalanobis distances across all timepoints with each respiratory phase and then averaged them across cycles to assess the mean Mahalanobis distance.

3.2.6 Statistics

We tested the assumptions of homogeneity of variance and normal distribution using the Brown–Forsythe ($\alpha = 0.05$) and Shapiro–Wilk ($\alpha = 0.05$) tests, respectively. Comparisons between injection locations were carried out across time bins using a two-way repeated-measures analysis

of variance (two-way RM ANOVA; one repeated factor; $\alpha = 0.05$) where appropriate. In case of significant main effects, we conducted pairwise multiple comparisons post-hoc procedures (Bonferroni method; $\alpha = 0.05$). Analysis of the peak response across injection locations and in comparison to baseline, was done using a repeated measures analysis of variance (one-way repeated measures ANOVA; $\alpha = 0.05$). Upon finding significant main effects, we used Bonferroni post hoc test ($\alpha = 0.05$). In cases where assumptions of normality were rejected ($p < 0.05$), we compared responses across injection location via a Kruskal-Wallis test and following with a post-hoc Dunn test, adjusting the alpha value for multiple comparisons with Sidak's method.

3.3 Results

3.3.1 Histological Analysis

For each rat, we precisely identified the core of the injection sites by assessing the rostrocaudal coordinates obtained from sections containing fluorobeads. Based on the core coordinates, experiments were divided into 5 groups in which injection spanned from -0.2 mm caudal to the tip of the facial nucleus (VIIc) to +0.8 mm rostral to VIIc (as illustrated in Fig 2 B). It is noteworthy that all injections were consistently positioned ventrolateral to the facial nucleus, and there was no overlap observed between the fluorobead-marked injection sites and PHOX2B+ cells within the more ventro-medial retrotrapezoid nucleus (RTN), as depicted in Figure 3.2 A-B. Additionally, the injection sites were confirmed not to overlap with the soma of TH+ cells in either the caudal C1 or the more rostral A5 areas, as shown in Figure 3.2 A-B.

To assess the cellular responses surrounding the injection sites, we quantified both cFos+ and cFos+/PHOX2B+ cells within a defined region surrounding the fluorobead-marked areas in the pFL (as outlined in Figure 3.2 A). In rats injected with HEPES buffer (control group), we observed an average activation of 44.7 ± 4.0 cells per hemisection along the rostrocaudal axis of the ventral medulla (n=7). Among these activated cells, an average of 2.3 ± 1.0 cells per hemisection were also positive for PHOX2B, as illustrated in the inset of Figure 3.2 C. In contrast, rats injected with bicuculline displayed a distinct response pattern, characterized by a peak activation with an average of 104.5 ± 5.1 cFos+ cells localized at the core of each injection site (-0.2 mm = 89.7; +0.1mm = 123.1; +0.4mm = 110.2; +0.6mm = 98.3; +0.8mm = 101.2) (Figure 3.2C). Importantly, the number of cFos+ cells decreased to 44.8 ± 1.2 per section beyond the boundaries of the

injection area for each experimental group. On the other hand, the number of cFos+/PHOX2B+ cells remained consistent between the control (CTRL) animals (2.3 ± 1.0 cFos+/PHOX2B+ cells per hemisection) and those injected with bicuculline (2.4 ± 0.4 cFos+/PHOX2B+ cells). These findings strongly suggest that bicuculline specifically activated cells within the vicinity of the injection sites and did not spread and activate PHOX2B+ cells in the RTN area, beyond their baseline level of activity.

3.3.2 Characteristics of ABD signals across the rostrocaudal axis of the pFL

We successfully elicited ABD responses with the administration of bicuculline at all tested injection sites. The ABD response was most reliably triggered at locations rostral to the tip of VIIc. This observation is supported by the fact that the caudal location (-0.2 mm from VIIc) elicited responses in only 3 out of 5 rats, whereas all other groups consistently induced responses in all rats (n=5-7 rats /group). The elicited response was characterized by a late-E component in the ∫ABD$_{EMG}$ trace across all experimental groups (Figure 3.2 D), as well as a downward deflection in airflow, signifying forced exhalation of the respiratory reserve volume preceding inspiration (i.e., active expiration; Figure 3.2 D). Remarkably, in the most rostral groups (+0.6 and +0.8 mm rostral to VIIc), the ∫ABD$_{EMG}$ traces exhibited a tonic expiratory component, which preceded the late-E peak and was absent in the most caudal locations (-0.2 mm, +0.1 mm, and +0.4 mm). Additionally, 5 out of 6 rats in the group with injection sites at +0.6 mm rostral to VIIc, exhibited a post-I ABD peak, a feature that was absent in all other groups (Figure 3.2 D).

3.3.3 Temporal dynamics of the ABD response reveal a longer-lasting and fastest response at rostral locations

The temporal characteristics of the ∫ABD$_{EMG}$ signal elicited by bicuculline injections at different rostrocaudal locations exhibited notable variations. Overall, responses had a shorter duration in the most caudal locations (-0.2 mm; +0.1 mm; + 0.4 mm) compared to the rostral locations (+0.6 mm; +0.8 mm) (Figure 3.3 A). In all groups, the ABD response initiated following the second bicuculline injection, except at location +0.6 mm, where it commenced following the first injection and became more pronounced with the second injection (Figure 3.3 A). Across all groups, the most robust ABD responses, as measured by ∫ABD$_{EMG}$ amplitude, were observed within the first 2 min of the response, declining to zero in the last 2 min (18 min post-injection) in the most caudal groups

(-0.2 mm; +0.1 mm; + 0.4 mm). In contrast, these responses remained present, albeit weaker, in the most rostral groups (+0.6 mm; +0.8 mm) after 20 min from injection (Figure 3.3 B-C).

The coupling of the $\int$ABD$_{EMG}$ and $\int$DIA$_{EMG}$ signals, which reflects the robustness of the response and the coupling between inspiratory and expiratory oscillators, was notably weaker at the most caudal location (-0.2 mm = 0.6 ± 0.2) in comparison to the most rostral groups (+0.4 mm = 0.96 ± 0.02; +0.6 mm = 0.89 ± 0.05; +0.8 mm = 0.97 ± 0.02; One-Way ANOVA p = 0.015; Tukey -0.2 mm vs +0.4 mm: p = 0.024; -0.2 mm vs +0.6 mm: p = 0.048; -0.2 mm vs +0.8 mm: p = 0.029; Figure 3.3 D). Similarly, the ABD response duration was longer at the two most rostral locations (+0.6 mm = 17.6 ± 2.7 min; +0.8 = 17.1 ± 3.3 min) compared to the most caudal group (-0.2 mm = 2.4 ± 1.1 min; One-Way ANOVA p = 0.043; Tukey -0.2 mm vs +0.6 mm: p = 0.048; -0.2 mm vs +0.8 mm: p = 0.041; Figure 3.3 E). Lastly, the group with injection sites located at +0.6 mm initiated responses sooner than all other groups (-0.2 mm = 20.3 ± 13.4 sec; +0.1 mm = 32.5 ± 20.6 sec; +0.4 = 40.1 ± 28.7 sec; +0.8 = 23.1 ± 19.8 sec), with an average response delay of 88.7 ± 32.3 sec previous to the second injection (but after the first one), which is represented as negative values (One-Way ANOVA p= 0.041; Tukey -0.2 mm vs +0.6 mm: p = 0.039; +0.1 mm vs +0.6 mm: p = 0.040; +0.4 mm vs +0.6 mm: p = 0.045; +0.8 mm vs +0.6 mm: p = 0.049; Figure 3.3 F). In summary, these results underscore that injections at the most rostral locations (+0.6 mm and +0.8 mm) elicit more robust and prolonged ABD responses than the caudal location (-0.2 mm). Furthermore, bicuculline injections at +0.6 mm from VIIc initiated the fastest response, suggesting proximity to the cells responsible for ABD recruitment following bicuculline injection.

3.3.4 Bicuculline injection elicited stronger respiratory effects at the rostral locations

The ABD response elicited by bicuculline injection generated a late-E downward inflection in airflow that was absent in baseline conditions (Figure 3.4 A). We measured the late-E peak amplitude and area to assess the strength of the response across different rostrocaudal locations. On average, the late-E peak amplitude and area values reached a maximum between 2- and 4-min post-second injection for all rostrocaudal locations except the most rostral injection site (+0.8 mm from the tip of VIIc), which peaked between 6- and 8-min post-second injection (Figure 3.4 B,D). Although the late-E peak amplitude seemed to reach a higher maximum in the two most rostral groups (+0.6 mm = -0.033 ± 0.007 V; +0.8 mm = -0.027 ± 0.011 V), these values were not

significantly different when compared to the remaining locations (-0.2 mm= -0.014 ± 0.004 V; +0.1 mm = -0.021 ± 0.007 V; +0.4 mm = -0.023 ± 0.004 V; One-Way ANOVA p= 0.41; Figure 3.4 C). Similarly, the late-E peak area also seemed to reach a higher maximum in the two most rostral locations (+0.6 mm = -0.0056 ± 0.0010 V.s; +0.8 mm = -0.0047 ± 0.0019 V.s), but these values were not significantly different from the rest of the injection sites (-0.2 mm= -0.0014 ± 0.0007 V.s; +0.1 mm = -0.0035 ± 0.0015 V.s; +0.4 mm = -0.0038 ± 0.0011 V.s; One-Way ANOVA p= 0.30; Figure 3.4 E).

The injection of bicuculline along the rostrocaudal axis of the ventral medulla induced a drop in respiratory frequency in all the injection sites tested (Figure 3.4 F), but this drop in frequency was only significant in comparison to baseline in the two most caudal groups (One-Way repeated measures ANOVA p = 0.003; Bonferroni: -0.02 mm baseline vs injection, p = 0.03; +0.1 mm baseline vs injection, p = 0.005; Figure 3.4 G). The respiratory rate reached a minimum value of 37.08 ± 1.36 bpm (12% drop from baseline) at 2 min post-injection in the most caudal location (-0.2 mm), whereas the minimum respiratory frequency value was reached at 4 min for the middle groups (+0.1 mm = 37.2 ± 2.0 bpm – 17% drop from baseline; +0.4 mm = 40.1 ± 1.6 bpm – 9% drop from baseline) and 6 min for the most rostral injection sites (+0.6 mm = 38.6 ± 2.6 bpm – 10% drop from baseline; +0.8 mm = 39.1 ± 2.2 bpm – 11% drop from baseline; Figure 3.4 F). Interestingly, the duration of inspiration during the response was found to decrease in all groups relative to baseline respiration (T_i response = 0.279 ± 0.034s, T_i baseline = 0.318 ± 0.043s, Wilcoxon rank sum: Z = 3.24, p = 0.001), whereas the total expiratory time was observed to increase in all groups and remained elevated compared to baseline (T_E response = 1.313 ± 0.188s, T_E baseline = 1.029 ± 0.161s, Wilcoxon rank sum: Z = 4.49, p = 0.001). Overall, these results suggest that the most caudal locations (-0.2 mm and +0.1 mm) experienced a faster and more drastic drop in respiratory frequency following bicuculline injection, and this reduction in frequency was driven by an increase in expiratory period accompanied by a reduction in the inspiratory time.

The amount of inspired air per each breath, measured as V_T, increased when compared to baseline in all the injection sites tested except the most caudal location (-0.2 mm from VIIc) (One-Way repeated Measures ANOVA, p = 0.01; Figure 3.4 H-I). In all the groups, the increase in V_T peaked at 4 min post-injection (Figure 3.4 H). Of particular interest is that the peak V_T observed in the

69

+0.6 mm location (V_T = 10.8 ± 0.5 ml/kg – 29% increase from baseline) was higher than that observed in the two most caudal groups (-0.2 mm = 7.0 ± 0.4 ml/kg – 8% increase from baseline and +0.1 mm = 8.0 ± 0.3 ml/kg – 16% increase from baseline; One-Way ANOVA p = 0.01; Bonferroni p = 0.03; Figure 3.4 I). On the other hand, V_E decreased compared to baseline in the most caudal group (-0.2 mm = 255.4 ± 16.2 ml x min^{-1} x kg^{-1} – 12% drop from baseline, One-Way Repeated Measures ANOVA, p= 0.001), whereas at the +0.6 mm location, V_E increased following bicuculline injection (V_E = 414.3 ± 22.7 – 16% increase from baseline, One-Way Repeated Measures ANOVA, p = 0.001; Figure 3.4 J-K). Interestingly, the change produced in V_E after injection of bicuculline at the most rostral locations (+0.4 mm; +0.6 mm and +0.8 mm) was larger than that produced after injection at -0.2 mm from VIIc (One-Way ANOVA p = 0.0006, Bonferroni p = 0.0004; Figure 3.4 K). These results suggest that the V_E was mostly driven by the drop in respiratory frequency at the two most caudal locations (-0.2 mm and +0.1 mm), whereas V_T drove the increase in V_E observed in the most rostral groups (+0.4 mm; +0.6 mm; +0.8 mm), which resulted in a more drastic increase in V_E.

3.3.5 Injection of bicuculline decreased oxygen consumption at the rostral locations

To evaluate the metabolic effects of the respiratory changes induced by bicuculline injections along the rostrocaudal axis of the ventral medulla, we measured the amount of oxygen consumption in the experimental animals (V_{O2}). Overall, V_{O2} remained similar to baseline at the 3 most caudal locations (-0.2 mm; +0.1 mm and +0.4 mm; Figure 3.4 L-M) and dropped from baseline only at the most rostral sites (+0.6 mm and +0.8 mm) (One-Way Repeated Measures ANOVA p = 0.0001). Similarly, the minimum V_{O2} achieved at the rostral groups (+0.6 mm = 11.8 ± 0.8 ml x min^{-1} x kg^{-1} – 33% drop from baseline and +0.8 mm = 12.2 ± 6.1 ml x min^{-1} x kg^{-1} – 25% drop from baseline) was different from the values achieved at the most caudal locations (-0.2 mm = 17.3 ± 3.3 ml x min^{-1} x kg^{-1} – 10% drop from baseline; +0.1 mm = 17.6 ± 1.3 ml x min^{-1} x kg^{-1} – 17% drop from baseline; One-Way Repeated Measures ANOVA p = 0.0001, Bonferroni p = 0.005; Figure 3.4 M). Additionally, the ratio of V_E/V_{O2} remained unchanged from baseline following bicuculline injection, except at the two most rostral locations, where it increased (+0.6 mm and +0.8 mm) (One-Way Repeated Measures ANOVA p = 0.001; Figure 3.4 N-O). The maximum V_E/V_{O2} was achieved at 6-8 min post-second injection at the two most rostral locations (+0.6 mm = 34.8 ± 3.0 – 73% increase from BL; +0.8 mm = 38.7 ± 12.8 – 82% increase from

baseline; Figure 3.4 N), and these values were different from the values observed at the two most caudal groups (-0.2 mm = 20.0 ± 6.7 – 3% increase from baseline and +0.1 mm = 18.7 ± 2.8 – 15% increase from BL; One-Way ANOVA p = 0.0006, Bonferroni p = 0.003; Figure 3.4 O). In summary, these results suggest that bicuculline injection and the resulting respiratory effects led to a reduction in oxygen consumption, especially at the +0.6 mm and +0.8 mm locations. Furthermore, the reduction in V_{O2} paired with the increases in V_E observed at the most rostral injection sites (+0.6 mm and +0.8 mm), resulted in hyperventilation, an effect which was not observed in the two most caudal groups (-0.2 mm and +0.1 mm).

3.3.6 Rostral bicuculine injection induces more prominent changes to all phases of the respiratory cycle

To further differentiate the responses elicited by bicuculine injections at each location along the rostrocaudal axis of the ventral medulla, we subdivided our analysis by respiratory phase (late-E, inspiratory, and post-I) and measured the differences in the area of respiratory signals (airflow, ∫DIA_{EMG} and ∫ABD_{EMG}) as per the algorithm described in the methods section (Figure 3.5 A-C).

Injections at all locations induced negative deflections in the airflow signal (Figure 3.5D) and were concomitant with potent increases to the ∫ABD_{EMG} within the late-E phase (Figure 3.5 D,F), whereas there was no change in ∫DIA_{EMG} signal during this phase (Figure 3.5 E). The observed differences tended to be more prominent in rostral locations and tended towards significance ($p <$ 0.1) when comparing the late-E responses from the +0.6mm and +0.8mm injection groups to control injections for the entire duration of the 20-minute post-injection response. The expiratory airflow reached significance ($\alpha = 0.05$) when comparing the second most rostral location (+0.6mm) relative to control injections at timepoints from 4 min (KW test: $H(5) = 14.66$, $p = 0.012$, Dunn: p , 0.001) to 12 min post-injection (KW test: $H(5) = 18.35$, $p = 0.003$, Dunn: $p < 0.001$; Figure 3.5D). Moreover, airflow responses were more negative following bicuculline injections in the +0.6mm group compared to the -0.2mm group, and remained different at several timepoints from 8 min (KW test: $H(4) = 11.41$, $p = 0.022$, Dunn: $p < 0.001$) to the last 20 min of the post-injection period (KW test: $H(4) = 10.65$, $p = 0.031$, Dunn: $p = 0.002$; Figure 3.5 D). In a similar manner, increases in the ∫ABD_{EMG} response differed relative to those elicited by control injections only for the 2 most rostral injection locations (+0.6mm, +0.8mm) at timepoints from 6 min (KW test: $H(5) = 16.23$, p

= 0.006, Dunn: +0.6mm: $p < 0.001$; +0.8mm: $p = 0.002$) to 12 min (KW test: $H(5) = 20.81$, p <0.001, Dunn: +0.6mm: $p < 0.001$; +0.8mm: $p < 0.001$; Figure 3.5 F). Correspondingly, the increases in $\int ABD_{EMG}$ activity evoked by these rostral locations (+0.6mm: Purple, +0.8mm: Orange) were significant as compared to the response at the most caudal location (-0.2mm: Red) for a similar range of timepoints from 8 min (KW test: $H(4) = 14.60$, $p = 0.006$, Dunn: +0.6mm: $p < 0.001$; +0.8: $p = 0.002$) to 14 min (KW test: $H(4) = 13.93$, $p = 0.008$, Dunn: +0.6mm: $p = 0.002$; +0.8mm: $p < 0.001$) with the +0.8mm group remaining elevated at 16 min (KW test: $H(4) = 13.56$, $p = 0.009$, Dunn: +0.8: $p = 0.002$; Figure 3.5 F). Thus, our results in the Late-E phase demonstrate that the rostral regions of the ventral medulla are the most sensitive to bicuculline-induced increases in expiratory airflow, presumably elicited via a prominent activation of ABD activity.

For the inspiratory phase, bicuculline injections evoked strong increases in the respiratory airflow and $\int DIA_{EMG}$ signal, which were strongest in the rostral locations (+0.6mm, +0.8mm) and relatively weaker in more caudal locations (-0.2mm). Inspiratory airflow was increased relative to control injections compared to the +0.6mm group for timepoints extending from 2 min (KW test: $H(4) = 13.25$, $p = 0.021$, Dunn: $p < 0.001$) to 12 min post-injection (KW test: $H(4) = 14.58$, $p = 0.012$, Dunn: $p = 0.001$; Figure 3.5 D). Unlike the effects noted above within the Late-E phase, airflow increases in this group were found to only reach significance for a shorter portion of the response from 10 min (KW test: $H(4) = 10.50$, $p = 0.033$, Dunn: $p = 0.004$) to 12 min (KW test: $H(5) = 10.93$, $p = 0.027$, Dunn: $p = 0.003$) post-injection when compared to the +0.4mm group (Figure 3.5 D). $\int DIA_{EMG}$ activity did not differ when compared between injection locations or to control injections, despite the increases in mean $\int DIA_{EMG}$ area in the +0.6mm and +0.8mm injection groups which peaked early in the time course of the response and are visible in Figure 3.5 E. Contributions of the ABD muscle to the respiratory changes during inspiration (Figure 3.5 F, inspiratory phase) were determined to be negligible as the raw ABD_{EMG} is not active during this phase and the remaining signal in the $\int ABD_{EMG}$ can be accounted for by exponential decay induced by the integration algorithm used to pre-process these signals (see methods section). These results illustrate that the increases in inspiratory airflow and $\int DIA_{EMG}$ activity evoked by bicuculline injections are stronger when targeting more rostral injection locations. However, these changes are relatively weak and, on average, remain altered for a much shorter period of time relative to the effects noted above for the Late-E phase.

Negative deflections in the airflow signal during the post-I phase were observed in several responses and were most pronounced in the 2 most rostral injection groups consistent with the results above (Purple and Orange, Figure 3.5 D). However, the area-under-the-curve measure used here to quantify changes in expiratory airflow relative to baseline did not reach the level of significance at $\alpha = 0.05$ when comparing injection locations as was described above for the other respiratory phases. Bicuculline injections into the most rostral group (+0.8mm: Orange) did, however, evoke substantial increases in $\int ABD_{EMG}$ activity during the post-I phase which were elevated during the 6 minute (KW test: $H(4) = 10.37$, $p = 0.035$, Dunn: $p = 0.002$) and 16 minute time bins (KW test: $H(4) = 9.52$, $p = 0.049$, Dunn: $p = 0.001$) when compared to injections into the most caudal group (-0.2mm). These effects were unlikely to be related to any changes in the DIA signal, as the DIA muscle activity is quiescent during the post-I period (Figure 3.5 A) and the $\int DIA_{EMG}$ is contaminated by the pre-processing as noted above for the ABD muscle during inspiration (see methods section).

Altogether, the area-under-the-curve analysis in Figure 3.5 shows that airflow is substantially altered in all 3 phases of the respiratory cycle and the ABD muscle is strongly activated in several groups in the late-E and post-I periods with injections of bicuculline along the pFL axis. Importantly, these effects are stronger when targeting the rostral areas of the pFL (+0.6mm and +0.8 mm from VIIc) compared to injections that target the more caudal regions.

3.3.7 Bicuculline responses following injections along the rostrocaudal axis of the ventral medulla can be differentiated by the deviations of their 3D trajectories at different phases of the respiratory cycle

We next sought to determine whether responses to bicuculline injections across the rostrocaudal axis of the pFL could be more precisely differentiated from each other when combining the responses in all three recorded signals (airflow, together with $\int DIA_{EMG}$ and $\int ABD_{EMG}$) evoked within the periods of late-E, inspiration, and post-I. Our approach was to represent all three signals as axes in a 3-dimensional space wherein each point corresponds to an individual timepoint during our recordings. When plotting the measurements across an entire respiratory cycle, this multidimensional representation resembles a looped trajectory as shown in Figure 3.1 D for cycles recorded during the baseline and post-injection periods. Indeed, each phase of the cycle (late-E,

inspiration, and post-I) could be recognized as a particular region along the 3D trajectory. Inspiration, for example, occupies the space where airflow and $\int DIA_{EMG}$ are positive (Figure 3.1 D: red). In baseline conditions, the loop is largely confined to the plane defined by the airflow-$\int DIA$ axes, as the ABD muscles are not activated during resting states (Figure 3.1 E, left). Following bicuculline injections, respiratory loops became more complex, involving marked perturbations occurring in this first plane, together with novel deformations extending along the $\int ABD_{EMG}$ axis as shown in the right-hand plane in Figure 3.1 E, described by airflow and the $\int ABD_{EMG}$. The relative amplitudes of these complex deviations from the baseline cycle could then be used to characterize the degree of change caused by our injections across pFL sites.

Figures 3.6 A-E demonstrate how the trajectories computed during the baseline (shown in black) are altered as the response evolves across each time bin spanning the full 20-minute post-injection period for all injection locations. Supplementary videos of each example recording in Figure 3.6, along with their cycle-by-cycle variability, further clarify their 3D shape as the trajectory is rotated about the $\int DIA_{EMG}$ axis (Supplementary Materials 1-5). We noted several key deformations to baseline loops including a "bulb" of activation on the outermost edge of the loop during the peak of inspiration when airflow is at its maximum. These "bulbs" are similarly confined to the $\int DIA_{EMG}$-airflow axis as both of these signals are involved in shaping their overall prominence. Baseline loops are also perturbed during the late-E period as a result of $\int ABD_{EMG}$-airflow activation which can be seen as "tails" which extend upwards in the right-most plots of Figure 3.6 A-E. Abdominal-airflow activation during the post-I period manifests as an upwards "foot-like" extension of the cycle in left-most portion of the Figure 3.6 A-E, most prominently displayed in the representative recording of Figure 3.6 D. The example trajectories in Figure 3.6 A-E demonstrate how the deformations in each phase can be used as features to distinguish the responses of each injection location.

Consistent with our analyses above, the late-E tails of the response loops elicited by caudal injection locations are relatively smaller compared to those observed in rostral locations (Figure 3.6 A). Moreover, these "tails" in the -0.2mm, +0.1mm, and +0.4mm groups last for a shorter duration than the two most rostral locations as can be determined by their more bluish-yellowish color (Figure 3.6 A-E: rightmost panel). Inspiratory bulbs appear to be more similar across groups and are most prominent in the +0.6mm group (Figure 3.6 A-E: middle panel). Lastly, post-I "feet"

are largely absent in the example responses of the three most caudal groups (-0.2mm, +0.1mm, +0.4mm) and are particularly noticeable in the +0.6mm and +0.8mm groups.

Quantifying the extent of these 3 features as the Euclidean distance between bicuculline injection and baseline in each respiratory phases is displayed in Figure 3.6 F. Compared to control injections of HEPES buffer, bicuculline evoked pronounced Late-E "tails", as well as inspiratory "bulbs", and post-I "feet" in all injection groups which lasted throughout the 20 min response, with the notable exception of the most caudal group (-0.2mm) which returned to a baseline trajectory by 8 min post-injection (Figure 3.6 G). Consistent with the results in Figure 3.5, the most rostral injections at +0.6mm and +0.8mm elicited the largest Late-E deformations. The 3D approach applied here further differentiated the responses of these two groups, as the Late-E "tails" of the +0.6mm group were longer than those observed in the -0.2mm group early in the response from 8 min (KW test: $H(4) = 12.22$, $p = 0.016$, Dunn: $p < 0.001$) to 12 min (KW test: $H(4) = 12.34$, $p = 0.015$, Dunn: $p = 0.002$), while those in the +0.8mm group peaked later in the response and were longer than in the -0.2mm group from 12 min (KW test: $H(4) = 12.34$, $p = 0.015$, Dunn: $p = 0.001$) to 16 min (KW test: $H(4) = 10.89$, $p = 0.028$, Dunn: $p = 0.001$; Figure 3.6 G). These results are consistent with the observations in Figure 3.3 F, which indicate that responses in the +0.6mm group begin earlier relative to other groups. Moreover, the +0.6mm group produced the largest deformations to the inspiratory "bulb" which were greater than those in the -0.2mm group from 8 min (KW test: $H(4) = 12.59$, $p = 0.013$, Dunn: $p < 0.001$) to 14 min (KW test: $H(4) = 10.27$, $p = 0.036$, Dunn: $p = 0.001$) (Figure 3.6 G). On the contrary, the largest post-I "feet" were observed in the +0.8mm group and were greater than the -0.2mm group from 4 min (KW test: $H(4) = 10.01$, $p = 0.040$, Dunn: $p = 0.002$) to 16 min (KW test: $H(4) = 9.70$, $p = 0.046$, Dunn: $p = 0.001$), excluding at the 10 minute (KW test: $H(4) = 8.93$, $p = 0.063$) and 14 minute time bins (KW test: $H(4) = 8.10$, $p = 0.088$; Figure 3.6 G).

As demonstrated in the representative graphs in Figure 3.6 A-E, the variability of the respiratory trajectories within the baseline or response periods (shown as clouds around the trajectory "loop"), differs between experiments. To account for the impact of this variability on our quantification of trajectory deformations, we computed the mean Mahalanobis distance within the late-E, inspiratory, and post-I phases (see methods). Our results revealed a gradient of response intensities relative to respiratory variability, with the two most rostral groups producing the strongest

deformations to breathing trajectories (Figure 3.6 H). Similar to our results above, these groups differed in the time course and relative strength of their responses in each phase. Injections at +0.6mm produced more pronounced late-E "tails" compared to caudal injection responses from 6 min (KW test: $H(4) = 11.80$, $p = 0.019$, Dunn: $p = 0.001$) for 12 min (KW test: $H(4) = 12.24$, $p = 0.016$, Dunn: $p = 0.001$; Figure 3.6 H). Late-E "tails" from the +0.8mm group were more prominent than "tails" evoked by caudal bicuculline injections for much greater proportion of the 20minute response compared to the +0.6mm group, ranging from 6 min (KW test: $H(4) = 11.80$, $p = 0.019$, Dunn: 0.002) to 20 min post-injection (KW test: $H(4) = 11.01$, $p = 0.026$ Dunn: $p < 0.001$; Figure 3.6 H). Deformations to the inspiratory "bulb" relative to respiratory variability were larger in the +0.6mm group compared to caudal responses and peaked at the 12minute time bin post-injection (KW test: $H(4) = 10.63$, $p = 0.031$, Dunn: $p = 0.002$)(Figure 3.6 H). In contrast, the extent of post-I "feet" was greater in the +0.8mm group than the -0.2mm group from 6 min (KW test: $H(4) = 11.00$, $p = 0.027$, Dunn: $p = 0.002$) to 20 min (KW test: $H(4) = 10.74$, $p = 0.030$, Dunn: $p < 0.001$), where as the extent of post-I "feet" in the +0.6mm group was greater than in caudal injections only at the 8 minute (KW test: $H(4) = 11.65$, $p = 0.020$, Dunn: $p = 0.002$) and 12 minute time bins (KW test: $H(4) = 12.23$, $p = 0.016$, Dunn: $p = 0.001$). Thus, while response intensity in all respiratory periods was strongest in the two most rostral injection groups, overall changes in the late-E and post-I period were strongest in the +0.8mm group, while changes in inspiration were strongest in the +0.6mm group.

3.4 Discussion

In this study, our primary aim was to investigate the rostrocaudal distribution of the source of active expiration within the lateral parafacial region (pFL). To accomplish this objective, we used bicuculline, a GABA-A receptor antagonist known for its ability to disinhibit pFL cells (de Britto & Moraes, 2017; Huckstepp et al., 2015; Pagliardini et al., 2011; Silva et al., 2019). Bicuculline was administered at various rostrocaudal coordinates, and we methodically assessed the resulting respiratory responses to pinpoint the location within this region that induced the most significant and relevant changes to the respiratory cycle. Our findings offer valuable insights into the neural circuitry governing active expiration in the brainstem, with a particular focus on less-explored, more rostral areas of the pFL.

3.4.1 Histological Analysis

We adopted a stereological approach to identify the central region of the injection sites by visualizing sections containing fluorobeads. Experimental subjects were categorized based on the proximity of the injection sites, spanning from -0.2 mm to +0.8 mm from VIIc. We took measures to ensure that injections were positioned ventrolateral to the facial nucleus (VIIc) and did not overlap with PHOX2B+ cells within the more ventromedial retrotrapezoid nucleus (RTN). Evaluation of cellular activity following bicuculline activation, as measured by cFos staining, confirmed minimal baseline activity of the PHOX2B+ cells in all groups as compared to the control group. These results confirm very limited mediolateral spread of the drug from the core site of injection and support previous findings indicating that PHOX2B is not a marker for the expiratory oscillator (de Britto & Moraes, 2017; Magalhães et al., 2021).

3.4.2 Characteristics of ABD Signals

Our efforts successfully elicited expiratory ABD responses and active expiration at all tested injection sites, consistent with previous reports (Boutin et al., 2017; de Britto et al., 2020; de Britto & Moraes, 2017; Huckstepp et al., 2015; Huckstepp et al., 2016; Huckstepp et al., 2018; Magalhães et al., 2021; Pagliardini et al., 2011; Silva et al., 2019; Zoccal et al., 2018). Previous work has primarily examined the core of the pFL at locations ranging from -0.2 mm to +1.0 mm from the caudal tip of the facial nucleus, a range similar to the one explored in the current study (-0.2 mm to +0.8 mm from VIIc). However, it is important to note that those studies have traditionally used the presence or absence of active expiration in response to a stimulus as the only measure to determine the location of the pFL. Our study reveals that this metric is not the most accurate in determining the closest proximity to the pFL core, as we found that all locations within that range in which injections were made exhibited active expiration. Consequently, we employed a combination of diverse respiratory measures to assess the injection site that induced the most robust respiratory effect.

Remarkably, the ABD response was consistently generated at locations rostral to VIIc, aligning with previous observations that did not find a reliable triggering of the ABD response at caudal positions ranging from -0.2 mm to -0.4 mm from VIIc (Pagliardini et al., 2011). This response was characterized by a late-E component at all rostrocaudal locations and, in the most rostral groups

(+0.6 mm and +0.8 mm from VIIc), an additional tonic post-I component that was absent in the injections at more caudal locations. Although the configuration of the ABD response, whether late-E only, tonic, or a combination of the two, has not been extensively discussed in the literature, these distinctions may provide valuable insights into the involvement of distinct neuronal circuits in mediating the ABD response. For example, sample traces from the injection of bicuculline/strychnine from 0 to +1.0 mm from VIIc with 4-5% CO_2 exposure exhibited a tonic ABD response throughout the entire expiratory phase (without post-I or late-E peaks) (Silva et al., 2019), whereas sample traces from injections spanning from -0.2 mm to +0.4 mm from VIIc suggest a combination of tonic and late-expiratory ABD responses (de Britto & Moraes, 2017; Pagliardini et al., 2011). Interestingly, the latter studies also observed tonic increases in ABD_{EMG} (without a late-expiratory peak), but only during baseline conditions and not in response to drug injection. In our study, we also observed a post-I ABD activation that only appeared at the +0.6 mm location. This post-I peak was previously observed in neonate rats (postnatal day 5) during ABD activation occurring throughout apneic periods induced by systemic fentanyl injection (Janczewski et al., 2002). A similar biphasic pattern (late-E/post-I) was also observed in facial nerve recordings of *in vitro* preparations and associated with neuron activity in the parafacial area (Onimaru & Homma, 2003; Onimaru et al., 2006). The presence of these unique response features at different rostrocaudal locations suggests a complex interplay among neural populations within the ventral medulla, necessitating further investigation beyond the scope of the present study.

3.4.3 Temporal dynamics of the ABD response reveal a longer-lasting and shortest latency response at rostral locations

The temporal dynamics of the ABD response exhibited significant variations along the rostrocaudal axis. Responses at rostral locations displayed prolonged durations and stronger coupling with DIA signals compared to caudal locations. Previous research employing bicuculline injections to induce active expiration have reported an increase in the coupling of ABD/DIA signals +0.1mm to +0.3 mm from VIIc in juvenile rats (de Britto & Moraes, 2017). Similarly, we observed good ABD/DIA coupling at locations rostral to +0.1 mm. Such coupling has been documented in other studies as an indicator of the robustness of the ABD response, either during hypercapnia/sleep or chemogenetic modulation during sleep (Leirão et al., 2018; Pisanski et al., 2019). Therefore, in our study, we used it as a measure of the strength of the achieved ABD

activation. Additionally, prior studies have indicated that the duration of effects induced by bicuculine/strychnine injections at locations spanning from -0.2 mm to +1.0 mm from VIIc can range from 16 to 30 min (Pagliardini et al., 2011; Silva et al., 2019). However, these studies did not specify whether there were disparities in the duration of ABD responses along the rostrocaudal axis. In our study, we have conclusively established that there are indeed variations in the robustness (as denoted by ABD/DIA coupling) and duration of ABD responses, with the more rostral locations (+0.6 mm and +0.8 mm from VIIc) yielding the most potent responses in this regard. Importantly, the group with injection sites at +0.6 mm rostral to VIIc exhibited the swiftest response onset, suggesting the closest proximity to, or the largest density of, the cells responsible for ABD recruitment following bicuculline injection. Given that the total number of cFos+ cells did not vary across injection sites, it is conceivable to infer that the rostral pFL is in the closest proximity to the cells responsible for the generation of active expiration.

3.4.4 Bicuculline injection elicited stronger respiratory effects at rostral locations in the pFL

Bicuculline injections induced significant alterations in a number of respiratory parameters, reminiscent of previous studies exploring the effects of bicuculline/strychnine injections in the ventral medulla (de Britto & Moraes, 2017; Pagliardini et al., 2011; Silva et al., 2019). We observed a drop in respiratory frequency concomitant with the emergence of ABD recruitment in the caudal locations (-0.2 mm, +0.1 mm), similar to what was observed in those locations through pharmacological activation of pFL (Boutin et al., 2017; Pagliardini et al., 2011). However, in the most rostral locations in our study (+0.4 mm, +0.6 mm, +0.8 mm), the respiratory frequency remained unchanged. This dichotomy in the frequency response despite the presence of ABD recruitment in both cases may suggest that the slowing of the respiratory period in the most caudal locations may be a consequence of disinhibition of the adjacent Bötzinger complex. Additional evidence to support this view is that the nadir of respiratory frequency was achieved at increasing periods of time as the injections were located increasingly more rostrally, with the most caudal injection reaching the minimum respiratory frequency at 2 min post-injection, while at the most rostral injection site, the minimum respiratory frequency was observed at 6 min.

On the other hand, V_T increased by 16-29% in all the studied locations except -0.2 mm, similar to what was observed previously with activation of the pFL at locations ranging from -0.2 mm to +0.4 mm (Boutin et al., 2017; Pagliardini et al., 2011). However, minute ventilation increased above baseline at the +0.6 mm location in our study, whereas it decreased at the -0.2 mm location and remained unchanged in the rest of the sites. These results are in agreement with previous observations, where V_E remained unchanged at caudal locations after bicuculline injection (-0.2 mm to +0.4 mm) (Pagliardini et al., 2011). However, it is important to highlight the absence of studies that have measured V_T and V_E after eliciting active expiration at more rostral locations (+0.6 mm to +0.8 mm) (Silva et al., 2019). These results emphasize that the rostrocaudal organization of the pFL is not as simple as previously thought and particularly highlights the importance of studying more rostral locations that have previously been neglected.

3.4.5 Injection of bicuculline decreased oxygen consumption at the rostral locations

This research also explored the metabolic consequences of bicuculline-induced respiratory changes. We observed a decrease in V_{O2} at the most rostral locations (+0.6 mm, +0.8 mm), which were also the sites where we observed the largest changes in V_T and V_E produced by the injection of bicuculline. It is important to note that these changes in V_T and V_E were not due to physiological needs and, therefore, could be considered a form of artificial hyperventilation that would cause a drop in arterial pCO_2 (Md Fau - Hazzledine & Hazzledine, 1963) and affect the gas exchange processes in the blood and peripheral tissues to reduce V_{O2}. Alternatively, the abdominal recruitment induced by bicuculline might not only increase V_T and V_E but might also facilitate respiratory mechanics *in vivo* (Bosc et al., 2010; Giordano, 2005; Haupt et al., 2012; Ninane et al., 1992; Ninane et al., 1993), reducing the work of breathing and, subsequently, causing a reduction in O_2 consumption. This remains to be determined, however.

3.4.6 Rostral pFL bicuculline injections induces more prominent changes to all phases of the respiratory cycle

Here we introduced a novel, area-under-the-curve (AUC) analysis algorithm, aimed at dissecting the respiratory changes evoked within each phase of the respiratory cycle (late-E, Inspiration, post-I) as a result of the locale of injections and relative to baseline conditions for each of the airflow, DIA , and ABD signals. This method revealed that the two most rostral injection sites elicited the

most robust activation of ABD activity and induced the most significant alterations in expiratory airflow during both the late E and post-I phases. Similarly, during the inspiratory phase, rostral injections generated the most pronounced changes in inspiratory airflow and DIA activity - particularly when positioned +0.6mm from the VIIc. These findings align with the observed increases in tidal volume depicted in Figure 3.4 H-I at those specific locations. Moreover, in the post-I phase, we also observed the most prominent negative airflow deflections at the most rostral injection sites, corresponding to concurrent ABD activation during that same timeframe.

By applying this novel analytical approach, which, to the best of our knowledge, has not been previously employed in research evaluating ABD responses triggered by pFL activation (Boutin et al., 2017; de Britto & Moraes, 2017; Huckstepp et al., 2015; Huckstepp et al., 2016; Huckstepp et al., 2018; Magalhães et al., 2021; Pagliardini et al., 2011; Silva et al., 2019; Zoccal et al., 2018), we were able to reveal disparities in the AUC of ABD and airflow signals. These disparities, which went undetected with the analyses shown in Figure 3.4B to E, were particularly evident during the late-E and post-I periods. Furthermore, the division of the response into three distinct respiratory phases enabled a more precise assessment of how targeted stimulation affects a particular phase of the respiratory cycle, which could be used in future research to provide valuable insights into the underlying neural mechanisms of respiratory control.

3.4.7 Bicuculline responses following injections along the rostrocaudal axis of the ventral medulla can be differentiated by the time course and total extent of respiratory activation during late-E, inspiration and post-I phases.

Our results certainly indicate that bicuculline injections at various pFL locations induce a complex set of interactions between DIA and ABD muscle activation, as well as changes in airflow across the inspiratory and expiratory phases of respiration. Our final goal was to develop an algorithm which could accurately represent the complete "framework" of respiratory activation across each recorded signal with respect to each these phases. To this end, we introduced another novel analysis method that tracked the multivariate variations occurring throughout the respiratory cycle. We were able to visualize and highlight a number of features of the respiratory cycle including late-E "tails", inspiratory "bulbs" and post-I "feet" that allowed us to characterize alterations that are specifically relevant to active expiration. Given that this analysis is designed to maintain a

consistent representation across conditions within experiments, these features can be catalogued into a "framework" of the breathing cycle during both baseline and post-injection conditions. Thus, this method is both sensitive to subtle changes in the activations of each component signal, but also more importantly, it is highly robust to the variability inherent in the acquisition of respiratory physiological measurements *in vivo*.

By quantifying the respiratory cycle in terms of 3D measures of distance we were able to differentiate between the rostral and caudally evoked responses, as well as differences between the two most rostral locations which were previously undetected in the standard analyses as presented in Figure 3.4 B-E. Particularly, our findings were consistent with the other analyses applied here with regards to the significantly larger extent of respiratory loop distortions in the two most rostral positions in comparison to the more caudal injections. Furthermore, it was observed that injections in the +0.8mm group produced the highest amplitude changes to the late-E "tails" which also persisted for a more extended duration. Injections at this location also produced post-I "feet" for a longer period of time. Conversely, the most prominent inspiratory "bulbs" were observed in the +0.6 mm group, aligning with the most substantial changes in V_T observed in Figure 3.4 H-I.

Collectively, these results imply that while the combined effects of bicuculline injection on the respiratory cycle were most pronounced at the two most rostral positions, there were slight variations in the effects exhibited during each respiratory phase at this level of the ventral medulla. These nuanced effects may suggest differences in the functional characteristics, phenotypes and projections of cell populations at these specific coordinates. It is worth noting that the pFL neurons responsible for active expiration are typically quiescent in adults at rest (de Britto & Moraes, 2017; Magalhães et al., 2021; Pagliardini et al., 2011), making their phenotypic and functional characterization challenging. Recent research has indicated that the pFL cells exhibiting late-E firing during hypercapnia-induced active expiration are characterized as glutamatergic, phox2b-negative and NMB-negative, and possess TASK, GPR4, hyperpolarization-activated, cyclic nucleotide-gated, T-type Calcium, and twik related K+ leak channels, while they lack sodium persistent current channels (Magalhães et al., 2021). However, these observations were made in neurons situated closer to the tip of the facial nucleus in juvenile rats. It will be important to investigate now whether phenotypic and electrical properties of neurons at more rostral positions share the same identity.

3.4.8 pFL or RTN?

An ongoing debate centers on whether the neurons responsible for the generation of ABD recruitment are an independent oscillator composed of PHOX2B-, late-E firing neurons (pFL) (de Britto & Moraes, 2017; Magalhães et al., 2021; Pagliardini et al., 2011; Pisanski & Pagliardini, 2019) or part of the PHOX2B+/NMB+ chemosensitive neurons of the RTN/ventral paraFacial region (Abbott et al., 2011; George et al., 2020). While there is evidence that specific stimulation of PHOX2B+/NMB+ neurons causes ABD activity and active expiration (Abbott et al., 2011; George et al., 2020), these studies have not shown recordings from late-E PHOX2B/NMB+ neurons in their investigations. However, there is concrete evidence of the existence of PHOX2B-negative late-E firing neurons that are activated in response to bicuculline injections in the ventral medulla (de Britto & Moraes, 2017; Magalhães et al., 2021; Pagliardini et al., 2011) while PHOX2B/NMB+ chemosensitive neurons may send tonic excitatory drive to the expiratory oscillator when activated. Because our anatomical results show very little PHOX2B/cFos+ staining at injections sites rostral to +0.1 mm, is fair to conclude that the ABD activity generated at that level is likely not the direct result of RTN activation or driven by PHOX2B+ neurons.

3.4.9 Conclusion

The results of this study highlight the functional diversity of the lateral parafacial region and emphasize the strong role of the most rostral locations in generating active expiration. The use of our novel multi dimensional map to assess physiological responses highlighted the functional nuances in respiratory responses to bicuculline along the pFL rostrocaudal axis, and advanced our understanding of the parafacial region.

3.5 Figures and Figure captions
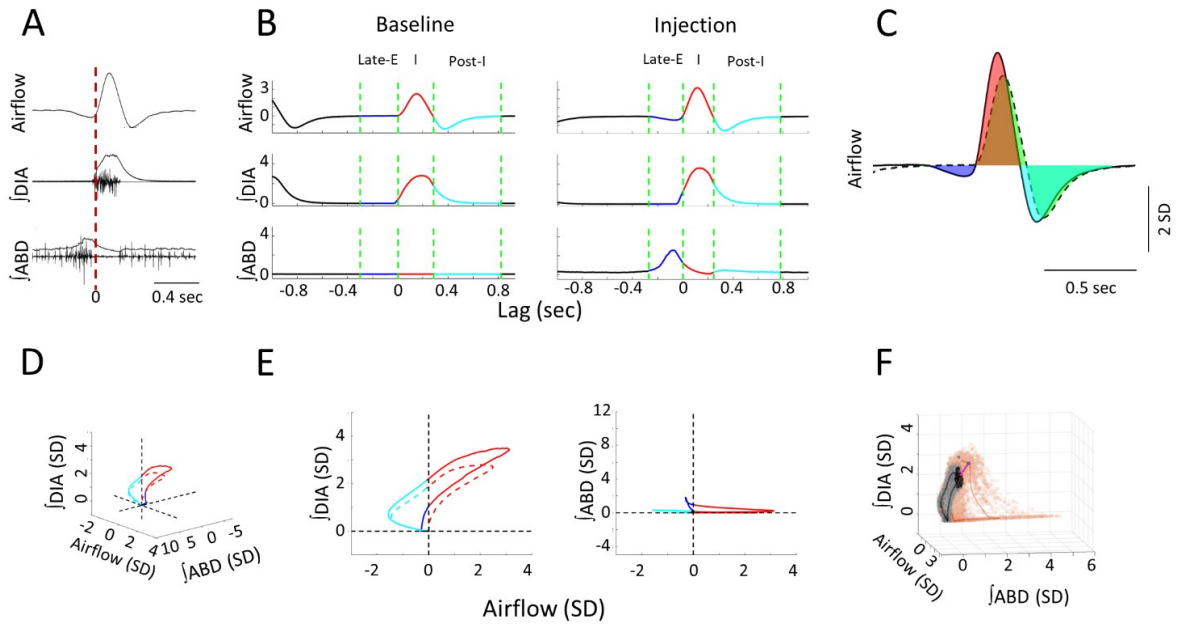
Figure 3.1 Measures used in quantifying respiratory responses to bicuculline injections

A: The time course of raw, and integrated EMG signals relative to recorded airflow during a sample breath. Vertical red line indicates the onset of inspiration as defined by positive airflow. **B**: Respiratory phases within a mean-cycle computed during baseline and post-injection for each recorded signal. Green lines mark the boundaries of each phase of the respiratory cycle, including the late-E (Blue), inspiratory (Red), and post-I (cyan) phases. **C**: Sample calculation of normalized area-under the-curve. Area under the baseline mean-cycle (dashed line, area in green) in each phase is subtracted from the corresponding colored area under the response mean-cycle (solid line, late-E: Blue, inspiration: Red, post-I: Cyan) to give a measure of how inspiratory airflow has changed relative to baseline. **D**: 3D representation of a representative baseline (dashed line) and response (solid line) mean-cycle. Each timepoint is a dot in 3D space defined by its airflow, $\int DIA_{EMG}$, and $\int ABD_{EMG}$ measurements. Colors indicate respiratory sub-periods as in **B**. Dashed lines indicate the origin for each measure. **E**: 2D projection of the mean-cycle in **D**. As per the colors in **B**, points on the left-hand side indicate expiration, points on the right-hand side indicate inspiration. **F**: Sample calculation of Euclidean and Mahalanobis distance measures for representative mean-

cycles during the baseline (gray) and response (orange). Pink line indicates the Euclidean distance between the response and baseline at a single timepoint. Black indicates the distribution of baseline values at the same timepoint used to calculate the Mahalanobis distance. Mean-cycles have been rotated relative to **D** to expose these distances to the viewer.

A

FB CFOS PHOX2B ChAT TH

Sp5

VII

200 μm

100 μm

B

NA

−0.2 mm

+0.1 mm   VII

+0.4 mm   VII

+0.6 mm   VII

+0.8 mm   VII

C

Number of cells

○ cFos
■ cFos-phox2b

○ cFos
■ cFos-phox2b

Distance from VIIc (μm)

Distance from VIIc (μm)

D

Airflow ∫ABD

Airflow ∫ABD

Airflow ∫ABD

Airflow ∫ABD

Airflow ∫ABD

0.008V.s

0.3V

2sec
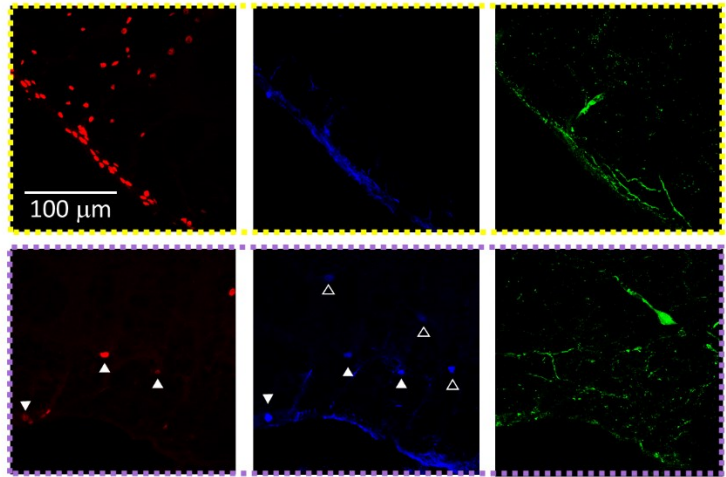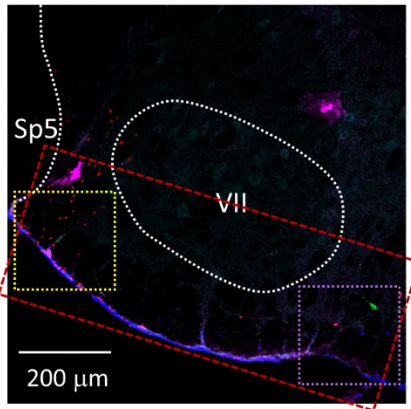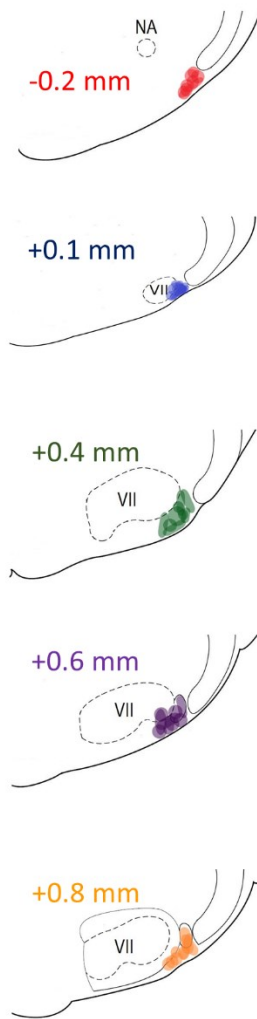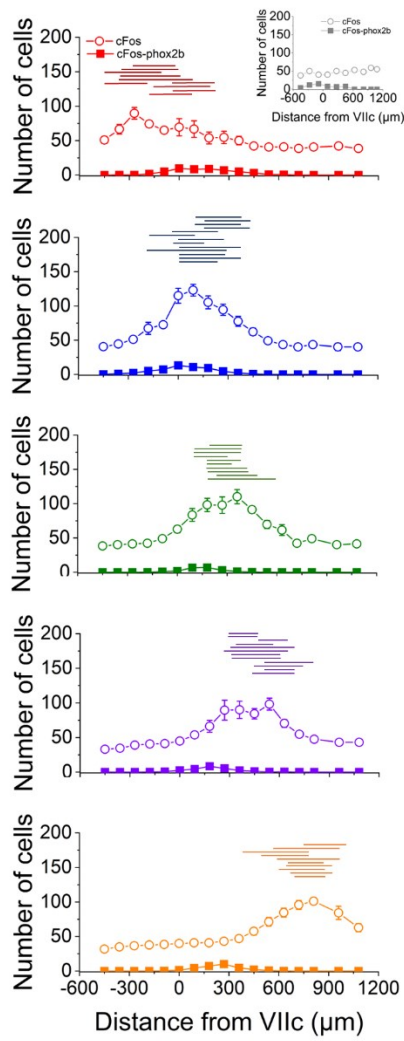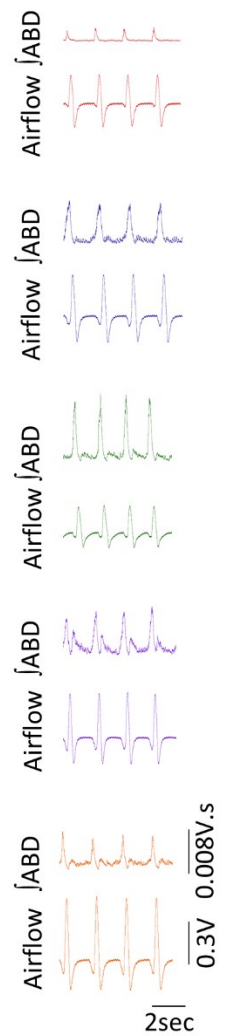
Figure 3.2 Location of bicuculline injections along the rostrocaudal axis of the ventral medulla

A: Representative confocal microscope images of immunohistochemistry performed at the injection sites. Red: cFos, Cyan: ChAT, Blue: PHOX2B, Green: TH, Magenta: fluorobeads. Red rectangle is a representative example of the area used for cell counting. Yellow and Purple squares are the areas represented on the right panel of **A**, notice the abundance of CFOS+ cells on the lateral area near the injection site (yellow square) compared to the fewer CFOS+ cells in the medial area (purple square). Closed white triangles are pointing out examples of CFOS-PHOXB+ cells, whereas open white triangles are pointing out examples of PHOX2B+ cells that were CFOS-negative. Magnification is the same for all images in the right panels of **A**. **B**: Schematic representation of the core of the injection sites and the group attribution, according to proximity of injection sites among experimental rats (-0.2 mm, n=5; +0.1 mm n=7; +0.4 mm, n=5; +0.6 mm, n=6; +0.8 mm, n=5). **C**: Cell counting colored coded according to the groups defined in **B** (CTRL, n=7; -0.2 mm, n=5; +0.1 mm n=7; +0.4 mm, n=5; +0.6 mm, n=6; +0.8 mm, n=5). Data points represents the Mean ± SEM of cells counted per hemisection at rostrocaudal locations ranging from -0.5 to +1.0 mm from VIIc. Open circles: CFOS+ cells; Closed squares: CFOS/PHOX2B+ cells. Inset in group -0.2 mm is the cell count obtained for the CTRL group. Horizontal lines above the cell count graphs represent the rostrocaudal extension in which fluorobeads were observed for each injection site. **D**: Representative examples of $\int ABD_{EMG}$ and Raw Airflow traces obtained after injection of bicuculline (color coded based on the groups defined in **B**).
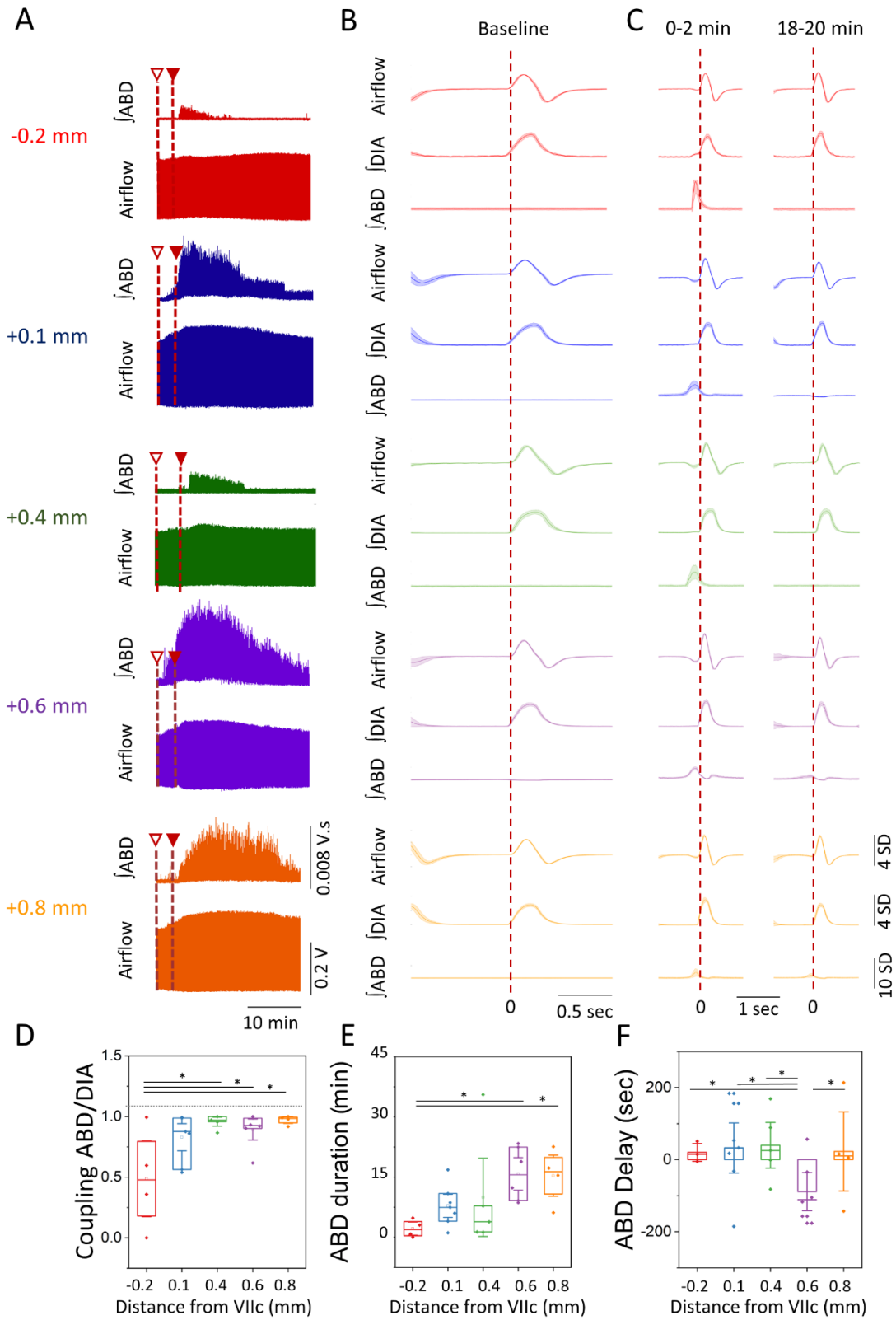
Figure 3.3 Temporal Characteristics of the ABD response elicited after bicuculline injection

A: Representative examples of raw traces of the Airflow and ∫ABD$_{EMG}$ signals for the entire duration of the response obtained at each injection site following the first (open triangle) and second injection (closed triangle) of bicuculline (examples are colored coded based on the groups obtained in Figure 3.2 B). **B-C**: Representative mean-cycles for the Airflow, ∫DIA$_{EMG}$, and ∫ABD$_{EMG}$ during baseline (**B**) and during the first two min and the last two min of the response (**C**) (traces are color coded based on the groups defined in Figure 3.2 B). Shaded areas indicate standard deviation of each signal. **D**: Coupling of the ∫ABD$_{EMG}$ and ∫DIA$_{EMG}$ following the injection of bicuculline at different rostrocaudal locations. **E**: Duration of the ABD response elicited. **F**: Delay in the onset of the ABD response following the second injection of bicuculline. Sample size for plots on D-F are as follow: -0.2 mm, n=5; +0.1 mm n=7; +0.4 mm, n=5; +0.6 mm, n=6; +0.8 mm, n=5. Boxplots represent the median, interquartile range, as well as the minimum and maximum values. Significance levels were obtained through a One-Way ANOVA followed by a Tukey Test, $p < 0.005$.
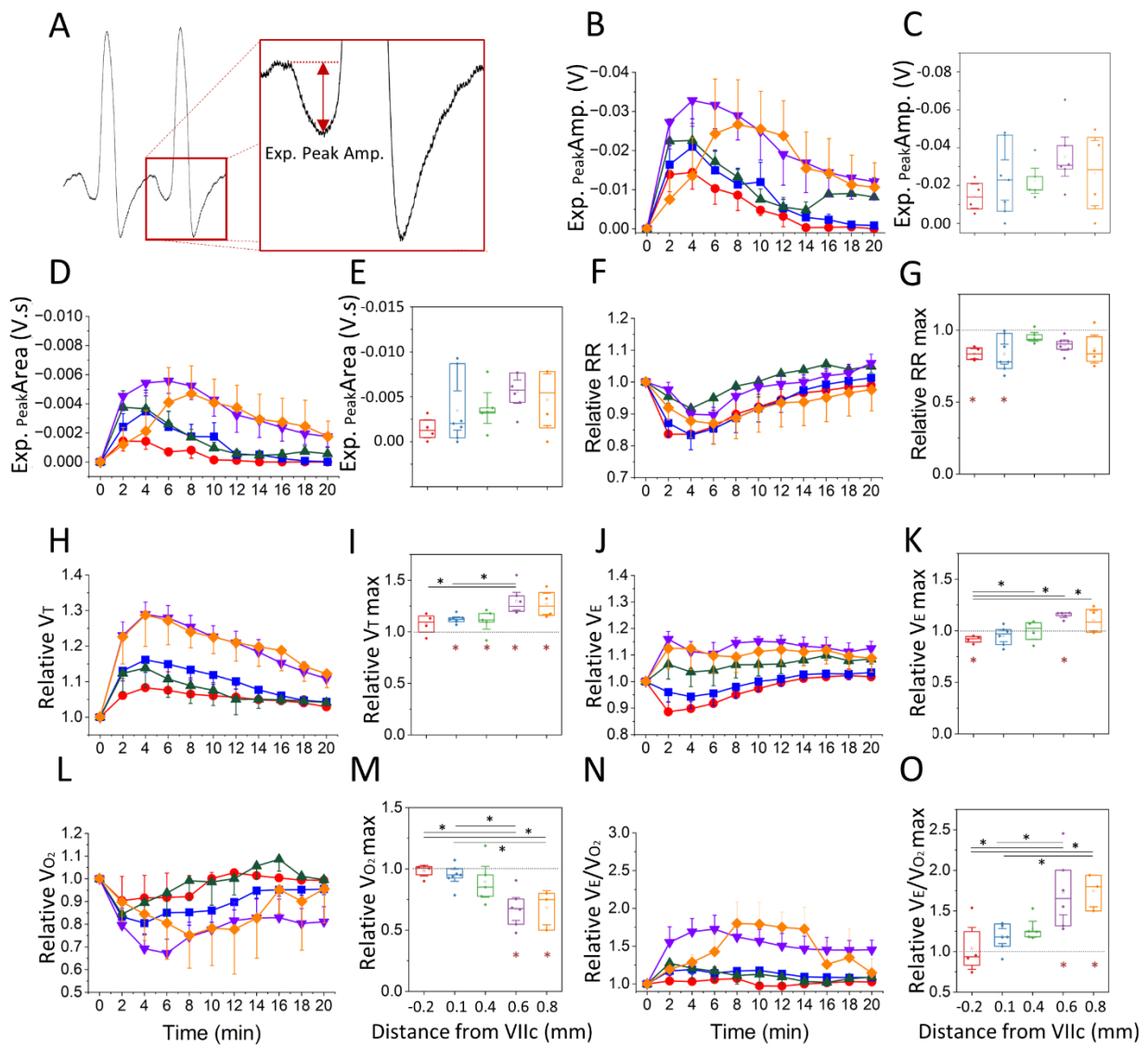
Figure 3.4 Respiratory Changes elicited following bicuculline injection

A: Airflow trace depicting the late expiratory (Late-E) inward airflow inflection induced during ABD recruitment, as well as the measure of Expiratory Peak Amplitude used in **B**. **B,D**: Expiratory Peak Amplitude (**B**) and Area (**D**), throughout the duration of the post-injection period for each group (color coded based in Figure 3.2 B). Values represent the Mean ± SEM at each time bin. **C,E**: Maximum Expiratory Peak Amplitude (**C**) and Area (**E**) obtained at each injection site. **F,H,J,L,N**: Relative change in respiratory rate (**F**), Tidal Volume (**H**), Minute Ventilation (**J**), Oxygen Consumption (**L**) and V_E/V_{O2} (**N**) with respect to baseline throughout the duration of the post-injection period for each group (color coded based on Figure 3.2 B). Values represent the

Mean ± SEM at each time bin. **G,I,K,M,O**: Maximum relative change in respiratory rate (**G**), Tidal Volume (**I**), Minute Ventilation (**K**), Oxygen Consumption (**M**) and V_E/V_{O2} (**O**) observed at each injection site. Sample size for plots on **B-O** are as follow: -0.2 mm, n=5; +0.1 mm n=7; +0.4 mm, n=5; +0.6 mm, n=6; +0.8 mm, n=5. Boxplots represent the median, interquartile range, as well as the minimum and maximum values. Significance levels were obtained through a One-Way Repeated Measures ANOVA followed by a Bonferroni Test, $p < 0.005$ (black asterisks represent significant comparisons between injection sites, red asterisks represent significant comparisons relative to baseline).

A

Airflow
∫DIA
∫ABD

0

0.4 sec

B

Baseline

Late-E I Post-I

Airflow
3
0

∫DIA
4
0

∫ABD

-0.8   -0.4   0   0.4   0.8

Injection

Late-E I Post-I

-0.8   -0.4   0   0.4   0.8

Lag (sec)

C

Airflow

2 SD

0.5 sec

CTRL   -0.2 mm   +0.1 mm   +0.4 mm   +0.6 mm   +0.8 mm

D

Late-E

Inspiration

Post-I

Airflow Area (norm.)

200

100

0

-100

E

DIA Area (norm.)

150

50

-50

Integration artifact

F

ABD Area (norm.)

1500

1000

500

Integration artifact

10   20

10   20

10   20

Time (min)

Time (min)

Time (min)

Figure 3.5 Rostral injections elicit more prominent changes to respiration in each signal and sub-period

A: Raw and integrated EMG activity relative to the onset of inspiration (vertical line). **B**: Representative mean-cycles during the baseline and post-injection, defining the late-E (Blue), inspiratory (Red), and post-I (Cyan) periods. **C**: Sample calculation of normalized area during each phase. **D-F**: Normalized response area across post-injection time for the Airflow (**D**), $\int DIA_{EMG}$ (**E**), and $\int ABD_{EMG}$ (F) signals following bicuculline injections into various coordinates along the rostral-caudal axis (colors as per label above figure). Sample size for plots on **D-F** are as follow: CTRL, n=7; -0.2 mm, n=5; +0.1 mm n=7; +0.4 mm, n=5; +0.6 mm, n=6; +0.8 mm, n=5. Stars indicate a significant difference (p <0.05) between the responses elicited by different injection locations (color-coded based on the groups defined in Figure 3.2 B) as assessed via Kruskal-Wallis test. Colored circles indicate the comparisons which were significant as per Dunn's post-hoc test with Sidak's correction. Shaded areas indicate mean + SEM.

A -0.2 mm

B +0.1 mm

C +0.4 mm

D +0.6 mm

E +0.8 mm

CTRL   -0.2 mm   +0.1 mm   +0.4 mm   +0.6 mm   +0.8 mm

F

Late-E   Inspiration   Post-I

G
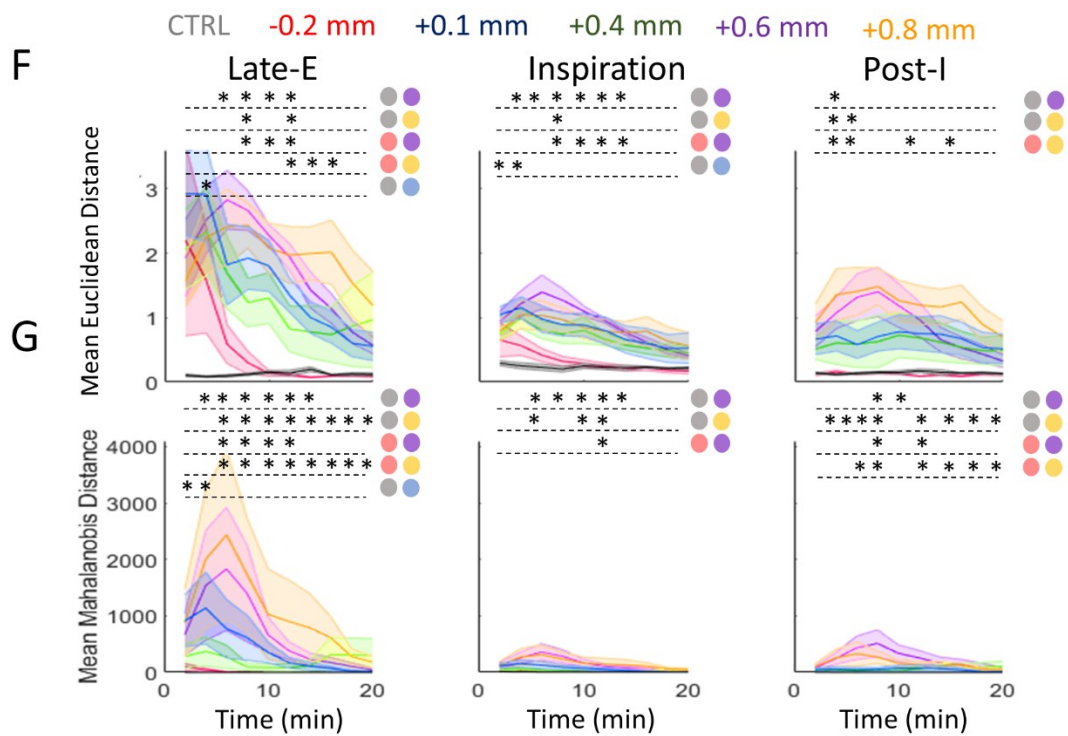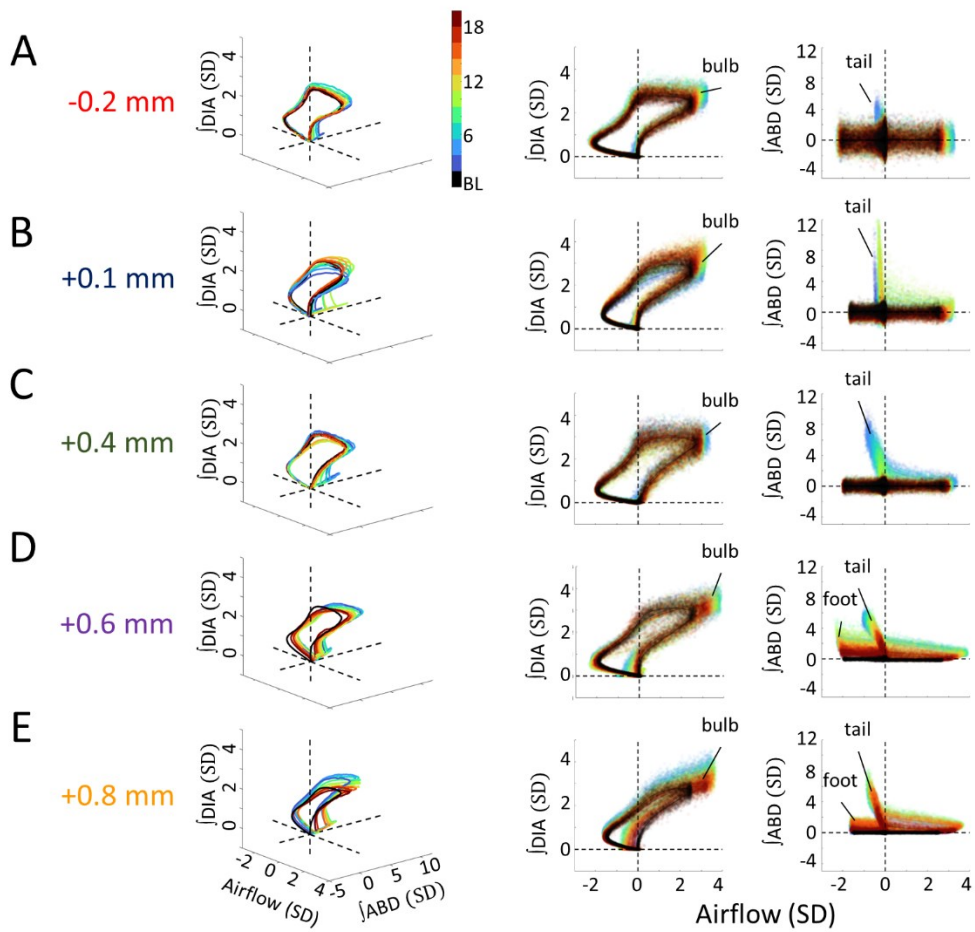
Figure 3.6 Deformations in multivariate respiratory trajectories differentiate the responses of various rostrocaudal coordinates following bicuculline injections

A-E: Representative respiratory trajectories from each injection location. Each row shows the 3D trajectories (solid lines) of the mean-cycle computed for baseline (black) and response time bins (blue to red), based on the color legend in the 3D panel of **A**. 2D projections of these trajectories onto the airflow-$\int$DIA$_{EMG}$ (middle), and airflow-$\int$ABD$_{EMG}$ planes (right) follow on the right of each 3D figure. Clouds of coloured points surrounding each trajectory indicate values from individual cycles of the corresponding time bin. Dashed lines indicate the origin of each axis. **F**: Mean Euclidean distance across response time bins comparing each injection location for the late-E, inspiratory, and post-I phases. Colours as per Figure 3.5, noted above the figure. Shaded areas indicate Mean +/- SEM. Stars indicate significance ($p < 0.05$) for a given time bin between injection locations or control injections as determined by Kruskal-Wallis test. Colored circles indicate which groups were different as per Dunn post-hoc testing with Sidak's correction. **G**: Mean Mahalanobis distance across the post-injection response for each injection location and respiratory phase. Colors as in **F**. Sample size for plots on **F-G** are as follow: CTRL, n=7; -0.2 mm, n=5; +0.1 mm n=7; +0.4 mm, n=5; +0.6 mm, n=6; +0.8 mm, n=5. Shaded areas indicate Mean +/- SEM. Stars indicate significance at the $p = 0.05$ level between injection locations for a given time bin as determined by Kruskal-Wallis test. Colored circles indicate which groups were different as per Dunn post-hoc with Sidak's correction.

Chapter 4.   Characterization of Respiratory Disturbances and Abdominal Recruitment during sleep in conditions of impaired inspiratory drive

4.1 Introduction

The regulation of breathing, a vital function of the brain, is orchestrated by neurons situated in the brainstem. The preBötzinger Complex (preBötC) plays a pivotal role in generating rhythmic inspiration, transmitting this activity to respiratory muscles through a network of premotor and motoneurons in the brainstem and spinal cord (Del Negro et al., 2018). Impairments such as neurodegeneration, reduced excitatory inputs to the preBötC (both centrally and peripherally), and altered connectivity within the preBötC itself can compromise the generation of a regular breathing rhythm, potentially leading to respiratory disorders (Benarroch, 2003; McKay & Feldman, 2008; Tan et al., 2008; Tsuboi et al., 2008).

Notably, disturbances in respiratory activity often manifest during sleep, and are characterized by a physiological decrease in excitatory drive, diminishing the electrical excitability of the network responsible for respiratory rhythm generation and motoneuron output (Orem et al., 2000; Orem et al., 2005). This phenomenon gives rise to sleep-disordered breathing (SDB), marked by central, obstructive, and mixed apneas and hypopneas (Dempsey et al., 2010). Epidemiologically, sleep-disordered breathing affects 24.1% of men and 18.0% of women (Balagny et al., 2023), and is defined by an elevated apnea-hypopnea index (AHI) exceeding 5. Although not within the common criteria used for sleep disordered breathing assessment in the human population, the occurrence of abdominal (ABD) activity has been documented during sleep in adult rodents as well as human and rodent neonates (Andrews & Pagliardini, 2015; Pisanski et al., 2019; Saini et al., 2022; Saini & Pagliardini, 2017). This activity, despite being linked to increase in minute ventilation and the stabilization of breathing, has never been quantified in naturally sleeping rodents under conditions of impaired inspiratory drive.

In the realm of sleep apnea research, animal models are instrumental for investigating the pathophysiology and consequences of breathing-related abnormalities during sleep. A prominent rodent model involves chronic intermittent hypoxia, complemented by variations such as sleep-induced intermittent hypoxia, hypercapnic stimuli, and models of mechanical upper airway obstruction (Ayyaswamy et al., 2023; Davis & O'Donnell, 2013; Fletcher, 1993, 1995; Salejee et

al., 1993; Tarasiuk et al., 1991). While rats and mice are considered natural models of sleep apnea by some (Christon et al., 1996; Davis & O'Donnell, 2013; Mendelson et al., 1988; Nakamura et al., 2003), caution arises due to the low number of respiratory disturbances they present (~ 2 per hour), as well as their healthy conditions and absence of pathologies like neurodegenerative diseases, comorbidities or craniofacial malformations. Alternative methods have involved inducing specific lesions in NK1R+ cells or inhibiting SST+ cells within the preBötC (McKay et al., 2005; Tan et al., 2008). Nevertheless, these investigations resulted in a highly severe phenotype, characterized by persistent apneas or respiratory disturbances not only during sleep but also during wakefulness, accompanied by episodes of ataxic breathing. On the other hand, other attempts with unilateral ablation of NK1R+ cells or bilateral preBötC ablation using viral vectors to transfect cells with diphtheria toxin A have succeeded at generating respiratory disturbances during sleep only (McKay & Feldman, 2008; Roberts et al., 2022). While these models prove valuable for comprehending sleep apnea in scenarios involving cell death, such as neurodegenerative diseases, it is essential to acknowledge the potential influence of neural plasticity on the observed outcomes.

In our study, we deviate from the conventional approaches, utilizing a pan-neuronal viral vector to transfect preBötC cells with a Kappa-Opioid-Receptor-DREADD (KORD). This strategy allows for temporary hyperpolarization of preBötC cells upon administration of the ligand Salvinorin B (SALB) without killing rhythmogenic neurons. Our investigation, monitoring breathing concurrently with sleep states and ABD activity, aimed to characterize breathing and ABD recruitment during sleep under conditions of impaired inspiratory drive.

Our results indicate a positive correlation between the number of transfected cells in the SST-core of the preBötC and the observed respiratory disturbances. Higher cell transfection corresponds to more disturbances, particularly during REM sleep. Moreover, our findings suggest an increase in ABD recruitment events during conditions of impaired inspiratory drive, especially in REM sleep, accompanied by a rise in the percentage of ABD events associated with apneas. These results underscore the robustness of the inspiratory rhythm, requiring a large number of inhibited cells to induce impaired inspiratory drive as previously observed with other lesioning approaches *in vivo* and *in vitro* (Gray et al., 2001; Hayes et al., 2012; McKay et al., 2005; Wang et al., 2014). Additionally, they highlight the enhanced ABD recruitment during impaired inspiratory drive

conditions. Further studies are essential to elucidate the precise role of ABD activity for breathing under conditions of a compromised inspiratory drive.

4.2 Materials and methods

4.2.1 Ethical approval

This study involved 30 male Sprague-Dawley rats. The rats were housed in a chamber with controlled temperature and pressure, following a 12-hour dark-light cycle and provided with water and food ad libitum. The University of Alberta's Health Science Animal Policy and Welfare Committees approved the animal care and experimental procedures (AUP#461) in compliance with the guidelines set by the Canadian Council on Animal Care.

4.2.2 Viral injection into the preBötC

For transfection of preBötC cells, we utilized a combination of two viruses: an adeno-associated virus (AAV, serotype 5) expressing Cre recombinase (Cre) and a fluorescent protein (eYFP) under the synapsin promoter (hSyn-Cre-eYFP), and a Cre-dependent AAV expressing the KORD receptor and hemagglutinin tag (HA) under the synapsin promoter (hSyn-DIO-KORD-HA). All viruses were produced, characterized, and titrated by the University of North Carolina Virus Vector Core Facility ($4x10^{12}$ molecules/ml).

We performed bilateral viral injections of the KORD expressing viruses (n = 23) into the preBötC of 200-300g Sprague Dawley rats. The injection procedure was carried out in anesthetized rats (ketamine 90mg/kg, xylazine 10 mg/kg) positioned on a stereotaxic frame with bregma 5 mm below lambda. The occipital bone was exposed, and a small window was opened for viral injections. Using a glass pipette with an external tip diameter of ~30 μm, the adenovirus mix (150nl of each virus) was delivered by controlled back-pressure injection (20 psi, 2-5 ms pulses; PicoSpritzer III) over 2-5 minutes. The injection coordinates were 0.9 mm rostral, 2.0 mm lateral, and 2.8 mm ventral to the obex. The electrode remained in place for 5 minutes after injection to minimize backflow of the virus. At the end of surgery, neck muscles and skin were sutured, and rats were allowed to recover with pain medication, food, and water ad libitum for at least 3 weeks.

4.2.3 Instrumentation of KORD injected rats

A total of 23 rats injected with the KORD virus and 5 naïve rats (CTRL) underwent EEG and EMG electrode instrumentation based on established protocols (Pagliardini, 2012; Andrews and Pagliardini, 2015; Pisanski et al., 2019). The procedure involved anesthetizing rats with ketamine (90mg/kg) and xylazine (10mg/kg). Bipolar multi-strand, Teflon-coated, stainless steel EMG electrodes (cat#AS633, CoonerWire) were inserted into the oblique abdominal (ABD), diaphragm (DIA), and neck muscles. The wires were tunneled under the skin and connected to a custom made electrical socket (Neurotekit Ink, ON) implanted on the neck.

Bipolar, multistranded PFA-insulated stainless steel wires (cat# 793500, AM-Systems) were also implanted in the neocortex (nCTX) and hippocampal formation (HPC) using specific coordinates relative to Bregma: nCTX (AP: +2.5; ML: -1.2; DV: -1.5 to -2.0mm) and HPC (AP: -3.3; ML: -2.4; DV: -2.5 to -3.0mm). The distance between wire ends was maintained at ~1mm for optimal recordings. For nCTX recordings, electrodes were lowered just below the position where an increase in multiunit discharge corresponds to the region just below layer V in the nCTX. HPC electrodes were positioned more ventrally, where a second audible multiunit discharge corresponding to the distal apical dendritic layer of CA1 pyramidal cells was identified. Electrodes were fixed to the skull with screws and dental acrylic. Three screws cemented to the skull ensured electrode stability and were soldered with Teflon-insulated wires to serve as additional cortical EEG signals and ground. These wires were then tunneled under the skin and connected to the same electrical socket on the rats' neck.

Post-surgery, rats received analgesics for two days (Metacam, 2mg/kg), had food and water ad libitum, and were maintained on a 12h/12hr dark-light cycle.

4.2.4 Recording procedures

In the first week after the EEG/EMG instrumentation surgery, rats were habituated to the whole-body plethysmograph during two five-hour sessions. Experimental recording sessions commenced 7-9 days post the instrumentation surgery. KORD injected rats were given a 2-hour acclimation period to the recording chamber, followed by a single injection of either vehicle (DMSO) or SALB (10mg/kg, s.c.) before further testing. The recording period lasted 3 hours post-injections.

Breathing variables were monitored in a 5L whole-body plethysmograph (Buxco chamber) utilizing the barometric method (Mortola & Frappell, 1998; Seifert, Knowles, & Mortola, 2000). Raw pressure signals were recorded using a Validyne differential pressure transducer connected to a CD15 carrier demodulator (Validyne Engineering, Northridge, CA, USA) and digitized through a Powerlab 8/35 (AD Instruments, Sydney, Australia). Chamber temperature and humidity were continuously tracked using an RH-300 water vapor analyzer (Sable Systems, Las Vegas, NV, USA) with additional readings from an HPR Plus Handheld PIT Tag reader (Biomark, Boise, ID, USA). Rectal temperature was monitored with a Homeothermic Monitor with Probe (507222F, Harvard Apparatus, Holliston, MA, USA).

Telemetry technology (Triangle Biosystem Inc., TBSI) was employed to measure EEG and EMG activity, with information sampled at 1 kHz using a transmitter connected to the rat socket during the recording session and TBSI receiver connected to PowerLab 16/30 data acquisition system (AD Instruments, Inc.). Field potential activity from nCTX and HPC was amplified at x1000 gain and filtered between 0.1Hz and 500Hz (amplifier model P511, Grass). EMG signals were amplified at x10000 and filtered between 100Hz and 500Hz (model 1700, AM Systems). Analysis was conducted using LabChart7 Pro (ADInstruments), Excel 2013, and Origin 9 (OriginLab Corp., Northampton, MA, USA).

4.2.5 Histology

At the conclusion of the experiment, KORD injected rats underwent transcardial perfusion with phosphate buffer (PB) followed by 4% paraformaldehyde dissolved in PB. The brains obtained were post-fixed for 24-48 hours, and 50 μm brainstem transverse sections were cut using a VT1000 Vibratome (Leica). Serial sections, spaced at 150 μm intervals, were immunoreacted to detect viral protein expression and specific preBötC markers.

Immunohistochemistry procedures followed established protocols (Boutin, 2015; Pagliardini, 2003). Free-floating sections were initially incubated for 60 minutes with 10% normal donkey antiserum (NDS) and 0.3% Triton X-100 to minimize nonspecific staining and enhance antibody penetration. Subsequently, sections were incubated overnight with primary antibodies diluted in PBS containing 1% NDS and 0.3% Triton X-100. The following day, sections underwent PBS washes, followed by a 2-hour incubation with specific secondary antibodies conjugated to

fluorescent probes (Cy2-conjugated donkey anti-chicken; Cy3-conjugated donkey anti-rabbit; Cy5-conjugated donkey anti-mouse; Jackson ImmunoResearch) diluted in PBS containing 1% NDS. After additional PBS washes, sections were mounted and coverslipped with Fluorsave mounting medium (Millipore). Primary antibodies included eYFP antibody (raised in chicken; Aves Labs Inc., dilution 1:500), hemagglutinin tag (HA, raised in rabbit; Cell Signaling, dilution 1:800), and somatostatin peptide (SST; raised in mouse, ThermoFisher Scientific, 1:600).

Subsequent analysis of slides and cell counting occurred using an Evos FL fluorescent microscope (Thermofisher Scientific, MA, US). Rostrocaudal acquisitions of serial sections were conducted along the respiratory column, spanning from the end of the lateral reticular nucleus to the caudal tip of the facial nucleus. Images were acquired within a 630x630 µm region below the nucleus ambiguus, positioned between the lateral edge of the inferior olive and the medioventral extension of the spinal trigeminal tract. Within this region, SST-expressing neurons were used to identify the core of the preBötC (Gray et al., 1999; S. Pagliardini et al., 2003; Ruth L. Stornetta et al., 2003). We used 16 out of the 23 brains infected with KORD virus for cell count. HA+ and SST+ neurons were then identified and counted in the SST-core of the preBötC and the surrounding area using ImageJ to determine the serial distribution of transfected neurons.

4.2.6 Data Analysis and Statistics

Sleep scoring was manually assessed based on visual assessment of HPC, nCTX, and neck EMG traces, following established criteria (Colin G. Andrews & Silvia Pagliardini, 2015; Pisanski et al., 2019). EEG traces were bandpass filtered (0.2–50 Hz) to minimize movement or electrical current-related noise. Wakefulness was identified by strong neck EMG activity coupled with activated EEG in the HPC (theta frequency; 4–10 Hz). During sleep, muscle tone was generally low, reaching even lower levels in the REM stage. The distinction between NREM and REM sleep was made through analysis of EEG and neck EMG signals. NREM sleep featured low-frequency (delta waves: 2–4 Hz) and high-amplitude signals in nCTX, while REM sleep showed theta activity in HPC (lasting 10 seconds or longer) and minimal neck EMG activity.

Diaphragmatic and abdominal raw EMGs were rectified and integrated digitally with a time-constant decay of 0.08s in LabChart 8 (v8.1.19, AD Instruments, Colorado Springs, CO, USA). Respiratory disturbances (apneas/hypopneas) were identified using the pressure signal from the

whole-body plethysmograph in combination with DIA$_{EMG}$. Apneas were recognized when breathing ceased for two breaths (2 seconds or more), while hypopneas occurred when the peak height of the barometric measurement decreased by more than half for a similar duration (>2 seconds). Apneas were further classified as post-sigh apneas if a sigh occurred 5 seconds or less before the apnea, or spontaneous apneas if no sighs immediately preceded the apnea. Animals were grouped based on the apnea/hypopnea index (AHI) after SalB injection: Affected (AHI > 5 over a period of 3 hours) or Unaffected (AHI < 5 over a period of 3 hours). ABD activity during sleep was evaluated to prevent confounding effects of potential vocalizations or behavioral ABD contractions during wakefulness. ABD recruitment was identified by expiratory modulated ABD$_{EMG}$ peaks lasting more than 5 seconds (i.e 3 consecutive breaths) and being more than double the height of the ABD$_{EMG}$ immediately preceding.

Assumptions of homogeneity of variance and normal distribution were tested using the Brown–Forsythe ($\alpha = 0.05$) and Shapiro–Wilk ($\alpha = 0.05$) tests, respectively. Comparisons on the number of transfected cells across the rostro-caudal axis between Affected and Unaffected groups and the comparisons between Affected and Unaffected animals under DMSO and SALB conditions were conducted using a two-way repeated-measures analysis of variance (two-way RM ANOVA; one repeated factor; $\alpha = 0.05$) where appropriate. In case of significant main effects, pairwise multiple comparisons were performed using the Bonferroni method ($\alpha = 0.05$). Additionally, a Pearson's correlation analysis was conducted with a significance level of $\alpha = 0.05$ to assess the association between the number of apneas per hour and the total transfected cells at the level of the SST-core of the preBötC, and assumptions of linearity and homoscedasticity were evaluated and met.

4.3 Results

4.3.1 Higher expression of KORD virus associated with higher number of respiratory disturbances

We administered a combination of viruses expressing Cre-recombinase (hSyn-Cre-eYFP) and Cre-dependent KORD receptor (hSyn-DIO-KORD-HA) to 23 rats. Rats injected with the KORD virus were categorized into two groups, Affected and Unaffected, based on the apnea/hypopnea index (AIH) observed after Salvinorin B injection. After 4 weeks, histological analysis of their brains revealed virus expression (hemagglutinin A marker, HA, indicative of KORD expression) in the

preBötC region marked with somatostatin (SST) cells in both groups, as depicted in Fig 1 A-B. Notably, although the virus was abundantly expressed in the area with SST+ cells, co-expression of HA tag with the SST marker was not observed in either the Affected or Unaffected animals (Fig 1 A-B). Quantifying cells expressing the HA marker, we found more transfected cells per hemisection in Affected (106.4 ± 2.7) than in Unaffected rats (74.2 ± 5.8) across a range from -300 μm to +450 μm from the beginning of the SST-core (Two-Way RM ANOVA, p = 0.047; Bonferroni p < 0.05; Figure 4.1 C). In both groups, HA tag expression declined to 47.0 ± 7.0 and 19.1 ± 1.4 cells per hemisection at -650 μm and +900 μm from the beginning of the SST-core, respectively.

To evaluate the association between apneas per hour and total transfected cells at the SST-core level, a Pearson's correlation analysis was performed following vehicle (DMSO) and SALB injections (Figure 4.1 D). While a moderate positive correlation was noted after DMSO (DMSO: r = 0.66, Pearson's correlation p = 0.004), a strong positive correlation was identified following SALB injection only (SALB: r = 0.87, Pearson's correlation p = 1 x 10 $^{-5}$). Furthermore, it was observed that the majority of KORD rats with a total of >900 transfected cells at the SST-core level (8 out of 9 rats) were also categorized as Affected based on AHI criteria (Figure 4.1 D, right panel).

4.3.2 Administration of Salvinorin B increases central apneas and reduces sighs in Affected rats

Four weeks post-viral injection, rats underwent whole-body plethysmography, with barometric pressure recordings obtained under the influence of both vehicle (DMSO) and SALB. Rats injected with the KORD virus were classified based on the frequency of respiratory disturbances per hour (RD/hr) observed following SALB administration, as Affected (RD/hr > 5) or Unaffected (RD/hr < 5).

Naïve rats (CTRL) exhibited an average of 2.2 ± 0.5 respiratory disturbances per hour, a value comparable to that observed in the Unaffected rats injected with the KORD virus (DMSO = 1.9 ± 0.4 RD/hr, SALB = 2.4 ± 0.5 RD/hr, Two-Way RM ANOVA, p = 0.5). Conversely, the Affected group displayed a higher incidence of respiratory disturbances, defined as apneas or hypopneas lasting longer than 2 seconds, upon SALB administration (Figure 4.2 A-C). Group data analysis

substantiated this observation, with the Affected group exhibiting an escalation in respiratory disturbances per hour from 5.5 ± 0.8 in DMSO to 11.4 ± 1.3 following SALB injection (Figure 4.2 D, Two-Way RM ANOVA p = 0.0002, Bonferroni p = 0.0001). Similarly, the number of respiratory disturbances per hour post-SALB injection in the Affected rats surpassed those observed following DMSO and SALB injections in the Unaffected group, as well as the observations made in the CTRL group (Two-Way RM ANOVA, p = 0.0002, Bonferroni p < 0.05; Figure 4.2 D).

The number of sighs per hour in CTRL animals paralleled that of the Unaffected group under both DMSO and SALB conditions (CTRL = 18.2 ± 1.9 sigh/hr, Unaffected-DMSO = 16.7 ± 1.0 sigh/hr, Unaffected-SALB = 17.4 ± 0.9 sigh/hr; Two-Way RM ANOVA, p = 0.5). In contrast, a reduction in the number of sighs was observed in the Affected group following SALB injection when compared to CTRL, as well as the DMSO and SALB conditions in the Unaffected group (Affected SALB = 12.4 ± 1.4 sigh/hr, Two-Way RM ANOVA, p = 0.0002, Bonferroni p < 0.05; Figure 4.2 E). Intriguingly, although the number of sighs decreased in the Affected group following SALB injection, the number of post-sigh apneas (PSA) and the ratio of PSA to sighs remained constant across all conditions (PSA/hr = 8.2 ± 0.5, Two-Way RM ANOVA p = 0.4; PSA/sighs = 0.5 ± 0.1, Two-Way RM ANOVA p = 0.3; Figure 4.2 F-G).

The duration of apneas in the Unaffected group under DMSO and SALB conditions (DMSO-Unaffected Apnea Length = 2.7 ± 0.1 sec; SALB-Unaffected Apnea Length = 3.0 ± 0.2 sec) resembled that of the CTRL group (Apnea Length = 2.6 ± 0.1 sec; Two-Way RM ANOVA, p = 0.5), whereas the duration of apneas following SALB injection in the Affected rats was prolonged compared to the CTRL and Unaffected groups in DMSO conditions (Affected-SALB Apnea Length = 3.5 ± 0.2 sec, Two-Way RM ANOVA, p = 0.04, Bonferroni p < 0.05; Figure 4.2 H). Conversely, PSA length remained consistent across conditions, with an average value of 3.9 ± 0.2 sec (Two-Way RM ANOVA, p = 0.7; Figure 4.2 I).

In summary, these findings indicate that in rats with a higher number of transfected cells at the SST-core in preBötC (i.e., Affected group), the injection of the KORD ligand SALB led to an increase in the frequency and duration of respiratory disturbances per hour, exceeding those observed in DMSO conditions as well as in the CTRL and Unaffected rats. Furthermore, in the

Affected group, transfection with the KORD virus affected the ability to generate sighs, as evidenced by a reduction in the frequency of sighs following SALB administration compared to CTRL and Unaffected groups.

4.3.3 Affected rats wake more often

Subsequently, we conducted a comprehensive assessment of the distinct sleep stages in CTRL, Unaffected, and Affected rats. Examples of each of the three sleep states quantified are depicted in Figure 4.3 A. Notably, the affected group exhibited heightened sleep fragmentation, characterized by an increased number of wake epochs per hour (Wake/hr = 8.2 ± 0.9) compared to both the Unaffected and CTRL groups (Wake/hr = 5.0 ± 0.6; Two-Way RM ANOVA, $p = 0.02$, Bonferroni, $p < 0.05$). Despite the more frequent awakening in Affected rats, the duration of wake epochs was shorter (Wake duration = 2.6 ± 0.4 min) compared to CTRL and Unaffected rats (Wake duration = 3.9 ± 0.3 min; Two-Way RM ANOVA, $p = 0.03$, Bonferroni, $p < 0.05$). Consequently, the total time spent awake per hour remained comparable across all conditions (Wake time/hr = 19.1 ± 1.6 min; Two-Way RM ANOVA, $p = 0.5$; Figure 4.3 B).

In contrast, NREM and REM sleep parameters exhibited no alterations across experimental conditions. The number of NREM epochs per hour, the duration of these epochs, and the time spent in NREM sleep per hour were consistent in CTRL, Unaffected, and Affected rats (pooled data from the three groups: NREM/hr = 9.8 ± 0.6; NREM duration = 3.3 ± 0.3 min; NREM time/hr = 28.0 ± 1.3 min; Two-Way RM ANOVA, $p > 0.05$; Figure 4.3 C). Similarly, the number of REM epochs per hour, the duration of these epochs, and the time spent in REM sleep per hour demonstrated no significant differences among CTRL, Unaffected, and Affected rats (REM/hr = 4.6 ± 0.3; REM duration = 0.8 ± 0.1 min; REM time/hr = 4.1 ± 0.2 min; Two-Way RM ANOVA, $p > 0.05$; Figure 4.3 D).

4.3.4 Affected rats have increased respiratory disturbances particularly during REM

We then conducted an assessment of respiratory disturbances during various sleep states in both Affected and Unaffected rats. Given the similarity in the number of respiratory disturbances and sleep characteristics between the CTRL and Unaffected groups, the CTRL group was excluded from all subsequent analyses, and we compared our results between Affected and Unaffected rats

instead. The number of respiratory disturbances per hour of sleep or apnea-hypopnea index (AHI) in the Unaffected rats averaged 5.4 ± 2.5 and remained consistent across conditions and sleep states (Two-Way RM ANOVA, $p = 0.22$; Figure 4.4 A). Conversely, in the Affected rats, the AHI averaged 17.8 ± 3.9 and exhibited no significant differences across conditions and sleep states (Two-Way RM ANOVA, $p = 0.43$; Figure 4.4 B).

During wakefulness, the AHI following SALB injection in the Affected rats was higher than that observed in Unaffected rats during DMSO conditions (Affected-SALB = 6.6 ± 2.1 vs Unaffected-DMSO = 2.3 ± 0.8, Two-Way RM ANOVA, $p = 0.04$, Bonferroni, $p < 0.05$), but it did not reach significance levels when compared to DMSO in the same group (Figure 4.4 C). Similarly, during NREM sleep, the AHI following SALB injection in the Affected rats was higher than that observed in Unaffected rats during both DMSO and SALB conditions but did not reach significance compared to DMSO conditions in Affected rats (Affected-SALB = 9.0 ± 2.8 vs Unaffected = 2.4 ± 0.5, Two-Way RM ANOVA, $p = 0.02$, Bonferroni, $p < 0.05$; Figure 4.4 D). Overall, the highest number of respiratory disturbances per hour of sleep state was observed during REM sleep in the Affected rats. Although the number of respiratory disturbances per hour of REM sleep in the Affected rats was not different in DMSO (AHI-DMSO = 22.9 ± 10.6) and SALB conditions (AHI-SALB = 39.0 ± 14.9), it was higher when compared to the DMSO and SALB conditions in the Unaffected animals (AHI-Unaffected = 4.0 ± 1.4; Two-Way RM ANOVA, $p = 0.001$, Bonferroni AHI-DMSO vs SALB, $p > 0.05$, Affected-SALB/DMSO vs Unaffected SALB/DMSO, $p < 0.05$; Figure 4.4 E).

4.3.5 Affected rats have more transitions to wakefulness associated with apneas

Next, we examined the association between apneas and transitions between different sleep states. To achieve this, we measured any sleep state transition occurring within a 10-second window of a respiratory disturbance, designating it as an apnea-induced transition (AIT). The occurrence of AITs was expressed as a percentage of the total number of that specific transition (% of TT) (refer to Figure 4.4 F).

Unaffected rats exhibited an average of $5.6 \pm 2.1\%$ of TT associated with respiratory disturbances, consistent across all evaluated sleep transitions (Two-Way RM ANOVA, $p = 0.3$; Figure 4.4 G, left panel). Whereas, Affected rats demonstrated an average of $7.6 \pm 1.5\%$ of TT associated with

respiratory disturbances, with a consistent pattern across all sleep transitions (Two-Way RM ANOVA, p = 0.3; Figure 4.4 G, right panel). Notably, we observed a higher percentage of awakenings from NREM sleep associated with respiratory disturbances in Affected rats compared to Unaffected rats (Affected NR-W% = 5.3 ± 1.6 vs Unaffected NR-W% = 0.8 ± 0.4, Two-Way RM ANOVA, p = 0.04, Bonferroni p < 0.05; Figure 4.4 H). Similarly, Affected rats exhibited a higher percentage of transitions from NREM to REM sleep associated with respiratory disturbances compared to Unaffected rats (Affected NR-R% = 9.7 ± 3.3 vs Unaffected NR-R% = 0, Two-Way RM ANOVA, p = 0.04, Bonferroni p < 0.05; Figure 4.4 I). For the remaining evaluated transitions (REM to NREM and REM to Wakefulness), no significant differences were observed between groups under either DMSO or SALB conditions (Two-Way RM ANOVA, R-NR p = 0.2, R-W p = 0.6; Figure 4.4 J-K). Overall, these results suggest that the higher amount of wakings observed in the Affected rats, could be the result of the increase in NR-W transitions associated with respiratory disturbances.

4.3.6 SalB injection induces an increase in ABD recruitment observed during sleep in Affected rats

Subsequently, we characterized the ABD activity during sleep. During DMSO conditions, the average frequency of ABD recruitment events per hour during sleep was 2.8 ± 0.7 events/hr. Notably, this rate remained consistent between the Affected and Unaffected groups across various sleep states (Two-Way RM ANOVA, one repeated factor, p = 0.4; Figure 4.5 A). Intriguingly, following the administration of SALB in Affected rats, the occurrences of ABD events per hour during NREM sleep escalated to 5.3 ± 1.5 events/hr. This observed increase was greater compared to the values recorded during DMSO conditions in both the Unaffected and Affected groups (Two-Way RM ANOVA p = 0.02, Bonferroni p < 0.05; Figure 4.5 A). Furthermore, the frequency of ABD recruitment events per hour during REM sleep exhibited a notable rise to 18.7 ± 5.6 events per hour following SALB injection in the Affected rats. This figure surpassed the values observed under DMSO conditions in both Unaffected and Affected rats and was also markedly higher than the values noted during NREM sleep in SALB conditions in the Affected rats (Two-Way RM ANOVA p = 0.02, Bonferroni p < 0.05; Figure 4.5 A). The average duration of ABD recruitment events was calculated to be 32.8 ± 3.5 seconds and evaluation of the event durations did not reveal any statistically significant differences across varied conditions or sleep states (Two-Way RM

ANOVA, p = 0.3). In conclusion, these findings collectively suggest that during instances of compromised inspiratory drive resulting from the hyperpolarization of >900 cells at the core of the preBötC, there is a notable increase in the frequency of ABD recruitment events during sleep, particularly evident in REM sleep.

Furthermore, we assessed the relationship between ABD events and respiratory disturbances by quantifying occurrences of ABD recruitment within a specified temporal proximity (10 seconds preceding or following) to apnea events. In the DMSO conditions for both Unaffected and Affected rats, our analysis revealed that 100% of the observed ABD recruitment events were not associated with the incidence of apneas. However, subsequent to SALB administration, an increase in the percentage of ABD recruitment events linked to respiratory disturbances was observed compared to DMSO conditions. Specifically, 7.5 ± 5.1% of ABD events occurred in the pre-apnea phase, and 5.4 ± 2.7% occurred in the post-apnea phase, resulting in a cumulative 13.0 ± 7.7 ABD events in the proximity of an apnea (peri-apnea) (Two-Way RM ANOVA p = 0.02, Bonferroni p < 0.05; Figure 4.5 B). These findings indicate a substantial augmentation in the proportion of ABD activity associated with respiratory disturbances under conditions of compromised inspiratory drive. Furthermore, our results show that the majority of ABD activity during sleep is not correlated with respiratory disturbances (refer to Figure 4.5 C, left panel). Nevertheless, in circumstances characterized by a compromised inspiratory drive, a notable escalation is evident in the percentage of ABD activity occurring in the proximity of an apnea event (refer to Figure 4.5 C, right panel).

4.3.7 The occurrence of ABD activity requires the presence of Inspiratory Drive

Throughout the course of our experimental recordings, three distinct patterns emerged in the occurrence of ABD activity specifically within the temporal confines of respiratory disturbance events, as illustrated in Figure 4.5 D. Quantification of these patterns revealed that a subset of respiratory disturbances, constituting approximately 1.0-1.5% of the total, exhibited what we termed "phasic ABD" activity during the event. These phasic events were characterized by rhythmic ABD activity coinciding with the duration of a respiratory disturbance. Remarkably, all instances of phasic ABD events were consistently observed during hypopneas and never during complete central apneas, identified by the cessation of DIA rhythm (Figure 4.5 D-E). In addition to phasic ABD responses, we also identified "tonic ABD" responses during respiratory

disturbances. This pattern manifested as a continuous firing pattern in the ABD_{EMG} once the DIA activity ceased, eventually terminating itself. Tonic ABD responses were observed in approximately 7.7-7.9% of the total respiratory disturbances (Figure 4.5 D-E). Notably, the most prevalent characteristic, accounting for 90.6-91.2% of observed instances, was the complete absence of ABD activity specifically during the duration of the respiratory disturbance (Figure 4.5 D-E). Furthermore, in every case where we observed tonic ABD or absence of ABD activity followed by post-apnea ABD activity, the resumption of DIA activity preceded the onset of ABD activity (Figure 4.5 F). In summary, these findings strongly support the notion that the manifestation of expiratory-related ABD activity is contingent upon the presence of an inspiratory drive.

4.4 Discussion

This study explores respiratory disturbances and ABD recruitment during sleep under conditions of impaired inspiratory drive. To induce impaired inspiratory drive, a viral vector expressing the KORD receptor (Marchant et al., 2016; Vardy et al., 2015), along with the HA-tag, was used to transfect preBötC. A positive correlation was observed between the number of transfected cells at the preBötC core and respiratory disturbances. Rats with higher KORD virus expression in the preBötC, categorized as Affected, exhibited increased respiratory disturbances, prolonged apnea duration, heightened wakefulness, and sleep fragmentation following SALB injection. Additionally, the Affected rats showed increased ABD recruitment during sleep, especially in REM sleep, suggesting a compensatory response to elevated respiratory disturbances. The study also revealed distinct abdominal muscle activity patterns during respiratory disturbances, highlighting the interplay between inspiratory and expiratory drives. These findings enhance our understanding of neural control of breathing during sleep, especially in conditions of impaired inspiratory drive.

4.4.1 Technical Considerations

The utilization of DREADD (Designer Receptors Exclusively Activated by Designer Drugs) technology in neuroscience research has experienced a significant surge since its inception and initial implementation (Blaine et al., 2007; Marchant et al., 2016; Vardy et al., 2015). Nevertheless, the integration of any emerging technology inevitably introduces unforeseen challenges that only

become apparent through repeated use. A noteworthy challenge concerning DREADD G-coupled receptors is the potential for constitutive activity in the absence of the ligand, as previously reported (Jami et al., 2016). Recent investigations reveal that the expression of Gi-DREADD in sensory neurons induces notable modifications in voltage-gated Ca^{2+} and Na^+ currents, even in the absence of the ligand clozapine-N-oxide (CNO) (Jami et al., 2016). Additionally, an upregulation in the expression of the Na^+ channel NaV1.7 is observed (Jami et al., 2016). Furthermore, mice subjected to these manipulation exhibit alterations in CNO-independent excitatory and inhibitory second-messenger signaling pathways (Jami et al., 2016). While there are currently no documented reports specific to the KORD (κ-opioid receptor DREADD) receptor, it is essential to acknowledge the potential for intrinsic activity of the transfected ectopic receptor in this context. The presence of constitutive activity could explain the respiratory disturbances observed in the Affected animals, even in the absence of the KORD ligand. Specifically, an indication of potential intrinsic activity on preBötC neurons was the reduction in sigh frequency, the duration of respiratory disturbances, and the total number of respiratory disturbances during REM sleep which suggest a reduced preBötC activity in absence of evident neuronal damage. Despite this unexpected increased KORD activity under DMSO conditions, we were able to discern significant differences between DMSO and SALB conditions in the Affected rats. Notably, these differences were particularly evident in respiratory disturbances independent of sleep state, as well as in the frequency of ABD recruitment and the percentage of ABD events associated with apneas suggesting that further activation of KORD receptors, and consequent hyperpolarization of preBötC neurons occurred with SALB application.

4.4.2 Higher expression of KORD virus associated with higher number of respiratory disturbances

Immunohistochemical analysis revealed a distinct expression pattern of the KORD receptor, labeled with the HA-tag, in rats exhibiting a higher incidence of respiratory disturbances compared to those without such disturbances. Specifically, the induction of impaired inspiratory drive necessitated the inhibition of over 900 cells at the level of the SST-core in the preBötC. This contrasts with prior studies reporting the induction of ataxic breathing, respiratory disturbances and SDB in unanesthetized animals by ablating between 300-450 total NK1R+ cells unilaterally or bilaterally (McKay & Feldman, 2008; McKay et al., 2005; Roberts et al., 2022). In our

investigation, a larger number of neurons had to be inhibited to observe respiratory disturbances during sleep, likely attributed to the use of a pan-neuronal promoter for KORD receptor expression and the preservation of rhythmogenic cells in our approach, which were hyperpolarized, rather than killed, upon the injection of the KORD ligand. Absence of secondary toxic effects (e.g., inflammation, gliosis) due to cell death may also be a reason for the distinct cell number involvement.

Interestingly, our histological analysis revealed that KORD receptor expression was confined to SST-negative neurons, despite a significant number of receptor-expressing cells being located among SST+ cells. The documented differential expression of Adeno-Associated Viruses (AAV) in various cell types depending on the serotype employed (Ellis et al., 2013) raises considerations about the serotype's capability to infect SST+ cells. While the AAV5 serotype used for KORD receptor transfection in our study can transfect central nervous system cells (Davidson et al., 2000), including respiratory network neurons (Alsahafi et al., 2015; Huckstepp et al., 2016; Huckstepp et al., 2015), its ability to infect SST+ cells specifically, has not been fully explored. It is plausible that SST+ cells in the preBötC lack the receptor for AAV5, specifically the platelet-derived growth factor receptor (PDGFR-α-polypeptide) (Pasquale et al., 2003). Nevertheless, existing proposals suggest that SST+ cells in the preBötC contribute to the generation of respiratory rhythm patterns rather than the direct generation of the rhythm itself (Cui et al., 2016; de Sousa Abreu et al., 2022). Thus, the absence of KORD receptor expression in these cells does not compromise the interpretation of our results.

4.4.3 Administration of Salvinorin B increases central apneas particularly during REM sleep

In this study, rats with a higher concentration of KORD-transfected cells at the SST-core in the preBötC demonstrated an increase in the frequency of respiratory disturbances per hour, specifically during REM sleep, subsequent to the administration of SALB. These results parallel previous findings observed in studies involving unilateral ablation of NK1R+ cells using Substance-P conjugated to saporin (McKay & Feldman, 2008). However, they diverge from outcomes reported by Roberts et al., 2022, where bilateral focal ablation of preBötC cells using DTA led to a higher prevalence of respiratory disturbances during NREM sleep.

The discrepancies in sleep stage specificity between our results and those of Roberts et al., 2022, may be attributed to nuanced variations in the quantification protocols employed. For instance, our study and McKay et al., 2008, utilized a 2.0-second criterion for quantifying apneas/hypopneas, while Roberts et al., 2022, employed a slightly shorter duration of 1.8 seconds. Alternatively, differences induced by the experimental methodologies used in itself may also account for these differences. For example, the study conducted by Roberts et al., 2022 involved preBötC cell ablation which induces a chronic state of sleep disordered breathing leading to long term intermittent hypoxia, neuroinflammation and neural plasticity, vs our study that involves acute inhibition of preBötC cells for short periods of time without the effects of cell loss, or possible neuroinflammation. Such differences in methodology could contribute to the observed distinctions in the prevalence of respiratory disturbances between studies.

4.4.4 Administration of Salvinorin B increases the duration of apneas and decreases sighs

In addition to the observed increase in respiratory disturbances, the Affected group also exhibited prolonged apnea durations compared to both CTRL and DMSO conditions in Unaffected rats. Intriguingly, a study involving NK1R+ cell ablation did not report alterations in the duration of respiratory disturbances relative to pre-injection (McKay & Feldman, 2008). The distinctive focus of the prior study on NK1R+ cells may contribute to the disparities noted when compared to our study, where all transfected cells in the preBötC were inhibited, as opposed to the selective ablation of NK1R+ cells. Contemporary hypotheses regarding the origin of the respiratory rhythm suggest that the summation and synchronization of subthreshold recurrent excitatory postsynaptic potentials (EPSPs) within the preBötC play a pivotal role in generating inspiratory bursts (Ashhad et al., 2022; Del Negro et al., 2018; Feldman & Kam, 2015; Kam et al., 2013; Phillips & Rubin, 2022; Prajkta et al., 2020). In the context of our investigation, the introduction of the KORD ligand would have induced hyperpolarization in the preBötC transfected cells. This hyperpolarization could have disrupted the requisite accumulation and coordination of recurrent EPSPs, consequently leading to an elevated incidence of missing bursts and prolonged apneas.

Similarly, Salvinorin B (SALB) administration in the Affected rats resulted in a reduction in sigh frequency compared to CTRL and Unaffected rats, suggesting the inhibition of neurons involved in the preBötC circuit for generating sighs (Li et al., 2016). It is proposed that an increase in the

excitability of preBötC NMBR or GRPR expressing neurons engages partially overlapping pathways for sigh generation. Furthermore, preBötC SST+ neurons are considered downstream elements in the sigh generation circuit (Li et al., 2016). Significant discrepancies in outcomes have been observed in prior investigations concerning the ablation of NK1R+ cells in the preBötC, as documented by McKay et al. (2005) and Roberts et al. (2022). Specifically, McKay et al. (2005) documented a decrease in the frequency of sighs upon ablation of NK1R+ cells, while Roberts et al. (2022) did not result in alterations in sigh frequency.

Interestingly, despite the absence of KORD HA-tag overlap with SST+ cells in our study, the activation of KORD receptors still resulted in a reduction in sigh frequency. This supports the notion that SST+ neurons in the preBötC function as downstream elements in the sigh generation circuit rather than being the originators of sighs. Inadvertently, our study likely inhibited NMBR or GRPR neurons in the preBötC, which are proposed as the origin of sighs, through the expression of KORD receptors using a pan-neuronal promoter (Peng Li et al., 2016). Collectively, the examination of these studies indicates that the cells accountable for generating sighs in the preBötC may potentially be neurons characterized by the absence of SST paired with the expression of NMBR and GRPR. Further experimental clarification on the role of NK1R+ cells on sigh generation and confirmation of the complete phenotype of the cells involved in the generation of sighs is still required.

4.4.5 Sleep fragmentation is heightened in Affected rats

Sleep fragmentation characterized by recurrent night awakenings is a prominent symptom of sleep-disordered breathing, and its impact on mood, concentration, vigilance, and attention has been documented (Gagnon et al., 2014; Sforza & Roche, 2016; Sforza et al., 2016). In our study, we observed that Affected rats, characterized by a higher frequency of respiratory disturbances, experienced more frequent awakenings during the sleep period compared to Unaffected rats and CTRL, although the total amount of sleep was not affected. Notably, these awakenings were more prevalent during NREM sleep and were closely associated with the occurrence of respiratory disturbances. While there was a discernible trend toward increased awakenings from REM sleep, it did not attain statistical significance. Our findings align with existing literature from both animal studies and clinical research, where increased awakenings in SDB have been reported (Roberts et

al., 2022; Swihart Bruce et al., 2008). Particularly noteworthy is the evidence showing that patients with sleep-disordered breathing exhibit elevated transitions from NREM to wakefulness (NR-W) and from REM to wakefulness (R-W) compared to healthy individuals, with NR-W transitions being more prominent (Swihart Bruce et al., 2008).

4.4.6 SALB administration in Affected rats increases ABD activity during sleep

In the realm of respiratory research, recent attention has shifted towards understanding the role of expiratory ABD activity and the potential involvement of the expiratory oscillator or lateral parafacial area (pFL) in generating this activity during sleep (Andrews & Pagliardini, 2015; Pisanski et al., 2019; Saini et al., 2022; Saini & Pagliardini, 2017). Given that this activity has been linked to enhanced ventilation and increased respiratory stability during sleep (Andrews & Pagliardini, 2015), a fundamental question arises: can the augmentation of this activity contribute to stabilizing breathing in conditions characterized by impaired inspiratory drive? In this study, we demonstrate that in the presence of heightened respiratory disturbances, there is indeed an increase in the number of ABD recruitment events observed, particularly during sleep. Moreover, in-depth analyses unveiled that under conditions of impaired inspiratory drive (SALB), the percentage of ABD activity associated with respiratory disturbances increased compared to DMSO conditions. While this evidence is solely observational, it constitutes an initial step supporting the notion of the expiratory oscillator and ABD recruitment serving as a backup mechanism in conditions marked by impaired inspiratory drive.

Alternatively, it has been shown that the pFL is silent at rest and disinhibition results in the generation of active expiration (de Britto & Moraes, 2017; Pagliardini et al., 2011; Silva et al., 2019). However, the source of this inhibitory control remains unresolved and awaits empirical validation. The Kölliker-Fuse nucleus has been strongly implicated in instigating active expiration in response to hypercapnia by disinhibiting the pFL (Barnett et al., 2018; Jenkin et al., 2017). Nevertheless, it is plausible that the modulatory influence of the Kölliker-Fuse on the pFL is mediated by inhibitory neurons situated in the Bötzinger or preBötzinger regions (Barnett et al., 2018; Flor et al., 2020). Given that in our study we hyperpolarized KORD-transfected cells, it is conceivable that this intervention might have indirectly alleviated inhibition of the pFL by

hyperpolarizing inhibitory neurons within the preBötC that project to the pFL (Yang & Feldman, 2018).

Additionally, the repetitive respiratory disruptions resulting from hyperpolarizing preBötC cells may induce transient hypoxic/hypercapnic conditions, potentially affecting blood gas levels (Panossian & Daley, 2013). Furthermore, it has been posited that during sleep in human infants, the activation of ABD muscles could enhance ventilation by counteracting airway resistance and reducing oxygen desaturation across various sleep stages (Saini et al., 2022). However, to validate these hypotheses thoroughly, it is imperative to conduct further experiments involving the manipulation of the expiratory oscillator, both in terms of silencing and activation, particularly under conditions of reduced inspiratory drive. Simultaneous measurements of oxygen saturation and sleep stages will be essential for a comprehensive understanding of these observed phenomena.

4.4.7 The occurrence of ABD activity requires the presence of Inspiratory Drive

Studies exploring the interaction between expiratory and inspiratory oscillators in adult rodents have indicated that the lateral parafacial area (pFL) struggles to sustain activity when the inspiratory oscillator is compromised (Huckstepp et al., 2016). However, these experiments were conducted in anesthetized preparations, where autoresuscitation processes are impaired (Krause et al., 2016), raising uncertainties about the persistence of this incapacity in freely behaving, unanesthetized rats. While evidence from awake rats with strong inhibition of preBötC SST+ cells suggests an inability to sustain any breathing pattern once the preBötC is entirely silenced (Tan et al., 2008), such investigations have not been conducted in a less severe phenotype of compromised inspiratory drive where abdominal (ABD) activity is concurrently measured until now.

A recent study has substantiated that chemogenetic modulation of the lateral parafacial area influences the occurrence of ABD activity during sleep (Pisanski et al., 2019), affirming the likelihood that the expiratory oscillator is responsible for these events. In our study, under conditions of moderately impaired inspiratory drive, we observe that approximately 98% of complete central apneas (absence of inspiratory drive) during sleep are characterized by the complete absence of expiratory ABD activity (90%) or a brief burst of tonic ABD activity that concludes before the end of the apnea (8%). This encompasses instances where ABD activity was

present before the apnea and resumed immediately after the apnea. Only about 2% of respiratory disturbances exhibited phasic ABD activity, and this was observed exclusively when the inspiratory drive was not completely absent (hypopneas). Moreover, in all instances where ABD activity resumed after the apnea, the inspiratory rhythm resumed first. In summary, this evidence supports the notion that the expiratory oscillator necessitates the presence of an intact inspiratory drive to be operational (Huckstepp et al., 2016).

4.4.8 Conclusions

Our study aimed to explore the impact of impaired inspiratory drive on respiratory patterns and ABD recruitment during sleep. Rats categorized as Affected, with a higher number of KORD-transfected cells, displayed notable changes, including increased respiratory disturbances, prolonged apnea duration, heightened wakefulness, and sleep fragmentation following SALB administration. Notably, the heightened sleep fragmentation in Affected rats paralleled clinical findings in sleep-disordered breathing. Furthermore, this investigation unveiled distinctive ABD activity patterns during respiratory disturbances, shedding light on the intricate interplay between inspiratory and expiratory drives, and affirming the necessity of an intact inspiratory drive for the existence of ABD activity. Additionally, the exploration into ABD recruitment suggested a potential compensatory role in conditions of impaired inspiratory drive, warranting further investigation. Technical considerations brought attention to potential intrinsic activity in KORD receptors, influencing outcomes even in the absence of the ligand. In essence, these findings collectively provide valuable insights into the complex mechanisms governing respiratory regulation during sleep under compromised conditions.

4.5 Figures and Figure captions
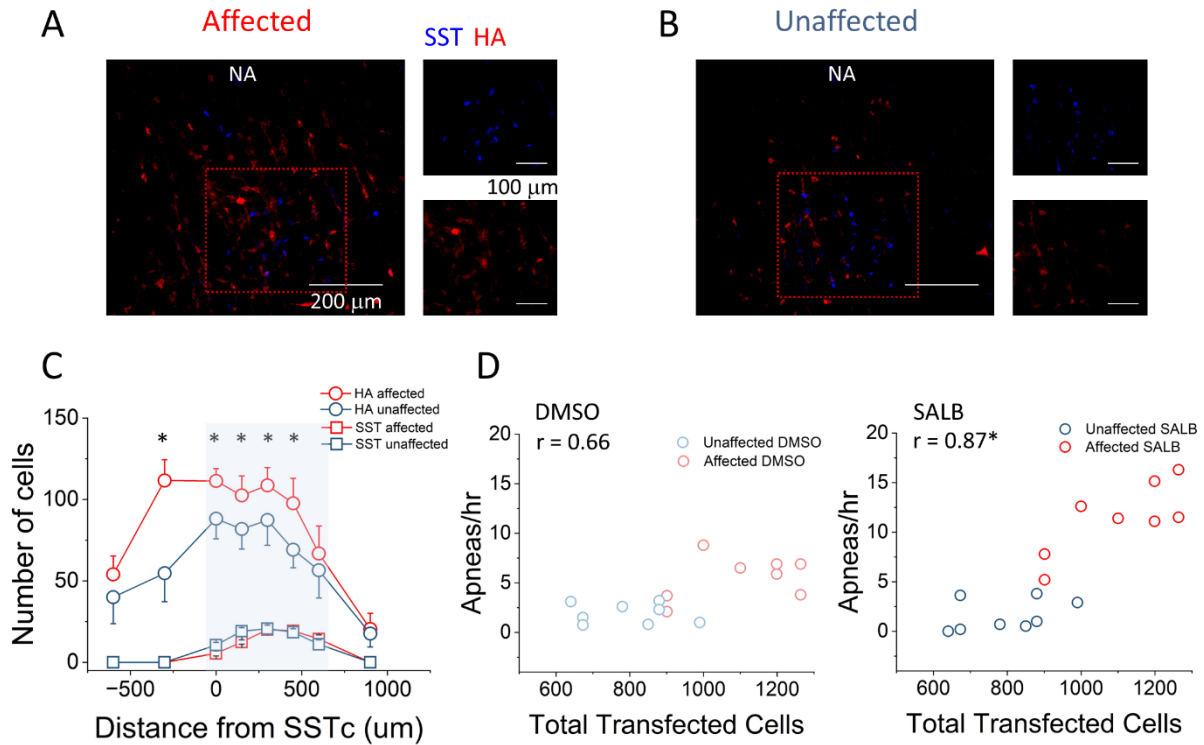
Figure 4.1 Differential expression of the KORD virus in Affected and Unaffected rats

A-B: Illustrated are representative immunohistological staining for Affected (**A**) and Unaffected (**B**) rats. In blue, Somatostatin (SST) positive cells are highlighted within the preBötC core, while red indicates Hemagglutinin (HA) positive cells, signifying successful transfection with the KORD receptor. The red square denotes the area depicted in smaller insets to the right of each image. Notably, there is an absence of co-localization of the HA and SST markers in the preBötC core and affected animals display a larger number of KORD-transfected cells. **C**: Cell counts were obtained within the preBötC core area at a 10X magnification under a Leica Fluorescent Microscope. Red represents Affected rats, and blue represents Unaffected rats. Open circles represent HA+ cells, and open squares represent SST+ cells. Statistical significance was determined using a Two-Way RM ANOVA followed by a Bonferroni Test ($\alpha = 0.05$). **D**: Illustrates the relationship between the number of apneas per hour and the total KORD-transfected cells at the SST-core level in the preBötC under DMSO (left) and SALB (right) administration. Red

denotes Affected rats, and blue denotes Unaffected rats. Lighter colors depict the DMSO conditions (left panel), while darker colors represent the SALB conditions (right panel). The correlation was assessed through Pearson's correlation coefficient (r).
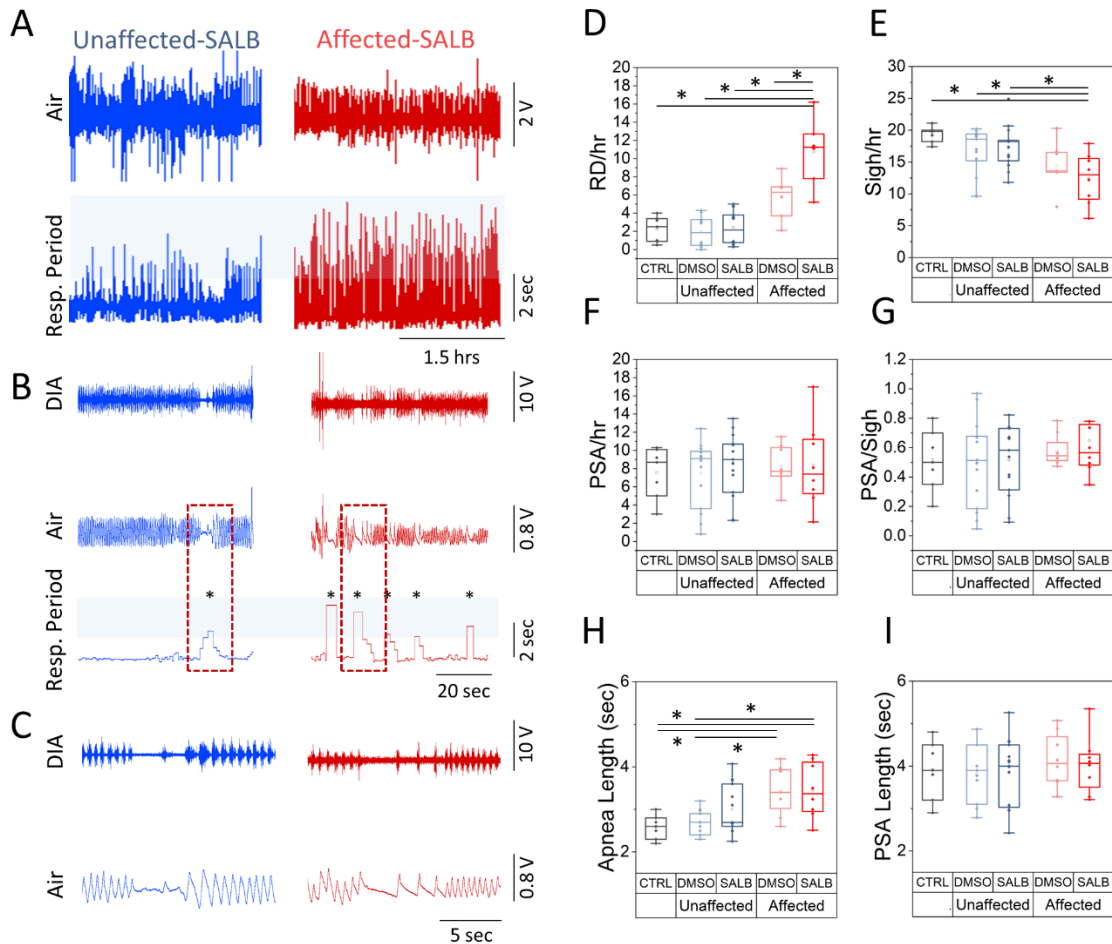
Figure 4.2 Administration of SALB leads to an increase in the frequency and duration of respiratory disturbances, accompanied by a reduction in sigh frequency in Affected rats

A-C: Illustrated are representative traces from barometric plethysmography recordings (Air), respiratory period (the time interval between two inspiratory bursts), and Diaphragmatic electromyogram signals (DIA) under SALB conditions. Blue represents Unaffected rats, while Red represents Affected rats. **A**: Depicts an entire 3-hour recording for the plethysmograph signal (Air) and the Respiratory Period. The shaded blue area on the respiratory period signal indicates the time threshold designating respiratory disturbances as apneas or hypopneas (2 seconds). **B**: Shows a 1-minute recording for DIA, Air, and Respiratory period signals. The shaded blue area above the respiratory period denotes the time threshold for identifying respiratory disturbances as

apneas or hypopneas (asterisks). Notably, Affected rats exhibit a higher incidence of respiratory disturbances, with 5 occurrences within this 1-minute example compared to only 1 in Unaffected rats. **C**: Zoomed-in representations of the dashed rectangles in **B** reveal that respiratory disturbances have a central origin in both cases, as evidenced by the absence of respiratory effort in the DIA signal. **D-I**: Number of respiratory disturbances (RD) per hour (**D**), sighs/hr (**E**), Post-sigh apnea per hour (PSA/hr) (**F**), PSA/sigh (**G**), Apnea length (**H**), PSA length (**I**) in CTRL group, as well Unaffected and Affected rats in DMSO and SALB conditions. In all plots, Gray represents the CTRL group, while Blue and Red represent Unaffected and Affected rats, respectively. Lighter colors correspond to the DMSO conditions, and darker colors represent the SALB conditions. Statistical significance was determined using a Two-Way RM ANOVA followed by a Bonferroni Test ($\alpha = 0.05$).
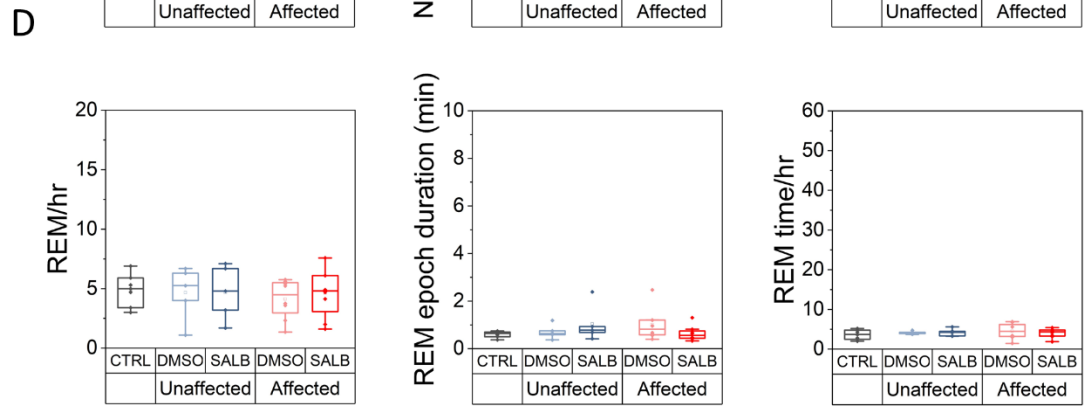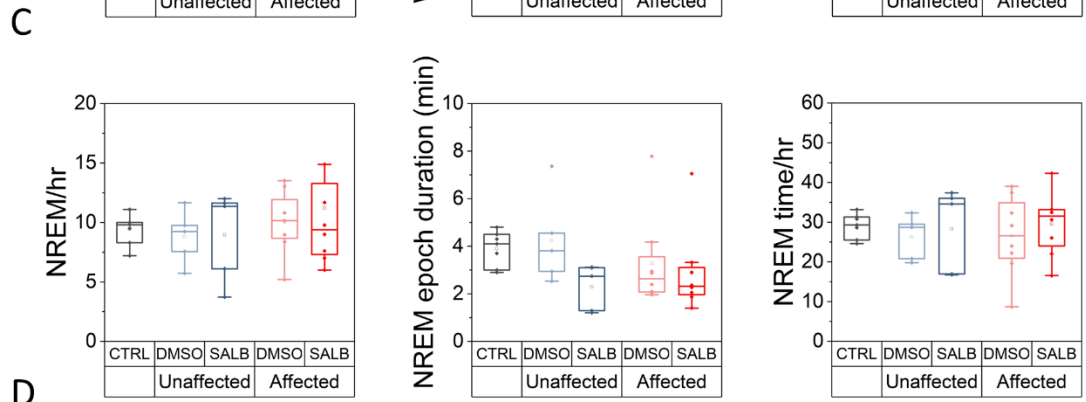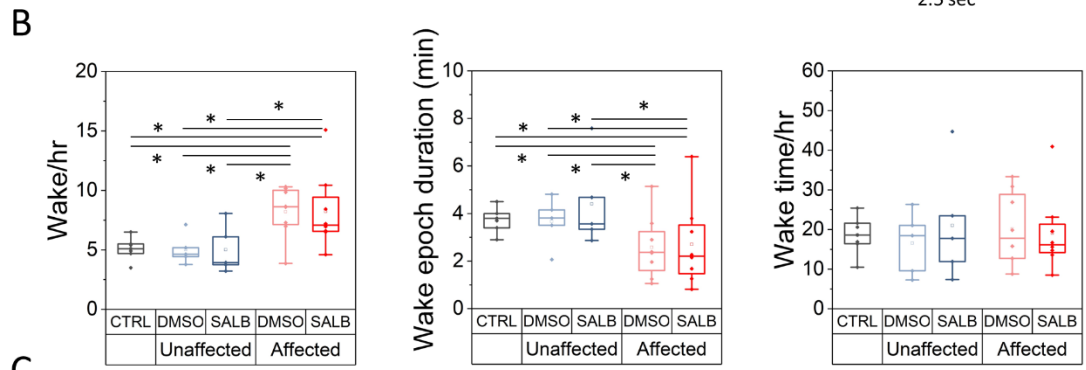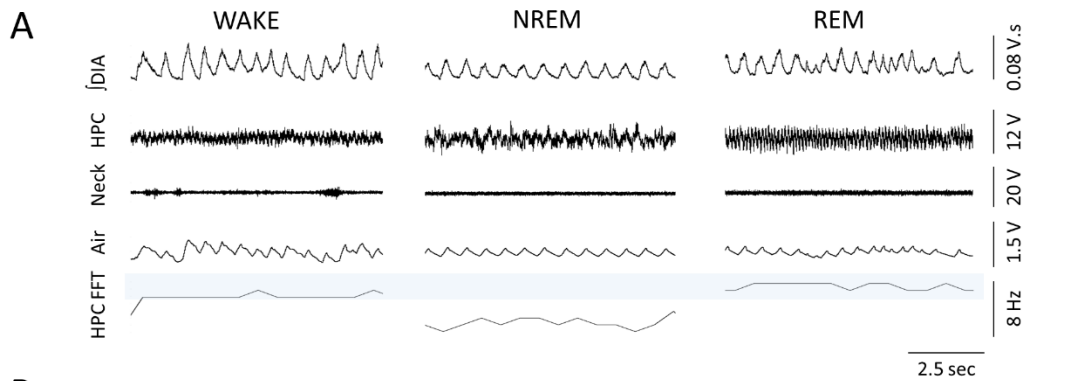
Figure 4.3 Examination of sleep characteristics indicates that Affected rats experience more frequent wakefulness

A: Illustrative traces include Diaphragm Integral (∫DIA), Hippocampus (HPC), Neck electromyogram, Plethysmography signal (Air), and Fast Fourier Transform of the HPC (FFT) during Wakefulness (left panel), NREM sleep (middle panel), and REM sleep (right panel). The blue shaded area on the HPC FFT indicates the frequency range from 6 to 8 Hz. Notably, the HPC signals display a frequency of 6-8 Hz (Theta waves) during Wakefulness and REM sleep, while it is between 2-4 Hz (Delta waves) during NREM sleep. Additionally, the absence of Neck muscle tone in REM sleep facilitates differentiation between Wakefulness and REM states. **B-D**: Depiction of the number of epochs per hour (left), epoch duration (middle), and total time spent on each epoch per hour of recording (right) for Wakefulness (**B**), NREM sleep (**C**), and REM sleep (**D**). In all plots, Gray represents the CTRL group, while Blue and Red represent Unaffected and Affected rats, respectively. Lighter colors correspond to the DMSO conditions, and darker colors represent the SALB conditions. Statistical significance was determined using a Two-Way RM ANOVA followed by a Bonferroni Test ($\alpha = 0.05$).
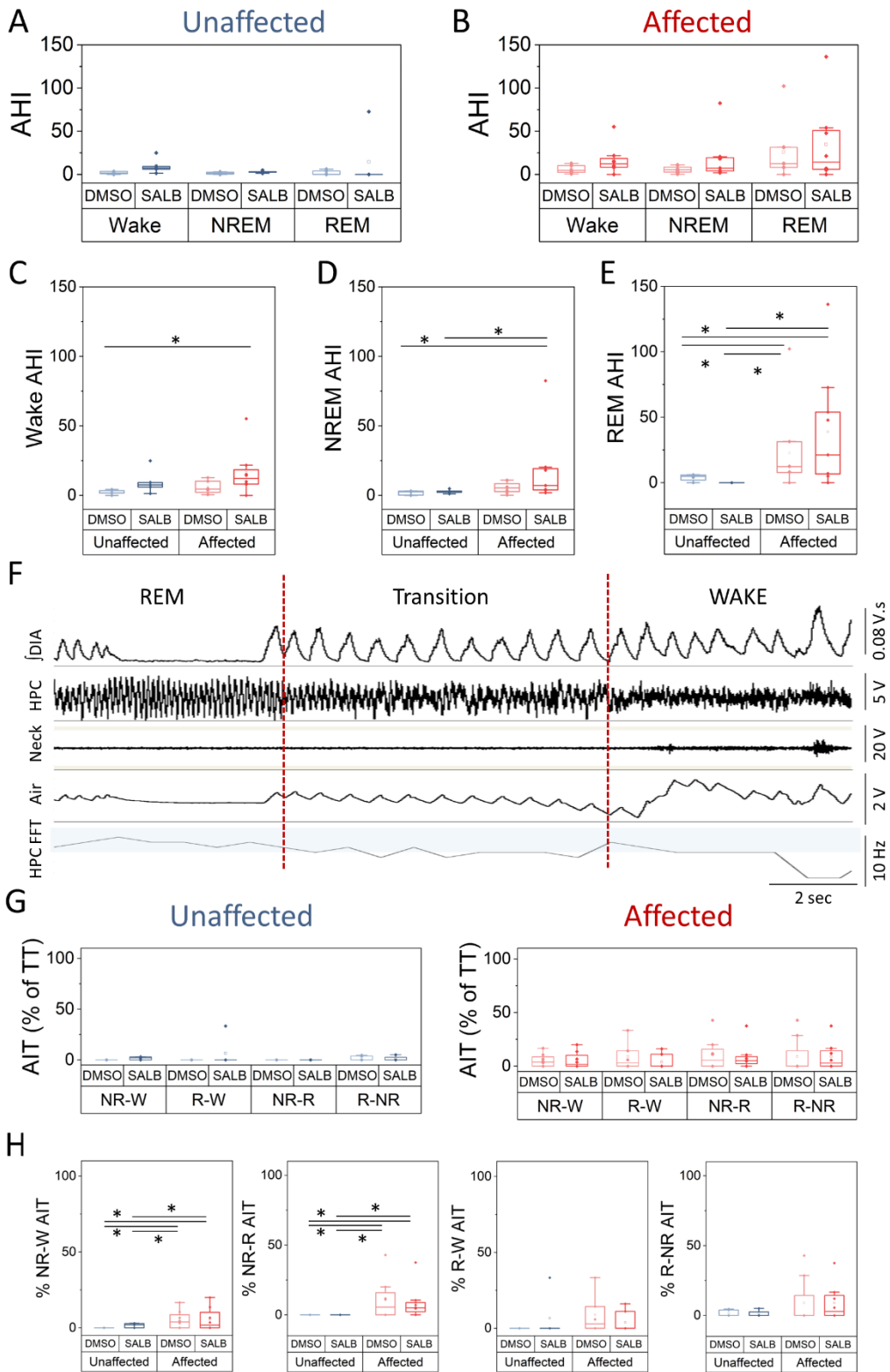
Figure 4.4 Affected rats exhibit heightened sleep fragmentation and an increased occurrence of respiratory disturbances, particularly during REM sleep

A-B: The Apnea Hypopnea Index (AHI) per hour of sleep, categorized by sleep state, in both DMSO and SALB conditions for Unaffected (blue, **A**) and Affected (red, **B**) rats. **C-D**: A comparison of AHI during Wakefulness (**C**), NREM sleep (**D**), and REM sleep (**E**) between Affected and Unaffected rats. **F**: Demonstrative traces of the Integral of the Diaphragmatic Electromyogram (∫DIA), Hippocampus EEG (HPC), Neck EMG, Plethysmograph signal (Air), and the Fast Fourier Transform (FFT) of the HPC. The shaded blue area on the HPC FFT indicates the Theta frequency range (6-8 Hz). This example illustrates an apnea-induced transition of sleep state, where following the apnea, the HPC signal shifts to a transitional state, and the rat awakens (evidenced by the presence of muscle tone in Neck EMG) within 10 seconds of the apnea occurrence. **G**: Apnea-induced transitions (AIT) as a percentage of Total Transitions (TT) for Unaffected (blue, left panel) and Affected rats (red, right panel) in DMSO and SALB conditions. Represented transitions include NREM-Wake (NR-W), REM-Wake (R-W), NREM-REM (NR-R), and REM-NREM (R-NR). **H**: Percentage of transitions representing an AIT for NR-W, NR-R, R-W, and R-NR transitions in Unaffected and Affected animals under DMSO and SALB conditions. In all plots, Blue and Red represent Unaffected and Affected rats, respectively. Lighter colors correspond to the DMSO conditions, and darker colors represent the SALB conditions. Statistical significance was determined using a Two-Way RM ANOVA followed by a Bonferroni Test ($\alpha = 0.05$).
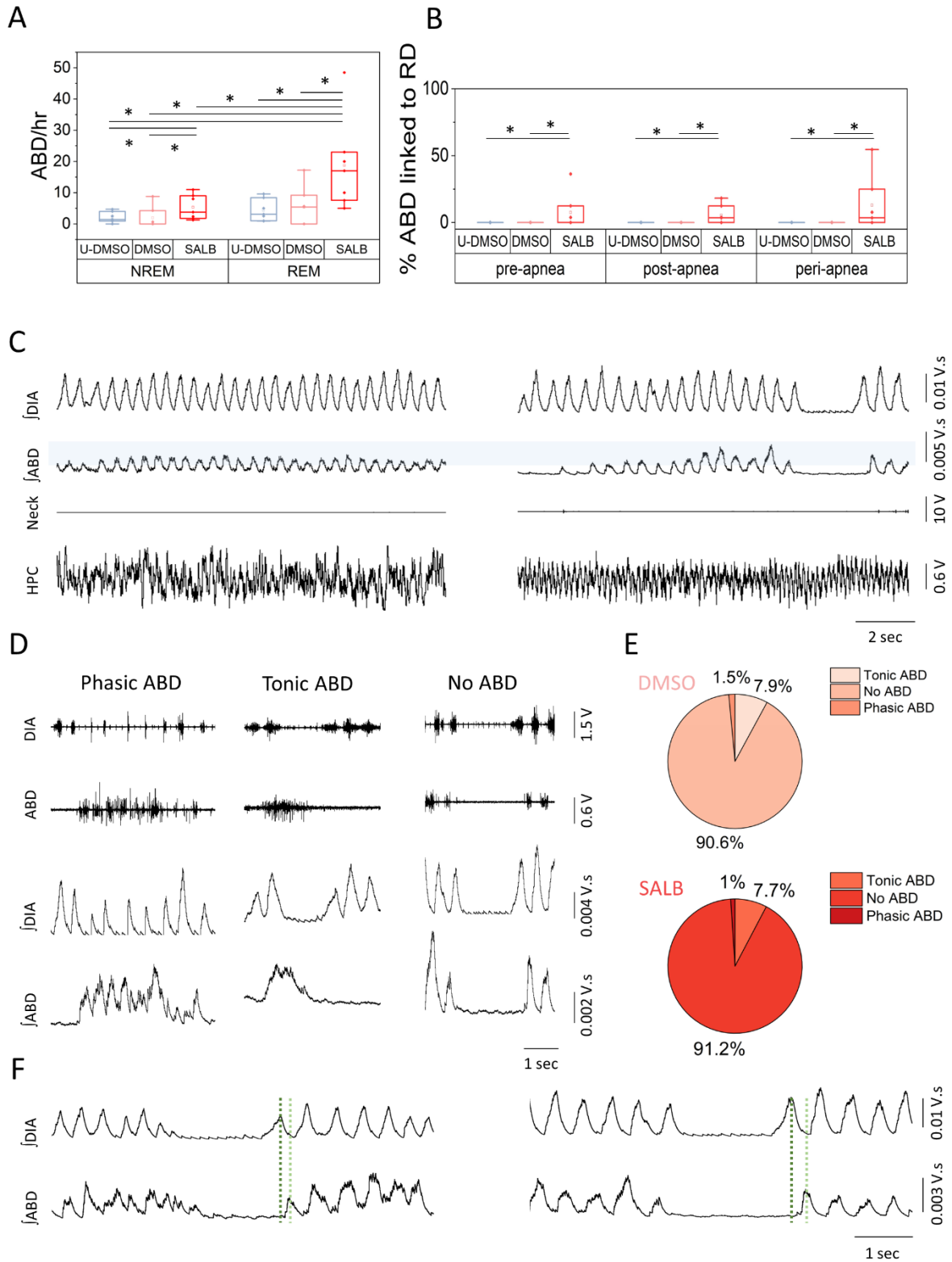
Figure 4.5 Affected rats exhibit a higher occurrence of abdominal (ABD) recruitment during sleep, and a greater percentage of this activity is associated with apneas in the Affected group

A: Depicts the number of Abdominal recruitment events per hour (ABD/hr) during NREM and REM sleep in Unaffected (Blue) and Affected (Red) rats. **B**: Illustrates the percentage of ABD events linked to respiratory disturbances (RD), categorized based on the timing of ABD events concerning apneas/hypopneas—Pre-apnea (within 10 seconds prior to RD), Post-apnea (within 10 seconds following RD), and Peri-apnea (a combination of events before and after RD. Notably, in DMSO conditions for both Unaffected and Affected rats, 100% of ABD events were unrelated to respiratory disturbances, while in SALB conditions, Affected rats showed a higher incidence of ABD events linked to RD. Blue and Red represent Unaffected and Affected rats, respectively. Lighter colors correspond to DMSO conditions, and darker colors represent SALB conditions. Statistical significance was assessed using a Two-Way RM ANOVA followed by a Bonferroni Test ($\alpha = 0.05$). **C**: Demonstrative traces of Diaphragmatic ($\int$DIA) and Abdominal ($\int$ABD) EMG integral, Neck EMG, and HPC EEG. The left panel shows an example of ABD activity unrelated to any respiratory disturbance, while the right panel depicts ABD activity associated with a respiratory disturbance. **D**: Exemplifies cases of respiratory disturbances with observed phasic ABD activity (left), tonic ABD activity (middle), or no ABD activity (right) during the respiratory disturbance itself. **E**: Utilizes pie charts to represent the percentage of respiratory disturbances exhibiting tonic ABD, no ABD, or phasic ABD patterns in DMSO and SALB conditions for Affected rats. Legends are shown in the figure. **F**: Illustrates representative traces of $\int$DIA and $\int$ABD during apneas, emphasizing that cases where ABD activity resumed after an apnea, it consistently initiated bursting activity following the resumption of the Diaphragmatic EMG. This pattern occurred in 100% of cases where ABD activity resumed after an apnea.

Chapter 5.   Discussion

Throughout my research endeavors, I employed a diverse array of methodologies and experimental approaches to address significant knowledge gaps within the realm of respiratory control. The primary objective of this work revolved around describing active expiration through the contraction of ABD muscles, during sleep in cases marked by an impaired inspiratory drive and following modulation of the parafacial region of the ventrolateral medulla (pFL). An additional aim that emerged as the result of the investigation on the modulation of the pFL, was to elucidate the rostrocaudal extension of the pFL. To achieve these goals, I conducted a multifaceted investigation involving chemogenetic and pharmacological interventions, followed by response-based analyses.

Specifically, this research entailed the following key components:

I.   Investigating the Role of the pFL in the generation of Active Expiration during Sleep: A chemogenetic study aimed to unravel the contributions of the pFL in the recruitment of ABD activity during sleep. My findings demonstrated that chemogenetic modulation of the pFL influenced the frequency, prevalence, and amplitude of ABD recruitment during REM sleep. Remarkably, these effects were not observed during quiet wakefulness or non-rapid eye movement (NREM) sleep, suggesting a vigilance state-dependent mechanism for the occurrence of active expiration during sleep (Chapter 2).

II.   Uncovering the Rostro-Caudal Distribution of the pFL: My investigation into the rostro-caudal distribution of the pFL unveiled significant insights. The most pronounced and enduring alterations in tidal volume, minute ventilation, and combined respiratory responses occurred at more rostral pFL locations, specifically at +0.6 mm and +0.8 mm from the VIIc. Moreover, I consistently observed the fastest onset of responses at the +0.6 mm location, highlighting its proximity to the core of the pFL. These findings underscore the crucial significance of examining the rostral pFL regions, which have received relatively limited attention in the existing body of literature.

III.   Assessing Active Expiration during Sleep with Impaired Inspiratory Drive: I embarked on a comprehensive exploration by inhibiting the preBötC via a chemogenetic approach, successfully creating a condition of impaired inspiratory drive. This alteration led to an

augmented occurrence of respiratory disturbances during sleep, while wakeful breathing remained unaffected. Notably, my observations revealed an increased incidence of ABD recruitment events under these conditions, in comparison to control scenarios.

In conclusion, my research efforts have shed light on the intricate mechanisms governing respiratory control and active expiration during sleep. The findings from the multifaceted approach used, suggest an enhancement of active expiration in conditions of an impaired inspiratory drive, emphasize the role of vigilance states on the recruitment of ABD activity, demonstrates the involvement of the pFL in active expiration during sleep and highlight the significance of the pFL's rostral regions for the recruitment of ABD muscles.

5.1 Role of the pFL in Active Expiration during sleep

Using a chemogenetic approach, this research aimed to investigate whether the lateral parafacial region (pFL) could be responsible for the previously documented recruitment of the abdominal muscles (ABD) during sleep (Andrews & Pagliardini, 2015; Leirao et al., 2017; Saini & Pagliardini, 2017; Sherrey et al., 1988). The findings from this study indicate that the modulation of the pFL influences the frequency, prevalence, and amplitude of ABD recruitment, specifically during REM sleep, while it does not appear to affect ABD activity during periods of quiet wakefulness and non-REM (NREM) sleep. These results suggest that the mechanism driving the generation of ABD recruitment during sleep may be dependent on the individual's state of vigilance. Furthermore, this investigation also revealed that the enhanced ventilation observed at the onset of ABD recruitment under control (CTRL) and excitatory conditions was notably reduced in inhibitory conditions. Lastly, it was observed that the modulation of the pFL and the occurrence of ABD recruitment did not contribute to stabilizing breathing by decreasing the number of respiratory disturbances but instead had an impact on a breath-to-breath basis.

5.1.1 Histological analysis and extent of pFL chemogenetic modulation

The identification of specific markers for pFL cells remains elusive. In this research, the selection of injection coordinates for targeting the pFL was informed by previous studies on active expiration recruitment using various manipulations of the ventrolateral area adjacent to VII (Boutin et al., 2017; de Britto & Moraes, 2017; Huckstepp et al., 2016; Huckstepp et al., 2015;

Pagliardini et al., 2011). In this study, viral expression extended approximately 1200 μm along the rostro-caudal axis around the caudal tip of the facial nucleus, with most transfected cells concentrated within a smaller 600 μm area (from -0.3 mm to +0.3 mm from VIIc). While the DREADD receptor expression did not rely on a specific marker, impacting potential non-respiratory structures, the majority of transfected cells were positioned ventrolateral to the facial nucleus. The nonspecific transfection of cells in the parafacial area, combined with the localized injection focus, may have contributed to the incomplete silencing or activation of the pFL, and consequently ABD recruitment, during sleep in this study. As seen in chapter 3 of this thesis, the rostro-caudal extension of the pFL may expand more rostrally than previously thought, and the lack of DREADD expression at locations rostral to +0.3 mm from VIIc in this study may have influenced these results. Alternatively, the presence of competing inhibitory and excitatory modulatory mechanisms on pFL neurons in the absence of anesthesia could explain the incomplete effects on ABD muscle recruitment in DREADD-Gi and DREADD-Gq rats compared to prior pharmacological studies in anesthetized preparations (Boutin et al., 2017; Huckstepp et al., 2015; Huckstepp et al., 2018; Huckstepp et al., 2016; Pagliardini et al., 2011).

5.1.2 The mechanism for ABD recruitment during sleep may depend on vigilance state

Previous research has documented the presence of expiratory abdominal (ABD) recruitment during REM sleep, with limited occurrences during NREM sleep (Andrews & Pagliardini, 2015; Leirao et al., 2017; Saini & Pagliardini, 2017; Sherrey et al., 1988). This study shows that chemogenetic manipulation of the expiratory oscillator has a specific impact on the frequency and strength of ABD activity during REM sleep, in contrast to NREM sleep, where no such effects were observed. These results contrast with findings from manipulations of the RTN, where it was observed that optogenetic stimulation of the RTN during REM sleep had no discernible impact on respiratory frequency, tidal volume, or minute ventilation. However, when such stimulation occurred during NREM sleep and wakefulness, it led to alterations in breathing, as reported by Burke et al. in 2015. These distinctions in the vigilance state-dependency of active expiration generation by the pFL (as demonstrated in this study) and the respiratory modifications induced by the RTN (Burke et al., 2015) underscore the likelihood of the parafacial area housing two distinct neuronal populations, namely the pFV and the pFL, each with unique functions and modulatory mechanisms during sleep, as proposed by Pisanski and Pagliardini in 2018. Similarly, previous studies have reported

vigilance state-dependent alterations in respiratory parameters and chemosensory mechanisms during sleep (Lydic et al., 1991; Megirian et al., 1980; Phillipson et al., 1976b; Sherrey et al., 1988; Smith et al., 1997; Souza et al., 2018). The mechanisms underlying these state-dependent variations are not well understood and may explain the distinct effects of chemogenetic manipulations across different vigilance states in this study.

The activity of the pFL is hypothesized to be governed by a complex interplay of inhibitory and excitatory mechanisms (Boutin et al., 2017; Huckstepp et al., 2016; Pagliardini et al., 2011). Cholinergic neurons in the laterodorsal and pedunculopontine tegmental nucleus (LDT/PPT) play a role in initiating REM sleep, while cholinergic cells in the basal forebrain influence the duration of REM epochs and the homeostatic sleep response (Han et al., 2014; Kalinchuk et al., 2015; Van Dort et al., 2015). Therefore, cholinergic modulation was hypothesized to potentially be involved in the state-dependent expiratory ABD activity (Boutin et al., 2017; Pisanski & Pagliardini, 2018) either through direct or indirect projections to the pFL. Interestingly, a recent study unveiled that there are no direct cholinergic projections from the LDT/PPT to the pFL area and these projections are glycinergic, GABAergic and Glutamatergic instead (Biancardi et al., 2021). Based on these anatomical data, selective ABD recruitment during REM sleep could include the withdrawal of inhibitory inputs or the activation of glutamatergic pathways from LDT/PPT to pFL (Biancardi et al., 2021; Huckstepp et al., 2018; Pagliardini et al., 2011) or could involve projections from different brain areas with state dependent activity. Vigilance state-dependent variations in neurotransmitter release in various brain regions have been observed in previous studies (Léna et al., 2005; Lopez-Rodriguez et al., 2007; Vanini et al., 2011), suggesting that these variations may also influence pFL activity. One possible research avenue to investigate the state-dependent ABD recruitment during sleep, may be to specifically manipulate the activity of GABAergic, glycinergic and glutamatergic projections from LDT/PPT to pFL through chemogenetic inhibition and excitation in unanesthetized freely behaving rodents during their resting period.

5.1.3 Breathing enhancement following the recruitment of ABD muscles

My findings reveal that augmenting pFL excitability through chemogenetic modulation increases the frequency of REM events featuring ABD recruitment, while its inhibition diminishes the occurrence of such events. In CTRL and excitatory conditions, ABD recruitment events

correspond to a decrease in respiratory variability and an increase in ventilation, consistent with prior reports (Andrews & Pagliardini, 2015; Saini & Pagliardini, 2017). However, during chemogenetic inhibition of the pFL, ABD recruitment does not lead to stabilization of breathing or increased ventilation. It has been previously suggested that pFL activation may stabilize breathing through mechanisms like the mechanical facilitation of air outflow via ABD muscle recruitment or through direct and indirect excitation of the preBötC (Pisanski & Pagliardini, 2018). As the facilitation of air outflow persists in the inhibitory conditions of this study, without producing a reduction in respiratory variability or increasing ventilation, it is possible that the respiratory improvements associated with ABD activity in CTRL and excitatory conditions might be attributable to central mechanisms linked to pFL activation. The existence of direct and/or indirect excitatory connections from the pFL to the preBötC has been proposed in embryonic and neonatal stages (see Figure 9 in Huckstepp et al., 2016; Thoby-Brisson et al., 2009) and inferred from physiological evidence in adult rats (Pagliardini et al., 2011). Recent anatomical studies revealed the existence of direct GABAergic, Glycinergic and Glutamatergic projections from preBötC to pFL (Biancardi et al., 2021; Yang & Feldman, 2018), as well as monosynaptic connections from the parafacial area to inhibitory and excitatory preBötC neurons (Yang et al., 2020). To better understand the functionality of the pFL projections to preBötC, it will be necessary to specifically excite pFL neurons that project to the preBötC, for example through an optogenetic approach, in anesthetized and unanesthetized preparation. If these neurons are involved in stabilization of breathing only, we should expect a reduction in breathing variability without the occurrence of ABD activity. Similarly, inhibition of these neurons during a condition that induces sustained ABD activity (e.g. hypercapnia/hypoxia or bicuculline injection) would provide insight into whether they are directly involved in the recruitment of ABD activity or have a singular role in stabilization of breathing through excitatory projections to the preBötC.

ABD muscle recruitment in REM sleep is known to coincide with reduced respiratory variability during its transient occurrence (Andrews & Pagliardini, 2015; Saini & Pagliardini, 2017). Hence, I hypothesized that impairment of ABD recruitment might lead to an increased number of respiratory disturbances in healthy rats, while enhancing these events could reduce the natural respiratory disturbances in healthy rats. Nevertheless, the analysis of respiratory disturbance frequency showed that chemogenetic modulation of the expiratory oscillator had no impact on apnea occurrence. Respiratory disturbances in healthy rats are minimal, with an average rate of

approximately 2 apneas per hour (Carley et al., 1996). In conditions where apneas are nearly absent, such as in this current study, augmenting pFL activity may not provide an accurate assessment of the benefits associated with enhancing ABD recruitment during sleep, although these effects may prove beneficial in pathological conditions like sleep-disordered breathing.

5.2 Rostrocaudal distribution of the pFL

In this study, the primary objective was to investigate the distribution of the source of active expiration along the rostro-caudal axis within the lateral parafacial region (pFL). To achieve this goal, I employed bicuculline, a GABA-A receptor antagonist recognized for its ability to disinhibit pFL cells (de Britto & Moraes, 2017; Huckstepp et al., 2015; Pagliardini et al., 2011; Silva et al., 2019). Bicuculline was administered at various rostro-caudal coordinates, and I rigorously examined the resulting respiratory responses to pinpoint the precise location within this region that elicited the most significant alterations. These findings provide valuable insights into the neural circuitry that governs active expiration in the brainstem, with a particular emphasis on the relatively unexplored, more rostral areas ventrolateral to the facial nucleus.

5.2.1 Histological Analysis

During the histological analysis, I adopted a stereological approach to identify the central region of the injection sites by averaging sections containing fluorobeads. Experimental subjects were categorized based on the proximity of the injection sites, spanning from -0.2 mm to +0.8 mm from VIIc. I took measures to ensure that injections were positioned ventrolateral to the facial nucleus (VIIc) and did not overlap with PHOX2B+ cells within the more ventromedial retrotrapezoid nucleus (RTN). Evaluation of cellular activity following bicuculline activation, as measured by cFos staining, confirmed minimal baseline activity of the PHOX2B+ cells in all groups compared to the control group and limited mediolateral spread of the drug from the core site of injection.

5.2.2 Temporal dynamics of the ABD response reveal a longer-lasting and fastest response at rostral locations

Active expiration was effectively induced across all injection sites within the rostro-caudal range of -0.2 mm to +0.8 mm from the caudal tip of the facial nucleus, aligning with previous studies involving pharmacological disinhibition, excitation, chemogenetics, or optogenetics (Boutin et al.,

2017; de Britto et al., 2020; de Britto & Moraes, 2017; Huckstepp et al., 2015; Korsak et al., 2018; Magalhães et al., 2021; Pagliardini et al., 2011; Silva et al., 2019; Zoccal et al., 2018). While traditionally the pFL location is determined based on the presence of active expiration, my research reveals that this criterion alone may not precisely identify the pFL core. Instead, a comprehensive analysis incorporating multiple respiratory measures was employed to pinpoint the site generating the most robust respiratory effects. Noteworthy variations in the temporal dynamics of ABD responses along the rostro-caudal axis were observed, with rostral sites displaying longer durations and stronger synchronization with DIA signals compared to caudal sites. Robust ABD and DIA signal coupling, indicating the strength of the ABD response, was observed at rostral sites exceeding +0.1 mm up to +0.8 mm. Importantly, I established variations in the duration, amplitude, shape, and ABD/DIA coupling of responses induced by bicuculline along the rostro-caudal axis, with more rostral sites at +0.6 mm and +0.8 mm yielding the fastest, most potent and prolonged responses, suggesting proximity to cells responsible for ABD recruitment following bicuculline injection.

5.2.3 Bicuculline injection elicited stronger respiratory effects at the rostral locations

Bicuculline injections induced notable alterations in respiratory parameters, as consistently observed in prior research investigating the effects of bicuculline/strychnine injections in the ventral medulla (de Britto & Moraes, 2017; Pagliardini et al., 2011; Silva et al., 2019). Remarkably, a reduction in respiratory frequency, coupled with the emergence ABD recruitment, was evident in caudal locations (-0.2 mm, +0.1 mm), resembling the effects induced by pharmacological activation of the pFL in those specific regions (Boutin et al., 2017; Silvia Pagliardini et al., 2011). In contrast, at more rostral locations in this study (+0.4 mm, +0.6 mm, +0.8 mm), respiratory frequency remained unaltered despite concurrent ABD recruitment. This discrepancy suggests that the deceleration in respiratory period observed in caudal locations might stem from the disinhibition of the adjacent Bötzinger Complex. Tidal volume (V_T) exhibited a uniform increase of 16-29% at all studied locations, except for -0.2 mm, aligning with previous findings following pFL activation (Boutin et al., 2017; Pagliardini et al., 2011) and suggesting partial disinhibition of inhibitory Bötzinger complex neurons at the most caudal location. Notably, minute ventilation (V_E) increased at the +0.6 mm location, decreased at -0.2 mm, and remained unchanged at other sites, highlighting the nuanced rostro-caudal organization of the pFL. These

results emphasize the need to explore responses to diverse pharmacological pFL modulators across the rostro-caudal axis, particularly in less investigated, more rostral regions, where distinct responses may arise based on the specific pharmacological agent employed.

5.2.4 Injection of bicuculline decreased oxygen consumption at the rostral locations

This research also explored the metabolic implications of bicuculline-induced respiratory changes, a parameter not previously studied in similar investigations (de Britto & Moraes, 2017; Pagliardini et al., 2011; Silva et al., 2019). In this study, a reduction of 25-33% in oxygen consumption (V_{O2}) was observed at the most rostral injection locations (+0.6 mm, +0.8 mm). The drop in oxygen consumption observed in this study resembles previous findings in anesthetized rats exposed to hypoxia while maintaining a constant body temperature. In those studies, a decrease in metabolism during hypoxia (ranging from 18% to 40%) coincided with concomitant increases in ventilation (V_E) (Blatteis & Lutherer, 1973; Frappell et al., 1995; Gautier et al., 1991; Olson Jr & Dempsey, 1978; Pappenheimer, 1977). Interestingly, the observed drops in metabolism in this study, coincided with the sites where substantial alterations in tidal volume (V_T) and minute ventilation (V_E) were induced by Bicuculline injections. These changes in V_T and V_E, were not driven by physiological necessity and therefore can be considered artificial hyperventilation. The observed bicuculline-induced hyperventilation at the rostral sites likely led to a decrease in arterial pCO2, in accordance with previous studies demonstrating that artificial hyperventilation in anesthetized dogs leads to a drop in arterial pCO2 (Daly Md Fau - Hazzledine & Hazzledine, 1963). The decrease in V_{O2} at locations where V_T and V_E increased may be attributed to a reduction in pCO2 shifting the oxyhemoglobin dissociation curve to the left, resulting in reduced oxygen delivery to the tissues, thereby decreasing V_{O2}. Similar findings have been reported in experiments involving anesthetized dogs, where an allosteric modifier of hemoglobin shifting the oxyhemoglobin curve to the right resulted in an increase in maximal V_{O2} at the skeletal muscle level (Richardson et al., 1998). Consequently, the decrease in V_{O2} and the increase in V_E at the rostral locations led to an elevation in the V_E/V_{O2} ratio, supporting the assumption that artificial hyperventilation was induced by activating ABD recruitment while maintaining other physiological demands unchanged.

5.2.5 Bicuculline responses following injections along the rostrocaudal axis of the ventral medulla can be differentiated by the time course and strength of their activation during Late-E, Inspiration and Post-I periods

To further differentiate the responses elicited at the rostral level, I used a multidimensional analysis developed for this study, that combined the standardized airflow, ABD and DIA EMG signals in a 3D space to create a cycle-by-cycle loop of the respiratory phases. The analysis of the deformations elicited on the respiratory loop following injection of bicuculline, enabled the more effective distinction of bicuculline-induced effects at the two most rostral locations. These findings indicated that distortions in the respiratory loop during the late-E, Inspiratory, and Post-I periods were more pronounced at the +0.6 mm and +0.8 mm positions compared to caudal injections. Notably, the +0.8 mm group exhibited prolonged impacts during the late-E and post-I phases. Additionally, subtle distinctions in late-E responses between the two rostral locations, previously undetected, were revealed. Conversely, the most significant inspiratory deformations were observed in the +0.6 mm group, aligning with substantial changes in tidal volume, reported earlier in this research.

Collectively, these results suggest that while the combined effects of bicuculline injections on the respiratory cycle were most pronounced at the two most rostral positions, variations in the effects during each respiratory phase at this level of the ventral medulla were evident. These nuanced effects may indicate differences in the characteristics and phenotypes of cell populations at these specific coordinates. Further investigations into the phenotypic and electrical properties of neurons at the +0.6 mm and +0.8 mm levels are warranted, given the observed differences in our study. Previous research has shown variations in late-E neuron membrane potentials during hypercapnia at the caudal tip of VIIc (+0.1 mm to +0.3 mm), with depolarization during the post-I and late-E phases, resulting in firing during the latter. Additionally, distinct postsynaptic currents govern membrane potentials during each respiratory phase (Magalhães et al., 2021). Differences in these synaptic currents at the +0.6 mm and +0.8 mm locations may account for the subtle distinctions observed in the deformations of the respiratory loop during late-E, Inspiration, and Post-I phases, necessitating further investigation. While my study does not definitively determine whether bicuculline is exerting its effects through presynaptic or postsynaptic mechanisms, or whether it is acting at the dendritic or somatic level, previous research has provided insights. Late-E neurons in

the parafacial area have been found to be influenced by both GABAergic Inhibitory Postsynaptic Currents (IPSCs) during the inspiratory phase and Glycinergic IPSCs during both inspiration and post-inspiration, as noted in Magalhaes et al. in 2021. Therefore, it is plausible that the effects of bicuculline in the pFL are a result of blocking postsynaptic inhibition.

5.3 Respiratory Disturbances and Active Expiration in conditions of impaired inspiratory drive

This study investigates respiratory disturbances and abdominal (ABD) recruitment during sleep in the context of impaired inspiratory drive. Impairment was induced using a viral vector expressing the KORD receptor with the HA-tag, leading to hyperpolarization of the preBötC region upon SALB administration. A positive correlation linked the number of inhibited cells at the preBötC core to respiratory disturbances. Affected rats, presented with higher KORD expression, exhibited increased disturbances, prolonged apneas, heightened wakefulness, and sleep fragmentation post-SALB injection. Additionally, ABD recruitment rose, especially in REM sleep, suggesting compensation for elevated disturbances, whereas the distinct ABD activity patterns observed, underscore the interplay between inspiratory and expiratory drives. These findings advance our understanding of neural control of breathing during sleep, particularly in impaired inspiratory conditions.

5.3.1 Higher expression of KORD virus associated with higher number of respiratory disturbances

Immunohistochemical analysis revealed a distinctive expression pattern of the KORD receptor labeled with the HA-tag in rats with increased respiratory disturbances, indicating a correlation between receptor expression and disturbed breathing. To induce impaired inspiratory drive, over 900 cells at the SST-core in the preBötC were inhibited, a larger number compared to prior studies inducing respiratory disturbances by ablating 300-450 NK1R+ cells (McKay & Feldman, 2008; McKay et al., 2005; Roberts et al., 2022). The use of a pan-neuronal promoter for KORD receptor expression, the lack of secondary gliosis due to cell death, and the preservation of rhythmogenic cells (hyperpolarization rather than cell death) in this approach likely contributed to this difference. This investigation found that KORD receptor expression was limited to SST-negative neurons, excluding cells with this specific phenotype. This was not intentional, but possibly due to tropism

of the AAV5 serotype for selected cellular phenotype. Although AAV5 can generally transfect central nervous system cells (Davidson et al., 2000), its capability to infect preBötC SST+ cells specifically has not been fully explored. Previous studies in our laboratory (Alsahafi et al., 2015) used a AAV5 phenotype to optogenetically control respiratory rhythm, but the colocalization with SST+ cells was not specifically assessed, although NK1R+ cells were transfected with the virus. Despite this, the absence of KORD receptor expression in SST+ cells does not compromise the interpretation of the results, as SST+ cells are proposed to contribute to respiratory patterns rather than the direct generation of rhythm itself (Cui et al., 2016; de Sousa Abreu et al., 2022).

5.3.2 Salvinorin B administration in Affected rats increases central apneas, prolongs apneas, reduces sighs, and induces sleep fragmentation.

In this investigation, the Affected group of rats exhibited an elevated frequency of respiratory disturbances, particularly during REM sleep, following SALB administration. This aligns with findings from a study involving unilateral ablation of NK1R+ cells using Substance-P conjugated to saporin (McKay & Feldman, 2008). However, the results of this study diverge from those reported by Roberts et al., 2022, where bilateral focal ablation of preBötC cells using DTA resulted in a higher prevalence of respiratory disturbances during NREM sleep. Discrepancies in sleep stage specificity between my study and Roberts et al., 2022, may be attributed to nuanced variations in quantification protocols. Notably, my study and McKay et al., 2008, employed a 2.0-second criterion for quantifying apneas/hypopneas, whereas Roberts et al., 2022, used a slightly shorter duration of 1.8 seconds. These subtle methodological differences could contribute to the observed distinctions in the prevalence of respiratory disturbances between the studies. Alternatively, they could be explained by the neuroinflammation induced due to chronic respiratory disturbances in Roberts et al., 2022.

In addition to an elevated frequency of respiratory disturbances, the Affected group exhibited prolonged apnea durations when compared to CTRL and DMSO conditions in Unaffected rats, a characteristic not directly assessed in previous lesioning studies (McKay & Feldman, 2008; Roberts et al., 2022). Furthermore, SALB administration in Affected rats resulted in a decreased sigh frequency compared to CTRL and Unaffected rats, indicating the inhibition of neurons within the preBötC circuit responsible for generating sighs. Previous investigations on the ablation of

NK1R+ cells in the preBötC, as reported by McKay et al. (2005) and Roberts et al. (2022), have yielded conflicting outcomes. McKay et al. (2005) observed a sigh frequency decrease following the ablation of NK1R+ cells, while Roberts et al. (2022) did not detect alterations in sigh frequency. Despite the absence of KORD HA-tag overlap with SST+ cells in my study, the activation of KORD receptors still led to a reduction in sigh frequency. This supports the notion that SST+ neurons in the preBötC function as downstream elements in the sigh generation circuit rather than being the generators themselves. This study likely inhibited NMBR or GRPR neurons, proposed as the origin of sighs (Li et al., 2016), through the pan-neuronal promoter expression of KORD receptors. Collectively, these findings suggest that cells responsible for generating sighs in the preBötC may potentially be neurons characterized by the absence of SST, coupled with the expression of NMBR and GRPR. Further experimental clarification on the role of NK1R+ cells in sigh generation and confirmation of the complete phenotype of the cells involved in sigh generation is still required.

Sleep fragmentation, marked by recurrent night awakenings, is a notable symptom of sleep-disordered breathing, affecting mood, concentration, vigilance, and attention (Sforza & Roche, 2016; Sforza et al., 2016). In this study, rats with increased respiratory disturbances also exhibited more frequent awakenings during sleep compared to Unaffected rats and CTRL. These awakenings were particularly prevalent in NREM sleep and closely associated with respiratory disturbances. While a trend towards increased awakenings from REM sleep was observed, it did not reach statistical significance. These findings align with previous studies indicating elevated awakenings in sleep-disordered breathing (Roberts et al., 2022; Swihart Bruce et al., 2008). Notably, patients with sleep-disordered breathing display heightened transitions from NREM to wakefulness (NR-W) and from REM to wakefulness (R-W), with NR-W transitions being more pronounced (Swihart et al., 2010).

5.3.3 SALB administration in Affected rats increases ABD activity during sleep

One of the main interests of our laboratory is the understanding the role of expiratory abdominal (ABD) activity and the potential contribution of the expiratory oscillator located in the lateral parafacial area (i.e., pFL) in generating this activity during sleep (Andrews & Pagliardini, 2015; Pisanski et al., 2019; Saini et al., 2022; Saini & Pagliardini, 2017). As this activity is associated

with improved ventilation and respiratory stability during sleep (Andrews & Pagliardini, 2015), a key question arises: can enhancing this activity help stabilize breathing in conditions of impaired inspiratory drive? Although I am not reporting the measures of ventilation and respiratory variability in the KORD study (measurements are under way), this study demonstrates that in the presence of heightened respiratory disturbances, there is an increased occurrence of ABD recruitment events, especially during sleep. Furthermore, under conditions of impaired inspiratory drive (SALB), the percentage of ABD activity associated with respiratory disturbances rises compared to DMSO conditions. While this evidence is observational, it provides an initial step supporting the idea of the expiratory oscillator and ABD recruitment as a backup mechanism in conditions of impaired inspiratory drive. However, further experiments manipulating the expiratory oscillator, involving both silencing and activation, under impaired inspiratory drive conditions will be crucial for fully substantiating this hypothesis.

Previous studies investigating the dynamics between expiratory and inspiratory oscillators in adult rodents, specifically focusing on the pFL have indicated difficulties in sustaining active expiration when the inspiratory oscillator is compromised (Huckstepp et al., 2016). Uncertainties have arisen regarding the generalizability of these results to freely behaving rats due to experiments being conducted under anesthesia where autoresuscitation is impaired (Krause et al., 2016) and active expiration does not usually occur. Previous research, involving awake rats with strong inhibition of preBötC SST+ cells, suggested an inability to maintain breathing patterns when the preBötC is entirely silenced, but ABD activity was not measured in those cases (Tan et al., 2008). Chapter 2 of this thesis corroborated the notion that the pFL influences ABD activity during sleep (Pisanski et al., 2019), supporting the hypothesis that the expiratory oscillator plays a role in these events. Here, under conditions of moderately impaired inspiratory drive, I found that nearly 98% of complete central apneas during sleep were characterized by the complete absence of expiratory ABD activity or a brief burst of tonic ABD activity concluding before the end of the apnea. Only about 2% of respiratory disturbances exhibited phasic ABD activity, exclusively during incomplete inspiratory drive suppression. Overall, this suggests that the expiratory oscillator, responsible for ABD activity during sleep, requires the presence of an intact inspiratory drive to be operational (Huckstepp et al., 2016).

5.4 Technical Considerations

In this thesis, I employed an innovative approach known as chemogenetics to address crucial inquiries concerning the involvement of the pFL in the activation of active expiration during sleep, both in healthy conditions and under circumstances characterized by a compromised inspiratory drive. Additionally, I combined traditional pharmacological interventions and electromyogram recordings, with a newly developed methodology for respiratory cycle analysis to pinpoint the specific rostrocaudal location within the lateral parafacial area that elicited the most pronounced respiratory effects. Nonetheless, it is essential to acknowledge that this research is not exempt from limitations. This section delves into an analysis of the technical considerations inherent to this study and their impact on the interpretation of the findings.

5.4.1 DREADDs

In Chapter 2, a chemogenetic approach was employed to specifically modulate the activity of the pFL brain region. While DREADD technology is widely acknowledged as a potent method for remotely controlling cellular activity, it is important to note that certain limitations have been brought to attention, which could potentially affect the interpretation of results unless rigorous control experiments are conducted, as highlighted in prior reports (Gomez et al., 2017; MacLaren et al., 2016; Mahler & Aston-Jones, 2018; Manvich et al., 2018; Raper et al., 2017). For instance, it has been observed that the systemic administration of the supposedly "inert" ligand CNO may induce locomotion-related and behavioral effects, likely associated with CNO's conversion into clozapine and N-desmethylclozapine (MacLaren et al., 2016; Manvich et al., 2018; Raper et al., 2017). Furthermore, recent discussions have suggested that the effects attributed to DREADD technology might be mediated by clozapine rather than CNO itself. This is due to the limited penetration of CNO across the blood-brain barrier and the high affinity of DREADD receptors for clozapine (Gomez et al., 2017; Raper et al., 2017). Additionally, the slow conversion of CNO into clozapine can lead to the prolonged duration of DREADD-mediated effects, which can be advantageous for experiments lasting more than two hours, such as the one in this thesis (Mahler & Aston-Jones, 2018). Despite these acknowledged limitations, it is important to emphasize that DREADD technology remains a potent tool for the precise manipulation of brain activity, as supported by Roth in 2016 and Mahler and Aston-Jones in 2018. In chapter 2 of this thesis,

measures were taken to control for potential off-target effects resulting from the metabolic by-products of CNO. Identical, commonly used doses of CNO were administered to rats transfected with both DREADD and non-DREADD viruses, specifically the Cre-eYFP experimental group. The results obtained from experiments in chapter 2, indicate that CNO did not induce effects unrelated to DREADD activation in terms of sleep architecture, respiratory parameters, or the activation of ABD muscles during sleep. Therefore, it can be inferred that the observed outcomes are not linked to off-target effects caused by CNO and its metabolites.

An important challenge associated with DREADD G-coupled receptors is the potential for constitutive activity in the absence of the ligand, as highlighted in prior research (Jami et al., 2016). Recent investigations have demonstrated that the expression of Gi-DREADD in sensory neurons induces substantial alterations in voltage-gated Ca2+ and Na+ currents, even without the ligand clozapine-N-oxide (CNO), along with an upregulation of the Na+ channel NaV1.7. Mice subjected to this manipulation exhibit changes in CNO-independent excitatory and inhibitory second-messenger signaling pathways (Jami et al., 2016). While no specific reports currently address the KORD (κ-opioid receptor DREADD) receptor, it is crucial to recognize the potential for intrinsic activity in this context. The presence of constitutive activity may elucidate the heightened effects observed in the Affected group in chapter 4 of this thesis, particularly in terms of sigh frequency, the duration of respiratory disturbances, and the total number of respiratory disturbances during REM sleep. Despite increased activity under DMSO conditions, notable differences between DMSO and SALB conditions were observed in the Affected rats, particularly in respiratory disturbances independent from sleep states, as well as in the frequency of ABD recruitment and the percentage of ABD events associated with apneas.

In Chapter 4, our investigation revealed a correlation between the quantity of cells expressing the KORD receptor in the preBötC and the incidence of respiratory disturbances. Notably, an aggregate of over 900 transfected cells was imperative to elicit an observable effect. This stands in contrast to prior studies, wherein a lower number of cell ablations (ranging from 300 to 450) sufficed to induce respiratory disturbances (McKay et al., 2008; Roberts et al., 2022). This could be the result of our study having an absence of toxicity and neuroinflammation resulting from cell death, distinguishing it from previous investigations (McKay et al., 2008; Roberts et al., 2022). Alternatively, it is conceivable that the KORD receptor may induce only a mild hyperpolarization

in preBötC cells, resulting in attenuated effects. However, the lack of recorded membrane potentials in preBötC cells transfected with the KORD receptor in response to the SALB ligand precludes definitive confirmation of this hypothesis. Furthermore, it is also possible that the KORD system used in this thesis may have different tropism from the system used by Roberts et al,. (2022) and therefore affected different cell populations.

5.4.2 Abdominal EMG recordings

To pinpoint the core location of the pFL in chapter 3, I conducted bicuculline injections at various rostrocaudal positions within the ventral medulla and measured the resulting respiratory responses. One notable challenge in the data collection was the variability in ABD_{EMG} amplitude among different rats, which was influenced by the proximity of the electrode placements in the muscles. Despite my efforts to maintain a consistent electrode placement within a maximum distance of 2 mm during instrumentation, there remained an inherent variability in the ABD signal across experiments as amplitude of the ABD signal may be influences by other experimental factors, such as anesthetic levels, pCO2, pO2, airflow resistance. This limitation is not unique to the present study, but it becomes more apparent as the main aim of this research is to compare the ABD response elicited at different injection sites to pinpoint the location producing the strongest response.

Originally, my plan involved performing multiple injections at various sites within a single rat to allow for direct comparisons while keeping the ABD_{EMG} variability consistent. However, this approach presented logistical challenges, such as ensuring the overall well-being of the anesthetized rats over extended periods (more than a total of 10 hours) during the injections and waiting for drug effects to dissipate. Therefore, I decided to perform one single injection per rat. I also experimented with inducing hypoxia before the bicuculline injections to establish a baseline measurement of ABD activity during this challenge. The goal was to then express ABD activity during injection as a percentage of the ABD activity observed during hypoxia for each rat, thereby facilitating comparisons between injection sites. Unexpectedly, I discovered that the hypoxia response also varied across rats (results not shown). Some rats exhibited very weak ABD recruitment during the hypoxic response, despite arterial pO2 levels indicating hypoxia and other respiratory parameters showing typical hypoxic responses, such as increased breathing rate, tidal

volume, and minute ventilation with subsequent respiratory depression, whereas in other rats with the same arterial pO2 values, the ABD response was robust. I verified that the lack of a strong ABD response during hypoxia was not due to electrode placement, as bicuculline injections consistently generated a strong response in those rats. Therefore, due to the inconsistent ABD response during hypoxia across rats, I was unable to employ it as a reliable baseline for ABD activity. Consequently, owing to these challenges, raw ABD_{EMG} data was not included in the results. Instead, we focused on the induced respiratory changes, and adopted a multidimensional approach, incorporating standard deviation values of the respiratory signals we measured in order to overcome these limitations. This approach allowed us to identify the locations where bicuculline injections produced the most pronounced respiratory effects.

5.4.3 Lack of unit recordings

Another significant limitation common to all three research projects within my thesis is the absence of single-unit neuronal recordings from the pFL region. This limitation hinders our ability to fully confirm whether the observed active expiration in all three projects directly results from the firing of late-expiratory neurons within the pFL. Notably, the recording of late-expiratory neurons within the putative expiratory oscillator in the pFL has thus far been achieved in adult and juvenile rats, either in anesthetized or in-situ preparations (de Britto & Moraes, 2017; Magalhães et al., 2021; Pagliardini et al., 2011), which are similar experimental conditions to the one I used in the study of the pFL location along the rostrocaudal axis of the ventral medulla. However, finding late-expiratory neurons for single-unit recordings is a time-consuming task and would require prolonged activation of the pFL. In my study, I found that injections of bicuculline at more caudal locations produced relatively short responses, which would make it difficult to find late-E neurons and sample from them in that time frame.

Chronic electrophysiological recordings within the ventral medulla, present added technical challenges when compared to similar recordings in forebrain regions, which are more commonly performed (Fu et al., 2016; Thompson & Best, 1990). One of the significant challenges arises from the fact that respiratory neurons are situated in the lower brainstem, a region that moves relative to the surrounding bones with locomotion and changes in posture. This movement makes it challenging to employ conventional rigid metal or glass electrodes for recording in the ventral medulla in behaving animals (Martial et al., 2005). Efforts have been made to develop techniques

suitable for this purpose (Martial et al., 2005). However, these attempts have resulted in the acquisition of multiunit recordings rather than single units. Additionally, the stability of these recordings was limited to only a few days. In the first two projects of my research with freely behaving rats, it was imperative that the recordings remained stable for a minimum of two weeks following surgery to allow the rats to fully recover and engage in normal sleep patterns without post-operative discomfort.

5.4.4 Quantification of hypopneas

In the fourth chapter of this dissertation, we evaluated the frequency of respiratory disturbances through the quantification of apneas and hypopneas. Specifically, hypopneas were assessed based on a criterion of a >50% reduction in the peak of the respiratory related pressure changes in our barometric system. Existing clinical literature has commonly employed varying thresholds, with some studies defining hypopnea as reductions in airflow ranging from 30% to 50%, accompanied by a concurrent decrease of 3-4% in oxygen saturation (Xie et al., 2002; Casey and Tiwari, 2018; Hadj-Amar et al., 2021). Alternatively, hypopneas are also quantified as a 50% reduction in minute ventilation coupled with a 4% decline in oxygen saturation (GC Mbata & Chukwuka, 2012). Considering the latter definition, it is plausible that the count of respiratory disturbances in this study may have been underestimated.

5.4.5 Lack of preBötC markers in addition to SST

During chapter 4 we identified the location of the cells transfected with the KORD receptor, using SST as the marker for preBötC. The lack of other preBötC markers such as NK1R or Glyt2, limit the interpretation of the results considering that I used a hSyn promoter and likely transfected both excitatory and inhibitory neurons in the preBötC. Future experiments will determine the phenotype of the infected neurons.

5.5 Future Directions

In this section, I will outline potential avenues for future research that emanate from the findings and insights gathered in the preceding chapters. The completion of this PhD thesis marks a point of departure rather than a conclusion, inviting a broader exploration into the intricate realms of the

role of active expiration in the modulation of breathing during sleep. These future directions aim to address existing gaps and expand upon novel methodologies.

5.5.1 To determine the effect of pFL stimulation on the rescuing of breathing in conditions of an impaired inspiratory drive

In Chapter 4 of this thesis, an increase in ABD recruitment events during sleep was observed under conditions of impaired inspiratory drive. This noteworthy finding paves the way for further investigation into the potential therapeutic research aspect of enhancing expiratory ABD activity in pathological conditions. Interestingly, Chapter 2 of this research revealed that chemogenetic modulation of the pFL in freely behaving, naturally sleeping rats had a direct influence on the frequency, robustness, and strength of ABD recruitment during sleep. Consequently, an intriguing avenue of research would involve exploring the feasibility of enhancing active expiration during sleep when faced with impaired inspiratory drive, aiming to assess whether this enhancement can rescue breathing. One conceivable approach to achieving this potentiation is by employing a chemogenetic method to stimulate the pFL in naturally sleeping rats under conditions of impaired inspiratory drive. Such a state of impaired inspiratory drive can be induced, as demonstrated in Chapter 4, either by inhibiting the preBötC or through NK1R-targeted lesions (McKay & Feldman, 2008; Roberts et al., 2022).

5.5.2 To investigate the vigilance-state dependency of the ABD recruitment observed during sleep

In Chapter 2 of this study, it was observed that chemogenetic modulation of the pFL influenced ABD recruitment specifically during REM sleep. This suggests the potential for a vigilance state-dependent modulation of active expiration during sleep. To delve further into the state-dependent ABD recruitment during sleep, a possible avenue for research could involve the targeted manipulation of GABAergic, glycinergic, and glutamatergic projections from state-dependent brain regions that have a direct target on the pFL, for example the LDT/PPT, the periaqueductal gray, the parabrachial nuclei and the ventral respiratory column, as demonstrated by Biancardi et al. in 2020. This manipulation would entail chemogenetic inhibition and excitation in unanesthetized, freely behaving rodents during their resting periods. By doing so, if it is indeed those projections that release inhibition from the pFL during REM sleep, causing its subsequent

excitation and ABD recruitment, then stimulating these neurons throughout the entire sleep period should result in a decrease in the number, robustness, and strength of ABD recruitment events during REM sleep. Conversely, inhibiting the GABAergic/glycinergic neurons may lead to an increase in ABD recruitment events during REM and NREM sleep. On the other hand, if the glutamatergic projections these areas are responsible for the vigilance state-dependent ABD recruitment observed during REM sleep, then exciting these neurons throughout the sleep period should lead to an increase in ABD recruitment not only during REM but also during NREM sleep. Conversely, inhibiting these neurons should result in a decrease in the number of ABD recruitment events observed during REM sleep.

5.5.3 To investigate the projections from the pFL to preBötC

Chapter 2 of this thesis shed light on the potential mechanism behind the observed breathing stabilization during ABD recruitment in sleep (Andrews & Pagliardini, 2015). It was suggested that this stabilization might not be a result of the mechanical facilitation of airflow from the lungs during ABD recruitment, but rather a consequence of direct excitation from the pFL to the preBötC. To gain a deeper understanding of the functional role of these newly described pFL projections to the preBötC (Yang et al., 2020), it would be intriguing to selectively activate pFL neurons projecting to the preBötC using an optogenetic approach in both anesthetized and unanesthetized preparations. If these neurons are solely involved in stabilizing breathing, one would anticipate a reduction in breathing variability without the occurrence of ABD activity when they are excited. Conversely, inhibiting these neurons under conditions that induce sustained ABD activity (such as hypercapnia, hypoxia, or bicuculline injection) could provide insights into whether they play a direct role in ABD activity recruitment or have a singular function in breathing stabilization through their excitatory projections to the preBötC.

5.5.4 To further investigate the rostrocaudal organization of the pFL

The findings of Chapter 3 underscore the intricate rostrocaudal organization of the pFL, challenging previous assumptions and underscoring the importance of exploring previously neglected, more rostral sites. Furthermore, they pave the way for investigating how responses to various pharmacological modulators of the pFL, such as muscarinic and glutamatergic agonists, may vary across the rostrocaudal axis of the ventral medulla, particularly in uncharted, more rostral

regions. If the distribution of inhibitory, muscarinic, and glutamatergic receptors in the lateral parafacial region does not precisely align along the rostro-caudal axis, we can anticipate distinct responses depending on the specific pharmacological agent employed. These proposed experimental approaches together with detailed histology procedures mapping the presence of GABA/Glycine, muscarinic and glutamatergic receptors along the ventral medulla would provide a better picture of the rostrocaudal organization or the pFL.

The frequency response exhibited a significant disparity between caudal and rostral locations, wherein the caudal sites displayed a discernible decrease in respiratory rate in response to bicuculline, a phenomenon not observed in the rostral locations. While our initial interpretation leaned towards the potential diffusion of the drug into the caudal Bötzinger Complex, an alternative explanation posits that these nuanced frequency responses may reflect compartmentalization of the pFL, leading to distinct reactions to varied stimuli. An intriguing avenue for further investigation would involve examining whether afferent projections to pFL differ between the caudal and rostral locations. Such an analysis could elucidate whether distinct brain regions, responsible for disparate functions, project to each of these delineated areas.

5.6 Conclusions

In summary, the second chapter of this research investigated the role of the lateral parafacial region (pFL) in active expiration during sleep using a chemogenetic approach. I found that modulation of the pFL influenced the frequency, prevalence, and amplitude of abdominal muscle (ABD) recruitment, particularly during REM sleep, while it did not affect ABD activity during periods of quiet wakefulness and non-REM sleep. This suggests that the mechanism driving ABD recruitment are state dependent. Additionally, the study showed that enhanced ventilation at the onset of ABD recruitment was notably reduced under inhibitory conditions despite the presence of ABD activity, albeit reduced, in those conditions. This suggests that direct excitation from pFL to preBötC may be the source of respiratory stabilization during ABD recruitment. Finally, the pFL's modulation and ABD recruitment did not contribute to stabilizing breathing by decreasing the number of respiratory disturbances but had an impact on a breath-to-breath basis, instead. Interestingly inhibition of the pFL did not completely silence the ABD recruitment observed during sleep but reduced its frequency and strength. Given the lack of a known genetic markers for the neurons

constituting the expiratory oscillator, we can only hypothesise that an incomplete transfection of all the pFL cells involved in ABD recruitment was achieved.

The third chapter of this study explored the rostro-caudal distribution of the pFL and found that Bicuculline injections induced active expiration at various rostro-caudal locations, with the more rostral sites (+0.6 mm and +0.8 mm from VIIc) showing longer and stronger ABD responses, as well as more pronounced changes in VT and VE. Additionally, respiratory changes elicited by bicuculline injections indicated that respiratory frequency was affected in caudal locations but remained unaltered in rostral locations, suggesting that frequency changes may be the result of stimulation of the adjacent Bötzinger Complex. Furthermore, metabolic implications of bicuculline-induced respiratory changes revealed a reduction in oxygen consumption (VO2) at rostral locations, likely due to artificial hyperventilation, driven by decreased arterial pCO2 and the leftward shift of the oxyhemoglobin dissociation curve, leading to reduced oxygen delivery to the tissues.

Chapter four of this study investigated abdominal (ABD) muscle recruitment during sleep in the context of impaired inspiratory drive. To induce respiratory disturbances, I employed chemogenetic inhibition of the inspiratory oscillator through the KORD receptor. While it is important to note the potential limitation of constitutive activity in the KORD receptor, this approach successfully established a state of impaired inspiratory drive when compared to the CTRL group. Notably, under impaired conditions, there was an augmentation in the occurrence of ABD recruitment events, particularly during REM sleep. Intriguingly, the results also suggest that an intact inspiratory drive is essential for the manifestation of expiratory activity from the lateral parafacial area (pFL).

In conclusion, this research highlights the complex role of the pFL in active expiration during sleep and in conditions of an impaired inspiratory drive, emphasizing the state-dependent nature of ABD recruitment. It also underscores the intricate rostro-caudal organization of the pFL, highlighting the need to explore more deeply the rostral locations. Additionally, the novel metabolic results explained here, open the avenue for further exploration of the metabolic implications of respiratory changes induced by ABD activity. The thesis's findings have implications for understanding the

neural circuits governing active expiration and its potential therapeutic applications in pathological conditions.

References

Abbott, S. B., Stornetta, R. L., Coates, M. B., & Guyenet, P. G. (2011). Phox2b-expressing neurons of the parafacial region regulate breathing rate, inspiration, and expiration in conscious rats. *J Neurosci, 31*(45), 16410-16422. doi:10.1523/JNEUROSCI.3280-11.2011

Abbott, S. B., Stornetta, R. L., Fortuna, M. G., Depuy, S. D., West, G. H., Harris, T. E., & Guyenet, P. G. (2009). Photostimulation of retrotrapezoid nucleus phox2b-expressing neurons in vivo produces long-lasting activation of breathing in rats. *J Neurosci, 29*(18), 5806-5819. doi:10.1523/JNEUROSCI.1106-09.2009

Abdala, A. P., Rybak, I. A., Smith, J. C., & Paton, J. F. (2009). Abdominal expiratory activity in the rat brainstem-spinal cord in situ: patterns, origins and implications for respiratory rhythm generation. *J Physiol, 587*(Pt 14), 3539-3559.

Al-Zubaidy, Z. A., Erickson, R. L., & Greer, J. J. (1996). Serotonergic and noradrenergic effects on respiratory neural discharge in the medullary slice preparation of neonatal rats. *Pflügers Archiv, 431*, 942-949.

Alsahafi, Z., Dickson, C. T., & Pagliardini, S. (2015). Optogenetic excitation of preBötzinger complex neurons potently drives inspiratory activity in vivo. *The Journal of Physiology, 593*(16), 3673-3692. doi:https://doi.org/10.1113/JP270471

Anderson, T. M., Garcia, A. J., 3rd, Baertsch, N. A., Pollak, J., Bloom, J. C., Wei, A. D., . . . Ramirez, J. M. (2016). A novel excitatory network for the control of breathing. *Nature, 536*(7614), 76-80. doi:10.1038/nature18944

Andrews, C. G., & Pagliardini, S. (2015). Expiratory activation of abdominal muscle is associated with improved respiratory stability and an increase in minute ventilation in REM epochs of adult rats. *Journal of Applied Physiology, 119*(9), 968-974. doi:10.1152/japplphysiol.00420.2015

Arata, A., Onimaru, H., & Homma, I. (1990). Respiration-related neurons in the ventral medulla of newborn rats in vitro. *Brain Res Bull, 24*(4), 599-604.

Arita, H., & Ochiishi, M. (1991). Opposing effects of 5-hydroxytryptamine on two types of medullary inspiratory neurons with distinct firing patterns. *Journal of Neurophysiology, 66*(1), 285-292.

Armbruster, B. N., Li, X., Pausch, M. H., Herlitze, S., & Roth, B. L. (2007). Evolving the lock to fit the key to create a family of G protein-coupled receptors potently activated by an inert ligand. *Proc Natl Acad Sci U S A, 104*(12), 5163-5168. doi:10.1073/pnas.0700293104

Ashhad, S., Kam, K., Del Negro, C. A., & Feldman, J. L. (2022). Breathing Rhythm and Pattern and Their Influence on Emotion. *Annual Review of Neuroscience, 45*(1), 223-247. doi:10.1146/annurev-neuro-090121-014424

Ayyaswamy, S., Shi, H., Zhang, B., Bryan Jr, R. M., & Durgan, D. J. (2023). Obstructive Sleep Apnea–Induced Hypertension Is Associated With Increased Gut and Neuroinflammation. *Journal of the American Heart Association*, e029218.

Baertsch, N. A., Baertsch, H. C., & Ramirez, J. M. (2018). The interdependence of excitation and inhibition for the control of dynamic breathing rhythms. *Nature communications*, 9(1), 843.

Balagny, P., Vidal-Petiot, E., Renuy, A., Matta, J., Frija-Masson, J., Steg, P. G., . . . Wiernik, E. (2023). Prevalence, treatment and determinants of obstructive sleep apnoea and its symptoms in a population-based French cohort. *ERJ Open Research, 9*(3).

Barnett, W. H., Jenkin, S. E. M., Milsom, W. K., Paton, J. F. R., Abdala, A. P., Molkov, Y. I., & Zoccal, D. B. (2018). The Kolliker-Fuse nucleus orchestrates the timing of expiratory abdominal nerve bursting. *J Neurophysiol, 119*(2), 401-412. doi:10.1152/jn.00499.2017

Benarroch, E. E. (2003). Brainstem in multiple system atrophy: clinicopathological correlations. *Cellular and molecular neurobiology, 23*(4-5), 519-526.

Benington, J. H., & Heller, H. C. (1994). Does the function of REM sleep concern non-REM sleep or waking? *Progress in Neurobiology, 44*(5), 433-449. doi:https://doi.org/10.1016/0301-0082(94)90005-1

Benington, J. H., Kodali, S. K., & Heller, H. C. (1994). Scoring Transitions to REM Sleep in Rats Based on the EEG Phenomena of Pre-REM Sleep: An Improved Analysis of Sleep Structure. *Sleep, 17*(1), 28-36. doi:10.1093/sleep/17.1.28

Biancardi, V., Saini, J., Pageni, A., Prashaad M, H., Funk, G. D., & Pagliardini, S. (2021). Mapping of the excitatory, inhibitory, and modulatory afferent projections to the anatomically defined active expiratory oscillator in adult male rats. *Journal of Comparative Neurology, 529*(4), 853-884.

Biancardi, V., Yang, X., Ding, X., Passi, D., Funk, G. D., & Pagliardini, S. (2023). Cholinergic projections to the preBötzinger complex. *Journal of Comparative Neurology, 531*(13), 1317-1332. doi:https://doi.org/10.1002/cne.25497

Blatteis, C. M., & Lutherer, L. O. (1973). Cold-induced thermogenesis in dogs: its reduction by moderate hypoxia. *Journal of Applied Physiology, 35*(5), 608-612.

Böing, S., & Randerath, W. J. (2015). Chronic hypoventilation syndromes and sleep-related hypoventilation. *Journal of Thoracic Disease, 7*(8), 1273.

Bosc, L. V. G., Resta, T., Walker, B., & Kanagy, N. L. (2010). Mechanisms of intermittent hypoxia induced hypertension. *Journal of Cellular and Molecular Medicine, 14*(1-2), 3-17. doi:https://doi.org/10.1111/j.1582-4934.2009.00929.x

Boutin, R. C., Alsahafi, Z., & Pagliardini, S. (2017). Cholinergic modulation of the parafacial respiratory group. *J Physiol, 595*(4), 1377-1392. doi:10.1113/JP273012

Bouvier, J., Thoby-Brisson, M., Renier, N., Dubreuil, V., Ericson, J., Champagnat, J., . . . Fortin, G. (2010). Hindbrain interneurons and axon guidance signaling critical for breathing. *Nature Neuroscience, 13*(9), 1066-1074. doi:10.1038/nn.2622

Burke, P. G., Kanbar, R., Basting, T. M., Hodges, W. M., Viar, K. E., Stornetta, R. L., & Guyenet, P. G. (2015). State-dependent control of breathing by the retrotrapezoid nucleus. *J Physiol, 593*(13), 2909-2926. doi:10.1113/JP270053

Carley, D. W., Trbovic, S., & Radulovacki, M. (1996). Sleep apnea in normal and REM sleep-deprived normotensive Wistar-Kyoto and spontaneously hypertensive (SHR) rats. *Physiol Behav, 59*(4-5), 827-831.

Carskadon, M. A., & Dement, W. C. (2005). Normal human sleep: an overview. *Principles and practice of sleep medicine, 4*(1), 13-23.

Casey, K. R., & Tiwari, R. (2018). The (still) elusive definition of hypopnea. *Journal of Clinical Sleep Medicine*, 14(12), 1971-1972.

Chevalier, M., Toporikova, N., Simmers, J., & Thoby-Brisson, M. (2016). Development of pacemaker properties and rhythmogenic mechanisms in the mouse embryonic respiratory network. *eLife, 5*, e16125. doi:10.7554/eLife.16125

Chokroverty, S. (2010). Overview of sleep & sleep disorders. *Indian Journal of Medical Research, 131*(2).

Christon, J., Carley, D. W., Monti, D., & Radulovacki, M. (1996). Effects of inspired gas on sleep-related apnea in the rat. *Journal of Applied Physiology, 80*(6), 2102-2107. doi:10.1152/jappl.1996.80.6.2102

Clement, E. A., Richard, A., Thwaites, M., Ailon, J., Peters, S., & Dickson, C. T. (2008). Cyclic and sleep-like spontaneous alternations of brain state under urethane anaesthesia. *PLoS ONE, 3*(4), e2004.

Cregg, J. M., Chu, K. A., Dick, T. E., Landmesser, L. T., & Silver, J. (2017). Phasic inhibition as a mechanism for generation of rapid respiratory rhythms. *Proceedings of the National Academy of Sciences*, 114(48), 12815-12820.

Cui, Y., Kam, K., Sherman, D., Janczewski, W. A., Zheng, Y., & Feldman, J. L. (2016). Defining preBötzinger Complex Rhythm- and Pattern-Generating Neural Microcircuits In Vivo. *Neuron, 91*(3), 602-614. doi:10.1016/j.neuron.2016.07.003

Curran, A. K., Darnall, R. A., Filiano, J. J., Li, A., & Nattie, E. E. (2001). Muscimol dialysis in the rostral ventral medulla reduced the CO2 response in awake and sleeping piglets. *Journal of Applied Physiology, 90*(3), 971-980.

Daly Md Fau - Hazzledine, J. L., & Hazzledine, J. L. (1963). THE EFFECTS OF ARTIFICIALLY INDUCED HYPERVENTILATION ON THE PRIMARY CARDIAC REFLEX RESPONSE TO STIMULATION OF THE CAROTID BODIES IN THE DOG. (0022-3751 (Print)).

Davidson, B. L., Stein, C. S., Heth, J. A., Martins, I., Kotin, R. M., Derksen, T. A., . . . Chiorini, J. A. (2000). Recombinant adeno-associated virus type 2, 4, and 5 vectors: Transduction of variant cell types and regions in the mammalian central nervous system. *Proceedings of the National Academy of Sciences, 97*(7), 3428-3432. doi:10.1073/pnas.97.7.3428

Davis, E. M., & O'Donnell, C. P. (2013). Rodent models of sleep apnea. *Respiratory Physiology & Neurobiology, 188*(3), 355-361.

de Britto, A. A., Magalhães, K. S., da Silva, M. P., Paton, J. F. R., & Moraes, D. J. A. (2020). Active expiratory oscillator regulates nasofacial and oral motor activities in rats. *Experimental Physiology, 105*(2), 379-392. doi:https://doi.org/10.1113/EP088046

de Sousa Abreu, R. P., Bondarenko, E., & Feldman, J. L. (2022). Phase- and state-dependent modulation of breathing pattern by preBötzinger complex somatostatin expressing

neurons. *The Journal of Physiology, 600*(1), 143-165. doi:https://doi.org/10.1113/JP282002

Del Negro, C. A., Funk, G. D., & Feldman, J. L. (2018). Breathing matters. *Nat Rev Neurosci, 19*(6), 351-367. doi:10.1038/s41583-018-0003-6

Dempsey, J. A., Veasey, S. C., Morgan, B. J., & O'Donnell, C. P. (2010). Pathophysiology of sleep apnea. *Physiological reviews, 90*(1), 47-112.

Douglas, N. J., White, D. P., Weil, J. V., Pickett, C. K., Martin, R. J., Hudgel, D. W., & Zwillich, C. W. (1982). Hypoxic ventilatory response decreases during sleep in normal men. *American Review of Respiratory Disease, 125*(3), 286-289.

Ellis, B. L., Hirsch, M. L., Barker, J. C., Connelly, J. P., Steininger, R. J., & Porteus, M. H. (2013). A survey of ex vivo/in vitro transduction efficiency of mammalian primary cells and cell lines with Nine natural adeno-associated virus (AAV1-9) and one engineered adeno-associated virus serotype. *Virology Journal, 10*(1), 74. doi:10.1186/1743-422X-10-74

Feldman, J. L., & Kam, K. (2015). Facing the challenge of mammalian neural microcircuits: Taking a few breaths may help. *Journal of Physiology, 593*(1), 3-23. doi:10.1113/jphysiol.2014.277632

Fletcher, E. C. (1993). Obstructive sleep apnea and the kidney. In (Vol. 4, pp. 1111-1121): LWW.

Fletcher, E. C. (1995). The relationship between systemic hypertension and obstructive sleep apnea: facts and theory. *The American journal of medicine, 98*(2), 118-128.

Flor, K. C., Barnett, W. H., Karlen-Amarante, M., Molkov, Y. I., & Zoccal, D. B. (2020). Inhibitory control of active expiration by the Bötzinger complex in rats. *The Journal of Physiology, 598*(21), 4969-4994. doi:https://doi.org/10.1113/JP280243

Frappell, P., Westwood, K., & Maskrey, M. (1995). Ventilatory and metabolic responses to hypoxia during moderate hypothermia in anesthetized rats. *Journal of Applied Physiology, 79*(1), 256-260.

Fu, T.-M., Hong, G., Zhou, T., Schuhmann, T. G., Viveros, R. D., & Lieber, C. M. (2016). Stable long-term chronic brain mapping at the single-neuron level. *Nature methods, 13*(10), 875-882.

Funk, G. D., Smith, J. C., & Feldman, J. L. (1993). Generation and transmission of respiratory oscillations in medullary slices: role of excitatory amino acids. *Journal of neurophysiology*, 70(4), 1497-1515.

Gagnon, K., Baril, A. A., Gagnon, J. F., Fortin, M., Décary, A., Lafond, C., . . . Gosselin, N. (2014). Cognitive impairment in obstructive sleep apnea. *Pathologie Biologie, 62*(5), 233-240. doi:https://doi.org/10.1016/j.patbio.2014.05.015

Gautier, H., Bonora, M., M'Barek, S. B., & Sinclair, J. D. (1991). Effects of hypoxia and cold acclimation on thermoregulation in the rat. *Journal of Applied Physiology, 71*(4), 1355-1363.

George, M. P. R. S., Ruth, L. S., Daniel, S. S., Stephen, B. G. A., & Patrice, G. G. (2020). Differential Contribution of the Retrotrapezoid Nucleus and C1 Neurons to Active Expiration and Arousal in Rats. *The Journal of Neuroscience, 40*(45), 8683. doi:10.1523/JNEUROSCI.1006-20.2020

Giordano, F. J. (2005). Oxygen, oxidative stress, hypoxia, and heart failure. *The Journal of Clinical Investigation, 115*(3), 500-508. doi:10.1172/JCI24408

Gomez, J. L., Bonaventura, J., Lesniak, W., Mathews, W. B., Sysa-Shah, P., Rodriguez, L. A., . . . Michaelides, M. (2017). Chemogenetics revealed: DREADD occupancy and activation via converted clozapine. *Science, 357*(6350), 503-507. doi:10.1126/science.aan2475

Gray, P. A., Hayes, J. A., Ling, G. Y., Llona, I., Tupal, S., Picardo, M. C. D., . . . Del Negro, C. A. (2010). Developmental origin of prebötzinger complex respiratory neurons. *Journal of Neuroscience, 30*(44), 14883-14895. doi:10.1523/JNEUROSCI.4031-10.2010

Gray, P. A., Janczewski, W. A., Mellen, N., McCrimmon, D. R., & Feldman, J. L. (2001). Normal breathing requires preBotzinger complex neurokinin-1 receptor-expressing neurons. *Nat Neurosci, 4*(9), 927-930.

Gray, P. A., Rekling, J. C., Bocchiaro, C. M., & Feldman, J. L. (1999). Modulation of respiratory frequency by peptidergic input to rhythmogenic neurons in the preBotzinger complex. *Science, 286*(5444), 1566-1568. doi:10.1126/science.286.5444.1566

Hadj-Amar, B., Finkenstädt, B., Fiecas, M., & Huckstepp, R. (2021). Identifying the recurrence of sleep apnea using a harmonic hidden Markov model. *The annals of applied statistics*, 15(3), 1171.

Han, Y., Shi, Y. F., Xi, W., Zhou, R., Tan, Z. B., Wang, H., . . . Yu, Y. Q. (2014). Selective activation of cholinergic basal forebrain neurons induces immediate sleep-wake transitions. *Current Biology, 24*(6), 693-698. doi:10.1016/j.cub.2014.02.011

Haupt, M. E., Goodman Dm Fau - Sheldon, S. H., & Sheldon, S. H. (2012). Sleep related expiratory obstructive apnea in children. (1550-9397 (Electronic)).

Hayes, J. A., Kottick, A., Picardo, M. C. D., Halleran, A. D., Smith, R. D., Smith, G. D., . . . Del Negro, C. A. (2017). Transcriptome of neonatal preBötzinger complex neurones in Dbx1 reporter mice. *Scientific Reports, 7*(1), 8669. doi:10.1038/s41598-017-09418-4

Hayes, J. A., Wang, X., & Del Negro, C. A. (2012). Cumulative lesioning of respiratory interneurons disrupts and precludes motor rhythms in vitro. *Proceedings of the National Academy of Sciences, 109*(21), 8286-8291. doi:10.1073/pnas.1200912109

Hinze-Selch, D., Mullington, J., Orth, A., Lauer, C. J., & Pollmacher, T. (1997). Effects of clozapine on sleep: a longitudinal study. *Biol Psychiatry, 42*(4), 260-266. doi:10.1016/S0006-3223(96)00347-2

Huckstepp, R. T., Cardoza, K. P., Henderson, L. E., & Feldman, J. L. (2015). Role of parafacial nuclei in control of breathing in adult rats. *J Neurosci, 35*(3), 1052-1067. doi:10.1523/JNEUROSCI.2953-14.2015

Huckstepp, R. T., Henderson, L. E., Cardoza, K. P., & Feldman, J. L. (2016). Interactions between respiratory oscillators in adult rats. *Elife, 5*. doi:10.7554/eLife.14203

Huckstepp, R. T. R., Cardoza, K. P., Henderson, L. E., & Feldman, J. L. (2018). Distinct parafacial regions in control of breathing in adult rats. *PLoS One, 13*(8), e0201485. doi:10.1371/journal.pone.0201485

Iizuka, M. (2001). Respiratory activity in glossopharyngeal, vagus and accessory nerves and pharyngeal constrictors in newborn rat in vitro. *J Physiol, 532*(Pt 2), 535-548.

Iizuka, M. (2003). GABAA and glycine receptors in regulation of intercostal and abdominal expiratory activity in vitro in neonatal rat. *J Physiol, 551*(Pt 2), 617-633. doi:10.1113/jphysiol.2003.042689

Jami, L. S., Nicole, N. S., Lindsey, M. S., Sarah, E. R., Brian, M. D., & Michael, S. G. (2016). Gi-DREADD Expression in Peripheral Nerves Produces Ligand-Dependent Analgesia, as well as Ligand-Independent Functional Changes in Sensory Neurons. *The Journal of Neuroscience, 36*(42), 10769. doi:10.1523/JNEUROSCI.3480-15.2016

Janczewski, W. A., & Feldman, J. L. (2006). Distinct rhythm generators for inspiration and expiration in the juvenile rat. *J Physiol, 570*(Pt 2), 407-420. doi:10.1113/jphysiol.2005.098848

Janczewski, W. A., Onimaru, H., Homma, I., & Feldman, J. L. (2002). Opioid-resistant respiratory pathway from the preinspiratory neurones to abdominal muscles: in vivo and in vitro study in the newborn rat. *J Physiol, 545*(Pt 3), 1017-1026.

Janczewski, W. A., Tashima, A., Hsu, P., Cui, Y., & Feldman, J. L. (2013). Role of inhibition in respiratory pattern generation. *Journal of Neuroscience*, 33(13), 5454-5465.

Jenkin, S. E., Milsom, W. K., & Zoccal, D. B. (2017). The Kolliker-Fuse nucleus acts as a timekeeper for late-expiratory abdominal activity. *Neuroscience, 348*, 63-72. doi:10.1016/j.neuroscience.2017.01.050

Jones, B. E. (1990). Immunohistochemical study of choline acetyltransferase-immunoreactive processes and cells innervating the pontomedullary reticular formation in the rat. *J Comp Neurol, 295*(3), 485-514. doi:10.1002/cne.902950311

Kalinchuk, A. V., Porkka-Heiskanen, T., McCarley, R. W., & Basheer, R. (2015). Cholinergic neurons of the basal forebrain mediate biochemical and electrophysiological mechanisms underlying sleep homeostasis. *Eur J Neurosci, 41*(2), 182-195. doi:10.1111/ejn.12766

Kam, K., Worrell, J. W., Ventalon, C., Emiliani, V., & Feldman, J. L. (2013). Emergence of population bursts from simultaneous activation of small subsets of preBötzinger complex inspiratory neurons. *Journal of Neuroscience, 33*(8), 3332-3338. doi:10.1523/JNEUROSCI.4574-12.2013

Kang, B. J., Chang, D. A., Mackay, D. D., West, G. H., Moreira, T. S., Takakura, A. C., . . . Stornetta, R. L. (2007). Central nervous system distribution of the transcription factor Phox2b in the adult rat. *J Comp Neurol, 503*(5), 627-641.

Kawai, A., Onimaru, H., & Homma, I. (2006). Mechanisms of CO2/H+ chemoreception by respiratory rhythm generator neurons in the medulla from newborn rats in vitro. *J Physiol, 572*(Pt 2), 525-537. doi:10.1113/jphysiol.2005.102533

Kleinfeld, D., Deschênes, M., & Ulanovsky, N. (2016). Whisking, Sniffing, and the Hippocampal θ-Rhythm: A Tale of Two Oscillators. *PLoS Biology, 14*(2), 1-8. doi:10.1371/journal.pbio.1002385

Koizumi, H., Mosher, B., Tariq, M. F., Zhang, R., Koshiya, N., & Smith, J. C. (2016). Voltage-dependent rhythmogenic property of respiratory pre-Bötzinger complex glutamatergic, Dbx1-derived, and somatostatin-expressing neuron populations revealed by graded optogenetic inhibition. *eNeuro, 3*(3), 1047-1061. doi:10.1523/ENEURO.0081-16.2016

Korsak, A., Sheikhbahaei, S., Machhada, A., Gourine, A. V., & Huckstepp, R. T. R. (2018). The Role Of Parafacial Neurons In The Control Of Breathing During Exercise. *Scientific Reports, 8*(1), 1-12. doi:10.1038/s41598-017-17412-z

Krause, A., Nowak, Z., Srbu, R., & Bell, H. J. (2016). Respiratory autoresuscitation following severe acute hypoxemia in anesthetized adult rats. *Respiratory Physiology and Neurobiology, 232*, 43-53. doi:10.1016/j.resp.2016.06.006

Kubin, L., Tojima, H., Davies, R. O., & Pack, A. I. (1992). Serotonergic excitatory drive to hypoglossal motoneurons in the decerebrate cat. *Neuroscience letters, 139*(2), 243-248.

Kuwaki, T., Li, A., & Nattie, E. (2010). State-dependent central chemoreception: a role of orexin. *Respiratory Physiology & Neurobiology, 173*(3), 223-229.

Kuwana, S. I., Tsunekawa, N., Yanagawa, Y., Okada, Y., Kuribayashi, J., & Obata, K. (2006). Electrophysiological and morphological characteristics of GABAergic respiratory neurons in the mouse pre-Bötzinger complex. *European Journal of Neuroscience*, 23(3), 667-674.

Lanuza, G. M., Gosgnach, S., Pierani, A., Jessell, T. M., & Goulding, M. (2004). Genetic identification of spinal interneurons that coordinate left-right locomotor activity necessary for walking movements. *Neuron*, 42(3), 375-386.

Le, S., Turner, A. J., Parker, L. M., Burke, P. G., Kumar, N. N., Goodchild, A. K., & McMullan, S. (2016). Somatostatin 2a receptors are not expressed on functionally identified respiratory neurons in the ventral respiratory column of the rat. *Journal of Comparative Neurology, 524*(7), 1384-1398. doi:https://doi.org/10.1002/cne.23912

Leirao, I. P., Silva, C. A., Jr., Gargaglioni, L. H., & da Silva, G. S. F. (2017). Hypercapnia-induced active expiration increases in sleep and enhances ventilation in unanaesthetized rats. *J Physiol*. doi:10.1113/JP274726

Léna, I., Parrot, S., Deschaux, O., Muffat-Joly, S., Sauvinet, V., Renaud, B., . . . Gottesmann, C. (2005). Variations in extracellular levels of dopamine, noradrenaline, glutamate, and aspartate across the sleep-wake cycle in the medial prefrontal cortex and nucleus accumbens of freely moving rats. *Journal of Neuroscience Research, 81*(6), 891-899. doi:10.1002/jnr.20602

Li, A., & Nattie, E. E. (1997). Focal central chemoreceptor sensitivity in the RTN studied with a CO2 diffusion pipette in vivo. *Journal of Applied Physiology, 83*(2), 420-428.

Li, P., Janczewski, W. A., Yackle, K., Kam, K., Pagliardini, S., Krasnow, M. A., & Feldman, J. L. (2016). The peptidergic control circuit for sighing. *Nature, 530*(7590), 293-297. doi:10.1038/nature16964

Lieske, S. P., Thoby-Brisson, M., Telgkamp, P., & Ramirez, J. M. (2000). Reconfiguration of the neural network controlling multiple breathing patterns: Eupnea, sighs and gasps. *Nature Neuroscience, 3*(6), 600-607. doi:10.1038/75776

Lindsay, A. D., & Feldman, J. L. (1993). Modulation of respiratory activity of neonatal rat phrenic motoneurones by serotonin. *The Journal of Physiology, 461*(1), 213-233.

Lopez-Rodriguez, F., Medina-Ceja, L., Wilson, C. L., Jhung, D., & Morales-Villagran, A. (2007). Changes in Extracellular Glutamate Levels in Rat Orbitofrontal Cortex During Sleep and Wakefulness. *Archives of Medical Research, 38*(1), 52-55. doi:10.1016/j.arcmed.2006.07.004

Lydic, R., Baghdoyan, H. A., & Lorinc, Z. (1991). Microdialysis of cat pons reveals enhanced acetylcholine release during state-dependent respiratory depression. *Am J Physiol, 261*(3 Pt 2), R766-770. doi:10.1152/ajpregu.1991.261.3.R766

MacLaren, D. A., Browne, R. W., Shaw, J. K., Krishnan Radhakrishnan, S., Khare, P., Espana, R. A., & Clark, S. D. (2016). Clozapine N-Oxide Administration Produces Behavioral Effects in Long-Evans Rats: Implications for Designing DREADD Experiments. *eNeuro, 3*(5). doi:10.1523/ENEURO.0219-16.2016

Magalhães, K. S., da Silva, M. P., Mecawi, A. S., Paton, J. F. R., Machado, B. H., & Moraes, D. J. A. (2021). Intrinsic and synaptic mechanisms controlling the expiratory activity of excitatory lateral parafacial neurones of rats. *The Journal of Physiology, 599*(21), 4925-4948. doi:https://doi.org/10.1113/JP281545

Mahler, S. V., & Aston-Jones, G. (2018). CNO Evil? Considerations for the Use of DREADDs in Behavioral Neuroscience. *Neuropsychopharmacology, 43*(5), 934-936. doi:10.1038/npp.2017.299

Malheiros-Lima, M. R., Silva, J. N., Souza, F. C., Takakura, A. C., & Moreira, T. S. (2020). C1 neurons are part of the circuitry that recruits active expiration in response to the activation of peripheral chemoreceptors. *eLife, 9*, e52572. doi:10.7554/eLife.52572

Malheiros-Lima, M. R., Takakura, A. C., & Moreira, T. S. (2017). Depletion of rostral ventrolateral medullary catecholaminergic neurons impairs the hypoxic ventilatory

response in conscious rats. *Neuroscience, 351*, 1-14. doi:10.1016/j.neuroscience.2017.03.031

Mandile, P., Vescia, S., Montagnese, P., Romano, F., & Giuditta, A. (1996). Characterization of transition sleep episodes in baseline EEG recordings of adult rats. *Physiology & behavior, 60*(6), 1435-1439.

Manvich, D. F., Webster, K. A., Foster, S. L., Farrell, M. S., Ritchie, J. C., Porter, J. H., & Weinshenker, D. (2018). The DREADD agonist clozapine N-oxide (CNO) is reverse-metabolized to clozapine and produces clozapine-like interoceptive stimulus effects in rats and mice. *Scientific Reports, 8*(1), 1-10. doi:10.1038/s41598-018-22116-z

Marchant, N. J., Whitaker, L. R., Bossert, J. M., Harvey, B. K., Hope, B. T., Kaganovsky, K., . . . Shaham, Y. (2016). Behavioral and Physiological Effects of a Novel Kappa-Opioid Receptor-Based DREADD in Rats. *Neuropsychopharmacology, 41*(2), 402-409. doi:10.1038/npp.2015.149

Marina, N., Abdala, A. P., Trapp, S., Li, A., Nattie, E. E., Hewinson, J., . . . Gourine, A. V. (2010). Essential role of Phox2b-expressing ventrolateral brainstem neurons in the chemosensory control of inspiration and expiration. *J Neurosci, 30*(37), 12466-12473. doi:10.1523/JNEUROSCI.3141-10.2010

Martial, F. P., Dunleavy, M., Nolan, P., McNicholas, W. T., O'Regan, R. G., & Bradford, A. (2005). Simultaneous recording of breathing and respiratory related neuronal activity in the brainstem of conscious rats. *Respiratory Physiology & Neurobiology, 145*(2-3), 301-306.

Mbata, G., & Chukwuka, J. (2012). Obstructive sleep apnea hypopnea syndrome. *Annals of medical and health sciences research*, 2(1), 74–77. https://doi.org/10.4103/2141-9248.96943

McGinty, D. J., Stevenson, M., Hoppenbrouwers, T., Harper, R. M., Sterman, M. B., & Hodgman, J. (1977). Polygraphic studies of kitten development: sleep state patterns. *Developmental Psychobiology: The Journal of the International Society for Developmental Psychobiology, 10*(5), 455-469.

McKay, L. C., & Feldman, J. L. (2008). Unilateral ablation of pre-Botzinger complex disrupts breathing during sleep but not wakefulness. *Am J Respir Crit Care Med, 178*(1), 89-95.

McKay, L. C., Janczewski, W. A., & Feldman, J. L. (2005). Sleep-disordered breathing after targeted ablation of preBotzinger complex neurons. *Nat Neurosci, 8*(9), 1142-1144.

Megirian, D., Ryan, A. T., & Sherrey, J. H. (1980). An electrophysiological analysis of sleep and respiration of rats breathing different gas mixtures: diaphragmatic muscle function. *Electroencephalogr Clin Neurophysiol, 50*(3-4), 303-313.

Mellen, N. M., Janczewski, W. A., Bocchiaro, C. M., & Feldman, J. L. (2003). Opioid-induced quantal slowing reveals dual networks for respiratory rhythm generation. *Neuron, 37*(5), 821-826.

Mendelson, W. B., & Bergmann, B. M. (1999). EEG delta power during sleep in young and old rats. *Neurobiology of aging, 20*(6), 669-673.

Mendelson, W. B., Martin, J. V., Perlis, M., Giesen, H., Wagner, R., & Rapoport, S. I. (1988). Periodic cessation of respiratory effort during sleep in adult rats. *Physiology & behavior, 43*(2), 229-234.

Mendonça-Junior, B. A., Fernandes, M. V., & Zoccal, D. B. (2021). Acute intermittent hypoxia evokes ventilatory long-term facilitation and active expiration in unanesthetized rats. *Respiratory Physiology & Neurobiology*, 294, 103768.

Menuet, C., Connelly, A. A., Bassi, J. K., Melo, M. R., Le, S., Kamar, J., . . . Allen, A. M. (2020). PreBötzinger complex neurons drive respiratory modulation of blood pressure and heart rate. *eLife, 9*, e57288. doi:10.7554/eLife.57288

Mortola, J. P., & Frappell, P. B. (1998). On the barometric method for measurements of ventilation, and its use in small animals. *Canadian Journal of Physiology and Pharmacology, 76*(10-11), 937-944. doi:10.1139/y99-001

Muere, C., Neumueller, S., Miller, J., Olesiak, S., Hodges, M. R., Pan, L., & Forster, H. V. (2012). Atropine microdialysis within or near the pre-Bötzinger Complex increases breathing frequency more during wakefulness than during NREM sleep. *Journal of Applied Physiology, 114*(5), 694-704. doi:10.1152/japplphysiol.00634.2012

Muere, C., Neumueller, S., Miller, J., Olesiak, S., Hodges, M. R., Pan, L., & Forster, H. V. (2015). Evidence for respiratory neuromodulator interdependence after cholinergic disruption in the ventral respiratory column. *Respiratory Physiology & Neurobiology, 205*, 7-15. doi:https://doi.org/10.1016/j.resp.2014.09.010

Mulkey, D. K., Stornetta, R. L., Weston, M. C., Simmons, J. R., Parker, A., Bayliss, D. A., & Guyenet, P. G. (2004). Respiratory control by ventral surface chemoreceptor neurons in rats. *Nat Neurosci, 7*(12), 1360-1369. doi:10.1038/nn1357

Nakamura, A., Fukuda, Y., & Kuwaki, T. (2003). Sleep apnea and effect of chemostimulation on breathing instability in mice. *Journal of Applied Physiology, 94*(2), 525-532. doi:10.1152/japplphysiol.00226.2002

Nattie, E., & Li, A. (2012). Central chemoreceptors: locations and functions. *Compr Physiol, 2*(1), 221-254. doi:10.1002/cphy.c100083

Nattie, E., Shi, J., & Li, A. (2001). Bicuculline dialysis in the retrotrapezoid nucleus (RTN) region stimulates breathing in the awake rat. *Respiration physiology, 124*(3), 179-193.

Ninane, V., Rypens F Fau - Yernault, J. C., Yernault Jc Fau - De Troyer, A., & De Troyer, A. (1992). Abdominal muscle use during breathing in patients with chronic airflow obstruction. (0003-0805 (Print)).

Ninane, V., Yernault Jc Fau - de Troyer, A., & de Troyer, A. (1993). Intrinsic PEEP in patients with chronic obstructive pulmonary disease. Role of expiratory muscles. (0003-0805 (Print)).

O'Halloran, K. D. (2017). Sleep awakens active expiration. *J Physiol*. doi:10.1113/JP275056

Oku, Y., Masumiya, H., & Okada, Y. (2007). Postnatal developmental changes in activation profiles of the respiratory neuronal network in the rat ventral medulla. *J Physiol, 585*(Pt 1), 175-186. doi:10.1113/jphysiol.2007.138180

Olson Jr, E. B., & Dempsey, J. A. (1978). Rat as a model for humanlike ventilatory adaptation to chronic hypoxia. *Journal of Applied Physiology, 44*(5), 763-769.

Onimaru, H., Arata, A., & Homma, I. (1987). Localization of respiratory rhythm-generating neurons in the medulla of brainstem-spinal cord preparations from newborn rats. *Neurosci Lett, 78*(2), 151-155.

Onimaru, H., & Homma, I. (1992). Whole cell recordings from respiratory neurons in the medulla of brainstem-spinal cord preparations isolated from newborn rats. *Pflugers Arch, 420*(3-4), 399-406.

Onimaru, H., & Homma, I. (2003). A novel functional neuron group for respiratory rhythm generation in the ventral medulla. *Journal of Neuroscience, 23*(4), 1478-1486.

Onimaru, H., Ikeda, K., & Kawakami, K. (2008). CO2-sensitive preinspiratory neurons of the parafacial respiratory group express Phox2b in the neonatal rat. *J Neurosci, 28*(48), 12845-12850. doi:10.1523/JNEUROSCI.3625-08.2008

Onimaru, H., Kumagawa, Y., & Homma, I. (2006). Respiration-Related Rhythmic Activity in the Rostral Medulla of Newborn Rats. *Journal of Neurophysiology, 96*(1), 55-61. doi:10.1152/jn.01175.2005

Orem, J. (1980). Neuronal Mechanisms of Respiration in REM Sleep. *Sleep, 3*(3-4), 251-267. doi:10.1093/sleep/3.3-4.251

Orem, J., Lovering, A. T., Dunin-Barkowski, W., & Vidruk, E. H. (2000). Endogenous excitatory drive to the respiratory system in rapid eye movement sleep in cats. *Journal of Physiology, 527*(2), 365-376. doi:10.1111/j.1469-7793.2000.00365.x

Orem, J., & Lydic, R. (1978). Upper airway function during sleep and wakefulness: experimental studies on normal and anesthetized cats. *Sleep, 1*(1), 49-68.

Orem, J., Osorio, I., Brooks, E., & Dick, T. (1985). Activity of respiratory neurons during NREM sleep. *Journal of Neurophysiology, 54*(5), 1144-1156. doi:10.1152/jn.1985.54.5.1144

Orem, J. M., Lovering, A. T., & Vidruk, E. H. (2005). Excitation of medullary respiratory neurons in REM sleep. *Sleep, 28*(7), 801-807.

Pagliardini, S., Funk, G. D., & Dickson, C. T. (2013). Breathing and brain state: urethane anesthesia as a model for natural sleep. *Respir Physiol Neurobiol, 188*(3), 324-332. doi:10.1016/j.resp.2013.05.035

Pagliardini, S., Gosgnach, S., & Dickson, C. T. (2013). Spontaneous sleep-like brain state alternations and breathing characteristics in urethane anesthetized mice. *PLoS ONE, 8*(7), e70411. doi:10.1371/journal.pone.0070411

Pagliardini, S., Greer, J., Funk, G., & Dickson, C. (2012). *Sleep and Breathing: State-dependent modulation of respiratory muscles under urethane anesthesia.* Paper presented at the XII Oxford Conference on breathing, emotion, evolution, Almelo, Netherlands.

Pagliardini, S., Janczewski, W. A., Tan, W., Dickson, C. T., Deisseroth, K., & Feldman, J. L. (2011). Active expiration induced by excitation of ventral medulla in adult anesthetized rats. *Journal of Neuroscience, 31*(8), 2895-2905. doi:10.1523/JNEUROSCI.5338-10.2011

Pagliardini, S., Ren, J., & Greer, J. J. (2003). Ontogeny of the pre-Botzinger complex in perinatal rats. *J Neurosci, 23*(29), 9575-9584.

Panossian, L., & Daley, J. (2013). Sleep-disordered breathing. *Continuum: Lifelong Learning in Neurology, 19*(1), 86-103.

Pappenheimer, J. R. (1977). Sleep and respiration of rats during hypoxia. *The Journal of Physiology, 266*(1), 191-207.

Pasquale, G. D., Davidson, B. L., Stein, C. S., Martins, I., Scudiero, D., Monks, A., & Chiorini, J. A. (2003). Identification of PDGFR as a receptor for AAV-5 transduction. *Nature Medicine, 9*(10), 1306-1312. doi:10.1038/nm929

Patrice, G. G., Charles, P. S., Matthew, C. W., & Ruth, L. S. (2002). Neurokinin-1 Receptor-Expressing Cells of the Ventral Respiratory Group Are Functionally Heterogeneous and Predominantly Glutamatergic. *The Journal of Neuroscience, 22*(9), 3806. doi:10.1523/JNEUROSCI.22-09-03806.2002

Paxinos, G., & Watson, C. (2005). *The rat brain in stereotaxic coordinates* (5th ed.). New York: Academic Press.

Phillips, R. S., & Rubin, J. E. (2022). Putting the theory into 'burstlet theory' with a biophysical model of burstlets and bursts in the respiratory preBötzinger complex. *eLife, 11*, e75713. doi:10.7554/eLife.75713

Phillipson, E. A., Murphy, E., & Kozar, L. F. (1976a). Regulation of respiration in sleeping dogs. *J Appl Physiol, 40*(5), 688-693. doi:10.1152/jappl.1976.40.5.688

Pisanski, A., Ding, X., Koch, N. A., & Pagliardini, S. (2019). Chemogenetic modulation of the parafacial respiratory group influences the recruitment of abdominal activity during REM sleep. *Sleep*. doi:10.1093/sleep/zsz283

Pisanski, A., & Pagliardini, S. (2018). The parafacial respiratory group and the control of active expiration. *Respir Physiol Neurobiol*. doi:10.1016/j.resp.2018.06.010

Prajkta, S. K., Cameron, G., Maria Cristina, D. P., & Christopher, A. D. N. (2020). Evaluating the Burstlet Theory of Inspiratory Rhythm and Pattern Generation. *eNeuro, 7*(1), ENEURO.0314-0319.2019. doi:10.1523/ENEURO.0314-19.2019

Raper, J., Morrison, R. D., Daniels, J. S., Howell, L., Bachevalier, J., Wichmann, T., & Galvan, A. (2017). Metabolism and Distribution of Clozapine-N-oxide: Implications for Nonhuman Primate Chemogenetics. *ACS Chem Neurosci, 8*(7), 1570-1576. doi:10.1021/acschemneuro.7b00079

Richardson, R. S., Tagore, K., Haseler, L. J., Jordan, M., & Wagner, P. D. (1998). Increased V˙o 2 maxwith right-shifted Hb-O2dissociation curve at a constant O2 delivery in dog muscle in situ. *Journal of Applied Physiology, 84*(3), 995-1002. doi:10.1152/jappl.1998.84.3.995

Roberts, R., Wall, M. J., Braren, I., Dhillon, K., Evans, A., Dunne, J., . . . Huckstepp, R. T. R. (2022). An Improved Model of Moderate Sleep Apnoea for Investigating Its Effect as a Comorbidity on Neurodegenerative Disease. *Frontiers in Aging Neuroscience, 14*.

Rogan, S. C., & Roth, B. L. (2011). Remote control of neuronal signaling. *Pharmacol Rev, 63*(2), 291-315. doi:10.1124/pr.110.003020

Roth, B. L. (2016). DREADDs for Neuroscientists. *Neuron, 89*(4), 683-694. doi:10.1016/j.neuron.2016.01.040

Saini, J. K., Janes, T. A., MacLean, J. E., & Pagliardini, S. (2022). Expiratory activity during sleep in children. *Journal of Sleep Research, 31*(4), e13539. doi:https://doi.org/10.1111/jsr.13539

Saini, J. K., & Pagliardini, S. (2017). Breathing during sleep in the postnatal period of rats: The contribution of active expiration. *Sleep, 40*(12), 1-13. doi:10.1093/sleep/zsx172

Sakai, K., & Crochet, S. (2001). Differentiation of presumed serotonergic dorsal raphe neurons in relation to behavior and wake–sleep states. *Neuroscience, 104*(4), 1141-1155.

Salejee, I., Tarasiuk, A., Reder, I., & Scharf, S. M. (1993). Chrol1ic Upper Airway Obstrudion Produces Right but Not Left Ventricular Hypertrophy in Rats. *Am Rev Respir Dis, 148*, 1346-1350.

Schmidt-Nowara, W. W., Coultas, D. B., Wiggins, C., Skipper, B. E., & Samet, J. M. (1990). Snoring in a Hispanic-American population: risk factors and association with hypertension and other morbidity. *Archives of internal medicine, 150*(3), 597-601.

Seifert, E. L., Knowles, J., & Mortola, J. P. (2000). Continuous circadian measurements of ventilation in behaving adult rats. *Respiration physiology, 120*(2), 179-183. doi:https://doi.org/10.1016/S0034-5687(00)00108-0

Sforza, E., & Roche, F. (2016). Chronic intermittent hypoxia and obstructive sleep apnea: an experimental and clinical approach. *Hypoxia, 4*(null), 99-108. doi:10.2147/HP.S103091

Sforza, E., Saint Martin, M., Barthélémy, J. C., & Roche, F. (2016). Mood disorders in healthy elderly with obstructive sleep apnea: a gender effect. *Sleep Medicine, 19*, 57-62. doi:https://doi.org/10.1016/j.sleep.2015.11.007

Shao, X. M., & Feldman, J. L. (2005). Cholinergic neurotransmission in the preBÖtzinger Complex modulates excitability of inspiratory neurons and regulates respiratory rhythm. *Neuroscience, 130*(4), 1069-1081. doi:https://doi.org/10.1016/j.neuroscience.2004.10.028

Shao, X. M., & Feldman, J. L. (2009). Central cholinergic regulation of respiration: nicotinic receptors. *Acta Pharmacologica Sinica, 30*(6), 761-770. doi:10.1038/aps.2009.88

Sherman, D., Worrell, J. W., Cui, Y., & Feldman, J. L. (2015). Optogenetic perturbation of preBötzinger complex inhibitory neurons modulates respiratory pattern. *Nature neuroscience*, 18(3), 408-414.

Sherrey, J. H., Pollard, M. J., & Megirian, D. (1988b). Proprioceptive, chemoreceptive and sleep state modulation of expiratory muscle activity in the rat. *Experimental Neurology, 101*(1), 50-62. doi:10.1016/0014-4886(88)90064-7

Shi, Y., Stornetta, D. S., Reklow, R. J., Sahu, A., Wabara, Y., Nguyen, A., . . . Bayliss, D. A. (2021). A brainstem peptide system activated at birth protects postnatal breathing. *Nature, 589*(7842), 426-430. doi:10.1038/s41586-020-2991-4

Silva, J. N., Oliveira, L. M., Souza, F. C., Moreira, T. S., & Takakura, A. C. (2019). Distinct pathways to the parafacial respiratory group to trigger active expiration in adult rats. *American journal of physiology. Lung cellular and molecular physiology, 317*(3). doi:10.1152/ajplung.00467.2018

Simor, P., van der Wijk, G., Nobili, L., & Peigneux, P. (2020). The microstructure of REM sleep: Why phasic and tonic? *Sleep medicine reviews, 52*, 101305.

Smith, C. A., Henderson, K. S., Xi, L., Chow, C., Eastwood, P. R., & Dempsey, J. A. (1997a). Neural-mechanical coupling of breathing in REM sleep. *J Appl Physiol (1985), 83*(6), 1923-1932. doi:10.1152/jappl.1997.83.6.1923

Smith, J. C., Ellenberger, H. H., Ballanyi, K., Richter, D. W., & Feldman, J. L. (1991). Pre-Bötzinger complex: A brainstem region that may generate respiratory rhythm in mammals. *Science, 254*(5032), 726-729. doi:10.1126/science.1683005

Souza, G., Kanbar, R., Stornetta, D. S., Abbott, S. B. G., Stornetta, R. L., & Guyenet, P. G. (2018). Breathing regulation and blood gas homeostasis after near complete lesions of the retrotrapezoid nucleus in adult rats. *J Physiol, 596*(13), 2521-2545. doi:10.1113/JP275866

Souza, G. M. P. R., Stornetta, R. L., Stornetta, D. S., Abbott, S. B. G., & Guyenet, P. G. (2019). Contribution of the retrotrapezoid nucleus and carotid bodies to hypercapnia-and hypoxia-induced arousal from sleep. *Journal of Neuroscience, 39*(49), 9725-9737.

Stornetta, R. L., Moreira, T. S., Takakura, A. C., Kang, B. J., Chang, D. A., West, G. H., . . . Guyenet, P. G. (2006). Expression of Phox2b by brainstem neurons involved in chemosensory integration in the adult rat. *J Neurosci, 26*(40), 10305-10314. doi:10.1523/JNEUROSCI.2917-06.2006

Stornetta, R. L., Rosin, D. L., Wang, H., Sevigny, C. P., Weston, M. C., & Guyenet, P. G. (2003). A group of glutamatergic interneurons expressing high levels of both neurokinin-1 receptors and somatostatin identifies the region of the pre-Bötzinger complex. *Journal of Comparative Neurology, 455*(4), 499-512. doi:https://doi.org/10.1002/cne.10504

Stornetta, R. L., Spirovski, D., Moreira, T. S., Takakura, A. C., West, G. H., Gwilt, J. M., . . . Guyenet, P. G. (2009). Galanin is a selective marker of the retrotrapezoid nucleus in rats. *J Comp Neurol, 512*(3), 373-383. doi:10.1002/cne.21897

Swihart Bruce, J., Caffo, B., Bandeen-Roche, K., & Punjabi Naresh, M. (2008). Characterizing Sleep Structure Using the Hypnogram. *Journal of Clinical Sleep Medicine, 04*(04), 349-355. doi:10.5664/jcsm.27236

Tan, W., Janczewski, W. A., Yang, P., Shao, X. M., Callaway, E. M., & Feldman, J. L. (2008). Silencing preBötzinger Complex somatostatin-expressing neurons induces persistent apnea in awake rat. *Nature Neuroscience, 11*(5), 538-540. doi:10.1038/nn.2104

Tarasiuk, A., Scharf, S. M., & Miller, M. J. (1991). Effect of chronic resistive loading on inspiratory muscles in rats. *Journal of Applied Physiology, 70*(1), 216-222.

Thoby-Brisson, M., Karlén, M., Wu, N., Charnay, P., Champagnat, J., & Fortin, G. (2009). Genetic identification of an embryonic parafacial oscillator coupling to the preBötzinger complex. *Nature Neuroscience, 12*(8), 1028-1035. doi:10.1038/nn.2354

Thoby-Brisson, M., Trinh, J. B., Champagnat, J., & Fortin, G. (2005). Emergence of the pre-Bötzinger respiratory rhythm generator in the mouse embryo. *Journal of Neuroscience, 25*(17), 4307-4318. doi:10.1523/JNEUROSCI.0551-05.2005

Thompson, L. T., & Best, P. J. (1990). Long-term stability of the place-field activity of single units recorded from the dorsal hippocampus of freely behaving rats. *Brain research, 509*(2), 299-308.

Touyz, S. W., Beumont, P. J., Saayman, G. S., & Zabow, T. (1977). A psychophysiological investigation of the short-term effects of clozapine upon sleep parameters of normal young adults. *Biol Psychiatry, 12*(6), 801-822.

Touyz, S. W., Saayman, G. S., & Zabow, T. (1978). A psychophysiological investigation of the long-term effects of clozapine upon sleep patterns of normal young adults. *Psychopharmacology (Berl), 56*(1), 69-73.

Trevizan-Baú, P., Dhingra, R. R., Furuya, W. I., Stanić, D., Mazzone, S. B., & Dutschmann, M. (2021). Forebrain projection neurons target functionally diverse respiratory control areas in the midbrain, pons, and medulla oblongata. *Journal of Comparative Neurology, 529*(9), 2243-2264. doi:https://doi.org/10.1002/cne.25091

Tsuboi, Y., Dickson, D. W., Nabeshima, K., Schmeichel, A. M., Wszolek, Z. K., Yamada, T., & Benarroch, E. E. (2008). Neurodegeneration involving putative respiratory neurons in Perry syndrome. *Acta neuropathologica, 115*, 263-268.

Tupal, S., Rieger, M. A., Ling, G.-Y., Park, T. J., Dougherty, J. D., Goodchild, A. K., & Gray, P. A. (2014). Testing the role of preBötzinger Complex somatostatin neurons in respiratory and vocal behaviors. *European Journal of Neuroscience, 40*(7), 3067-3077. doi:https://doi.org/10.1111/ejn.12669

Van Dort, C. J., Zachs, D. P., Kenny, J. D., Zheng, S., Goldblum, R. R., Gelwan, N. A., . . . Brown, E. N. (2015). Optogenetic activation of cholinergic neurons in the PPT or LDT induces REM sleep. *Proc Natl Acad Sci U S A, 112*(2), 584-589. doi:10.1073/pnas.1423136112

Vanini, G., Wathen, B. L., Lydic, R., & Baghdoyan, H. A. (2011). Endogenous GABA levels in the pontine reticular formation are greater during wakefulness than during rapid eye movement sleep. *J Neurosci, 31*(7), 2649-2656. doi:10.1523/JNEUROSCI.5674-10.2011

Vann, N. C., Pham, F. D., Hayes, J. A., Kottick, A., & Del Negro, C. A. (2016). Transient Suppression of Dbx1 PreBotzinger Interneurons Disrupts Breathing in Adult Mice. *PLoS ONE, 11*(9), e0162418. doi:10.1371/journal.pone.0162418

Vardy, E., Robinson, J. E., Li, C., Olsen, Reid H. J., DiBerto, Jeffrey F., Giguere, Patrick M., . . . Roth, Bryan L. (2015). A New DREADD Facilitates the Multiplexed Chemogenetic Interrogation of Behavior. *Neuron, 86*(4), 936-946. doi:https://doi.org/10.1016/j.neuron.2015.03.065

Wallén-Mackenzie, Å., Gezelius, H., Thoby-Brisson, M., Nygård, A., Enjin, A., Fujiyama, F., ... & Kullander, K. (2006). Vesicular glutamate transporter 2 is required for central respiratory rhythm generation but not for locomotor central pattern generation. *Journal of neuroscience*, 26(47), 12294-12307.

Wang, X., Hayes, J. A., Revill, A. L., Song, H., Kottick, A., Vann, N. C., . . . Del Negro, C. A. (2014). Laser ablation of Dbx1 neurons in the pre-Botzinger complex stops inspiratory rhythm and impairs output in neonatal mice. *Elife, 3*, e03427. doi:10.7554/eLife.03427

Winter, S. M., Fresemann, J., Schnell, C., Oku, Y., Hirrlinger, J., & Hülsmann, S. (2009). Glycinergic interneurons are functionally integrated into the inspiratory network of mouse medullary slices. *Pflügers Archiv-European Journal of Physiology*, 458, 459-469.

Woolf, N. J., & Butcher, L. L. (1989). Cholinergic systems in the rat brain: IV. Descending projections of the pontomesencephalic tegmentum. *Brain Res Bull, 23*(6), 519-540.

Xie, A., Skatrud, J. B., Puleo, D. S., Rahko, P. S., & Dempsey, J. A. (2002). Apnea–hypopnea threshold for CO2 in patients with congestive heart failure. *American Journal of Respiratory and Critical Care Medicine*, 165(9), 1245-1250.

Yackle, K., Schwarz, L. A., Kam, K., Sorokin, J. M., Huguenard, J. R., Feldman, J. L., . . . Krasnow, M. A. (2017). Breathing control center neurons that promote arousal in mice. *Science, 355*(6332), 1411-1415. doi:10.1126/science.aai7984

Yang, C. F., & Feldman, J. L. (2018). Efferent projections of excitatory and inhibitory preBötzinger Complex neurons. *Journal of Comparative Neurology, 526*(8), 1389-1402. doi:https://doi.org/10.1002/cne.24415

Yang, C. F., Kim, E. J., Callaway, E. M., & Feldman, J. L. (2020). Monosynaptic Projections to Excitatory and Inhibitory preBötzinger Complex Neurons. *Frontiers in Neuroanatomy, 14*. doi:10.3389/fnana.2020.00058

Zheng, F., Nixdorf-Bergweiler, B. E., Edelmann, E., van Brederode, J. F. M., & Alzheimer, C. (2020). Muscarinic Modulation of Morphologically Identified Glycinergic Neurons in the Mouse PreBötzinger Complex. *Frontiers in Cellular Neuroscience, 13*.

Zhu, H., & Roth, B. L. (2014). Silencing synapses with DREADDs. *Neuron, 82*(4), 723-725. doi:10.1016/j.neuron.2014.05.002

Zoccal, D. B., & Machado, B. H. (2010). Sympathetic overactivity coupled with active expiration in rats submitted to chronic intermittent hypoxia. *Respiratory physiology & neurobiology, 174*(1-2), 98-101.

Zoccal, D. B., Silva, J. N., Barnett, W. H., Lemes, E. V., Falquetto, B., Colombari, E., . . . Takakura, A. C. (2018). Interaction between the retrotrapezoid nucleus and the parafacial respiratory group to regulate active expiration and sympathetic activity in rats. *American Journal of Physiology-Lung Cellular and Molecular Physiology, 315*(5), L891-L909. doi:10.1152/ajplung.00011.2018